

The Cardiovascular Profile and Pharmacology of Vandetanib and Pazopanib

*Thesis submitted to the University of Nottingham for
the Degree of Doctor of Philosophy*

Joanne Carter, BSc (Hons)

2016



**The University of
Nottingham**

UNITED KINGDOM • CHINA • MALAYSIA

Cell Signalling Research Group

School of Life Sciences

University of Nottingham Medical School

Queen's Medical Centre

Nottingham

NG7 2UH

Acknowledgements.....	9
Declaration.....	10
Publications.....	10
Abbreviations.....	11
Abstract.....	16
Chapter 1 : General Introduction	18
1.1 General Introduction.....	19
1.2 VEGF	21
1.3 VEGF in Angiogenesis	30
1.3.1 Anti-VEGF Treatments in Cancer.....	35
1.3.1.1 Vandetanib	38
1.3.1.2 Pazopanib.....	42
1.3.1.3 Cediranib and Sorafenib	45
1.3.2 Cardiovascular Consequences of RTKIs.....	46
1.4 The Pathophysiology of Hypertension.....	48
1.4.1 Nervous Control of Vessel Tone	49
1.4.2 The Renin- Angiotensin-Aldosterone System and its Effect on Vessel Tone	50
1.4.3 Vascular Control of Vessel Tone.....	51
1.5 Current Theories on RTKI-Mediated Hypertension.....	53
1.6 Aims and Hypothesis	54
Chapter 2 : General Methods.....	56
2.1 NFAT-Luciferase Gene Reporter Assay	57
2.1.1 Cell Culture.....	58
2.1.2 Cell Passage	59
2.1.3 Long Term Storage	60

2.2	NFAT-Luciferase Assay	61
2.2.1	Experimental Method Protocol 1: The 'non-confluent monolayer' Method	62
2.2.2	Experimental Method Protocol 2: The 'suspension' Method	63
2.2.3	Data Analysis	64
2.3	Telemetry	65
2.3.1	Telemetry Variables	68
2.3.2	Surgical Procedures	68
2.3.2.1	Animals.....	68
2.3.2.2	Implantation of Telemetry Devices	69
2.3.2.3	Telemetry Experimental Method	73
2.3.2.4	Statistical Analysis.....	73
2.4	Mesothelium Panel Staining for ECs	74
2.4.1	Method of Tissue Isolation	75
2.4.2	Staining Procedure	76
2.4.3	Analysis	77
2.4.3.1	AngioTool 0.6b.....	77
2.5	The Measurement of Regional Haemodynamics in Conscious Rats	78
2.5.1	The Pulsed Doppler Method.....	79
2.5.2	Construction of Doppler Flow Probes	81
2.6	Surgical Procedures	84
2.6.1	Animals.....	84
2.6.2	Implantation of Doppler Flow Probes.....	84
2.6.2.1	Implantation of Intra-vascular Catheters	88
2.6.2.2	Intra-venous Catheters	89

2.6.2.3	Intra-Arterial Catheters	89
2.6.2.4	Intra-peritoneal Catheters	90
2.6.3	Doppler Experimental Set Up	90
2.6.4	Statistical Analysis	93
2.7	Isobaric Myography	94
2.7.1	Preparation of Small Mesenteric Arteries.....	94
2.7.2	Myography System	95
2.7.3	Statistical Analysis	98

Chapter 3 : Effects of Receptor Tyrosine Kinase Inhibitors on VEGF₁₆₅- and VEGF_{165b}-Stimulated NFAT-Luciferase Gene Transcription in HEK-293 Cells Expressing Human VEGFR2 99

3.1	Introduction	100
3.2	Methods.....	102
3.2.1	Experimental Method Protocol 1: The 'non-confluent monolayer' Method	102
3.2.2	Experimental Method Protocol 2: The 'suspension' Method	102
3.2.3	Data Analysis	103
3.3	Results	104
3.3.1	Characterisation of the VEGF ₁₆₅ -Mediated NFAT Luciferase Response, in the Presence and Absence of RTKIs	104
3.3.2	Characterisation of the VEGF _{165b} Mediated NFAT Luciferase Response, in the presence and absence of RTKIs	114
3.4	Discussion.....	117
3.4.1	Methodology	117

3.4.2	Characterisation of the VEGF ₁₆₅ and VEGF _{165b} Mediated NFAT Luciferase Response	118
3.4.3	The Action of RTKIs on the VEGF ₁₆₅ and VEGF _{165b} Mediated NFAT Luciferase Response	119
3.4.4	Conclusion	120

Chapter 4 : The *In Vivo* Cardiovascular Actions of Vandetanib 121

4.1	Introduction	122
4.2	Methodology.....	124
4.2.1	Time Course of the Effects of Vandetanib on Cardiovascular Variables, Measured By Radio-Telemetry	124
4.2.1.1	Statistical Analysis.....	124
4.2.2	The Action of Vandetanib on Mesenteric Vessel Structure Following <i>In Vivo</i> Dosing For 21 Days and a Post-Treatment Period of 10 Days.....	125
4.2.2.1	Data Analysis.....	125
4.2.3	Regional Haemodynamic Effects of Vandetanib Measured by Pulsed Doppler Flowmetry (i.v)	126
4.2.4	Regional Haemodynamic Effects of Vandetanib Measured by Pulsed Doppler Flowmetry (i.p)	126
4.2.4.1	Statistical Analysis.....	127
4.3	Results	128
4.3.1	Time Course of Effects of Vandetanib on Cardiovascular Variables Measured By Radio-Telemetry	128
4.3.1.1	Mean Arterial Blood Pressure	128
4.3.1.2	Heart Rate.....	134

4.3.2	The Effects of Vandetanib on Mesenteric Vessel Structure Following <i>In Vivo</i> Dosing For 21 Days and a Post-treatment Treatment Period of 10 Days	139
4.3.3	Regional Haemodynamic Effects of Vandetanib Measured by Pulsed Doppler Flowmetry (i.v)	143
4.3.4	Regional Haemodynamic Effects of Vandetanib Measured by Pulsed Doppler Flowmetry (i.p)	147
4.4	Discussion	156
4.4.1	Methodology	156
4.4.2	Mean Arterial Blood Pressure.....	157
4.4.3	Vascular Conductance	160
4.4.4	Heart Rate	161
4.4.5	Conclusion	162

Chapter 5 : The *In Vivo* Cardiovascular Actions of Pazopanib 164

5.1	Introduction	165
5.2	Methodology.....	166
5.2.1	Time Course of Effects of Pazopanib on Cardiovascular Variables Measured By Radio-Telemetry	166
5.2.1.1	Statistical Analysis.....	166
5.2.2	Regional Haemodynamic Effects of Pazopanib Measured by Pulsed Doppler Flowmetry (i.p)	167
5.2.2.1	Statistical Analysis.....	167
5.3	Results	169
5.3.1	Time Course of Effects of Pazopanib on Cardiovascular Variables Measured By Radio-Telemetry	169
5.3.1.1	Mean Arterial Blood Pressure	169

5.3.1.1	Heart Rate.....	174
5.3.2	Regional Haemodynamic Effects of Pazopanib Measured by Pulsed Doppler Flowmetry (i.p)	179
5.4	Discussion	188
5.4.1	Methodology	188
5.4.2	Mean Arterial Blood Pressure.....	191
5.4.3	Vascular Conductance	193
5.4.4	Heart Rate	193
5.4.5	Conclusion	194
Chapter 6 : The Actions of Vandetanib, Pazopanib, hVEGF₁₆₅ and Acetylcholine on Vessel Diameter		196
6.1	Introduction	197
6.2	Methodology	199
6.2.1	Living Systems Pressure Myography	199
6.2.2	DMT 120CP myography	200
6.2.3	Statistical Analysis.....	201
6.3	Results	203
6.3.1	The Effects of Vandetanib and Pazopanib on Pressurised Vessel Diameter.....	203
6.3.2	The Effects of Vandetanib on the Vessel Diameter of Pre-Constricted Pressurised Vessels.....	205
6.3.3	The Effects of Vandetanib on hVEGF ₁₆₅ Mediated Vessel Dilatation	207
6.3.4	The Effects of Vandetanib on ACh Mediated Vessel Dilatation	209
6.4	Discussion.....	211

6.4.1	The Effect of Vandetanib and Pazopanib on Pressurised Vessel Diameter.....	211
6.4.2	The Effect of Vandetanib on the Vessel Diameter of Pre-Constricted Pressurised Vessels	213
6.4.3	The Effects of Vandetanib on hVEGF _{165a} -Mediated Vessel Dilatation	214
6.4.4	The Effects of Vandetanib on ACh-Mediated Vessel Dilatation	216
6.4.5	Conclusion	217
Chapter 7 : General Discussion		218
7.1	Introduction	219
7.2	The Pharmacological Characteristics of a Panel of Receptor Tyrosine Kinase Inhibitors (RTKIs) (Cediranib, Sorafenib, Pazopanib and Vandetanib) in a Whole Cell System.....	220
7.3	The Chronic Effects of Vandetanib and Pazopanib on Heart Rate and Blood Pressure in Male Sprague Dawley Rats	222
7.4	The Effect of Various Concentrations of Vandetanib and Pazopanib on Heart Rate, Mean Arterial Blood Pressure, Hindquarter, Renal and Mesenteric Vascular Conductances in Male Sprague Dawley Rats.....	224
7.5	The Action of Vandetanib and Pazopanib on Isolated Pressurised Mesenteric Arterioles, and the Effect of Vandetanib on VEGF and Acetylcholine Mediated Vessel Dilatation.....	226
7.6	Overall Conclusion.....	228
References		231

Acknowledgments

I would like to thank Dr Jeanette Woolard for her support throughout my studies. My sincere thanks also go to Professor Stephen Hill, who has compassionately taken me under his wing. His mentorship, patience and devotion to this project have been instrumental. I would also like to also extend my gratitude to Dr Tom Bellamy and Phillip Kemp for their support, teaching, patience and guidance throughout this process, as well as to Julie March for her support in the surgical theatre.

I would like to especially thank the Cell Signalling Research Group for their unwavering emotional and scientific support. The lows and highs of this process have been innumerable but your consistent belief in me and encouragement has made this experience unforgettable.

I would also like to thank The University of Nottingham for the opportunity to carry out this work and for funding this project.

Last, but by no means least, I would like to thank my family for their incredible and unwavering support. Without their guidance, love and encouragement I would never have had the courage to start or the determination to finish. Their collective belief that one can do anything she puts her mind to has been a tremendous inspiration!

Declaration

Cells used in Chapter 3 were provided by Promega. In Chapters 4 and 5, the principle surgeon was Julie March with myself acting as assistant surgeon. All results documented in this thesis are from my own work.

Publications

Published papers

JJ Carter, AJ Wheal, SJ Hill, J Woolard (2015) Effects of receptor tyrosine kinase inhibitors on VEGF₁₆₅ a- and VEGF₁₆₅ b-stimulated gene transcription in HEK-293 cells expressing human VEGFR2. *Br J Pharmacol.* 172(12):3141-50.

JJ Carter, LV Fretwell, J Woolard (2016) The effects of four multi-targeted receptor tyrosine kinase inhibitors on regional haemodynamics in conscious, freely-moving rats. FASEB J [epub ahead of print]

Published abstracts

JJ Carter, AJ Wheal, SJ Hill, J Woolard (2014). A Pharmacological Profile of Receptor Tyrosine Kinase Inhibitors on VEGFR2-stimulated NFAT Signalling in HEK-293 Cells. *Proceedings of the British Pharmacological Society at* <http://www.pA2online.org/abstracts/Vol12Issue3abst038P.pdf>

AJ Wheal, JJ Carter, SJ Hill, J Woolard (2014). Agonist Activity of VEGF_{165b} in HEK 293 Cells Expressing the Human VEGF Receptor 2. *Proceedings of the British Pharmacological Society at* <http://www.pA2online.org/abstracts/Vol12 Issue3abst131P.pdf>

JJ Carter, J Woolard (2014). The Hypertensive and Haemodynamic Actions of Vandetanib and Pazopanib, Two VEGF Receptor Tyrosine Kinase Inhibitors, *In Vivo. Angiogenesis* 17(4):935-984.

JJ Carter, J Woolard (2015). The Chronic Hypertensive Actions of Vandetanib and Pazopanib *In Vivo. J Vasc Res* 52 (1):1-88.

Abbreviations

ACh Acetylcholine

APES 3-Aminopropyltriethoxysilane

BAD Bcl-2-associated death promoter

BPM beats per minute

BSA Bovine serum albumin

Casp (3, 7, 9) Cysteine-dependent aspartate-directed protease

CD34 Cluster of differentiation 34

c-kit Stem cell growth factor receptor

DBP Diastolic blood pressure

dH₂O Distilled water

DII4 Delta-like ligand 4

DMEM Dulbecco's modified Eagle's medium

DMSO Dimethyl sulfoxide

EC Endothelial cell

EC₅₀ Molar concentration of agonist required to generate 50% of the maximal response

ECG Electrocardiogram

ECM Extracellular matrix

EGFR Epidermal growth factor receptor

E_{max} The maximal response of an agonist

eNOS Endothelial nitric oxide synthase

ETDA ethylene-diamine-tetraacetic acid

ERK Extracellular signal regulated kinase

FAK Focal adhesion kinase

FCS Foetal calf serum

FGFR Fibroblast growth factor receptor

FIH factor inhibiting hypoxia inducible factors

FLT fms (colony stimulating factor)-like tyrosine kinase

GDNF Glial cell line derived neurotrophic factor

GRB2 Growth factor receptor-bound protein 2

GS-IB4 *Griffonia simplicifolia*- isolectin type IB4

GSK3 Glycogen synthase kinase 3

GST Glutathione S-transferase

G418 Geneticin

HEK Human embryonic kidney

HIF Hypoxia inducible factor

His Histamine

HSG Heparan sulphate glycoprotein

i.a Intra-arterial

Ig Immunoglobulin

IGFR Insulin-like growth factor 1 receptor

i.p Intra-peritoneal

ITK Interleukin-2-inducible T-cell kinase

i.v Intra-venous

IQGAP IQ motif containing guanosine-5'-triphosphatase activating protein

JNK c-Jun N-terminal kinase

K_A The dissociation constant of the agonist

K_E The system coupling efficiency (the concentration of agonist receptor complex which produces a half maximal response)

LCK Lymphocyte-specific protein tyrosine kinase

L-NAME L-NG-Nitroarginine Methyl Ester

MAP Mean arterial blood pressure

MAPK Mitogen activated protein kinase

MEK Mitogen activated protein kinase

NFAT Nuclear factor of activated T-cells

NO Nitric oxide

NP Neuropillin

PBS Phosphate-buffered saline

PBX 0.5% triton-X100 in PBS

PDGFR Platelet derived growth factor receptor

PDK 3-phosphoinositide dependent protein

PECAM Platelet EC adhesion molecule

PHD Prolyl hydroxylase domain

PDGF Platelet-derived growth factor

PI3K Phosphatidylinositide 3-kinase

PKB/AKT Protein kinase B

PKC Protein kinase C

PLA₂ Phospholipase A2

PLC Phospholipase C

PMCA plasma membrane Ca²⁺ ATPase

PRF Pulse repetition frequency

PSS Physiological salt solution

PGI₂ Prostaglandin 2

Raf Rapidly accelerated fibrosarcoma

RET Rearranged during transfection

R_T The total receptor concentration within the system

RTKI Receptor tyrosine kinase inhibitor

SA Stretch activated

SBP Systolic blood pressure

SERCA Sarcoendoplasmic reticulum calcium transport ATPase

sGC Soluble guanylyl cyclase

sVEGFR Soluble vascular endothelial growth factor receptor

SRE Serum response factor

SHB SH2 domain-containing adapter protein B

SH2 src homology domain 2

TAF Tumour angiogenesis factor

TIE2 Angiopoietin receptor

TP Thromboxane receptor

TRITC Tetramethyl-rhodamine-isothiocyanate

TxA₂ Thromboxane A₂

U46619 9, 11-dideoxy-9 α , 11 α -methanoepoxy
prostaglandin F_{2 α}

VE-Cadherin Vascular endothelial cadherin

VEGF Vascular endothelial growth factor

VEGFR Vascular endothelial growth factor receptor

VPF Vascular permeability factor

Y Tyrosine

Abstract

Angiogenesis, a process that enables the growth of blood vessels from a pre-existing vasculature and is common to all solid tumours greater than 1 mm³ in size (Gacche and Meshram, 2014). The angiogenic process is heavily promoted by vascular endothelial growth factor (VEGF). Compounds able to inhibit VEGF signalling have been shown to reduce cancer mass (Arjaans *et al.*, 2016). However, VEGF receptor tyrosine kinase inhibitors (RTKIs), a class of anti-VEGF treatment, have been shown to cause cardio-toxicity, with hypertension being a commonly reported, and often severe, side effect (Eskens and Verweij, 2006; Widakowich *et al.*, 2007; Abi Aad *et al.*, 2015). Depending on the nature of the study, the incidence of hypertension in the VEGF RTKI patient population ranges from 23% to 90% (Hamberg *et al.*, 2010; La Vine *et al.*, 2010; Aparicio-Gallego *et al.*, 2011; Bible *et al.*, 2014). Due to the increasing incidence and seriousness of hypertension observed in oncology clinics, it is clear that there are important cardiovascular issues relating to the use of RTKIs, particularly those that target VEGF, that require further exploration. This body of work set out to determine the *in vitro* potencies of vandetanib, pazopanib, cediranib and sorafenib at VEGFR2, alongside the *in vivo* cardiovascular haemodynamic and vasoactive profile of vandetanib and pazopanib, two VEGF RTKIs shown to cause hypertension in approximately 32% (Wells *et al.*, 2012) and 33%-40% of the patient population, respectively (Bible *et al.*, 2014).

In NFAT luciferase assays cediranib, sorafenib, pazopanib and vandetanib were shown to inhibit, in a non-competitive fashion, VEGF₁₆₅ mediated signalling *in vitro*. In haemodynamic studies, using Doppler flowmetry and

telemetry methodologies, both vandetanib and pazopanib caused significant hypertension ($P < 0.05$, in comparison to vehicle). Pazopanib and vandetanib lead to significant vasoconstriction of the mesenteric and hindquarter vascular beds, pazopanib also produced significant vasoconstriction in the renal vascular bed ($P < 0.05$, in comparison to vehicle). None of the variables measured in the haemodynamic studies significantly differed between the $30 \text{ mgkg}^{-1}\text{day}^{-1}$ pazopanib and $25 \text{ mgkg}^{-1}\text{day}^{-1}$ vandetanib groups. In chronic radio-telemetric studies, vandetanib was shown to cause a significantly greater but more transient increase in mean arterial blood pressure in comparison to pazopanib ($P < 0.05$). Vandetanib was also shown to inhibit VEGF and ACh-mediated vessel dilatation in pressure myography experiments. Finally, vandetanib and pazopanib were shown to induce vasodilatation in the presence of a vasoconstrictor (U46619), a previously unseen finding.

In conclusion, the body of work undertaken here has given novel insight into the ability of non-competitive anti-VEGF RTKIs to inhibit VEGF-mediated signalling and vessel dilatation as well as produce direct effect of vessel diameter in the absence of VEGF. It has also produced a validated method of hypertension in a rat model, both in the short and long term. These models have shown that different anti-VEGF RTKIs have different regional haemodynamic and post-treatment hypertensive side effect profiles. These findings are important for understanding the mechanisms behind the therapeutic and non-therapeutic effects of VEGF RTKIs and allow for further research into the signalling mechanism involved in VEGF RTKI-mediated hypertension and the potential therapeutic treatments that could treat this.

Chapter 1: General Introduction

1.1 General Introduction

Cancer is a complex group of diseases, with over 100 different known classifications (Stewart, 2014). It is a leading cause of morbidity worldwide, with 14 million newly diagnosed cases and 8.2 million cancer related deaths in 2012 (Stewart, 2014; World Health Organisation, 2016). The development and progression of cancer involves multiple changes and/or mutations in gene expression, leading to up- or down-regulation of specific signalling pathways (Hanahan and Weinberg, 2011). Common to all solid tumours is the ability to induce angiogenesis, a process that enables the growth of blood vessels from the pre-existing vasculature (Gacche and Meshram, 2014). Increasing blood flow to the tumour mass is a requirement for tumour growth beyond 2-3 mm³ in size (Folkman, 1971). Pathological angiogenesis results in the development of blood vessels that are unstructured, tortuous and innately leaky (Ferrara, 2001). The resultant enhanced vessel permeability facilitates the escape of tumour cells from the tumour mass as well as their transportation to distant sites, wherein secondary metastases may form (Wong *et al.*, 2015). One of the key, and most potent, mediators of angiogenesis is vascular endothelial growth factor (VEGF). The inhibition of tumorigenic processes, such as angiogenesis, is critical to preventing cancer progression. The recent development of several anti-angiogenic drugs that target VEGF, or its receptors, has highlighted the important relationship between the cardiovascular system and the tumour microenvironment. This relationship has become one of the main focuses of oncology and cardiovascular research.

VEGF is important for cell survival, proliferation, increased vascular density and vasodilatation (Liang *et al.*, 2013;

Domigan *et al.*, 2014). Neutralisation or blockade of VEGF signalling, either by inhibiting the VEGF ligand directly, i.e. with the humanised monoclonal antibody bevacizumab that prevents the VEGF ligand from interacting with the receptor, or by targeting the associated VEGF receptor 2 (VEGFR2) signalling pathway, generally with receptor tyrosine kinase inhibitors (RTKIs), has been shown to decrease these events (Liang *et al.*, 2014). There are several RTKIs such as vandetanib (Zactima™), pazopanib (Votrient®), sorafenib (Nexavar®) and cediranib (Recentin™) (Knosel *et al.*, 2014) that are currently used or are in late Phase trials as adjuvant treatments alongside current chemotherapeutic agents (Herbst *et al.*, 2010; Arjaans *et al.*, 2016).

VEGF RTKIs are a multi-targeted drug class. This approach was first designed to reduce the likelihood of drug resistance (Huang and Kauffman, 2013). However, it has been shown that anti-angiogenic/anti-VEGF treatments can lead to cardio-toxicity, with hypertension being a commonly reported and severe side effect (Eskens and Verweij, 2006; Widakowich *et al.*, 2007; Abi Aad *et al.*, 2015). Depending on the nature of the study, the incidence of hypertension in the clinical setting ranges from 23% to 90% of the patient population (Hamberg *et al.*, 2010; La Vine *et al.*, 2010; Aparicio-Gallego *et al.*, 2011; Bible *et al.*, 2014), with approximately 32% of the patient population taking vandetanib (Wells *et al.*, 2012) and 33%-40% of the patient population prescribed pazopanib (Hamberg *et al.*, 2010; Bible *et al.*, 2014) developing hypertension. Moreover, the development and escalation of pre-existing hypertension in these patient populations has been linked to multiple severe complications including venous or arterial thrombo-embolisms, acute heart failure,

intracerebral haemorrhage and reversible posterior leukoencephalopathy syndrome (Govindarajan *et al.*, 2006; Chu *et al.*, 2007; Pouessel and Culine, 2008; Eschenhagen *et al.*, 2011). The resultant hypertension caused by treatment with VEGF RTKIs has proven difficult to treat clinically, as many patients appear to be resistant to conventional anti-hypertensive therapies, including angiotensin converting enzyme inhibitors, calcium channel blockers, beta blockers and thiazide diuretics; all of which appear to have little or no effectiveness in this patient population (Kruzliak *et al.*, 2013).

VEGF blockade, by therapeutic compounds such as RTKIs, has been shown to produce cardiotoxic effects. To date, the role of VEGF in the cardiovascular system is poorly understood, under both normal and pathophysiological conditions. A better understanding of the mechanisms by which hypertension occurs in the absence of VEGF signalling would help to improve the side effect profile of current and future anti-angiogenic treatments.

1.2 VEGF

VEGF represents a ligand family of dimeric polypeptides, of approximately 46 kDa, which propagate pro-survival and pro-angiogenic signals (Liang *et al.*, 2013).

In the early 1970's, J. Folkman first reported that a secreted tumour factor, initially termed tumour angiogenesis factor (TAF), was required for the initiation of tubule formation (Folkman, 1971; Folkman, 1972). TAF was shown to induce angiogenesis and allow tumour growth past 2-3 mm³ in size (Folkman, 1971). Several years later, TAF was isolated and partially purified (Senger *et al.*, 1983), in a study that

demonstrated its role in vascular permeability. Thereafter, it was termed vascular permeability factor (VPF). Subsequently TAF and VPF were recognised to be the same factor and it was ultimately renamed as VEGF by Ferrara, who fully sequenced the human and bovine VEGF in 1989 (Senger *et al.*, 1983; Senger *et al.*, 1986; Leung *et al.*, 1989; Ferrara and Henzel, 1989).

The mammalian VEGF family consists of 5 members, namely, VEGF-A, VEGF-B, VEGF-C, VEGF-D and placental-derived growth factor (PlGF) (Olsson *et al.*, 2006). VEGFs propagate their signal through binding to VEGF receptors. The VEGFR family of receptor tyrosine kinases (VEGFR1, VEGFR2, VEGFR3 and soluble (s) VEGFR1) are structurally comprised of a 7 immunoglobulin like (Ig) extracellular domain, a linked hydrophobic transmembrane domain and multiple intracellular kinase domains (Koch *et al.*, 2011). However, the soluble form of VEGFR1 (sVEGFR1) comprises of only the extracellular domain of the receptor. The intracellular portion of VEGFR1, VEGFR2 and VEGFR3 contain a juxta-membrane domain, a kinase insert domain, an ATP binding domain, a phosphotransferase domain and a C-terminal domain (Figure 1.1) (Stuttfield and Ballmer-Hofer, 2009; Brozzo *et al.*, 2012). VEGF ligands have differing affinities for different members of the VEGF receptor family (Woolard *et al.*, 2009) as well as for heparan sulphate glycoproteins (HSG) and neuropilin (NP) (a 130-140 kDa co-receptor which also interact with semaphorin) (Soker *et al.*, 1998). There are two NPs, namely, NP1 which is able to bind to VEGF-A, -B and PlGF and is found in arterial endothelial cells (ECs) and NP2 which is able to bind to VEGF-A, -C and -D and is found in venous and lymphatic ECs (Djordjevic and Driscoll, 2013).

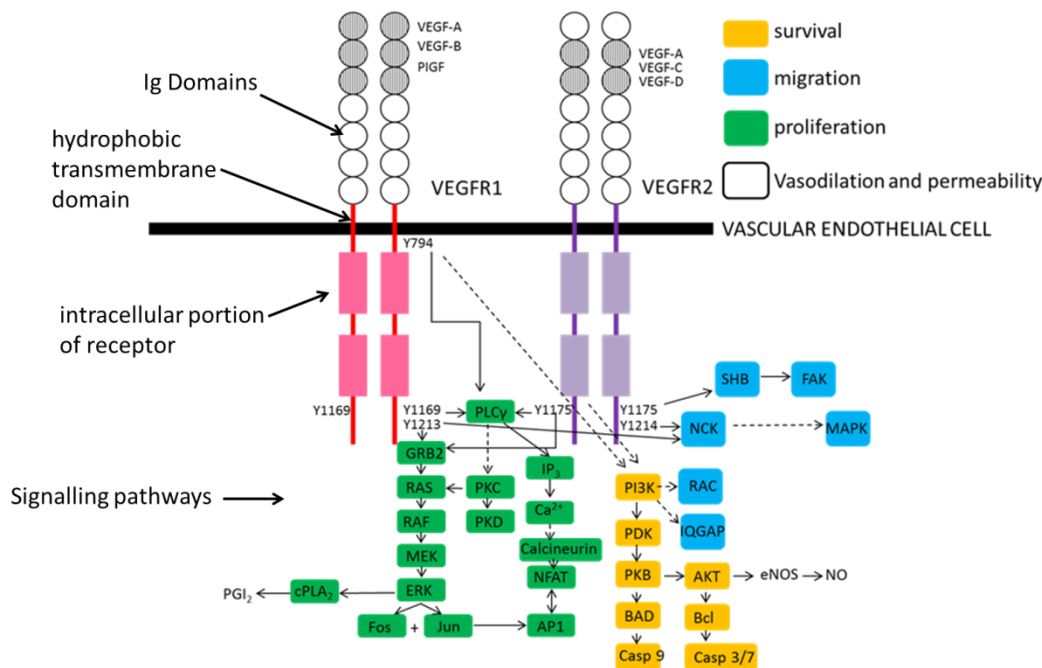


Figure 1.1 Diagrammatical representation of VEGFR1 and VEGFR2 receptor structure, their corresponding ligands and signalling pathways. The VEGFR comprises of 7 immunoglobulin like (Ig) extracellular domain of each receptor, linked to a hydrophobic transmembrane domain. The intracellular portion of each receptor contains a juxta-membrane domain, a kinase insert domain, an ATP binding domain, a phosphotransferase domain and a C-terminal domain. The VEGFR1 and 2 cononical signalling pathways comprise of the PLC γ , PI3K and MAPK pathways, allowing these receptors to influence cell survival (yellow), cell migration (blue), cell proliferation (green) and vessel permeability and vasodilatation (clear). Adapted from information in Olsson *et al.*, 2006; Stuttfeld and Ballmer-Hofer, 2009; Brozzo *et al.*, 2012; Bretz *et al.*, 2013; Domigan *et al.*, 2014;.

VEGF-A is able to bind to NPs (expressed on tumour cells and ECs), VEGFR1, a 180 kDa protein also referred to as Flt1, (expressed on monocytes and vascular ECs) and VEGFR2 (expressed on vascular ECs) (Zachary and Gliki, 2001). VEGF-B and PlGF are able to bind NP as well as VEGFR1. Lastly, VEGF-C and VEGF-D both bind to VEGFR3 (a 195 kDa protein also referred to Flt4) found on lymphatic ECs (Zachary and Gliki, 2001).

The extent of production and secretion of VEGF is determined by the extracellular environment, in particular the availability of oxygen (Kaur *et al.*, 2005). When oxygen is freely available, factor inhibiting hypoxia inducible factors (FIH) and prolyl hydroxylase domain proteins (PHDs) (Maxwell *et al.*, 2001) degrade cytoplasmic hypoxia inducible factors (HIF) such as HIF-1 α (Ahn *et al.*, 2014) reducing the ability of HIF to transcribe the *vegf* gene.

However under hypoxic conditions, FIHs and PHDs are inhibited. This allows HIF-1 α to translocate to the nucleus, whereupon it is able to increase both VEGF production and secretion, through its action as a transcription factor (Semenza *et al.*, 1997; Ferrara, 2001). This action also positively feeds-back to further up-regulate HIF expression levels (Blancher *et al.*, 2001).

VEGF-A is currently the most studied VEGF variant (Goel and Mercurio, 2013). The VEGF-A gene is alternatively spliced to give multiple VEGF-A isoforms with differing bioavailability's (Woolard *et al.*, 2009). These isoforms include VEGF₁₂₁, VEGF₁₄₅, VEGF₁₄₈, VEGF₁₆₅, VEGF₁₈₃, VEGF₁₈₉ and VEGF₂₀₆ (Koch *et al.*, 2011). Each isoform differs in its specificity for VEGFR2, as well as HSG and NP binding (Pan *et al.*, 2007;

Koch *et al.*, 2011). VEGF-A isoforms fall into two major groups: VEGF_{xxx} and VEGF_{xxx}b, with xxx symbolising amino acid number. VEGF_{xxx} and VEGF_{xxx}b isoforms differ primarily as a consequence of alternative splicing within exon 8 (Bates., 2013). This leads to the terminal 6 amino acids, and therefore tertiary structure of VEGF_{xxx} and VEGF_{xxx}b isoforms to differ, for example cysteine-160 in VEGF₁₆₅ is changed to a serine in VEGF₁₆₅b (Woolard., 2009). This alters the tertiary structure of VEGF₁₆₅b, in comparison to VEGF₁₆₅, by removing a disulphide bond formed between cysteine-160 and cysteine-146 in the VEGF₁₆₅ isoform (Woolard *et al.*, 2009). There are also a number of charged amino acids (such as arginine) in the C-terminus of VEGF₁₆₅, which are supplemented by neutral amino acids, such as lysine in VEGF₁₆₅b, further varying each isoform's tertiary structure. Although these structural changes do not greatly affect the affinity of VEGF₁₆₅b for VEGFR2 in comparison to VEGF₁₆₅ (Kawamura *et al.*, 2008), they are thought to reduce VEGF₁₆₅b efficacy at the VEGFR2 receptor by reducing the probability of receptor transphosphorylation (Kawamura *et al.*, 2008). This reduces the probability and amplification of receptor-mediated downstream signalling. It has also been shown that VEGF₁₆₅b is unable to bind to the VEGFR2 co-receptor, NP1 which acts to enhance the cell migratory and cell proliferative signalling of VEGFR1 and VEGFR2 (Kawasaki *et al.*, 1999; Chaudhary *et al.*, 2014; Zachary, 2014). The reduced efficacy of VEGF₁₆₅b at VEGFR2 and reduced affinity for NP1, in comparison to VEGF₁₆₅, has led to VEGF₁₆₅b being referred to as 'anti-angiogenic' due to its weak agonist action and its ability to competitively inhibit the receptor binding of more efficacious VEGFs such as VEGF₁₆₅a (Woolard *et al.*, 2004; Kawamura *et al.*, 2008; Carter *et al.*, 2015). VEGF₁₆₅b comprises around 50% of the VEGF₁₆₅

isoforms found in tissues such as the lung, kidney, bladder and colon (Cheung *et al.*, 1998). However, in relatively angiogenic tissues, such as the placenta, VEGF_{165b} expression is low (Bates *et al.*, 2006). It has also been noted that tumours that express abnormally high amounts of VEGF_{165b} grow more slowly in comparison to those expressing high amount of VEGF₁₆₅, further supporting the hypothesis that VEGF_{165b} is a weaker promoter of angiogenesis (Pritchard-Jones *et al.*, 2007). The presence of VEGF_{165b} has also been shown to reduce the potency of Avastin (bevacizumab) (Varey *et al.*, 2008). This is thought to be due to VEGF_{165b} competitively binding to Avastin leaving VEGF₁₆₅ able to activate VEGFR2-mediated angiogenesis. As VEGF_{165b} has been shown to be overexpressed in various tumours (Rennel *et al.*, 2008), understanding the effect of VEGF_{165b} on RTKI action is important for future drug development and has potential clinical applications regarding treatment choice.

Binding of VEGF-C and VEGF-D to VEGFR3 leads to the activation of the Phosphatidylinositide 3-kinase (PI3K) and mitogen activated protein kinase (MAPK) pathways (Salameh *et al.*, 2005). This is important for lympho-EC survival and proliferation. VEGFR3 signalling has also been shown to have a role in cardiovascular development with *vegfr3* *-/-* mice dying at embryonic day 9.5 due to impaired cardiovascular and vessel development (Dumont *et al.*, 1998). However, VEGFR3 signalling has not been shown to be integral to adult vascular development, and therefore will not be discussed further.

VEGFR1, VEGFR2 and the co-receptor NP1 are known to facilitate a number of processes in the vasculature, including EC survival, vessel sprouting and vasodilatation (Olsson *et al.*, 2006). The activation of VEGFR2, via VEGF-A isoforms, has the

most prominent promotional effect on these processes (Koch *et al.*, 2011). NP1 is able to bind VEGF-A, VEGF-B and PlGF. This interaction allows it to form an oligomeric complex with VEGFR1 or VEGFR2 and enhance the resultant cell migration and proliferation (Kawasaki *et al.*, 1999; Parker *et al.*, 2012).

VEGFR1 binds to its ligand via extracellular Ig domains 1-3 (Nieminen *et al.*, 2014). This interaction induces receptor dimerisation and trans-phosphorylation of intracellular tyrosine residues, subsequently leading to activation of phospholipase C (PLC) and MAPK signalling cascades (Sawano *et al.*, 1997) increasing cell migration, proliferation and vascular permeability (Ito *et al.*, 1998). Although it is clear that VEGFR1 causes downstream signalling when activated, the current level of involvement of VEGFR1 in EC proliferation, migration and vascular permeability is debated in the literature. It has been shown *in vitro* that VEGFR1 is not essential for these processes to occur (Gille *et al.*, 2001). However, contrary to this, phosphorylation of VEGFR1 tyrosine residue 1213 has been shown to cause sustained activation of angiogenesis through its interaction with the p85 subunit of PI3K, leading to the induction of the PI3K pathway (Cai *et al.*, 2003). Although the full role of VEGFR1 remains to be determined, its presence has been shown to be important in development, with the *vegfr1* *-/-* knockout being lethal in mice at embryonic day 8.5 (Fong *et al.*, 1999). Interestingly, deletion of the tyrosine kinase domain of VEGFR1 in mice leads to normal development (Hiratsuka *et al.*, 1998). This has led to the theory that sVEGFR1 and VEGFR1 may act as anti-angiogenic decoy receptors, by sequestering VEGF and therefore reducing the extent of the angiogenic response (Carmeliet *et al.*, 2001; Murakami *et al.*, 2006).

Like VEGFR1, VEGFR2 knockout mice also experience embryonic lethality at embryonic day 8.5-9 (Shalaby *et al.*, 1995). This, and the embryonic lethality of *vegfa* *-/-* (lethal at embryonic day 9.5-10.5) and *vegfa* *+/-* (lethal at embryonic day 11-12) in mice, highlights the importance of the VEGF-A/VEGFR2 signalling pathway in EC survival, proliferation and angiogenesis (Ferrara *et al.*, 1996; Carmeliet *et al.*, 1996). VEGF-A or C-terminal truncated forms of VEGF-C and VEGF-D bind to the Ig 2 and 3 domains of VEGFR2. This leads to activation, dimerization and trans-phosphorylation of the receptor (Dougher-Vermazen *et al.*, 1994), allowing VEGFR2 to activate various pathways, including the PLC γ , MAPK, focal adhesion kinase (FAK), PI3K and phospholipase A₂ (PLA₂) pathways (Figure 1.1). These interactions lead to VEGF-A/VEGFR2- induced proliferation, migration, cell survival, cell permeability and angiogenesis, as well as vasodilatation through the production of nitric oxide (NO) and prostaglandin (PGI₂), two potent vasodilatory factors (Horii *et al.*, 1978; Kitsukawa *et al.*, 1995; Bauer and Sotnikova, 2010). NP1/VEGFR2 oligomeric complex signalling has been shown to increase cell migration, cell survival, permeability and angiogenesis, compared to that of VEGFR2 alone (Pan *et al.*, 2007; Jia *et al.*, 2010). The involvement of NP1 in VEGF signalling is important in the regulation of vascular development and tone, with *np1* *-/-* being lethal in mice at embryonic day 12.5, due to reduced vasculature and irregular neuronal patterning (Kawasaki *et al.*, 1999). Overexpression of NP1 leads to constitutive vessel dilatation and heart malformation (Kitsukawa *et al.*, 1995). Due to VEGFR2 signalling having the most influence over angiogenesis and cell survival, this receptor along with its ligand VEGF-A, have been

targeted pharmacologically in diseases where angiogenic regulation is abnormal, e.g. cancer.

In addition to its role in angiogenesis (discussed in Section 1.3.1.1), VEGF/VEGFR2 also promotes vascular permeability (Senger *et al.*, 1986). Although it is not fully understood how VEGF increases vascular permeability, its strong affiliation with the production of vesicular-vacuolar organelles is thought to be integral (Feng *et al.*, 1996). Vesicular-vacuolar organelles are able to form channels through the EC by fusing with each other, therefore facilitating the diffusion of molecules (Feng *et al.*, 1996). Murohara *et al.* (1998) demonstrated that NO and PGI₂ have been linked to the formation of vesicular-vacuolar organelles, showing that VEGF induced permeability was substantially reduced in the presence of N ω -Nitro-L-arginine methyl ester (L-NAME; eNOS inhibitor) and indomethacin (cyclooxygenase inhibitor) *in vitro* (Murohara *et al.*, 1998).

VEGF not only contributes to the progression of cancer through stimulating angiogenesis and increasing vascular permeability, but has also been linked to tumour initiation and tumour survival (Goel and Mercurio, 2013). Autocrine VEGF signalling has been observed in multiple tumour types (Bachelder *et al.*, 2001; Hamerlik *et al.*, 2012), and has been suggested as a characteristic of aggressive cancer types (Mak *et al.*, 2010; Cao *et al.*, 2012). It is thought that the ability of the tumour cell to signal independently through VEGF-A, in an autocrine manner, helps to increase its survival. The inhibition of VEGF-A has been shown to reduce tumour cell growth and survival (Lee *et al.*, 2012). The presence of VEGF in micro-dissected tumours and its role in cell de-differentiation have garnered interest in the function of VEGF in tumour initiation (Senger and Van De Water, 2000; Bates *et al.*, 2003;

Mak *et al.*, 2010). How cells increase their expression of VEGF-A and VEGFRs in order to promote a tumour phenotype is currently unknown. However, it is thought that environmental hypoxia may be an important driver. The sustained activation of HIF-1 α , the hypoxic-inducible transcription factor for VEGF-A, in certain tumour types goes some way to supporting this hypothesis (Mimeault and Batra, 2013). Finally, the presence of VEGFRs on T-cells (Hansen *et al.*, 2012) and macrophages (Galdiero *et al.*, 2013) has been associated with the progression of tumour growth. It has been hypothesised that VEGF, secreted by macrophages located in the hypoxic tumour environment, may act to further contribute to tumour growth by increasing tumour cell survival and angiogenesis (Goel and Mercurio, 2013).

The high expression of VEGF-A in certain tumour types, e.g. breast and colorectal cancer, has also been associated with increased tumour aggressiveness, poorer responses to chemotherapy and increased mortality rates (Toi *et al.*, 2001; Foekens *et al.*, 2001; Cao *et al.*, 2012). Due to this, chemotherapies have been designed to target the VEGF-A/VEGFR2 pathway, with some also targeting VEGF-A/VEGFR1 and VEGFR3 signalling in order to reduce tumour cell survival and tumour angiogenesis.

1.3 VEGF in Angiogenesis

Since the initial demonstration of the importance of the vasculature in the development of solid tumours (Folkman, 1971), the wider understanding of angiogenic processes in health and disease has quickly developed and is now recognised as the process of vessel sprouting and extension from the pre-existing vasculature (Carmeliet and Jain, 2011).

In order for this to occur, Pericyte cells, an EC phenotype located on the luminal side of the vessel, act to monitor oxygen levels (De Bock *et al.*, 2009). When hypoxic conditions are detected, HIF-1 α translocates to the nucleus (Maxwell *et al.*, 2001) and promotes the transcription of pro-angiogenic signalling molecules such as VEGF (Semenza *et al.*, 1997; Ferrara, 2001). This action also positively feeds back to up-regulate HIFs, which are able to independently activate the PI3K and PLC γ pathways, further compounding the pro-angiogenic signal (Blancher *et al.*, 2001).

VEGF causes ECs to release matrix metalloproteases (MMPs). MMPs degrade the vascular basement membrane (Ohuchi *et al.*, 1997) allowing the ECs to migrate to the outer layers of the vessel, as well as cause the release of basement membrane-sequestered VEGF that further promotes the angiogenic process (Lee *et al.*, 2005).

In order for the vessel to branch, the now motile ECs begin to segregate themselves phenotypically into either tip or stalk cells (Eilken and Adams, 2010). Tip cells, characterised by their motility and expansive filopodia, lead the branching process, whereas stalk cells, typically characterised by their high proliferation rate, fewer filopodia in comparison to tip cells and excretion of basement membrane proteins, follow the tip cell toward the concentrated end of the VEGF gradient and help to form the vessel lumen (Gerhardt *et al.*, 2003). The identity of the cell as either a tip or stalk cell is versatile and changes throughout the branching process according to the expression of notch (Hellstrom *et al.*, 2007); a single pass transmembrane receptor which is involved in the control of cell differentiation and cell fate. The VEGF/VEGFR-2 signalling pathway is able to stimulate tip cell induction, by increasing

production of the notch receptor ligand: delta like ligand-4 (Dll4) (Gerhardt *et al.*, 2003). Dll4 binds to notch on neighbouring cells and reduces the likelihood of them becoming tip cells by decreasing expression levels of VEGFR2, VEGFR3 and NP1, while increasing the expression level of VEGFR1. Once a new vessel has branched, the vessel lumen is formed (Bentley *et al.*, 2009; Potente *et al.*, 2011).

Currently, it is thought that vessel lumen formation occurs via the 'cord-hollowing' process; a mechanism by which the ECs orientate themselves into an apical/basal polarity, with expression of negatively charged CD34-sialomucins (CD34) on the apical (luminal) membrane (Strilic *et al.*, 2009) (Figure 1.2). The negative charge leads to membrane repulsion and the opening of a gap between the ECs. CD34 then interacts with cytosolic F-actin via moesin. This interaction allows for cytoskeletal retraction, lumen formation and blood flow (Strilic *et al.*, 2009). Perfusion of the vessel increases local oxygen and nutrient concentrations leading to remodelling of the lumen and vessel maturation (Nicoli *et al.*, 2010).

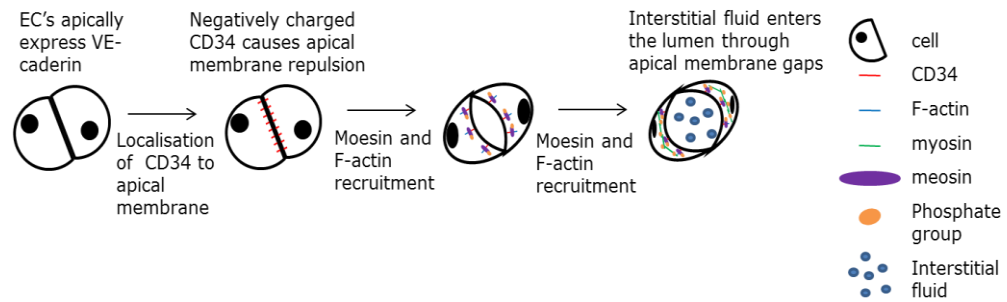


Figure 1.2 Illustration of vessel lumen formation. ECs create VE-cadherin expressing junctions with each other while forming the protruding vascular stalk. This interaction causes EC polarisation where ECs express negatively charged CD34-sialomucins on their apical membrane. CD34-sialomucin recruits F-actin via binding to moesin, this and the negative charge of CD34-sialomucins, lead to apical-membrane retraction and lumen formation. Figure adapted from Strillic *et al.*, 2009.

The stimulation of vessel growth surrounding and within a tumour increases the likelihood of tumour metastasis, as tumour cells are able to disseminate through intravasation (Wyckoff *et al.*, 2000). Once this occurs, the cell is transported via the vasculature to a distant organ/site. The tumour cell is able to extravasate into the surrounding tissue and new tumour formation occurs. As tumour cells must adapt to be able to survive within the circulating blood, these micro-metastases tend to create more malignant tumour types (Chambers *et al.*, 2002).

There are several different mechanisms by which a tumour mass can initiate angiogenesis. Amongst the most well-known is constitutive up-regulation of the production and secretion of pro-angiogenic factors, such as VEGF (Hanahan and Weinberg, 2000; Hanahan and Weinberg, 2011). However, the pathological vessels created by this process are disorganised in structure and placement, as well as leaky and tortuous due to weak intercellular connections (Ehling and Mazzone, 2016). This increases the likelihood of tumour metastasis and

decreases vessel perfusion, thereby reducing the ability of the vessel to deliver oxygen, nutrients and chemotherapeutic agents. These pathological vessels are also less able to remove waste, causing the tumour microenvironment to become toxic. This is thought to promote the selection of more malignant tumour cell phenotypes and to maintain the constitutive up-regulation of pro-angiogenic factors (Potente *et al.*, 2011).

As well as tumour cells being able to cause vessel sprouting and extension, other mechanisms by which tumour cells access the vascular system have been noted. The most prominent of these are the induction of intussusceptive angiogenesis, allowing directed vessel growth through endothelial and mural cell reorganisation (Djonov *et al.*, 2003); co-option, where cancerous cells grow directly around vessels; and vascular mimicry, where tumour cells line the internal and external vessel walls. Finally some 'stem cell-like' cancer cells are able to differentiate into an EC phenotype which incorporates into the vessel wall in a process known as postnatal vasculogenesis (Carmeliet and Jain, 2011). Tumour cells are also able to aid vessel repair by recruiting endothelial progenitor cells, which strengthen and repair the vascular wall, ensuring blood flow to the tumour (Wang *et al.*, 2010).

Through the above mechanisms, neoplastic tumour cells are able to access oxygen and nutrients via the pre-existing vascular system. Therefore, the pharmacological targeting of signalling molecules that allow tumour cells to promote angiogenesis, or maintain vessel structure and permeability is seen as a key treatment strategy in cancer. Amongst the pro-angiogenic factors produced, VEGF is one of the principal mediators of angiogenic progression and maintenance, EC

survival and vessel permeability and has hence become the main target of anti-angiogenic treatments.

1.3.1 Anti-VEGF Treatments in Cancer

Pharmaceutical companies have harnessed a variety of techniques to neutralise the action of VEGFs. Currently there are a range of compounds which inhibit VEGF-A, VEGFR1, VEGFR2 and/or VEGFR3 and have been approved for use in the treatment of cancer, or are currently undergoing clinical trials (Arjaans *et al.*, 2016; Bible and Ryder, 2016).

Of the current therapeutic strategies which target VEGF signalling, the first to be clinically approved was the monoclonal humanised VEGF antibody, bevacizumab (Avastin™). Bevacizumab is approved as a treatment in advanced metastatic cancers such as colorectal and non-squamous, non-small cell lung cancer. It acts by binding free VEGF, reducing its availability to bind to VEGFR2 and therefore its ability to subsequently promote angiogenesis (Bagri *et al.*, 2010). Ranibizumab is another immuno-pharmacological agent (humanised antibody Fab fragment) that binds to VEGF and is FDA approved for use in the treatment of age-related macular degeneration (Lowe *et al.*, 2007).

Another strategy pharmaceutical companies have adopted to target VEGF signalling involves decoy receptors, such as Aflibercept. Aflibercept was approved for use in colorectal cancer in 2012 (Sharma *et al.*, 2013) and works by binding to extracellular VEGF, again reducing circulating VEGF levels and inhibiting receptor downstream signalling. Aflibercept is a soluble humanised immunoglobulin antibody constant region

fused to the extracellular Ig 1-3 domains of VEGFR1 (Gomez-Manzano *et al.*, 2008). This allows Aflibercept to bind to and inhibit the actions of VEGF-A, VEGF-B and PDGF.

A further pharmacological strategy clinically approved for the inhibition of VEGF signalling is the use of RTKIs (Table 1.1). There are three classes of RKTIs. Class I RKTIs are able to bind to the active conformation of the receptor, competitively antagonising ATP binding at various intracellular kinase groups (Gotink and Verheul, 2010). Examples of this group include vandetanib, cediranib and pazopanib (Hennequin *et al.*, 2002; Wedge *et al.*, 2002; Knowles *et al.*, 2006; Gotink and Verheul, 2010; Davis *et al.*, 2011; Blanc *et al.*, 2013). Class II RTKIs, such as sorafenib (Zhang *et al.*, 2009), bind to the non-active conformation of the receptor, at the hydrophobic pocket of the activation loop, and antagonise receptor activation by sterically blocking ATP binding. Finally, class III RTKIs work by covalently binding to sulphur-rich cysteine residues within the intracellular region of the receptor, regardless of receptor conformation. This action blocks ATP binding, reducing the ability of the receptor to enter its active conformational state. One example of a class III RKTi is neratinib (Gotink and Verheul, 2010; Davis *et al.*, 2011).

Unlike immunological compounds, RTKIs are multi-targeted (Table 1.1) (Belcik *et al.*, 2012). The multi-targeted aspect of these compounds makes them a popular therapeutic tool, as the ability for the tumour to act independently of multiple signalling pathways is less likely.

RTKI	Targets	Indications	Adverse effects	Reference
Vandetanib	VEGFR2,3, EGFR, RET	Medullary thyroid cancer Phase III: Non-small cell lung cancer	Hypertension, haemorrhage, QT prolongation, diarrhoea, rash	(Wedge <i>et al.</i> , 2002)
Pazopanib	VEGFR1,2,3, PDGFR, c-kit	Renal cell carcinoma, advanced tissue sarcoma	Hypertension, diarrhoea, fatigue, weight loss	(Bible <i>et al.</i> , 2012)
Sorafenib	VEGFR2,3, PDGFR, Flt-3, c-kit	Advanced renal cell carcinoma, hepatocellular carcinoma	Hypertension, cardiac ischemia, diarrhoea, dermatological effects,	(Eskens and Verweij, 2006; Widakowich <i>et al.</i> , 2007)
Cediranib	VEGFR1,2,3, PDGFR, FGFR1	Phase III: Ovarian cancer Phase III: Cervical cancer	Hypertension, diarrhoea, nausea	(Mulders <i>et al.</i> , 2012; Schmidt, 2015; Minguet <i>et al.</i> , 2015; Ruscito <i>et al.</i> , 2016)

Table 1.1 Summary of four VEGFR RTKIs; their targets, indications and adverse effects.

All treatments which block VEGF have been shown to have VEGF-related side effects. These include rash, proteinuria, cardiomyopathy, haemorrhage, wound complications and hypertension amongst other effects (Eskens and Verweij, 2006; Widakowich *et al.*, 2007; Chen and Cleck, 2009; Hall *et al.*, 2013; Le *et al.*, 2014). These side effects are thought to be related to the inhibition of VEGF, as VEGF-specific compounds such as bevacizumab display these alone, whereas compounds that are multi-targeted to VEGF and other signalling molecules show these toxicities as well as other adverse effects, such as weight loss and nausea (Table 1.1). In order to improve cancer treatment and therefore prognosis and outcome, it is important to investigate why anti-angiogenic treatments display particular side effects and how these can be reduced.

1.3.1.1 Vandetanib

Vandetanib (otherwise known as ZD6474 or Zactima™, produced by AstraZeneca) is a Class I VEGFR2, VEGFR3, epidermal growth factor receptor (EGFR), rearranged during transfection (RET) kinase specific RTKI which is FDA approved for use in the treatment of medullary thyroid cancer. It is also known to inhibit many other kinases (Table 1.2); however, the significance of this on its anti-tumorigenic action and adverse effect profile has not been analysed.

Vandetanib is able to cross the cell membrane and bind to the intracellular portion of the active conformation of the VEGFR2 receptor, inhibiting ATP binding, receptor phosphorylation and consequent downstream signalling (Figure 1.3). Its action on VEGFR2, VEGFR3 and EGFR leads to a reduction in MAPK, PI3K and PLC γ pathway activation, subsequently reducing cell

growth, proliferation and survival (Thornton *et al.*, 2012). Vandetanib has been shown to reduce tumour angiogenesis via inhibition of VEGFR2; and tumour cell survival, growth and morphogenesis due to its inhibition of EGFR (Grandis and Sok, 2004; Thornton *et al.*, 2012). Interestingly, the overexpression of EGFR has been shown in multiple cancer types including breast, lung and prostate (Klijn *et al.*, 1992; Visakorpi *et al.*, 1992; Fujino *et al.*, 1996). Therefore, vandetanib demonstrates dual action through its multi-targeted design; able to inhibit blood supply and metastasis through its inhibition of VEGFRs, while reducing tumour cell growth and survival via EGFR inhibition. The anti-tumour effects of EGFR inhibition have also been observed with EGFR-specific inhibitors, such as erlotinib, a RKTi which is FDA approved for the treatment of non-small cell lung cancer (Smith, 2005). Finally, vandetanib inhibits RET, a tyrosine kinase receptor whose activation via glial cell line derived neurotrophic factor (GDNF) increases neuronal cell survival. It has been shown that the development of medullary thyroid cancer is strongly associated with gain of function mutations in RET (Vidal *et al.*, 2005; Knowles *et al.*, 2006). It is thought that the multi-targeted action of vandetanib reduces the likelihood of tumour cells to develop 'by-pass' mechanisms through progressive mutations, therefore reducing the ability of the tumour to become resistant to treatment.

Vandetanib binds to VEGFR2 with a half maximal inhibitory concentration (IC₅₀) of 0.38 µM, to VEGFR3 with an IC₅₀ of 0.26 µM and to EGFR with an IC₅₀ of 0.043 µM (IC₅₀ gained from purified Glutathione S-transferase (GST) or histidine (His) tagged proteins assays; (Davis *et al.*, 2011)) (Table 1.2). However, its potency at tyrosine kinases can vary, with

inhibition of RET being reduced in cases where particular point mutations in the kinase insert domain are present, e.g. valine 804 (Carlomagno *et al.*, 2004).

Kinase	Vandetanib ($\mu\text{M IC}_{50}$)	Pazopanib ($\mu\text{M IC}_{50}$)
VEGFR1	0.15 (His tagged)	0.01
VEGFR2	0.38 (His tagged)	0.03
VEGFR3	0.26 (His tagged)	0.047
AKT3	>100	>20
EGFR	0.043	>20
EPHB4	0.32	>20
FAK	>100	0.8
FGFR1	0.58	0.14
FGFR3	0.75	0.13
FGFR4	5.8	0.8
IGFR1	>100	8
GSK3 β	>100	3.4
ITK	26	0.43
JNK3	>100	4.06
LCK	0.37	0.41
PDGFR α	1.1	0.071
PDGFR β	5.3	0.084
PKC β 1	>100	>20
PKC β 2	>100	>20
SRC	0.42 (His tagged)	3.1
TIE2	0.52 (His tagged)	4.5
Side effects	Vandetanib	pazopanib
Percentage of patient populations with hypertension	32-33%	33%-40%

Table 1.2 Summary of the IC_{50} (μM) values of vandetanib and pazopanib against various kinases, and the percentage of their patient population who develop hypertension, respectively (Hamberg et al., 2010; Wells et al., 2012; Bible et al., 2014). IC_{50} s for vandetanib were gained from a cell based assay where all kinases were expressed as human recombinant GST-fusion proteins or as His tagged proteins (labelled in table) (Leigh Verbois, 2011). Pazopanib IC_{50} s were gained using recombinantly expressed catalytic domains of the kinases stated above (Kumar et al., 2007).

Following oral administration in humans (300 mg day^{-1}), vandetanib reaches its peak plasma volume concentration between 4-7.5 h depending on the dose given (50-600 mg)

with a plasma half-life of approximately 19 days. Vandetanib metabolism occurs primarily via cytochrome-P4503A4 (Ton *et al.*, 2013), leading to the potential for drug-drug interaction with concomitantly prescribed compounds such as methadone and cisapride. The major metabolite of vandetanib, N-desmethyl-vandetanib, which circulates at 11% of vandetanib's total plasma concentration in humans, is produced via cytochrome-P4503A4 oxidation (Leigh Verbois, 2011; Kandel and Lampe, 2014). It also has a large volume of distribution (2680 l) and a low clearance from the body (8.47 l h^{-1}) (Holden *et al.*, 2005), signifying its presence in the body long after dosing. Vandetanib was approved for the treatment of medullary thyroid cancer in April 2011 (Chau and Haddad, 2013).

In humans, vandetanib has been shown to cause various documented side effects including nausea, rash, ECG prolongation, vomiting, anorexia, diarrhoea and hypertension. Hypertension is a common side effect among the patient population with 33% of those taking vandetanib developing graded hypertension and 9% of those developing grade 3+ hypertension (Wells *et al.*, 2012).

1.3.1.2 Pazopanib

Pazopanib, like vandetanib, is a multi-targeted RTKI approved for the treatment of advanced stage renal cell carcinoma and soft tissue sarcoma (Cella *et al.*, 2016) Developed by Glaxo Smith Kline and commercially known as Votrient, pazopanib is a synthetic class I RTKI small molecule inhibitor of VEGFR1, VEGFR2, VEGFR3, PDGFR α , PDGFR β and c-kit (Figure 1.3). By inhibiting all 3 forms of VEGFR, pazopanib is able to reduce

cell growth, cell proliferation, angiogenesis and vascular permeability (Verbois *et al.*, 2008; Thornton *et al.*, 2012).

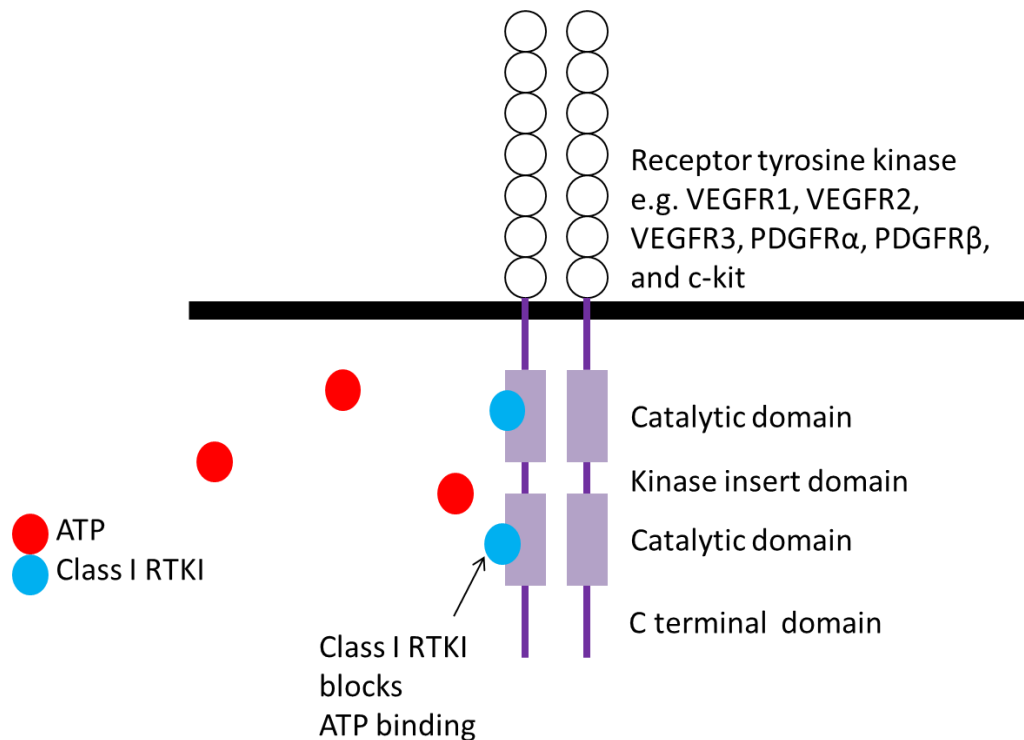


Figure 1.3 Diagrammatical representation of class I RTKI mechanism of action. Class I RTKIs competitively bind to the ATP binding site on the intracellular part of its target receptor antagonising receptor activation and signalling. Adapted from Gotink and Verheul, 2010

Pazopanib's inhibition of PDGFR α and PDGFR β has been shown to reduce tumour angiogenesis and metastasis through reducing PDGFR α and PDGFR β associated MAPK, PI3K and PLC γ pathway activation. In particular the reduction of PDGF signalling has been shown to reduce pericyte recruitment during angiogenesis, therefore reducing vessel stability (Heldin, 2013).

c-kit, also known as the stem cell factor receptor, has been shown to play a role in cell survival and proliferation. Its constituent activation has been noted in multiple malignancies such as gastrointestinal stroma and melanoma. The inhibition of c-kit is thought to reduce cell survival and proliferation,

therefore, reducing tumour size (Verbois *et al.*, 2008; Stankov *et al.*, 2013). It was shown that tumours implanted into CB-17 SCID mice reduced in size by 90%, 77%, and 99% at doses of 10, 30, and 100 mgkg⁻¹, respectively (Verbois *et al.*, 2008). Pazopanib has varying affinity for the VEGFR receptors (IC₅₀ values of 10, 30 and 47 nM, for the human VEGFR1, VEGFR2 and VEGFR3 receptors respectively) and has similar potencies at PDGFR- α (IC₅₀=71 nM), PDGFR- β (IC₅₀=84 nM) and c-Kit (IC₅₀ =74 nM) (Kumar *et al.*, 2007; Verbois *et al.*, 2008; Bible *et al.*, 2012).

Following oral administration in humans, pazopanib (800 mgday⁻¹) reaches its peak plasma volume concentration between 2.0 to 4.0 h with a mean plasma half-life of 30.9 h. Pazopanib is primarily metabolised by CYP3A4, and has been shown to be metabolised by breast cancer resistant protein and multi drug resistance protein 1 *in vitro*, indicating the possibility for tumour resistance to develop against pazopanib (Justice and Robertson, 2008; Weiss *et al.*, 2014; Cella and Beaumont, 2016).

Pazopanib has been shown to have multiple side effects in humans, with the most common being hair discolouration; thought to be linked to its action on c-kit, hepatic toxicity, hyperkalaemia, anorexia, vomiting, rash and hypertension. Hypertension occurs in 40% of the patient population, with 3% of those developing grade 3+ hypertension (Hamberg *et al.*, 2010). In a phase I study completed by GSK, where a custom measure of hypertension was used (patient populations who demonstrated >15 mmHg rise in mean arterial blood pressure on three separate occasions or whose anti-hypertensive medication had to be adjusted due to an increase in the severity of their hypertension (given when blood pressure

reached 160/100 mmHg on three separate occasions over 2 weeks)), found that 63% of the patient population taking pazopanib developed hypertension, with 23% of those having grade 3+ hypertension. In this study, the majority of the patient population developed hypertension within the first 4 weeks of treatment (Hamberg *et al.*, 2010), prompting the FDA to insist on blood pressure monitoring during treatment. These side effects may also arise from pazopanib's inhibition of various other kinases. It has been shown, that like vandetanib, pazopanib also inhibits a subset of cardio-active kinases such as TIE2 and EGFR (Kumar *et al.*, 2007)(Table 1.2).

1.3.1.3 Cediranib and Sorafenib

Sorafenib (produced by Bayer) and otherwise known as Nexavar or BAY 43-9006, is a class II RTKI that inhibits VEGFR2, VEGFR3, PDGFR, C-Raf, B-Raf, Flt-3 and c-kit among other tyrosine kinases (Davis *et al.*, 2011; Hasskarl, 2014). It has been FDA approved for the treatment of advanced renal cell carcinoma and hepatocellular carcinoma (Eskens and Verweij, 2006; Widakowich *et al.*, 2007). Sorafenib has been shown to reduce tumour angiogenesis and tumour size. This action is thought to be due to its inhibition of VEGFR2 and PDGFR (Heldin, 2013; Mahalingam *et al.*, 2014). In clinical trials where sorafenib was given orally at 400 mg twice daily it was shown to have a half-life of approximately 36 h with a peak plasma concentration after 3 h (Hasskarl, 2014). The side effect profile of sorafenib includes multiple cardiotoxic effects such as hypertension, haemorrhage, QT prolongation and cardiac ischemia as well as off target side effects such as diarrhoea and rash (Hasskarl, 2014).

Cediranib (produced by AstraZeneca and planned to be marketed under the name Recentin), is currently undergoing Phase III trials for ovarian cancer (Robinson *et al.*, 2010; Mulders *et al.*, 2012; Schmidt, 2015; Ruscito *et al.*, 2016). It has been shown to act as a class I inhibitor (Figure 1.3) of VEGFR1, VEGFR2, VEGFR3, PDGFR and FGFR1 (Wedge *et al.*, 2005; Mulders *et al.*, 2012; Minguet *et al.*, 2015; Ruscito *et al.*, 2016). Cediranib has been shown to lead to a reduction in tumour angiogenesis and tumour growth (Mulders *et al.*, 2012). In humans dosed orally, cediranib displays a half-life of 22 h and maximal plasma concentration at 3 h (Ruscito *et al.*, 2016). However it also produces hypertension, nausea, fatigue and diarrhoea in the patient populations taking it (Ruscito *et al.*, 2016).

1.3.2 Cardiovascular Consequences of RTKIs

VEGF is a key mediator of pathophysiological as well as physiological angiogenesis (Liang *et al.*, 2014; Shibuya, 2014). Therefore the inhibition of VEGF-VEGFR signalling not only reduces pathophysiological vessel growth but also leads to multiple cardiovascular-related adverse events (Hong *et al.*, 2015). VEGF inhibitors have been shown to increase a patient population's likelihood of developing venous or arterial thrombo-embolisms (Eschenhagen *et al.*, 2011), proteinuria, delayed wound healing (Veronese *et al.*, 2006), reversible posterior leukoencephalopathy syndrome (Govindarajan *et al.*, 2006), neutropenia, thrombocytopenia, haemorrhage (Hapani *et al.*, 2010) and hypertension (Hong *et al.*, 2015; Abi Aad *et al.*, 2015; Souza *et al.*, 2015).

The above side effects are serious for the patient's quality of life and chances of survival. They also have an impact on the

possible treatment regimens prescribed. For example, a patient taking a VEGF RTKI is unable to undergo surgery as the risks of haemorrhage and delayed wound healing are too great. In patient populations with metastatic colorectal cancer, who had discontinued the anti-VEGF therapy bevacizumab for 60 days prior to surgery, 13% of patient populations experience grade 3 or 4 surgical complications, including haemorrhage, bowel perforation and delayed or abnormal wound healing (Scappaticci *et al.*, 2005). This study demonstrates the need to think carefully about the side effect profile of compounds when embarking on surgical intervention or when changing treatment regimens.

The occurrence of hypertension in anti-VEGF treatments has been commented on as a possible biomarker for drug efficacy, as patients who respond positively to anti-VEGF treatment also develop hypertension (Scartozzi *et al.*, 2009; Kieran *et al.*, 2012; Hong *et al.*, 2015). The percentage of patients who develop hypertension has been suggested to positively correlate with the specificity of an RTKI to VEGFRs (Sleijfer *et al.*, 2009; Mourad and Levy, 2011).

It has been shown that approximately 23 to 90% of the anti-VEGF treatment population develop hypertension during treatment (Bible *et al.*, 2014; Hong *et al.*, 2014; Abi Aad *et al.*, 2015; Granito *et al.*, 2016). In light of this, many researchers have postulated reasons as to why reduced VEGF levels are linked to the development of hypertension. However, these hypotheses should be looked upon cautiously (discussed further in Section 1.5). Methodological flaws in blood pressure measurement, for example long time lags between blood pressure measurements (blood pressure is usually measured once every 15 or 21 days, clinically), may

lead to an underestimation of the number of patient populations who develop elevated blood pressure (Mir *et al.*, 2009). A study in which patient populations receiving sunitinib had their blood pressure measured weekly, found that 100% of the treatment cohort developed hypertension (Azizi *et al.*, 2008). An increase in the cohort of pazopanib patients who developed hypertension was also seen in phase I trials when GSK changed their definition of hypertension (study described previously) (Hamberg *et al.*, 2010). This result was mirrored in a phase II trial involving the treatment of soft tissue sarcomas with pazopanib, where almost all of the patient population treated with pazopanib developed some degree of hypertension (Sleijfer *et al.*, 2009).

Therefore, the connection between the level of hypertension development within anti-VEGF treatment groups and the anti-VEGF drug efficacy needs to be further explored.

1.4 The Pathophysiology of Hypertension

In order to understand how anti-VEGF/VEGFR treatments may cause hypertension, it is important to understand how hypertension can occur in the absence of pharmacological intervention.

Hypertension refers to an arterial blood pressure above 140 mmHg/90 mmHg (classed as grade I mild hypertension (McCormack *et al.*, 2012)). The maintenance of a steady blood pressure is important for the function and health of the cardiovascular system as well as the body as a whole. The incidence of hypertension increases the risk of developing renal disease, stroke, heart failure and cardiac infarction (Cutler, 1996).

Blood pressure is controlled by the heart and blood vessels. The heart acts to pump blood around the body, providing a pressure gradient to ensure blood flow, while the vessels allow for transportation of blood and act to maintain or change pressure through providing resistance (Katz, 2002).

Since vessel length doesn't change in the adult and under normal conditions blood viscosity remains relatively constant, resistance is largely determined by the radius of blood vessels and is mainly dependent on vessel tone. Vessel tone is controlled on 3 major levels: (1) the nervous system, (Chapleau *et al.*, 1991; Estanol *et al.*, 2011) (2) the endocrine system (Ponchon and Elghozi, 1996) and (3) local autocrine and paracrine signalling (Furchgott and Zawadzki, 1980).

1.4.1 Nervous Control of Vessel Tone

Immediate/ short term changes in blood pressure are detected by baroreceptors located in the aortic arch and the carotid sinuses (Chapleau *et al.*, 1991; Estanol *et al.*, 2011). An increase in blood pressure leads to vessel wall stretching and an increase in baroreceptor signalling (Estanol *et al.*, 2011). This primarily leads to the release of noradrenaline from sympathetic nerves innervating the vessel adventitia. Noradrenaline binds to and activates α and β adrenoceptors that can produce a change in vessel diameter (Joyner and Casey, 2014). The effect of noradrenaline on vascular tone depends on the type and subtype of adrenoceptor expressed (Joyner and Casey, 2014). Activation of α_1 -adrenoceptors leads to contraction of the vessel wall, whereas activation of β_2 -adrenoceptors leads to relaxation of the vessel wall and a reduction in heart rate. This allows the body, in a fight or flight situation, to reduce blood flow to organs such as the gut,

which are not necessary in crisis, and increase blood flow to necessary organs, for example the skeletal muscles and heart through vascular bed specific variation of the adrenoceptor subtype (Hauzer *et al.*, 2014). Compounds that inhibit α_1 -adrenoceptors, such as Doxazosin, and compounds that inhibit β_2 -adrenoceptors, such as propranolol, are used to treat hypertension (Levy, 1989).

1.4.2 The Renin- Angiotensin-Aldosterone System and its Effect on Vessel Tone

Endocrinological control of vascular tone is dominated by the renin-angiotensin-aldosterone system (Ponchon and Elghozi, 1996). The renin-angiotensin-aldosterone system is activated by the detection of low blood volume by baroreceptors in the kidney. This causes the release of renin from the juxta-glomerular cells of the kidney and in turn aldosterone release from the adrenal gland (Persson *et al.*, 2004). When renin enters the circulation it cleaves the plasma protein angiotensinogen into angiotensin I. Angiotensin I is further cleaved into angiotensin II by angiotensin converting enzyme, located in the lungs and vascular endothelium. Angiotensin II is a very potent vasoconstrictor. This action is achieved through its interaction with angiotensin II receptor I receptors on smooth muscle cells and sympathetic nerve endings. Angiotensin II and aldosterone have both been shown to have an anti-natriuretic effect, increasing blood volume (Lamas and Rodriguez-Puyol, 2012). Compounds such as losartan, a selective, competitive angiotensin II receptor 1 type 1 antagonist (Mavromoustakos *et al.*, 2001) and Ramipril, a angiotensin converting enzyme inhibitor (Yasky *et al.*, 1996), can be used to inhibit the vasoconstrictive actions of the renin-angiotensin-aldosterone system, therefore reducing

blood pressure. Thiazide diuretics, such as chlorthalidone, and aldosterone antagonists, such as spironolactone, can also be used to treat sodium dependent hypertension as they inhibit the reabsorption of sodium and chloride from the distal convoluted tubules of the kidney, reducing blood volume (Blowey, 2016).

1.4.3 Vascular Control of Vessel Tone

Furchgott and Zawadzki (Furchgott and Zawadzki, 1980) showed that the removal of ECs from the vessel lumen removed the ability of the vessel to dilate in response to acetylcholine (ACh), demonstrating the importance of endothelial signalling in the control of vessel tone. As well as responding to endocrine and neural signalling molecules mentioned previously, ECs are able to release their own vasoactive compounds such as nitric oxide (NO) (Moncada and Higgs, 2006), VEGF (see Section 1.1.1) and prostacyclin (PGI₂) in response to various signals such as shear stress, ACh and bradykinin (Cahill and Redmond, 2016).

Prostacyclin production is a calcium dependent process involving the oxidation and peroxidation of arachidonic acid via the PLA₂- COX signalling pathway (Nakayama, 2006). Once released by the EC it is able to signal via IP receptors to reduce platelet activation, cause vasodilatation and reduce smooth muscle cell remodelling (Stitham *et al.*, 2007) via the IP₃ and PKC γ signalling pathways (Mitchell *et al.*, 2008). Its vasodilatory actions have been harnessed in the treatment of pulmonary hypertension with the use of synthetic analogues like iloprost (Fallah, 2015).

NO, made from the enzymatic conversion of arginine by endothelial nitric oxide synthase (eNOS) diffuses into the smooth muscle cell cytosol where it induces a vasodilatory effect (Gelinias *et al.*, 2002). This occurs through its interaction with soluble guanylate cyclase (sGC), which in turn produces cyclic guanosine monophosphate (cGMP). cGMP has been linked with the opening of Kir K⁺ channels leading to membrane hyperpolarisation and vascular smooth muscle cell relaxation (Levick *et al.*, 2010). It has also been associated with the activation of protein kinase G (PKG), which phosphorylates myosin light chain phosphatase. PKG activation leads to the reduction of intracellular calcium concentrations through phosphorylation of the sarco-endoplasmic reticulum calcium channel (SERCA) and the plasma membrane calcium channel (PMCA). Overall these actions lead to smooth muscle cell relaxation and vasodilatation (Horowitz *et al.*, 1997; Hood *et al.*, 1998). NO has also been shown to be important for the kidney's tubule-glomerular feedback. When NO levels are reduced, the kidney retains excess sodium and therefore fluid, leading to hypertension through increased blood volume (Zou and Cowley, 1999). Nitric oxide can be given to relieve angina and causes a reduction in blood pressure (Abrams, 1996).

Finally, calcium channel blockers, like amlodipine, are also used in the treatment of hypertension (Mason *et al.*, 2003). They act by inhibiting calcium influx into smooth muscle cells, therefore reducing the ability of the smooth muscle cell to constrict, leading to vasodilatation (Mason *et al.*, 2003).

1.5 Current Theories on RTKI-Mediated Hypertension

The reason why anti-VEGF therapies cause hypertension is unknown. Currently it is thought that it may be due to a reduction in NO/PGI₂ and/or a reduction in vessel number or number of functioning vessels (vascular rarefaction (Hayman *et al.*, 2012)). It is presently believed that a reduction in VEGF leads to the down regulation of eNOS. Under normal physiological conditions, VEGF is able to stimulate eNOS to produce NO via the PI3K, MAPK and PLC γ pathways (Gelinias *et al.*, 2002) (Figure 1.1). When VEGF action is blocked, eNOS is down-regulated and the vessel constitutively constricts leading to hypertension. Within the microcirculation this leads to rarefaction, reducing the density of the microvascular network and therefore increasing blood pressure (Feihl *et al.*, 2006). Rarefaction can be classed as either functional, where there is a high density of unperfused micro vessels, or as structural, where there is a reduction in the density of the microvasculature. Both forms of rarefaction lead to an increase in blood pressure (Feihl *et al.*, 2006). It has been shown that anti-VEGF therapies, such as bevacizumab, cause rarefaction and that this positively correlates to the severity of the hypertension developed (Mourad *et al.*, 2008). However, whether rarefaction leads to hypertension or hypertension leads to rarefaction remains unclear.

VEGF RTKI-mediated hypertension has been shown to be resistant to pharmacological intervention with angiotensin converting enzyme inhibitors, calcium channel blockers, beta blockers and thiazide diuretics (Rini *et al.*, 2011; Kruzliak *et al.*, 2013). The lack of treatment available for VEGF RTKI-mediated hypertension further increases the need to understand its aetiology.

1.6 Aims and Hypothesis

Through characterising the cardiovascular action of RTKIs *in vivo* and their pharmacology at VEGFR2 *in vitro*, the detrimental cardiovascular effects of these compounds and the possible mechanisms of action by which VEGF is important for vascular tone will be explored. With this in mind, the aims of the present investigations were:

- a) To determine the pharmacological characteristics of a panel of receptor tyrosine kinase inhibitors (RTKIs) (cediranib, sorafenib, pazopanib and vandetanib) in a whole cell system using VEGF-stimulated nuclear factor of activated T-cell (NFAT) signalling in HEK-293 cells expressing the human VEGFR2 and an NFAT reporter gene linked to firefly luciferase. The actions of the above RTKIs were also explored in the presence of two VEGF-A isoforms, VEGF_{165a} and VEGF_{165b}.

Null hypotheses:

1. There will be no difference in IC₅₀ between cediranib, sorafenib, pazopanib and vandetanib in the presence VEGF_{165a} or VEGF_{165b}.
 2. There will be no difference in agonist action (eg, EC₅₀ or E_{MAX} values) between VEGF_{165a} and VEGF_{165b}.
- b) To assess the effect of various concentrations of vandetanib and pazopanib on heart rate, mean arterial blood pressure, hindquarter, renal and mesenteric vascular conductances in male Sprague Dawley rats.

Null hypotheses:

1. There will be no vandetanib or pazopanib mediated effect on heart rate, mean arterial blood pressure,

hindquarter, renal and mesenteric vascular conductances in male Sprague Dawley rats.

2. There will be no vandetanib mediated effect on vessel structure or number.
 3. There will be no difference in heart rate, mean arterial blood pressure, hindquarter, renal and mesenteric vascular conductances in male Sprague Dawley rats given vandetanib or pazopanib.
- c) To investigate the chronic effects of vandetanib and pazopanib on heart rate and blood pressure in male Sprague Dawley rats.

Null hypothesis:

1. There will be no chronic effects of vandetanib and pazopanib on heart rate and blood pressure in male Sprague Dawley rats.
- d) To assess the action of vandetanib and pazopanib on isolated pressurised mesenteric arterioles, and to elucidate the effect of vandetanib on VEGF and ACh-mediated vessel dilatation.

Null hypotheses:

1. There will be no vandetanib or pazopanib mediated effects on isolated pressurised mesenteric arterioles.
2. Vandetanib or pazopanib will not effect VEGF or ACh-mediated vessel dilatation.

Chapter 2: General Methods

2.1 NFAT-Luciferase Gene Reporter Assay

In order to look at the downstream signalling of VEGFR2 in a whole cell system, the NFAT reporter gene was used. NFAT leads to the transcription of target genes which contribute to cell growth and proliferation (Bretz *et al.*, 2013). The activation, dimerisation and transphosphorylation of VEGFR2 leads to the downstream activation of calcineurin and in turn the dephosphorylation and translocation of NFAT into the nucleus (Figure 2.1) (Armesilla *et al.*, 1999). NFAT, once in the nucleus, forms a transcription complex with Fos and Jun (Hogan *et al.*, 2003) allowing it to bind to DNA and transcribe various gene products, in the VEGFR2 NFAT cells used here (Section 2.1.1), this includes the reporter gene product: firefly luciferase (Figure 2.1). By measuring the amount of luminescence emitted from the mono-oxygenation of 5'fluoroluciferin by firefly luciferase (*photinus pyralis*), the extent of VEGFR2 activation and signalling via the calcium-calcineurin pathway in VEGFR2 NFAT cells can be quantified.

Luciferase is an enzyme capable of catalysing the mono-oxygenation of 5'fluoroluciferin, causing it to produce yellow/green light (550-570 nm) (Figure 2.1). The ONE-Glo™ Luciferase Assay System (Promega ONE-Glo™ Luciferase Assay System Literature # TM292) can be used to measure NFAT linked firefly luciferase reporter gene expression in mammalian cells.

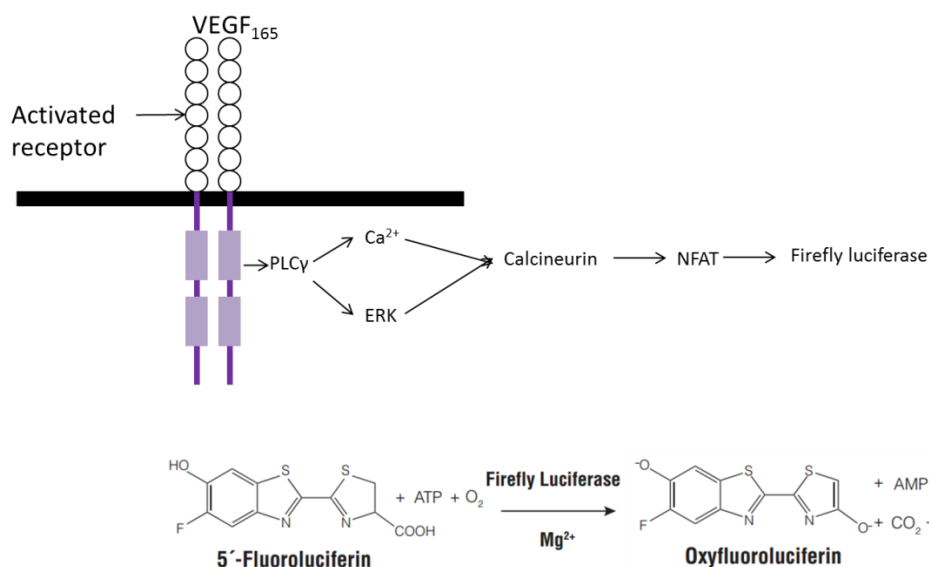


Figure 2.1. Schematic Representation of the NFAT Luciferase Assay. The activation of VEGFR2 by VEGF causes the receptor to dimerise and phosphorylate specific intracellular tyrosine kinases. This in turn leads to the activation of calcineurin, which dephosphorylates NFAT, leading to the transcription of firefly luciferase through the PLCγ pathway. The addition of 5'fluoroluciferin allows for the linear measurement of firefly luciferase production and in turn NFAT activation through the measurement of oxyfluoroluciferin using a microplate luminescence counter (Perkin Elmer Topcount). Chemical reaction taken from Promega ONE-Glo™ Luciferase Assay System Literature # TM292.

2.1.1 Cell Culture

HEK 293 cells, from the human embryonic kidney, are commonly used as an *in vitro* model due to their amenable transfection rate and reliable growth rate in the cell culture environment. This allows them to be used in experiments where the activity of an induced component is of interest (Thomas and Smart, 2005). As HEK 293 cells do not natively express VEGFR1, VEGFR2 or VEGFR3, unlike more physiologically relevant endothelial cell models, they provide the opportunity to study the effects of multi-targeted RKTIs on VEGFR2-NFAT signalling without interference from native receptor-NFAT signalling that may also be activated by VEGF_{165a} or VEGF_{165b}; the chosen agonists in these experiment.

HEK 293 cells were first isolated in 1977 by Graham *et al.*, who transformed them into an immortal cell line by transfecting chromosome 19 with human adenovirus type 5 (Ad5) DNA (Graham *et al.*, 1977). The HEK 293 cells used here have been further modified with an NFAT-RE-luc2P vector, which leads to the transcription of firefly luciferase when the NFAT response element (NFAT-RE) is activated. They have also been transfected with a KDR-5K vector which causes the HEK 293 cell to transcribe and translate human VEGFR2.

All sterile procedures were performed in the Cell Signalling Research Group Cell Culture Facility. Dulbecco's Modified Eagle's Media (DMEM) and Dulbecco's phosphate buffered saline (PBS) were purchased from Sigma, while heat-treated foetal calf serum (FCS) came from PAA labs. Adherent human embryonic kidney 293 cells (HEK 293) stably transfected with an NFAT-RE-luc2P vector (Promega pGL4.30, E8481) and KDR-5K vector were provided by Promega Corporation (Madison, USA) and are referred to as VEGFR2 NFAT cells hereafter.

Cells were maintained in DMEM supplemented with 10% FCS and 0.5% G418 (Life Technologies) (subsequently referred to as growth media) in humidified conditions at 37°C/ 5% CO₂ + 95% air. All sterile cell culture techniques were performed in a class 2 laminar flow cell culture hood with pre-warmed liquids so as not to cause excessive shock to the cells.

2.1.2 Cell Passage

Cells were generally maintained in T75 flasks containing 20 ml growth media and grown to between 80-90% confluency before passaging. In order to passage the cells, media was

removed and they were washed with 5 ml PBS. One ml trypsin-Ethylenediaminetetraacetic acid (EDTA)(0.5% and 0.2%, respectively) was added to the cells in order to hydrolyse membrane bound adhesion proteins (via trypsin), and to chelate Ca^{2+} ions, reducing cell clumping by reducing cadherin binding (via EDTA), allowing the cells to enter suspension. Once cells began to detach from the flask, 9 ml of growth media was added. The cell suspension was transferred into a 25 ml universal tube and centrifuged at 1000 rpm for 5 min and the supernatant was discarded. This was done to remove any cell debris and trypsin-EDTA solution. The pellet was suspended in 10 ml of media. This was divided into new flasks containing 20 ml growth media. Cells were routinely passaged at ratios of 1:5 and 1:10 in order to keep the passage number below 15 post-purchase.

2.1.3 Long Term Storage

For long-term storage, cells were suspended (Section 2.1.2) in sterile (filtered with a 0.2 μm syringe filter) FCS with 10% (v/v) DMSO in order to reduce ice crystal formation during freezing. 500 μl of cell suspension was aliquoted into cryogenic tubes, which were placed into an isopropanol-filled container. This allowed for controlled cell freezing at a rate of 1°C per min in a -80°C freezer. After 24 h the aliquots were transferred to liquid nitrogen storage until use.

Cells were thawed rapidly before use, through the addition of 500 μl warmed growth media. Once thawed, the cells were immediately transferred to a T75 flask containing 20 ml pre-warmed growth media. After 24 h the media in the flask was replaced with fresh media in order to remove DMSO and cell debris. This increased the likelihood of cells growing

healthily. Finally, cells were passaged a minimum of once before experimental use.

2.2 NFAT-Luciferase Assay

VEGFR-NFAT cells, used in this assay, artificially expressed firefly luciferase downstream of the NFAT promoter.

Physiologically, NFAT leads to the transcription of target genes which contribute to cell growth and proliferation (Hogan *et al.*, 2003, Armesilla *et al.*, 1999). However, in the VEGFR2 NFAT cells, NFAT activation also leads to the transcription of firefly luciferase. At the end of the experimental procedure, addition of the ONE-Glo assay reagent, lyses the cell membrane. The ONE-Glo assay reagent also contains the firefly luciferase substrate, 5-fluoroluciferin. Firefly luciferase catalyses the mono-oxygenation of 5-fluoroluciferin to oxyfluoroluciferin (Figure 2.1). This reaction produces energy in the form of luminescence that can be measured via a luminescence counter, allowing the extent of VEGFR2-mediated activation of NFAT signalling to be quantified.

Reporter gene systems have previously been used as an alternative to biochemical assays, and allow for compound efficacy at specific receptors to be measured. Unlike other assays, reporter gene assays do not involve radiation, have been shown to be highly sensitive and are relatively cheap due to their ability to be used in 96 well and 384 well plate systems, reducing the requirement for expensive reagents (Hill *et al.*, 2001). The NFAT-luciferase reporter gene assay is also very sensitive because the signal measured is at the terminal portion of the signalling pathway, allowing for maximal amplification (Hill *et al.*, 2001).

2.2.1 Experimental Method Protocol 1: The 'non-confluent monolayer' Method

Reagents received in the Promega ONE-Glo™ kit were prepared according to the manufacturer's instructions, aliquoted and stored at -20°C. Reagents were used within one freeze thaw cycle to reduce any freeze-thaw initiated breakdown of reagent components. Cells were suspended in 10 ml media and counted using a haemocytometer. Cells were then suspended in DMEM and seeded at a density of 30000 cells per well in white 96 well plates with clear flat bases (Greiner Bio-one, Stonehouse, UK). Prior to cell seeding, wells were coated with 5 mgml⁻¹ poly-D-lysine (Sigma) for a minimum of 30 min to enhance cell adherence. The plates were then washed with media, to remove any residual unbound poly-D-lysine before the cells were added.

After 24 h, media was replaced with FCS free media. This was done to reduce FCS interference within the measured pathway. FCS, and growth factors contained within FCS, have been shown to activate multiple signalling pathways within the cell (Even *et al.*, 2006). 'Serum-starving' helps to reduce this effect and produce a more specific readout (Hill *et al.*, 2001). After 24 h the FCS free media was removed and replaced with DMEM containing 0.1% bovine albumin serum (BSA). VEGF was incubated with the cells at 37°C/ 5% CO₂ for 5 h. After the 5 h incubation, the experimental media was removed from the wells and 50 µl of DMEM and 50 µl ONE-Glo™ Luciferase Assay reagent was added to the wells. A white plastic cover was placed over the bottom of the plate to ensure no signal was lost, and luminescence was measured using a microplate scintillation and luminescence counter (TopCount NXT Packard) set to read at 19.1 °C (the one-Glo™ Luciferase

Assay reagent is temperature sensitive and is more stable at lower temperatures (Promega ONE-Glo™ Luciferase Assay System Literature TM292)) with a 5 min delay, to allow for the biochemical reaction to take place and for background luminescence absorbed by the plate from indoor fluorescent lighting to fade, before reading relative luminescence units. An average of the counts per second, taken over 3 seconds, was used in all experimental analyses. Each individual experiment was performed in triplicate or quadruplicate and repeated a minimum of 4 times.

2.2.2 Experimental Method Protocol 2: The 'suspension' Method

Cells were seeded in a T75 at 5×10^6 using DMEM + 10% FCS and incubated at 37°C/ 5% CO₂ for 3 days (until the media turned yellow and the flask was 100% confluent). As DMEM contains a phenol red pH indicator, colour change from red to yellow indicates a more acidic pH, inferring high cell confluence. On the 4th day, cells were washed with 5 ml PBS and detached using 3 ml Versene (0.02% EDTA in PBS: as versene contains only a chelating agent, it is used as a gentle method of lifting cells from a surface into suspension (Chen *et al.*, 2015)). Once cells had detached, 6 ml of DMEM + 0.1% BSA was added. Cells were centrifuged at 1000 rpm for 5 min, counted using a haemocytometer and suspended in DMEM + 0.1% BSA. They were subsequently seeded at a density of 40000 cells per well in white sided, clear flat-bottomed, 96 well plates which had been coated with poly-D-lysine. Cells were incubated for 1 h at 37°C/ 5% CO₂ to allow them to settle within the wells. Cells were then incubated with set concentrations of RTKI (10x final concentration) at 37°C/ 5% CO₂ for 1 h prior to the addition of

VEGF. VEGF was incubated with the cells at 37°C/ 5% CO₂ for 5 h. After the 5 h incubation, the experimental media was removed from the wells and 50 µl of DMEM and 50 µl ONE-Glo™ Luciferase Assay reagent was added to the wells. A white plastic cover was placed over the bottom of the plate and luminescence was measured using a microplate scintillation and luminescence counter (TopCount NXT Packard). Each individual experiment was performed with triplicate or quadruplicate replicates and the experiment was repeated a minimum of 4 times.

2.2.3 Data Analysis

All data were fitted using non-linear regression in GraphPad Prism 6 (San Diego, CA). VEGF₁₆₅ and VEGF_{165b} concentration response curves were fitted to the following equation:

$$Response = \frac{E_{max} \times [A]}{[A] + EC_{50}}$$

Where [A] is the concentration of VEGF and EC₅₀ is the molar concentration of agonist required to generate 50% of the maximal response. E_{max} was defined as the maximal response of an agonist. In experiments where a VEGF concentration-response curve in the presence of RTKI was generated, data were also fitted to the above equation, where either the EC₅₀ or E_{max} were shared between curves.

Inhibition curves obtained with RTKIs in the presence of a fixed concentration of VEGF₁₆₅ or VEGF_{165b} were fitted to the following equation:

$$\% \text{ Response to VEGF} = \frac{100 \times IC_{50}}{[I] + IC_{50}}$$

Where IC_{50} is the molar concentration of RTKI required to inhibit 50% of the response to VEGF and $[I]$ is the concentration of RTKI.

All data have been presented as mean \pm SEM. Statistical significance was determined by Student's unpaired t-test or by a one or two-way ANOVA with Dunnett's post-hoc analysis, where appropriate. $P < 0.05$ was considered statistically significant.

2.3 Telemetry

The use of radio-telemetry was first published in the early 1990's by Brockway *et al* (Brockway *et al.*, 1991), who demonstrated that it was possible to accurately measure mean arterial blood pressure (± 5 mmHg) and heart rate chronically (>1 month) while not interfering with the conscious, unrestrained experimental rat, thereby reducing external stressor effects (Brockway *et al.*, 1991; Guiol *et al.*, 1992; Kramer *et al.*, 1993). This is particularly relevant to studies directed at the cardiovascular system, where small interferences with an animal can have a detrimental effect on the experimental readouts (Lamprecht *et al.*, 1973; Gartner *et al.*, 1980; Kramer and Kinter, 2003). More recent advances in radio-telemetric methodologies have further increased the accuracy of blood pressure measurements to ± 3 mmHg (DSI, 2013) (Table 2.1).

For the studies described herein, the implanted radio telemetric device was placed in the intra-peritoneal cavity of

each rat. It consisted of a battery, a strain-gauge sensor and an electronic module, which was able to process information from the strain-gauge sensor and transmit this information to a receiver plate (RPC-1) (Figure 2.2) (Guiol *et al.*, 1992). Protruding from the radio telemetric device was one positive and one negative ECG lead, as well as a catheter (outer diameter 0.7 mm) (Guiol *et al.*, 1992) which was positioned in the abdominal aorta. The catheter tip contained an anti-thrombogenic film and gel membrane, ensuring catheter patency throughout the experiment (Brockway *et al.*, 1991).

Data recorded by the implanted radio-telemetric device were sent to the receiver plate via AM radio waves (DSI, 2013). Each receiver plate was programmed to receive data from one corresponding transmitter. All receiver plates used in an experiment electronically relayed data collected by their registered radio-telemetric device to a data exchange matrix (DSI, 2013) (Figure 2.2). The data exchange matrix then consolidated the information from multiple receiver plates before electronically sending it to a PC installed with DataSciences Dataquest A.R.T™ software (Guiol *et al.*, 1992; DSI, 2013). Finally, an ambient pressure reference module (Figure 2.2), which was able to measure atmospheric pressure, relayed the atmospheric pressure to the Dataquest A.R.T™ software (DSI, 2013). This allowed the software to subtract atmospheric pressure from the pressure detected by the radio-telemetric device and convert it into mmHg, as well as display, plot and store all data collected (Guiol *et al.*, 1992; DSI, 2013) (Figure 2.2).

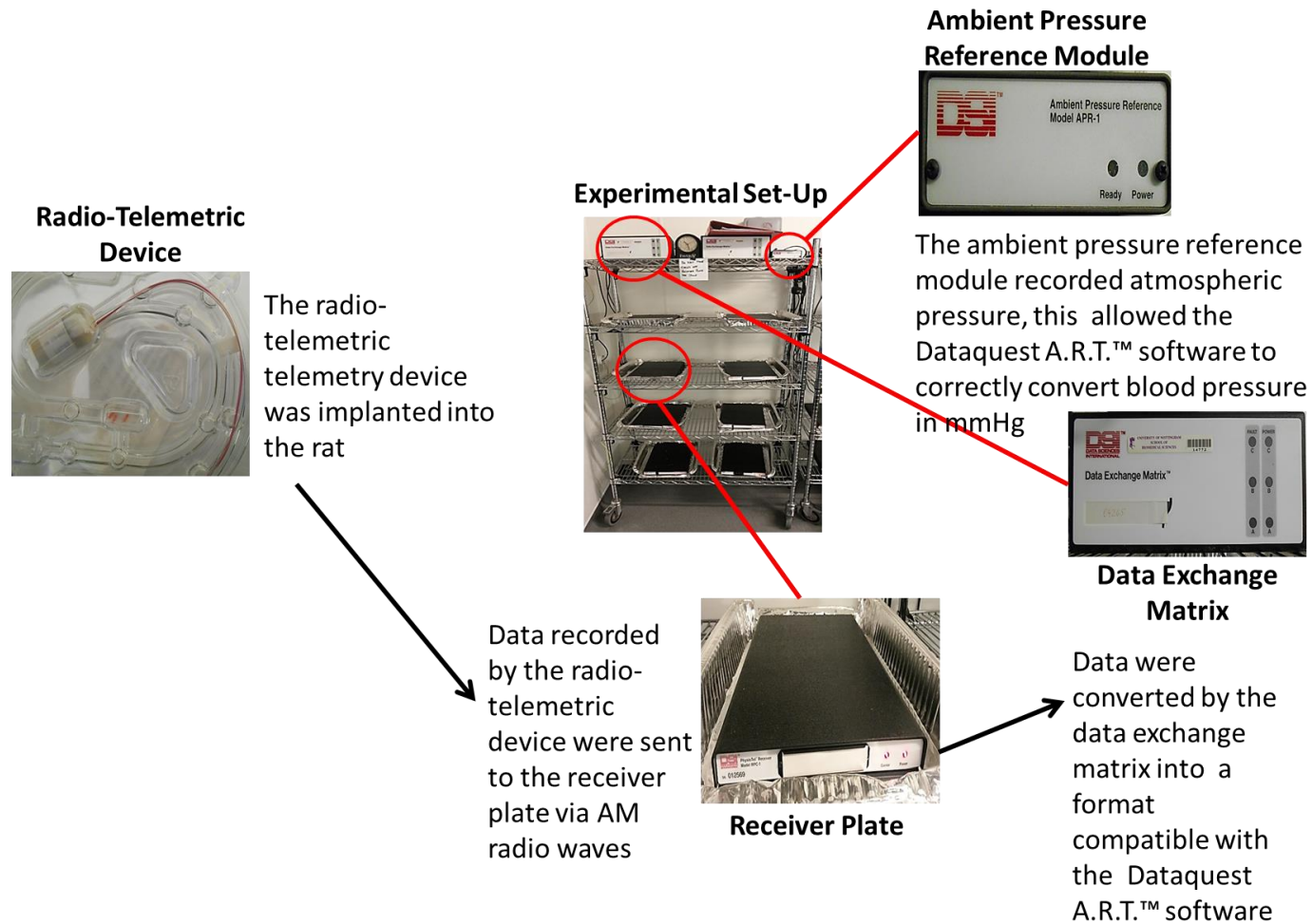


Figure 2.2 Illustration of the DSI radio-telemetric experimental set up. The DSI radio-telemetric telemetry device was implanted into the rat, which was then housed in a cage placed on top of a receiver plate. This received information from the radio-telemetric device and relayed it to the data exchange matrix, and finally to a computer for observation and analysis.

2.3.1 Telemetry Variables

Heart rate was derived from electrocardiogram (ECG) measurements, taken via two ECG leads positioned at the rat's lower sternum and manubrium (Kramer *et al.*, 1993).

Dataquest A.R.T™ software isolated the R wave from each QRS complex. The time between each ECG R wave, also known as the inter-beat interval (s) was calculated. With this information heart rate (beats per minute, BPM) was derived (heart rate=60/inter-beat interval (s)) (DSI, 2013).

The radio telemetric device also measured mean arterial blood pressure via an intra-arterial catheter positioned in the abdominal aorta. Pressure values received from the implanted telemetry device were averaged over 50 sub-segments of each pressure segment length (one pressure segment was defined as one systolic and two diastolic values) to give a mean arterial blood pressure value (mmHg) (DSI, 2013).

2.3.2 Surgical Procedures

2.3.2.1 Animals

Male Sprague-Dawley rats (Charles River, Margate, UK), weighing between 200-300 g, were used for all telemetry studies. This outbred strain was chosen due to their genetic heterogeneity and calm nature (Ghirardi *et al.*, 1995; Rex *et al.*, 2007). Animals were housed in temperature (21-23°C) and light (12 h light/dark cycles from 6 am/6 pm) controlled conditions. All animals had free access to food and water and were allowed to acclimatise to the housing conditions for ≥ 10 days before any surgery was performed. Animals were housed in pairs prior to telemetry device implantation. They were then singly housed overnight after telemetry device

implantation, and subsequently pair housed for the remainder of the experiment. Pair housing was maintained to ensure effects from long term isolation, such as increased locomotor activity, anxiety and aggression were mitigated (Arakawa, 2005). This was not only important for animal welfare but also experimental results (Malkesman *et al.*, 2006). All *in vivo* experimentation was approved by the Animal Welfare and Ethical Review Body (University of Nottingham) and performed in keeping with the Scientific Procedures Animals Act (1986), under U.K Home Office approved Project Licence (40/3466) and Personal License authority.

2.3.2.2 Implantation of Telemetry Devices

Animals were initially anaesthetised with fentanyl citrate, ($300 \mu\text{gkg}^{-1}$, Jansen-Cilac Ltd, opioid agonist) mixed with medetomidine (Domitor, $300 \mu\text{gkg}^{-1}$, Pfizer, α_2 -adrenergic agonist), i.p (supplemented with 0.5 ml fentanyl citrate $50 \mu\text{gml}^{-1}$ and 1mgml^{-1} medetomidine to maintain anaesthetic depth throughout the surgery) (Flecknell, 2010). Once animals were fully anaesthetised (no flinch response after firmly pinching the hind-paw), their weight was recorded and their abdominal midline, and neck were shaved. The shaved areas, paws and tail were cleaned with chlorhexidine gluconate (0.5% w/v in 70% v/v IMS, Adams Healthcare) and the animal was wrapped in a clear surgical drape (cling film, Glad, USA) before being placed on a heated surgical table, set at 37°C , in the dorsal recumbent position. From this point onwards surgery was completed under aseptic conditions, which were approved and monitored by the Home Office.

The telemetry device DSI C50-PXT was used in the vandetanib studies and DSI HD-S11 in the pazopanib studies (Table 2.1).

Both implants were activated using a magnet and their activity was checked using an AM radio receiver, prior to implantation. A 4-5 inch midline abdominal incision was made along the *linea alba*. The contents of the abdomen were wrapped in sterile, saline-saturated tissue and pushed to one side, exposing the vasculature underneath. The distal abdominal aorta was identified and cleared of adipose and connective tissue using blunt dissection techniques. This reduced surgical trauma, helping to ensure blood flow post-catheterisation (Huetteman and Bogie, 2009). The vessel was occluded superiorly and an incision made using a 21 gauge needle bent 90° at the bevelled end. The gel filled catheter of the telemetry device was inserted into the distal abdominal aorta (approximately 1 cm below the renal artery) and the vessel closed using Vet Bond (3M) and cellulose patching (DSI) (Huetteman and Bogie, 2009). The vessel was then released, to ensure blood flow returned through the artery and no blood leaked from the incision. The content of the abdomen was then carefully replaced. A pouch was made on the underside of the xiphisternum using blunt dissection and the tip of the positive ECG lead was stripped of insulation and secured into a loop before being attached into the pouch using suture (3/0) (Huetteman and Bogie, 2009). A 1 cm incision was made on the anterior of the neck and the negative ECG lead was tunneled subcutaneously from the abdomen to the opening in the neck (Deveney *et al.*, 1998). The tip of the ECG lead was stripped of insulation and secured into a loop at the manubrium with suture (3/0) (Sgoifo *et al.*, 1996). The body of the telemetry device was attached to the body wall via suture (4/0) and the abdomen and neck were then closed and all wounds were dusted with surgical wound powder. The animal was given 5 ml saline, 0.02 mgkg⁻¹ Vetergesic

(Buprenorphine, Alstoe Animal Health, partial opioid agonist) and 1 mgkg⁻¹ Antisedan (Atipamezole hydrochloride, Pfizer α_2 -adrenergic antagonist), i.p. Vetergesic (0.02 mgkg⁻¹) was given as an analgesic 4 h after surgery. Animals were then rehoused singularly in an individually ventilated cage overnight before being reintroduced to their cage mate. This period of individual housing allowed for the rat to rest and for the skin and muscle incisions to begin healing. Greene *et al* demonstrated that recovery from telemetry surgery, where parameters such as heart rate, body temperature, mean arterial blood pressure and activity return to post-surgical readings, takes approximately 1 week (Greene *et al.*, 2007). Therefore, rats were given a 10-14 day recovery period with free access to food and water. They were monitored daily and satisfactorily inspected by the Named Veterinary Surgeon before recording took place.

	C50-PTX	HD-S11
Accuracy (mmHg)	±3 mmHg	±3 mmHg
Pressure Range (mmHg)	-20 - 300	-20 - 300
Approx. Transmitter Body Dimensions :		
Length (mm)	30.8	34.8
Weight (g)	10.6	8
Volume (cc)	5.5	5.9
Biopotential Lead Dimensions :		
Length (cm)	30	30
Outer Diameter (mm)	0.94	0.94
Coil Diameter (mm)	0.46	0.46
Catheter Dimensions:		
Length (mm)	80	80
Outer Diameter (mm)	0.7	0.7
Summary of the differences between the C50-PXT and HD-S11 radio-telemetric implants		
<ul style="list-style-type: none"> • The HD-S11 is lighter with a flatter body shape making it more comfortable for the rat. • The HD-S11 sends its implant ID with each data point thus eliminating any potential animal mix ups or cross talk issues. • The HD-S11 automatically sends its calibration values and ID to the Dataquest A.R.T™. software thus eliminating any human error. • The HD-S11 device displays remaining battery life via the Dataquest A.R.T™. Software whereas the C50-PXT requires a manual log. This allows for easier experimental planning. 		

Table 2.1 Summary of the differences between the C50-PXT and HD-S11 radio-telemetric implants (DSI, 2013).

2.3.2.3 Telemetry Experimental Method

Each telemetry device was turned on using a magnet which was run down the flank of the animal, ensuring its close proximity to the telemetry device. Heart rate and mean arterial blood pressure were recorded every 15 min for 1 min for 9 days (vandetanib) or 3 days (pazopanib) before the compound of interest was given either i.p in vehicle (2% Tween, 5% propylene glycol in 0.9% saline solution) or vehicle was administered i.p, once every 24 h for 21 days. A 10 day off-treatment period was observed where recordings took place without the animal being disturbed. At the end of the study the animal was terminally anaesthetised with 50 mgkg⁻¹ pentobarbitone (Dolethal, Vetoquinol, UK), i.p.

2.3.2.4 Statistical Analysis

All data were expressed as mean \pm SEM. Data were displayed parametrically to follow scientific convention, but non-parametric statistical analyses were used, since not all the data were normally distributed (Kolmogorov-Smirnoff normality test). A Friedman test was performed to determine if within group changes from baseline values were significant. Between-group two tailed comparisons were made using the Mann Whitney-U test (for 2 groups) and the Kruskal Wallis test (more than 2 groups) with significance being accepted at $P < 0.05$. All statistical analysis was performed using Graphpad prism 6.00.

2.4 Mesothelium Panel Staining for ECs

To investigate the effects of vandetanib on the microvasculature, a pilot study was performed where mesothelium, from rats participating in the radio-telemetric vandetanib 25 mgkg⁻¹day⁻¹ vs vehicle study (Chapter 2, Section 2.3, and Chapter 4) were harvested and stained for ECs using the antibody Isolectin-B4 and for cell nuclei with Hoechst (Benest and Bates, 2009). The rat mesentery on average contains 30-50 mesothelium panels (Figure 2.3), with each panel consisting of microvessels, macrophages, lymphocytes, mast cells and fibroblasts (Norrby, 2006; Norrby, 2011). The rat mesothelium staining study was first introduced by Norrby in 1986 (Norrby *et al.*, 1986) and has been shown to have multiple advantages. For example the membranes harvested are easy to isolate and dissect, transparent and are only a few cells thick. They are ideal for histological staining as the antibody is able to penetrate the whole tissue without the need for tissue slicing. Therefore, there is a reduced risk of damaging vessel structure, ensuring the structures seen are as close to their native state as possible, and that the entire vascular network can be visualised (Norrby *et al.*, 1986; Norrby, 2008; Norrby, 2011). The transparency and thin width of these vessels makes this tissue attractive for use in microscopy, as the light transmitted from the microscope is able to penetrate through the tissue.

The total number of junctions (indication of vessel branching), and total vessel length (indication of rarefaction and vessel destruction) were measured (Gould *et al.*, 2011; Zudaire *et al.*, 2011).

2.4.1 Method of Tissue Isolation

At the end of the 25 mgkg⁻¹day⁻¹ i.p vandetanib telemetry experiment, each animal was terminally anaesthetised with 50 mgkg⁻¹ pentobarbitone (Dolethal, Vetoquinol, UK-GABA_A agonist) i.p, as described above (Section 2.3.2.3). A 5 cm abdominal midline incision was made and the mesentery isolated. The superior mesenteric artery was tied as a physiological marker to allow for subsequent tissue orientation and positioning. The mesentery was washed with PBS and fixed in 4% paraformaldehyde (pH 7.4) for 2 h at room temperature. Mesothelium panels (Figure 2.3) were isolated from the first 3rd of the mesentery (third closest to the superior mesenteric artery) using blunt forceps and spring action surgical scissors. Mesothelium panels were stored at 4°C in 8 well plates filled with PBS, prior to staining.

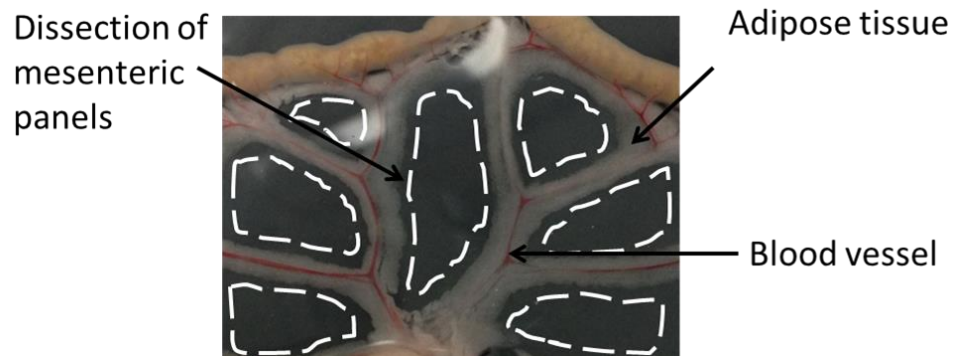


Figure 2.3 Illustration of mesothelium panel dissection. Each rat mesentery contains between 30-50 panels. Each panel consists of a mesothelium membrane containing microvessels, macrophages, lymphocytes and mast cells and fibroblasts (Norrby, 2006; Norrby, 2011). This image shows an isolated rat mesentery with the intestine, vessels, fat and mesothelium present. White dotted lines illustrate where panels were taken from.

2.4.2 Staining Procedure

Each panel was washed in PBX (0.5% Triton-X100 in PBS) for 1 h at room temperature with PBX solution being removed, discarded and replaced every 10 min. All wash and incubation steps were performed on a slow moving shaker. The mesothelium panels were incubated in 1% BSA in PBX (BSA-PBX) at room temperature to reduce the likelihood of antibody-nonspecific binding to reactive sites such as Fc receptors within the tissue (Ramos-Vara, 2005). The panels were then incubated overnight at 4°C with 10 µgml⁻¹ biotinylated Isolectin GS-IB4 (from *Griffonia simplicifolia* (Molecular Probes)). Panels were subsequently washed in PBX for 1 h at room temperature with PBX solution being removed, discarded and replaced every 10 min. Panels were then incubated at room temperature for 2 h with 1 µgml⁻¹ Tetramethyl-rhodamine-isothiocyanate (TRITC)-labelled streptavidin (S-870 Molecular Probes) before being washed in PBX (0.5% Triton-X100 in PBS) for 1 h at room temperature with the PBX solution being changed every 10 min. Finally, panels were incubated with Hoechst (2 µgml⁻¹ diluted in BSA-PBX), to label cell nuclei, before being placed onto 3-Aminopropyltriethoxysilane (APES) coated microscopy slides. APES coating was used to positively charge the slide and therefore reduce sample movement (Maddox and Jenkins, 1987). A coverslip (32 mm x 0.17 mm) was placed over the tissue sample and secured in place with DABCO Fluorescence Mounting Medium (200 mg DABCO (1-4-Diazabicyclo-2-2-2-octane), 14 ml PBS, 86 ml Glycerol), which has been shown to reduce fluorescence signal fading (Valnes and Brandtzaeg, 1985).

2.4.3 Analysis

16 bit images were taken on a Zeiss Axio observer Z1 using a Hamamatsu Orca flash 4 C11440 HD camera and an EC-Plan-neofluar 10x/-0.3 ph1 objective. Images were analysed using ImageJ and AngioTool 0.6b (Zudaire *et al.*, 2011). AngioTool 0.6b uses a subset of algorithms to map vessels within an image and calculate total vessel length and total number of vessel junctions. All analysis was blinded. Data were analysed using Microsoft Excel 2010 and GraphPad Prism 6.0. Statistical significance was determined using an unpaired one tailed Mann Whitney-U test ($P < 0.05$).

2.4.3.1 AngioTool 0.6b

AngioTool was used to gain a quantitative, non-subjective analysis of total vessel length and total number of branch points. AngioTool 0.6b is an open source analysis program written using Java script. It is compatible with the open source software ImageJ. The images analysed were converted into 16 bit grey scale using ImageJ and then uploaded to the AngioTool software. AngioTool analyses the image using a multiscale hessian-based enhancement filter (Zudaire *et al.*, 2011), allowing the program to distinguish linear structures from background (Sato *et al.*, 1998). Once the vessels are detected within the image, the software maps a skeleton onto the image (Chapter 4) (Arganda-Carreras *et al.*, 2010) and calculates user set parameters, such as total vessel length and total junction number (junction defined as a vessel branch point) (Zudaire *et al.*, 2011). The mapped skeleton layed over the original image allows the user to ensure that all vessel structures have been detected. If this is not the case the user can adjust pre-set parameters, which allow gaps in the

mapped skeleton to be filled or for background noise to be removed (Zudaire *et al.*, 2011). The 'mapped' image is saved along with the values for the measured parameters into an excel file.

2.5 The Measurement of Regional Haemodynamics in Conscious Rats

In order to measure the effect of RTKIs on regional haemodynamics in the rat, blood flow velocities were measured using the Doppler principle (Section 2.5.1). Small (1-2 mm in diameter) ultrasonic pulsed Doppler flow probes were implanted around vessels of interest (the mesenteric artery, renal artery and abdominal aorta), and the Doppler shift (difference in frequency transmitted and frequency received), was measured, allowing blood flow velocity to be subsequently derived (Hartley and Cole, 1974). This is described in detail below. Alongside pulsed Doppler flow probe implantation, an intra-arterial (i.a) catheter was implanted 10-14 days later to measure blood pressure and heart rate simultaneously. Intra-venous (i.v) and intra-peritoneal (i.p) catheters were also implanted to allow for drug administration. This method facilitated the measurement of regional haemodynamic changes in conscious, freely-moving animals for up to 4 days. Drugs were administered via intravascular catheters, allowing animals to remain undisturbed in their individual cages. The following sections will describe the theory behind the ultrasonic pulsed Doppler technique and describe the methodology used.

2.5.1 The Pulsed Doppler Method

The pulsed Doppler method was first developed by Hartley *et al.* (1974) for use in dogs (Hartley and Cole, 1974). By using a single piezoelectric crystal, capable of emitting and receiving sound waves, Hartley *et al.* were able to greatly reduce the size of the probes needed in comparison to methods like the continuous wave Doppler technique, which needs both emitting and receiving ultrasonic crystals. The first description of the use of Hartley *et al.*'s pulsed Doppler flowmetry technique in rats was by Haywood *et al.* in 1981 (Haywood *et al.*, 1981). This technique was improved further by Gardiner *et al.* (Gardiner *et al.*, 1990), who adapted the system to reduce 'aliasing' at high velocities (Section 2.6.3).

Doppler shift is measured via a small (1 mm) ultrasonic piezoelectric crystal embedded in a probe and held at a 45° angle to the specified vessel. When connected to a flowmeter, the piezoelectric crystal emits a short burst of ultrasonic energy at 20 MHz. When this comes into contact with a moving object, for example an erythrocyte, the ultrasonic energy is reflected back toward the crystal face. The energy reflected back is time-delayed and at a slightly different frequency compared to the energy emitted, and the shift in frequency (Doppler shift) is directly related to the velocity of the moving target (Hartley and Cole, 1974). The frequency at which the ultrasound is emitted (20 MHz) is higher than that used in systems such as the continuous wave Doppler system. This is advantageous as it produces a higher energy scatter allowing for a small crystal face to be used, as the energy returned is higher (Hartley and Cole, 1974). The time delay seen between the emission and detection of the ultrasonic signal is directly proportional to the distance between the

moving erythrocytes and the face of the crystal. The system used in these studies allows for the Doppler shift to be measured at various points across the lumen diameter (between 1-10 mm) by adjusting the time delay of the crystal (range setting). In order to make the most reliable measurements, the ultrasonic energy is pulsed to the middle of the vessel where there is maximal laminar flow. In practice, this is done by slowly adjusting the range of the probe until the largest signal is found.

By using the Doppler equation:

$$\Delta f = 2f_0 \frac{V}{C} \cos\theta$$

Where Δf = Doppler shift, f_0 = transmitted frequency in Hz, v = velocity of fluid, C = velocity of sound in the fluid, θ = angle between the flow axis and acoustic axis (the angle of the crystal in relation to the blood vessel), the difference between the frequency emitted and the frequency returned can be calculated.

In the days (prior to catheter implantation) following implantation of the pulsed Doppler flow probe, fibrous tissue grows to encapsulate the vessel and probe. The fibrous capsule acts to keep θ and the diameter of the vessel directly beneath the probe constant. As f_0 (20 MHz), C (velocity of sound in fluid) and θ (about 45°) remain constant, Δf is linearly related to the velocity of fluid, in this case blood flow velocity. As the diameter of the vessel directly under the cuff also remains constant, blood flow velocity is directly proportional to blood flow. This assumption was investigated by Haywood, who measured blood flow simultaneously using

the pulsed Doppler flowmeter method and the electromagnetic flowmeter method, Haywood showed measured changes in blood flow were directly proportional to changes in flow velocity across a range of pharmacologically-induced vasoconstriction and vasodilatation (Haywood *et al.*, 1981). The measurement of Doppler shift in conjunction with mean arterial blood pressure (measured via an i.a catheter attached to a pressure transducer) allows for vascular conductance (vascular conductance=mean Doppler shift/mean arterial blood pressure) (Gardiner *et al.*, 1990) to be calculated.

2.5.2 Construction of Doppler Flow Probes

Pulsed Doppler flow probes were assembled using a method similar to that described by Haywood (Haywood *et al.*, 1981). Piezoelectric crystals with attached wires were obtained from Crystal Biotech Inc (USA) and tested for their ability to send and receive ultrasonic signals. This was done by attaching the piezoelectric crystal to a flowmeter and dipping it in and out of distilled water; if the crystal was working, sound was produced through the flowmeter. Once this had been confirmed, the crystal was inserted in to a 3-4 mm length of medical grade silicone tubing (Figure 2.4). One side of the tubing was cut at a 45° angle, allowing the piezoelectric crystal to sit at a 45° angle to the vessel when it was implanted. The wires of the crystal were then pulled through the other side of the tubing, ensuring the face of the crystal was positioned toward the angled side of the tubing. The crystal was held in place with a small amount of dental wax until it was ready to be permanently fixed. On the opposite side of the tubing (where the wires protrude) a piece of polystyrene was attached as an acoustic baffle, ensuring the ultrasound was projected forward

(Figure 2.4). The probe was then left to set for 24 h (Gardiner *et al.*, 1990).

In order to form a cuff, which was later used to attach the crystal to the vessel, the piezoelectric crystal + acoustic baffle was mounted onto a needle by melting the dental wax on the crystal (Figure 2.4). A silastic cuff was then built up around the subunit and the needle. The probe was left overnight, allowing the silastic gel to set (Figure 2.4). Finally, the silastic cuff was cut along the underside of the needle, releasing the probe from the needle and forming two flaps, which subsequently had sutures (6/0 ophthalmic silk) sewn into them to provide ties; this later allowed for the probe to be secured around the vessel (Figure 2.4, Figure 2.5.a.).

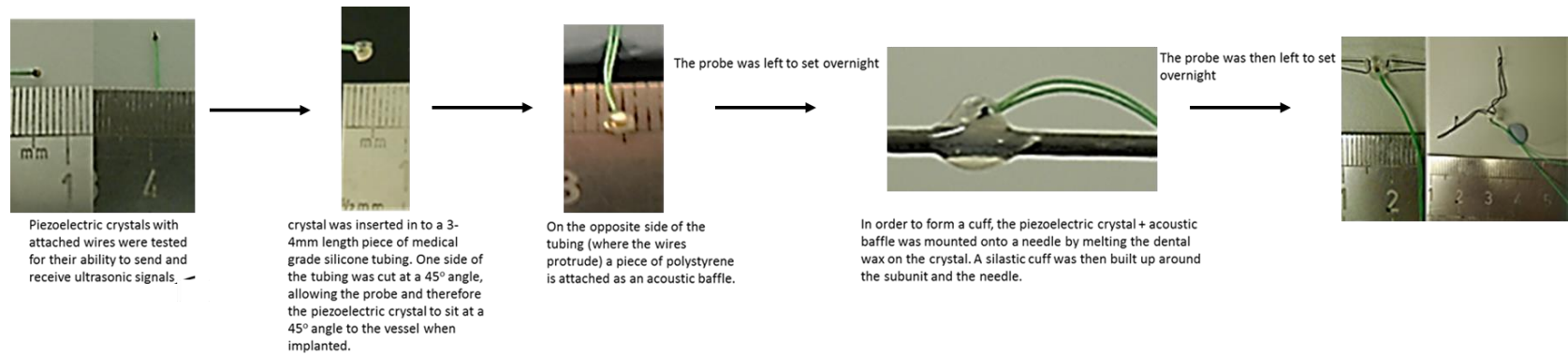


Figure 2.4 Labelled image of the pulsed Doppler probe construction process.

2.6 Surgical Procedures

2.6.1 Animals

Male Sprague-Dawley rats (Charles River, Margate, UK) weighing between 300-500 g were used for all pulsed Doppler flowmetry studies. Animals were housed in temperature (21-23°C) and light (12 h light/ dark cycles from 6 am/ 6 pm) controlled conditions. All animals had free access to food and water and were allowed to acclimatise to the housing conditions for ≥ 10 days before any surgery was performed. Animals were housed in pairs prior to Doppler flow probe implantation. They were then singularly housed overnight after pulsed Doppler flow probe implantation, pair housed again before catheterisation and single housed post-catheterisation surgery. All *in vivo* experimentation was approved by the Animal Welfare and Ethical Review Body (University of Nottingham), and performed in keeping with the Animals (Scientific Procedures) Act (1986), under UK Home Office approved Project Licence (40/3466) and Personal License authority.

2.6.2 Implantation of Doppler Flow Probes

Animals were initially anaesthetised with fentanyl citrate, ($300 \mu\text{gkg}^{-1}$, Jansen-Cilac Ltd, opioid agonist) mixed with medetomidine (Domitor, $300 \mu\text{gkg}^{-1}$, Pfizer, α_2 -adrenergic agonist), i.p (supplemented with 0.5 ml fentanyl citrate $50 \mu\text{gml}^{-1}$ and 1mgml^{-1} medetomidine to maintain anaesthetic depth throughout the surgery, as required) (Flecknell, 2010). Once animals were fully anaesthetised (assessed by firmly pinching the hind-paw), weight was recorded and the abdominal midline, posterior of the neck and left flank above the hind limb were shaved. The shaved areas, paws and tail

were cleaned with chlorohexidine gluconate (0.5% w/v in 70% v/v IMS, Adams Healthcare) and the animal was wrapped in a clear surgical drape (cling film, Glad, USA) before being placed on a heated surgical table, set at 37°C, in the dorsal recumbent position.

A 4-5 inch midline abdominal incision was made along the *linea alba*. The contents of the abdomen were wrapped in sterile, saline-saturated tissue and pushed to one side, exposing the vasculature underneath. Vessels of interest (left renal artery, superior mesenteric artery and the distal abdominal aorta) (Figure 2.5) were identified using a microscope. These vessels were cleared of adipose and connective tissue using blunt dissection techniques. An appropriate sized probe, with a lumen equivalent to the vessels diameter (renal/ mesenteric artery approximately 1 mm, aortic artery approximately 1.7 mm), was selected for each vessel and coupling gel (ultrasound gel, Henleys Medical, UK) was added to the centre of the probe, onto the face of the crystal. Each probe was then connected to a Doppler flowmeter and checked for acceptable signal detection. Providing the signal was of good quality, the probe was then sutured around the vessel (Haywood *et al.*, 1981; Gardiner *et al.*, 1990).

Probe wires were secured to the left abdominal wall with 2-0 vicryl suture (Ethicon, UK) and tunnelled via the left flank to the posterior of the neck, where signals were re-verified using the Doppler flowmeter. Wire ends were secured with suture and sterile tape to the nape of the neck (approximately 0.3 cm of wire/ tape was left exposed). The abdominal contents were carefully repositioned and the muscle wall sutured using 2-0 vicryl (Ethicon, UK). Excess wire was coiled

and anchored subcutaneously at the left flank. Finally, the abdominal skin layer was sutured using 4-0 vicryl (Ethicon, UK) and surgical wound powder (Battle, Hayward and Bower Ltd, UK) was dusted over all the wounds to reduce the likelihood of infection and promote wound healing. Animals were given 0.05 ml Amoxycare LA (150 mgml⁻¹ (15% w/v) ampicillin trihydrate, Animalcare, UK) intra-muscularly and 5 ml warmed saline i.p to aid post-surgical hydration and to ensure the abdominal cavity and its contents were moist, reducing the risk of post-surgical trauma (suggested best practice by the named veterinary surgeon). Anaesthetic was reversed using 0.02 mgkg⁻¹ Vetergesic (buprenorphine, Alstoe Animal Health, UK, partial opioid agonist) and 1 mgkg⁻¹ Antisedan (atipamezole hydrochloride, Pfizer α_2 -adrenergic antagonist). Animals were housed singly in cages positioned over heating pads for the first 6 h post-surgery, during this time their welfare was checked every 15 min and 0.02 mgkg⁻¹ Vetergesic was given 4 h after surgery as an analgesic top-up. Animals were then housed singularly in an individually ventilated cage over night before being reintroduced to their cage mate. This period of individual housing allowed for the rat to rest and for the skin and muscle incisions to begin to heal. Rats were allowed free access to food and water during their 10-14 day recovery period, and were monitored daily and satisfactorily inspected by the Named Veterinary Surgeon before catheterisation took place.

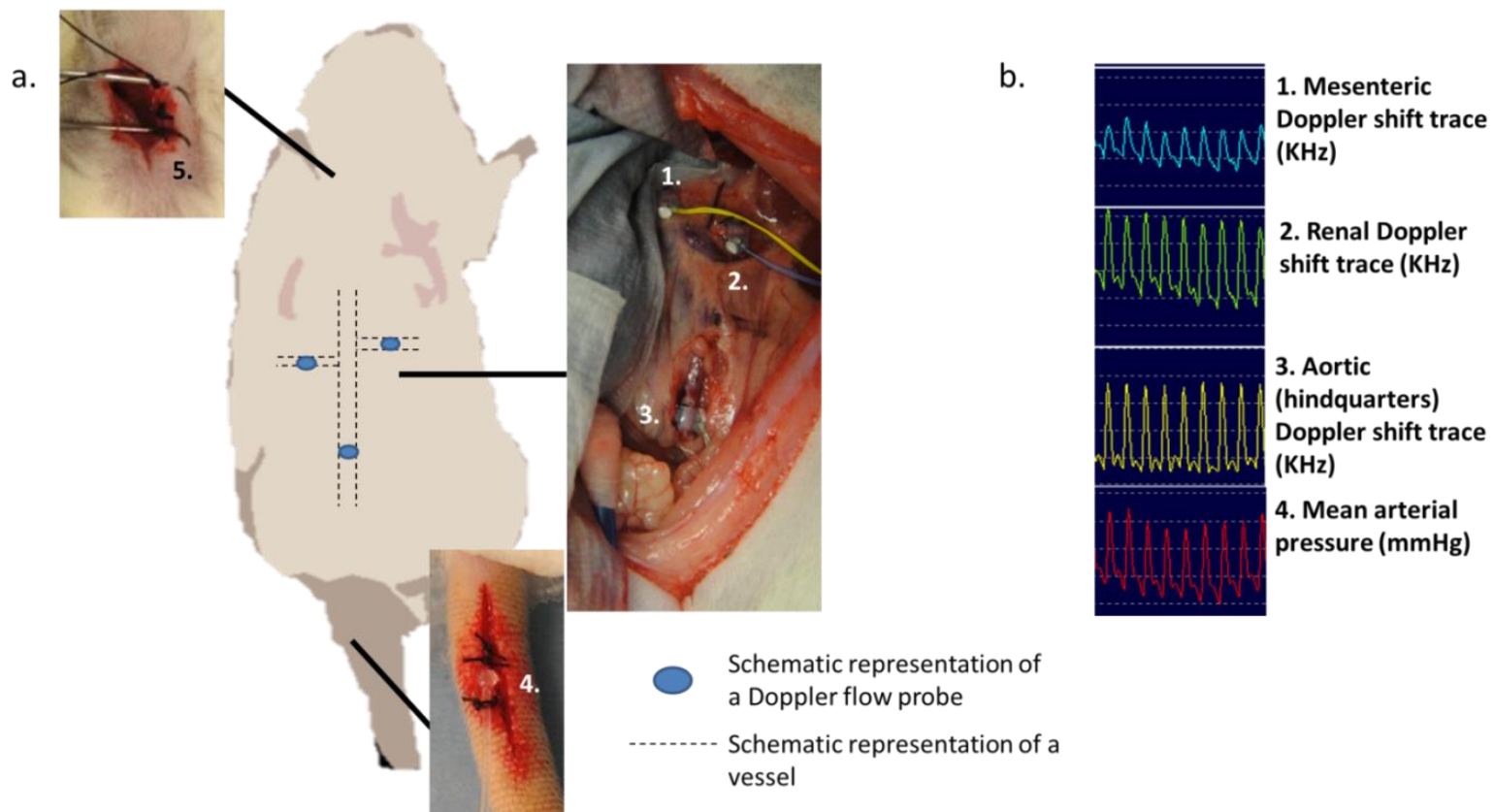


Figure 2.5 Illustration of flow probe, i.v. and i.a. catheter placement. Doppler flow probes were tied around the mesenteric (a.1.), renal (a.2.) and distal aortic (a.3.) arteries. 10-14 days later, catheters were introduced into the right jugular vein (i.v: a.4.) and ventral caudal artery (i.a: a5.). Post-catheterisation surgery, flow probes were connected to a flow meter, allowing Doppler shift to be recorded (b.1., b.2, b.3. representative trace). The i.a. catheter was connected to a pressure transducer in order to record mean arterial blood pressure (b.4). Representative Doppler shift and mean arterial blood pressure traces (b) were obtained from regions, as indicated in (a).

2.6.2.1 Implantation of Intra-vascular Catheters

Venous catheters consisted of 150 cm Portex polythene tubing (internal diameter 0.28 mm x outer diameter 0.61 mm) and intra-peritoneal catheters consisted of 150 cm Portex polythene tubing (internal diameter 0.40 mm x outer diameter 0.80 mm). The arterial line consisted of 6 cm Portex polythene tubing (internal diameter 0.28 mm x outer diameter 0.61 mm) heat-sealed to 85 cm Portex nylon tubing (internal diameter 0.58 mm x outer diameter 1.02 mm). All catheters were packed and sterilised with ethylene oxide before surgery. Prior to insertion all catheters were flushed with 15 Uml⁻¹ heparinised saline.

Animals were fully anaesthetised with fentanyl citrate (300 µgkg⁻¹, Jansen-Cilac Ltd) mixed with medetomidine (Domitor, 300 µgkg⁻¹, Pfizer) i.p, supplemented when required to maintain depth of anaesthesia. Depth of anaesthesia was monitored using the hind-paw toe pinch method. The weight of the animal was recorded and the anterior of the neck (between the larynx and sternum) and right flank were shaved and cleaned with chlorohexidine gluconate (0.5% w/v in 70% v/v IMS, Adams Healthcare). The wire tips protruding from the rat's posterior neck were freed and stripped of insulation allowing the signal from each probe to be verified using the flowmeter. The wires were then soldered into a 6-way miniature connector (Microtech, Boothwyn, PA, USA) (Figure 2.6). The rat was then wrapped in a clear surgical drape before being placed on the surgical table in the dorsal recumbent position.

2.6.2.2 Intra-venous Catheters

A 1 cm incision was made on the anterior of the neck. Connective tissue was parted using blunt dissection and the right jugular vein isolated and ligated posteriorly. Lidocaine (0.5% w/v, Antigen Pharmaceuticals) was used to relax the vessel and further numb the neck. Either 2 (i.p administration studies) or 3 (i.v administration studies) venous catheters were tunnelled from the nape of the neck to the exposed jugular vein, and then advanced (by 2 cm) into the jugular vein through a small incision made in the vein. Catheters were secured into place using suture (4-0 silk thread), flushed with heparinised saline (15 Uml⁻¹) and sealed with a wire spigot (Figure 2.5). The incision was then sutured closed and surgical wound powder dusted over the wound (Haywood *et al.*, 1981, Gardiner *et al.*, 1990).

2.6.2.3 Intra-Arterial Catheters

A 2 cm incision was made along the ventral side of the base of the tail and the ventral caudal artery exposed. Lidocaine (0.5% w/v, Antigen Pharmaceuticals) was applied to relax the vessel, the vessel was occluded by lifting on a pair of forceps and ligated; an arterial catheter was then advanced 6 cm into the distal aorta and secured in place with suture (4-0 silk thread) (Figure 2.5). The catheter was then flushed with heparinised saline (15 Uml⁻¹) and sealed with a wire spigot before it was tunnelled via the dorsal end of the tail superiorly to the nape of the neck, where the probe wires and venous catheters exited. The tail was sutured closed (Van Dongen, 1990).

2.6.2.4 Intra-peritoneal Catheters

An incision was made along the skin of the right flank and an intra-peritoneal catheter inserted through the abdominal wall by 4 cm. The catheter was secured to the muscle wall by suture (4-0 silk thread), both at the site of entry and 1-2 cm posterior to the incision. The catheter was tunneled subcutaneously to exit at the nape of the neck, flushed with heparinised saline (15 Uml^{-1}) and sealed with a spigot. The skin was sutured and surgical wound powder dusted over the incision.

2.6.3 Doppler Experimental Set Up

Post-surgery, the animals were transferred to a cage in the experimental room and fitted with a harness (Figure 2.6). The catheters were threaded through a hollow spring attached to a counter balance and a miniature 6 way plug (Figure 2.6.d.) and secured to the harness; any exposed wires and soldered joints were protected with tape (Figure 2.6.b., 2.6.c.). The connector was attached to an extension lead and the probe signals checked using a Doppler flowmeter. Anaesthesia was reversed using 0.02 mgkg^{-1} Vetergesic (buprenorphine, Alstoe Animal Health) and 1 mgkg^{-1} Antisedan (atipamezole hydrochloride, Pfizer). The arterial line was connected to a fluid-filled swivel (Gardiner *et al.*, 1990) which in turn was connected to an infusion pump set to infuse heparinised saline (15 Uml^{-1}) at 0.4 mlh^{-1} during non-experimental periods (Figure 2.6). Animals had free movement within the cage and free access to food and water.

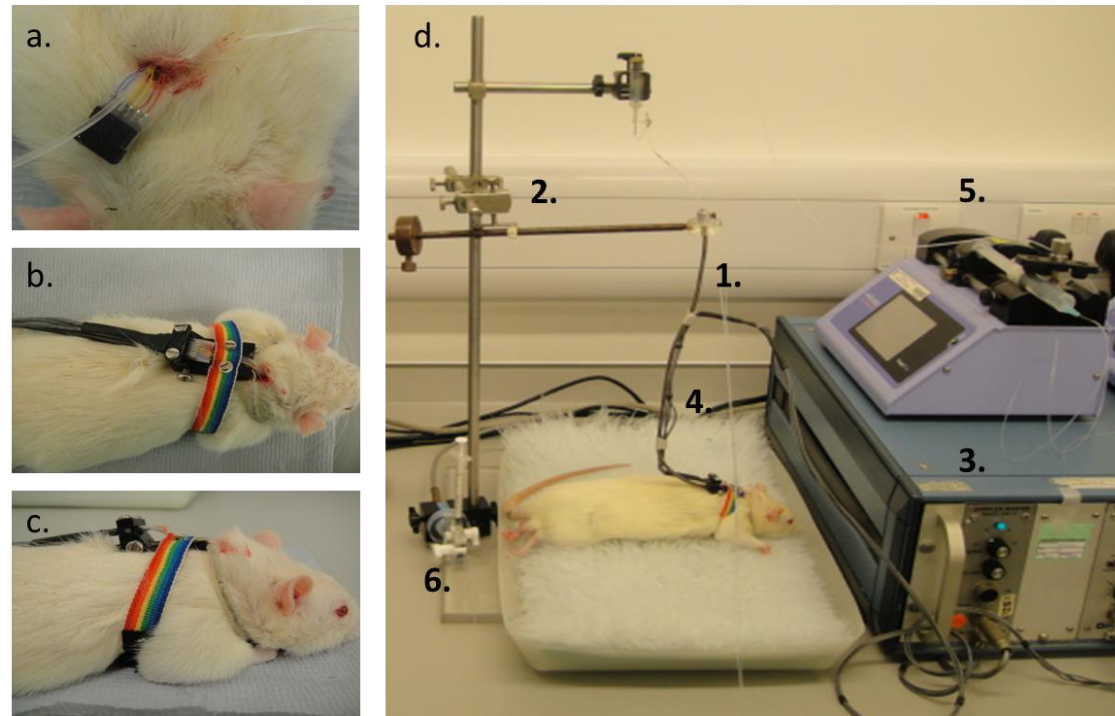


Figure 2.6 Illustration of exteriorised catheters, flow probe wires, harness placement and experimental set up (shown when the animal was recovering from anaesthesia post-catheterisation surgery). During flow probe implantation and catheterisation surgery, the catheters and flow probe wires were exteriorised at the back of the neck and a 6 way plug soldered to the wire ends (a.). While the animal was still anaesthetised a harness was attached (b., c.). The 6 way plug + wires were wrapped in tape, to protect the soldering joints, and secured to the back of the harness (b.). The catheters were fed through a steel spring for protection (d.1.). The spring was attached to a counter balance swivel (d.2) allowing the rat free movement within the cage. The 6 way plug was attached to the Doppler flow meter (d.3.) via a connector lead (d.4.). Finally the i.a catheter was attached to an infusion pump (d.5.) set to infuse heparinised saline (15 Uml^{-1}) at 0.4 mlh^{-1} during non-experimental periods. During experimental periods the i.a catheter was connected to a pressure transducer (d.6.).

After a 24 h recovery period, experiments began and lasted for a total of 4 days, with recordings taken continuously for 4.5 h per day. Baseline recordings were taken for a minimum of 30 min in all studies undertaken. Heart rate and blood pressure were continuously monitored via the i.a catheter connected to a pressure transducer (Gould, Eastlake, Ohio, USA) and a transducer amplifier (Gould, Eastlake, Ohio, USA) model 13-4615-50)), which interfaced with the IDEEQ recording system (Maastrich Instruments, The Netherlands). Pressure changes were detected by strain gauges, in the pressure transducer, as changes in resistance. The change in resistance was converted to a change in voltage by a Wheatstone bridge circuit. Calibration of the pressure transducer, using a sphygmomanometer, allowed changes in voltage to be converted into changes in mmHg by the IDEEQ software.

The catheter-transducer-IDEEQ recording system was able to follow a fundamental frequency of approximately 40 Hz. The ability to measure frequencies up to the 5th harmonic of the heart rate means that systolic and diastolic arterial blood pressures can be measured faithfully i.e., not over-dampened or under-dampened. Over-dampening of the blood pressure signal was reduced by using rigid arterial catheter tubing, and by using a custom 'low volume' transducer filled with de-gassed water. This reduced possible air spaces and bubbles within the transducer. Under-dampening, which would cause resonance, was avoided by the use of the flexible, small bore, intra-vascular section of the arterial catheter (Gardiner *et al.*, 1990).

The Doppler shift was measured by connecting the flow probes to a Doppler flowmeter (Crystal Biotech, Holliston, MA, USA) and in turn to the IDEEQ recording system. The Doppler flowmeter used here had been modified to detect pulse repetition frequencies (PRF) of 125 KHz. In 1990, Gardiner *et al.* demonstrated a PRF of 62.5 KHz was insufficient to accurately measure changes in rat aortic Doppler shift, in the presence of nitroprusside and methoxamine (Gardiner *et al.*, 1990). This was concluded to be due to the Nyquist (sampling) theorem (Cho *et al.*, 2011), which states that to accurately convert analogue signals to digital, the sampling frequency (pulse-repetition frequency (PRF)), which in this case is the number of times the piezoelectric crystal emits and receives a signal per second, must be greater than half of the maximum frequency, or over twice the frequency response (Stewart *et al.*, 1985). When this parameter is not met, a phenomenon called aliasing occurs. Alias signals are signals of the same value on corresponding sides of the waveform, when the maximum frequency response is not at least twice that of the PRF, these alias signals overlap leading to the loss of high frequency components of the signal and to a distortion of the continuous waveform (Cho *et al.*, 2011).

2.6.4 Statistical Analysis

All data were expressed as mean \pm SEM. Data were displayed parametrically to follow scientific convention, but non-parametric statistical analyses were used, since not all the data could be considered to be normally distributed. A Friedman test was performed to determine if within group changes from baseline values were significant. Between group two tailed comparisons were made using Mann Whitney-U test

(for 2 groups) and Kruskal Wallis test (more than 2 groups) with significance being accepted at $P < 0.05$. All statistical analysis was performed using Biomedical version 3.4 (Nottingham, UK).

2.7 Isobaric Myography

Isobaric (pressure) myography comprises of an isolated vessel segment being mounted and secured onto 2 glass micro-cannulae (Mulvany and Halpern, 1976). This allows the vessel to be exposed to transmural pressure and changes in vessel diameter (caused by vessel contraction/relaxation) to be measured. Unlike wire myography, which measures the force exerted by a vessel that is undergoing contraction (Mulvany and Halpern, 1977), pressure myography allows for changes in the diameter of the vessel to be measured. It has multiple advantages over wire myography including maintenance of the cross sectional shape of the vessel, as well as control over the intramural pressure within a vessel. It also ensures that the endothelium remains relatively untouched during the set-up of the experimental procedure, helping to reduce undue vessel trauma (Mulvany and Halpern, 1976; Halpern and Mulvany, 1977).

2.7.1 Preparation of Small Mesenteric Arteries

Male, Sprague Dawley rats, weighing between 150-200 g were killed by striking the cranium, followed by exsanguination. This technique was carried out in accordance with Schedule 1 of the UK, Animals Scientific Procedures Act (1986). The mesentery was removed and transferred to a dissection dish containing ice cold (0-4°C) Krebs-Henseleit physiological salt solution (PSS) (118 mM NaCl, 4.8 mM KCl, 1.1 mM

MgSO₄·7H₂O, 25 mM NaHCO₃, 1.2 mM KH₂PO₄, 12 mM Glucose, 1.25 mM CaCl₂·2H₂O) (White *et al.*, 2013). The PSS was gassed with 5% CO₂ 95% air prior to being used. This ensured the pH of the solution was 7.4 and that the solution was oxygenated. The mesentery was laid flat in PSS and pinned allowing for vessel isolation. The arteriole was identified by its 'V' shaped branching anatomy. The second order branch of the arteriole was carefully stripped of fat and connective tissue with forceps and spring action surgical scissors, ensuring vessel stretching and damage was kept to a minimum. Approximately 5-7 mm of the arteriole connected to a 0.5-1 mm side branch was transferred into either a living systems CH2 or DMT 120CP pressure myography chamber. Second order mesenteric arterioles (diameter 100-400 µm) were used as they are representative of the vessels in vascular beds that influence total peripheral resistance and blood pressure (Christensen and Mulvany, 2001).

2.7.2 Myography System

Due to equipment availability, two separate pressure myography systems were used to collect data, the living systems CH2 and DMT 120CP pressure myographs. This Section shall discuss how the vessel was mounted onto the myograph and highlight any differences between the two set-ups (Table 2.2).

The myography bath contained 10 ml PSS and was perfused with 95% air 5% CO₂ to maintain a pH of approximately 7.4. Temperature was maintained at 36-37°C. Both myography systems used self-heating baths. All tubing was filled with PSS solution ensuring all air bubbles were removed. This was done so that no air could enter the vessel when it was mounted. It

has been shown that perfusion of a vessel with air disrupts the endothelial layer affecting the ability for the endothelium to control vessel tone and, therefore, affecting the results gained (Falloon *et al.*, 1993). The side of the vessel which had an off branch attached was carefully slipped onto the right hand micro-cannula using forceps. It was then tied in place, ensuring the tie was placed after the off-branch, with a single strand of nylon thread. A small amount of PSS solution was allowed to flow through the micro-cannula and vessel to remove any residual blood in the vessel. The other side of the vessel was then carefully mounted onto the left hand micro-cannula and tied in place. The myography bath was then placed onto the microscope platform (Table 2.2).

90 mmHg was applied to the vessel and no flow of PSS was allowed to ensure no flow mediated vasoactivity (Ando and Yamamoto, 2009). Static pressure of the vessel was checked in the living systems CH2 system by switching the peristaltic pump to manual and checking for maintenance of pressure; on the DMT 120CP system maintenance of pressure was checked by comparing the pre-vessel and post-vessel pressure transducer readings and looking for pressure differences. One of the major differences between these two systems is how the vessel was pressurised. The Living Systems myograph used a pressure-servo peristaltic pump connected to a pressure transducer. The peristaltic pump worked by actively displacing fluid, therefore forcing it along the tubing. The DMT 120CP system used a flow control system, where a mixture of 95% air 5% CO₂ was used to pressurise a bottle containing PSS solution, the pressure in the bottle forced the fluid out of the bottle, and through the vessel, at a set pressure (detected by pressure transducers placed before and after the vessel).

Intraluminal pressure was set to 90 mmHg (Fenger-Gron *et al.*, 1995). Fenger *et al.* (1995) demonstrated that in conscious freely moving Wistar rats, the approximate blood pressure in the intestine was 96 mmHg. However, as these animals had recently undergone surgery prior to the blood pressure measurement, a procedure that has been shown to raise blood pressure for up to 10 days (Greene *et al.*, 2007) a pressure of 90 mmHg was chosen to reduce the likelihood of over-stretching and/or damaging the vessel.

Edge detection software (Table 2.2) was used to measure the distance between each of the vessel walls, giving a value for internal vessel diameter (μm). The edge detection software worked by identifying changes in brightness across an image. As the vessel wall is thicker and does not allow as much light to penetrate it, in comparison to the vessel lumen, the vessel lumen diameter can be easily distinguished and measured. Both edge detection systems allowed the user to adjust the edge detection in real time to ensure an accurate measurement was taken. The vessel was allowed to equilibrate to bath conditions for 30 min before the experimental procedure began (see Chapter 6 for further detail).

	Living Systems CH2	DMT 120CP
Pressurisation technique	Peristaltic pump	Flow control system using 95% air 5%CO ₂ mixture
Microscope	Olympus CK40	Zeiss Axio Vert A1
Edge detection and analysis software	Lab Chart 7 (ADInstruments)	MyoView II (DMT)

Table 2.2 Summary of the key differences between the Living Systems CH2 and DMT 120CP myography systems.

2.7.3 Statistical Analysis

Data collected from more than one system was not collated but instead has been shown and analysed independently. Data obtained from the DMT 120CP system were fitted using non-linear regression in GraphPad Prism 6 (San Diego, CA) to obtain EC₅₀ values.

$$Response = \frac{E_{max} \times [A]}{[A] + EC_{50}}$$

Where [A] is the concentration of VEGF or ACh and EC₅₀ is the molar concentration of agonist required to generate 50% of the maximal agonist response. In experiments where a VEGF/ ACh concentration- response curve in the presence of RTKI/ DMSO/ PSS control was generated, data were also fitted to the above equation.

All data were expressed as mean ± SEM. A non-parametric, two-tailed group comparison Friedman test was performed to determine if any changes seen from the baseline value were significant. Non-parametric between group two tailed comparisons (Mann Whitney (for 2 groups) and Kruskal Wallis (more than 2 groups) were performed to look for significant differences between groups. An unpaired student T test was used to compare E_{max} and EC₅₀. These were gained by averaging the individual experimental E_{max} and EC₅₀ values from each experimental non-linear regression curve fit (Graphpad prism 6.00). Significance was accepted at P<0.05.

**Chapter 3: Effects of
Receptor Tyrosine
Kinase Inhibitors on
VEGF₁₆₅- and
VEGF_{165b}-Stimulated
NFAT-Luciferase Gene
Transcription in
HEK-293 Cells
Expressing Human
VEGFR2**

3.1 Introduction

This Chapter will address the *in vitro* action of RTKIs on VEGFR2-mediated responses, by quantifying their ability to inhibit the VEGF-VEGFR2-mediated activation of the PLC γ -NFAT pathway in a whole cell system. This pathway was chosen as it is involved in the promotion of cell growth and proliferation (Figure 1.1) (Armesilla *et al.*, 1999; Hogan *et al.*, 2003). As these processes specifically contribute to the progression of angiogenesis and therefore, pathologically, the progression of solid tumour growth (Section 1.3), their inhibition by VEGF RTKIs is important for the successful treatment of cancer.

The use of an *in vitro* whole cell system allows for the inhibitory actions of vandetanib, pazopanib, cediranib and sorafenib at VEGFR2 to be quantified. Additional understanding of the RTKI mechanism of action at VEGFR2 *in vitro* is important. It is currently thought that the ability of RTKIs to elicit an effect is dependent on their capacity to bind to intracellular regions of VEGFR2 (Wedge *et al.*, 2002; Hennequin *et al.*, 2002; Knowles *et al.*, 2006; Gotink and Verheul, 2010; Davis *et al.*, 2011; Blanc *et al.*, 2013), therefore understanding the potency of these RTKIs when a cell membrane is present is important.

Finally, a better understanding of the mechanism of antagonism and order of potency of cediranib, sorafenib, pazopanib and vandetanib, against two VEGF-A splice variants: VEGF₁₆₅, the predominantly studied pro-angiogenic VEGFR2 ligand (Liang *et al.*, 2013), and VEGF_{165b}, a VEGF-A splice variant with reduced efficacy at VEGFR2 in comparison to VEGF₁₆₅ (Woolard *et al.*, 2009), may help to further the

understanding of how VEGFR inhibitors lead to varying levels of hypertension *in vivo* and in the clinic (Varey *et al.*, 2008) (Section 1.1). VEGF_{165b} has previously been shown to be over expressed in various tumour types (Rennel *et al.*, 2008) and to affect the growth of tumours (Pritchard-Jones *et al.*, 2007) (described fully in Section 1.2). It has also been shown to affect the potency of Avastin (Varey *et al.*, 2008), an anti-angiogenic monoclonal humanised VEGF antibody. Therefore, a better understanding of RTKI action against VEGF_{165b} is important for future drug development and has potential clinical applications regarding treatment choice.

3.2 Methods

3.2.1 Experimental Method Protocol 1: The 'non-confluent monolayer' Method

VEGFR2 NFAT cells were detached from the T75 flask (as described in Section 2.1.2) and seeded at a density of 30000 cells per well in white sided, clear flat-bottomed 96 well plates which had been coated with poly-D-lysine. After 24 h, media was replaced with FCS free media. 24 h later, the FCS free media was removed and replaced with DMEM + 0.1% BSA. 10 μ l DMEM + 0.1% BSA or VEGF₁₆₅ diluted in DMEM + 0.1% BSA (100 nM–30 pM final concentration) were then added and the cells incubated at 37°C/ 5% CO₂ for a further 5 h. After the 5 h incubation period, the experimental media was removed from the wells and 50 μ l of DMEM and 50 μ l ONE-Glo™ Luciferase Assay reagent was added to each well. A white plastic cover was placed over the bottom of the plate and luminescence was measured using a microplate scintillation and luminescence counter (TopCount NXT Packard) set to read at 19.1°C with a 5 min delay before reading relative luminescence units. An average of the counts per second, taken over 3 seconds, was used in all experimental analysis. Each individual experiment was performed in quadruplicate and repeated n number of times (n number per experiment specified in Section 3.3).

3.2.2 Experimental Method Protocol 2: The 'suspension' Method

VEGFR2 NFAT cells were seeded in a T75 at 5x10⁶ using DMEM + 10% FCS and incubated at 37°C/5% CO₂ for 3 days (until the media turned yellow and the flask was 100% confluent). On the 4th day cells were washed with PBS and

detached using 3 ml Versene. Once cells had detached, 6 ml of DMEM + 0.1% BSA was added and the cells were counted using a haemocytometer. Cells were centrifuged at 1000 rpm for 5 min and re-suspended in DMEM + 0.1% BSA. They were subsequently added to the well at a density of 40000 cells per well in white sided, clear, flat-bottomed, 96 well plates which had been coated with poly-D-lysine. Cells were incubated for 1 h at 37°C/5% CO₂ and then incubated with set concentrations of RTKI (10 µl diluted to 10x final concentrations in DMEM + 0.1% BSA) at 37°C/5% CO₂ for 1 h prior to the addition of 10 µl VEGF in DMEM + 0.1% BSA. VEGF was incubated with the cells at 37°C/5% CO₂ for 5 h. After the 5 h incubation, 100 µl ONE-Glo™ Luciferase Assay reagent was added to the wells and the plate was prepared and read as described in Section 3.2.1. Each individual experiment was performed in triplicate or quadruplicate and repeated n number of times (n number per experiment specified in Section 3.3).

3.2.3 Data Analysis

Data were fitted using non-linear regression (see Section 2.2.3). All data have been presented as mean ± SEM. Statistical significance was determined by either Student's T-test or a one or two way ANOVA with Dunnett's post-hoc analysis, where appropriate. P<0.05 was considered statistically significant. Data were fitted using non-linear regression (GraphPad Prism 6.00).

3.3 Results

3.3.1 Characterisation of the VEGF₁₆₅-Mediated NFAT Luciferase Response, in the Presence and Absence of RTKIs

VEGF₁₆₅ produced a concentration dependent increase in NFAT-mediated luciferase production (Figure 3.1). Cells cultured using the 'non-confluent monolayer method' gave a larger SEM and a lower signal: basal noise ratio between and within experiments (Figure 3.1) in comparison to experiments performed using the 'suspension method' (Figure 3.1). Due to this, it was decided that the more cell dense, suspension cell culture method, where cells were not allowed to form a monolayer would be used throughout the remainder of the study (protocol 2). VEGF₁₆₅ pEC₅₀ values obtained using this methodology were similar to those obtained using the non-confluent monolayer methodology, however the experimental window was larger and variation within and between experiments was reduced (Figure 3.1, Table 3.1).

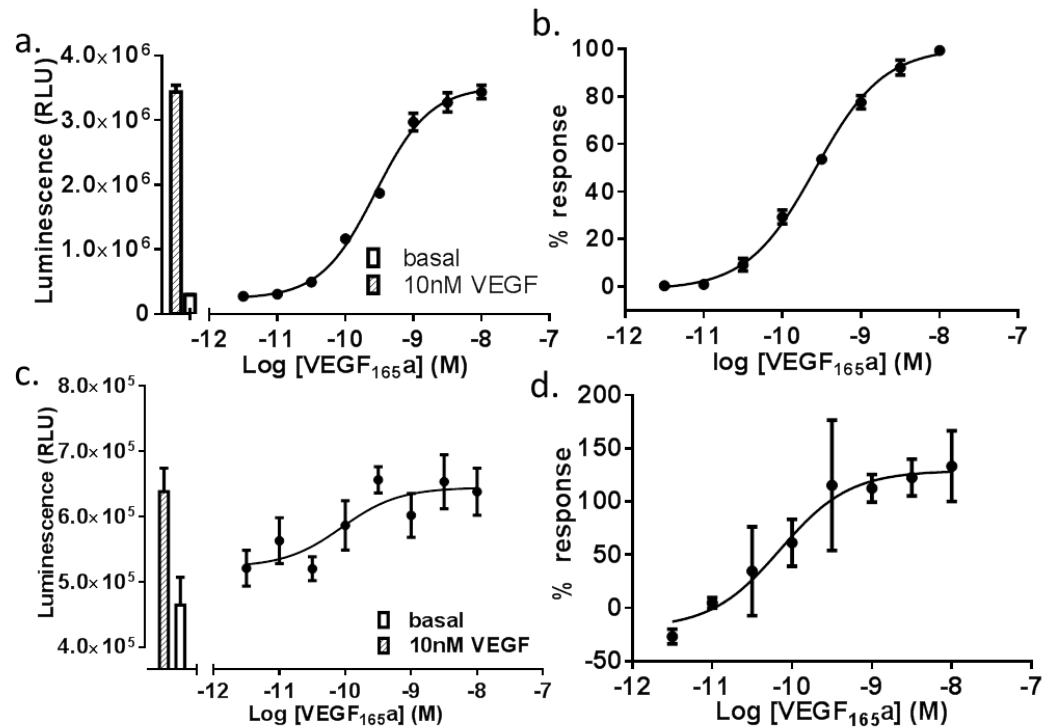


Figure 3.1 The effect of VEGF₁₆₅ on firefly luciferase production (luminescence measured using relative luminescence units (RLU)) in VEGFR2 NFAT Cells. Cells were treated with VEGF₁₆₅ either in suspension (a, b) or as a non-confluent monolayer (c, d). Graphs on the left are representative of one experiment (performed in quadruplicate), graphs on the right represent normalised pooled data (b n=10, d n=6), where 0% is defined as the basal luminescence count (RLU) and 100% is defined as the 10 nM VEGF₁₆₅ positive control luminescence count (RLU).

	VEGF ₁₆₅ mean±SEM (suspension)	VEGF ₁₆₅ mean±SEM (monolayer)
E _{max} (fold over basal)	8.30 ± 0.85	2.30±0.54
pEC ₅₀ (-log mol/L)	9.66 ± 0.05	10.09±0.27
n	10	6

Table 3.1 Comparison of the suspension or non-confluent monolayer cell culture methods on NFAT reporter gene responses following stimulation with VEGF₁₆₅. VEGFR2 NFAT cells were treated with VEGF₁₆₅ (in quadruplicate at each concentration in each experiment) either as suspension or as a non-confluent monolayer. Table 3.1 shows the E_{max} (fold over basal), demonstrating the size of assay window for each technique, the VEGF₁₆₅ pEC₅₀ (negative log of the EC₅₀ (mol/L)) and number of individual experiments performed (n) for each technique. Data are displayed as mean ± SEM. Students unpaired T test between group comparison demonstrated a significant difference between E_{max}.

Using the suspension method, all four VEGF RTKIs were shown to inhibit VEGF₁₆₅-NFAT-mediated luciferase production (Figure 3.2, Figure 3.3). The action of these compounds was not increased or diminished by DMSO (vehicle), which was used at a comparable concentration to the highest concentration of experimental compound used (as seen in Figure 3.2). pIC₅₀ values obtained for each compound were similar to the K_D values reported by Davis *et al.*, (Davis *et al.*, 2011), who used purified VEGFR2 kinase domains (Table 3.2) to look at RTKI binding. Although IC₅₀ values are related to affinity (K_D), they are an empirical measure which are dependent upon a number of different experimental factors. Perhaps most importantly, the IC₅₀ of competitive compounds is directly related to the concentration of agonist used to stimulate the system. In addition, where IC₅₀s are determined for compounds targeting intracellular binding sites, the membrane permeability of

compounds can have a significant impact on observed IC_{50} values, with poorly permeable compounds having much higher cellular IC_{50} s than their K_{is} measured against soluble purified catalytic domains. The observation that the cellular IC_{50} s observed in this study are similar to the K_D values reported for soluble catalytic domain (Gotink and Verheul, 2010; Davis *et al.*, 2011) suggests that these compounds are not competitive with VEGF and also readily cross the plasma membrane to access the intracellular binding site.

Sorafenib ($-25.0 \pm 2.6\%$, $n=5$) and vandetanib ($-23.0 \pm 3.7\%$, $n=5$) both caused a significant inhibition below constitutive (basal) activity ($P < 0.05$, paired T test, Figure 3.3 a, d). This may indicate that sorafenib and vandetanib have off target effects at higher concentrations. Cediranib and pazopanib did not show a marked inhibition below basal (Figure 3.3 b, c). However, when cediranib was incubated with unstimulated cells, an inhibition of basal readings was seen (Figure 3.4). This suggests that the inhibition below basal seen in these experiments is caused by off-target effects.

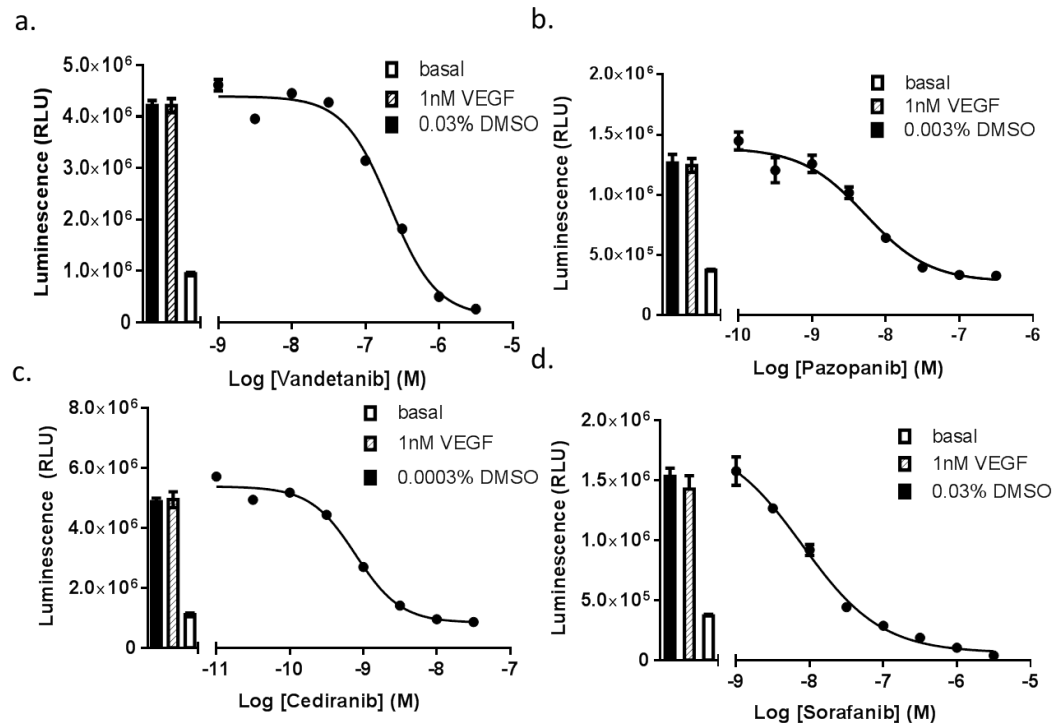


Figure 3.2 The effect of selected RTKIs on VEGF₁₆₅ stimulated firefly luciferase production in VEGFR2 NFAT cells in suspension (confluent method). VEGFR2 NFAT cells were pre-treated with vandetanib (n=1) (a), pazopanib (n=1) (b), cediranib (n=1) (c) and sorafenib (n=1) (d) for 1 h at 37°C/ 5% CO₂ before treatment with +1 nM VEGF₁₆₅ for 5 h at 37°C/ 5% CO₂. Data shows 1 representative experiment. Data are displayed as mean ± SEM. Each individual experiment was performed in quadruplicate. Student paired T test of basal value versus RTKI highest concentration showed vandetanib and sorafenib significantly inhibited constitutive activity.

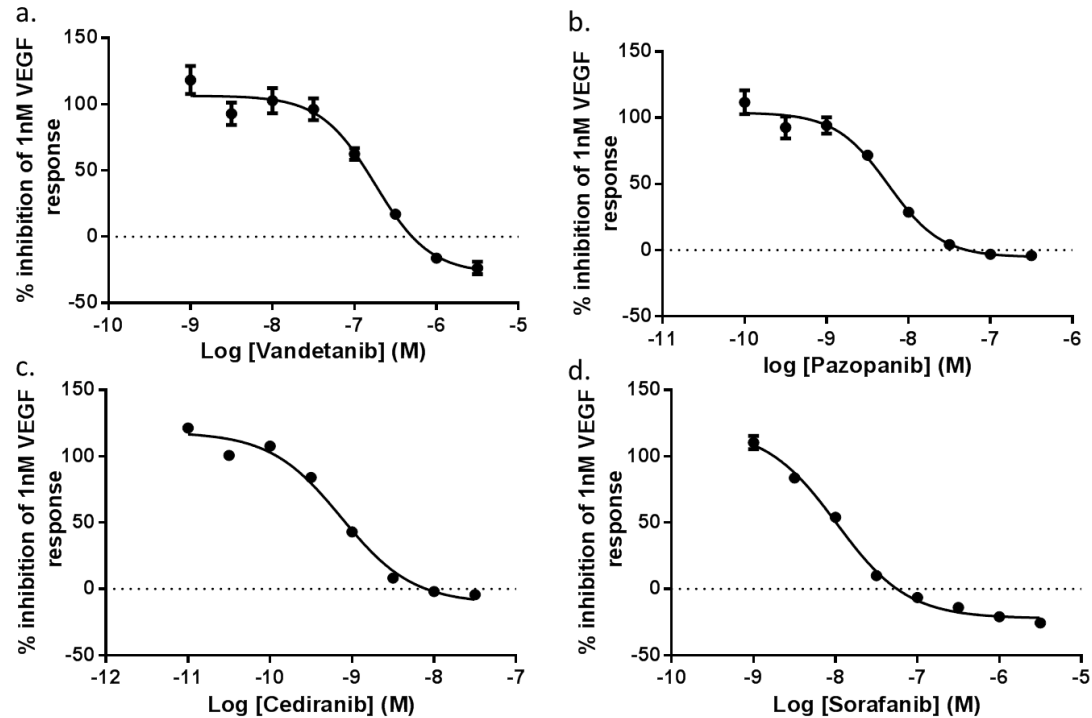


Figure 3.3 The effect of selected RTKIs on VEGF₁₆₅ stimulated firefly luciferase production in VEGFR2 NFAT cells in suspension (confluent method). VEGFR2 NFAT cells were pre-treated with vandetanib (n=5) (a), pazopanib (n=5) (b), cediranib (n=5) (c) and sorafenib (n=5) (d) for 1 h at 37°C/ 5% CO₂ before treatment with +1 nM VEGF₁₆₅ for 5 h at 37°C/ 5% CO₂. Data have been pooled and normalised to the corresponding basal and 1 nM VEGF₁₆₅ controls. Data are displayed as mean ± SEM. Each individual experiment was performed in quadruplicate. Student paired T test of basal value versus RTKI highest concentration showed vandetanib and sorafenib significantly inhibited constitutive activity.

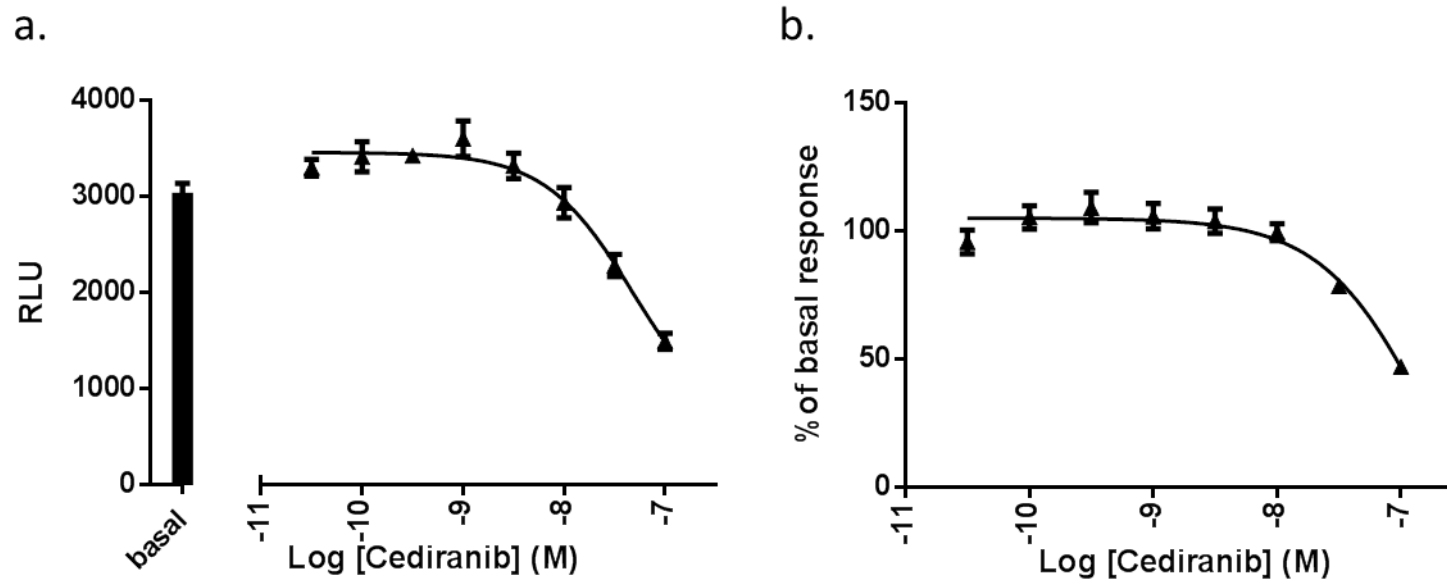


Figure 3.4. The effect of cediranib on basal NFAT-luciferase Production. VEGFR2 NFAT cells were pre-treated with cediranib for 1 h at 37°C/ 5% CO₂ before treatment with 10 µl DMEM+0.1% BSA for 5 h at 37°C/5% CO₂. Data shown in panel a. is representative of 1 experiment, whereas data shown in panel b. shows n=5 experiments which have been pooled and normalised to the basal response. Each individual experiment was performed in quadruplicate. Data are displayed as mean ± SEM.

	VEGF ₁₆₅ pIC ₅₀ mean±SEM (suspension)	n	Reported binding pK_D for purified kinase domain.*
Cediranib	9.13±0.01	5	8.96
Pazopanib	8.25±0.03	5	7.85
Sorafenib	8.01±0.06	5	7.23
Vandetanib	6.72±0.03	5	6.08

Table 3.2 RTKI pIC₅₀ values (negative log of the IC₅₀ (mol/L)) obtained from VEGF₁₆₅-mediated NFAT responses versus published pK_D values (negative log of the K_D (mol/L)) from purified kinase domains. VEGFR2 NFAT cells were treated with each RTKI + 1 nM VEGF₁₆₅. Data are presented as mean ± SEM of n separate experiments *pK_D values were taken from Davis *et al.*, 2011 (Davis *et al.*, 2011).

All four RTKIs inhibited VEGF₁₆₅-mediated NFAT activation in a non-competitive manner. This was demonstrated by the significant reduction in VEGF₁₆₅ E_{max} coupled with a relatively small shift in pEC₅₀ with increasing concentrations of each RTKI (Figure 3.5, Table 3.3). Each RTKI demonstrated a significant decrease in E_{max} (P<0.05, two-way ANOVA) between concentrations. VEGF₁₆₅ in the presence of the highest concentration of each RTKI showed a significant change in pEC₅₀ compared to VEGF₁₆₅ alone (P<0.05, two-way ANOVA).

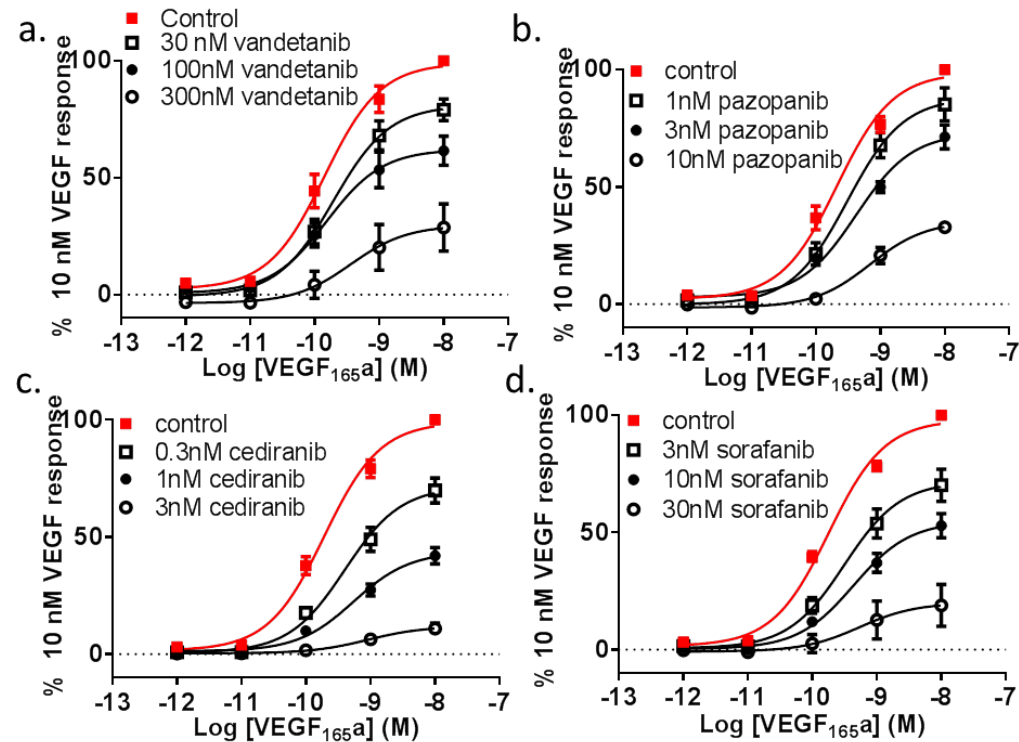


Figure 3.5 The effect of varying concentrations of RTKIs on VEGF₁₆₅-stimulated firefly luciferase production in VEGFR2 NFAT cells. VEGFR2 NFAT cells were treated with 10 nM VEGF₁₆₅ and varying concentrations of vandetanib (a), pazopanib (b), cediranib (c) and sorafenib (d). Data have been pooled and normalised to the corresponding basal and 10 nM VEGF₁₆₅ controls. Data displayed as mean ± SEM. Each individual experiment was performed in quadruplicate and repeated n=6 (cediranib), 5 (pazopanib), 7 (sorafenib) and 5 (vandetanib) times separately. Between group two-way ANOVA with dunnett's post hoc analysis was performed on E_{max} and EC₅₀ values.

vandetanib			pazopanib			cediranib			sorafenib		
nM	pEC ₅₀	% E _{max}	nM	pEC ₅₀	% E _{max}	nM	pEC ₅₀	% E _{max}	nM	pEC ₅₀	% E _{max}
0	9.90±0.14	100	0	9.66 ±0.11	100	0	9.68±0.09	100	0	9.72±0.06	100
30	9.77±0.10	81.0±4.1	1	9.50±0.09	85.2±7.0	0.3	9.40±0.10	64.8±10.4*	3	9.50±0.05	70.1±6.9*
100	9.75±0.12	58.5±5.7*	3	9.43±0.13	71.4±5.2*	1	9.28±0.12	31.1±6.6*	10	9.33±0.06*	52.9±5.1*
300	9.41±0.14*	29.5±7.9*	10	9.14±0.16*	32.8±2.0*	3	9.13±0.18*	8.8±1.9*	30	9.00±0.13*	18.9±8.9*

Table 3.3 The effect of pre-incubation with RTKI on VEGF₁₆₅-induced NFAT production. pEC₅₀ and E_{max} values for VEGF₁₆₅ were obtained in the presence of increasing concentrations of 4 RTKIs. Data shown are mean ± SEM. Each individual experiment was performed in quadruplicate and repeated n=6 (cediranib), 5 (pazopanib), 7 (sorafenib) and 5 (vandetanib) times separately. * P<0.05 compared to corresponding control in the absence of RTKI (between group two-way ANOVA with Dunnett's post-hoc analysis).

3.3.2 Characterisation of the VEGF_{165b} Mediated NFAT Luciferase Response, in the presence and absence of RTKIs

In comparison to VEGF₁₆₅, VEGF_{165b} was shown to be a lower efficacy agonist at VEGFR2 (Figure 3.6). VEGF_{165b} led to a concentration dependent NFAT-mediated luciferase production and had a pEC₅₀ of 9.21 ± 0.08 (n=5). When normalised to the 30 nM VEGF₁₆₅ response, VEGF_{165b} had an E_{max} of $62.1 \pm 1.2\%$ (n=5). As the EC₅₀ values demonstrated by VEGF₁₆₅ and VEGF_{165b} were similar, the data shown here suggest that although the efficacy between these two endogenous ligands is different, their potency is not.

As with VEGF₁₆₅, the four RTKIs inhibited VEGF_{165b} stimulation of the NFAT response element (Table 3.4). pIC₅₀ values for the four RTKIs in respect to inhibition of VEGF_{165b} signalling, were similar to those seen when using VEGF₁₆₅ stimulation (Table 3.2, Table 3.4).

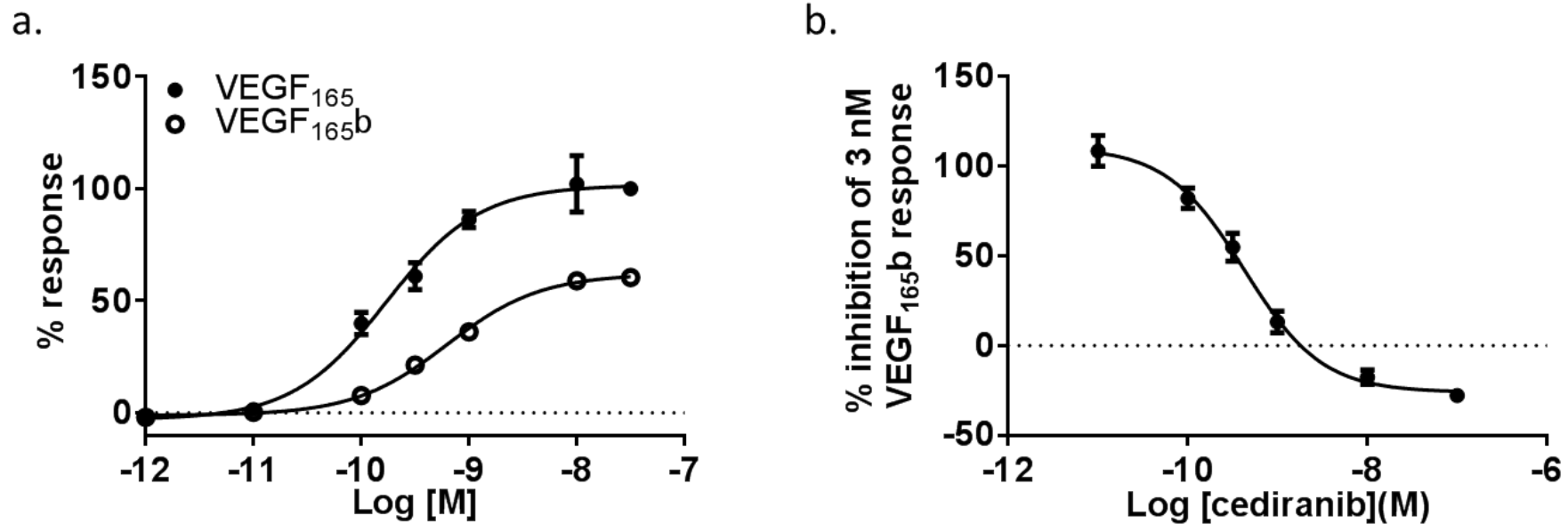


Figure 3.6 Characterisation of the VEGF_{165b}-mediated NFAT luciferase response. VEGFR2 NFAT cells were treated with increasing concentrations of VEGF₁₆₅ or VEGF_{165b} in order to investigate isoform specific differences in NFAT production (n=5) (a). VEGFR2 NFAT cells were also pre-treated with increasing concentrations of cediranib (1 h at 37°C/5% CO₂) followed by stimulation with 3 nM VEGF_{165b} (5 h at 37°C/5% CO₂) (n=5) (b). Data have been pooled and normalised to the corresponding basal and 30 nM VEGF₁₆₅ controls except for the data in b that have been normalised to 3 nM VEGF_{165b}. Data are displayed as mean ± SEM. Each individual experiment was performed in quadruplicate.

	Inhibition of 3nM VEGF₁₆₅b pIC₅₀	n
Cediranib	9.38±0.07	5
Pazopanib	8.29±0.10	8
Sorafenib	7.96±0.04	5
Vandetanib	7.00±0.04	6

Table 3.4 Inhibition of 3 nM VEGF₁₆₅b by four representative RTKIs. VEGFR2 NFAT cells were treated with increasing concentrations of each RTKI and 3 nM VEGF₁₆₅b. Data were presented as mean ± SEM of n separate experiments. Each individual experiment was performed in triplicate (vandetanib and sorafenib) or quadruplicate (cediranib and pazopanib). Individually fitted pIC₅₀ values were obtained from each individual experiment and then pooled to provide the mean ± SEM data provided here.

3.4 Discussion

In order to investigate the potency of vandetanib, sorafenib, cediranib and pazopanib at VEGFR2 in living cells, an NFAT reporter gene assay was used (Voon *et al.*, 2005). This also allowed for the quantitative analysis of RTKIs in the presence of VEGF₁₆₅ and VEGF_{165b} and for a comparison of VEGF₁₆₅ and VEGF_{165b}-mediated NFAT stimulation.

3.4.1 Methodology

Cells were treated either in a non-confluent monolayer (using protocol 1: Section 3.2.1) or in suspension (using protocol 2: Section 3.2.2). In experiments where cells were allowed to adhere to the base of the well, a large SEM and a low signal: basal noise ratio between and within experiments was seen (Figure 3.1c, d). However, when cells were grown to full confluence in a T75 flask and then used in suspension during the experimental procedure (Figure 3.1 a, b), the error within and between experiments was reduced. One reason for this difference may be the difference in cell cycle stage. Cells which have been cultured and maintained at 100% confluence (labelled here as suspension) are more likely to be in a state of quiescence (G0), or senescence (G1/S) where the cell is in a resting state and not preparing for mitosis (Patel *et al.*, 2005; Yoon and Seger, 2006), therefore the production and secretion of growth factors is reduced (Zhang *et al.*, 2004). Autocrine and paracrine signalling from growth factors produced by cells which are growing or preparing to go through mitosis would lead to a high basal level of bioluminescence (as seen in non-confluent monolayer experiments, Figure 3.1 c, d).

3.4.2 Characterisation of the VEGF₁₆₅ and VEGF_{165b} Mediated NFAT Luciferase Response

Both VEGF₁₆₅ and VEGF_{165b} were able to stimulate NFAT-mediated luciferase expression in a concentration dependent manner (Figure 3.6). Although both isoforms had very similar pEC₅₀ values (VEGF₁₆₅: 9.66 ± 0.05 vs VEGF_{165b}: 9.21 ± 0.08), VEGF_{165b} was a partial agonist of NFAT-luciferase production eliciting a maximal response that was $61.94\% \pm 2.26\%$ (mean \pm SEM) of that achieved by VEGF₁₆₅. The reduced efficacy of VEGF_{165b} at VEGFR2 compared with VEGF₁₆₅ had been previously reported by Woolard *et al* and others (Woolard *et al.*, 2004; Cebe Suarez *et al.*, 2006; Kawamura *et al.*, 2008; Catena *et al.*, 2010) and is thought to be caused by differences between the protein structure of VEGF₁₆₅ and VEGF_{165b} (Chapter 1, Section 1.2).

Another reason for the difference in the reported efficacy of VEGF_{165b} at VEGFR2 compared to VEGF₁₆₅ may be due to the cell type tested and/or the signalling cascade measured in the experiment. It has previously been shown that VEGF_{165b} is a lower efficacy agonist of VEGFR2-mediated MAPK phosphorylation in CHO cells transfected with VEGFR2 (Woolard *et al.*, 2004). However, VEGF_{165b} showed greater efficacy at VEGFR2 compared to VEGF₁₆₅ at the same signalling pathway in human microvascular ECs (Woolard *et al.*, 2004). This difference may be due to differences in receptor expression, downstream transcription machinery and/or receptor coupling efficiency between cell phenotypes.

3.4.3 The Action of RTKIs on the VEGF₁₆₅ and VEGF_{165b} Mediated NFAT Luciferase Response

The 4 RTKIs tested here (cediranib, vandetanib, sorafenib and pazopanib) demonstrated the ability to inhibit VEGFR2-NFAT signalling mediated by VEGF₁₆₅ and VEGF_{165b}. There was little difference in pIC₅₀ values for each RTKI between the two VEGF isoforms. As the binding target for all of the RTKIs tested is different from the binding site of VEGF₁₆₅ and VEGF_{165b} (intracellular kinase domain of the receptor vs Ig domain 2 and Ig domain 3 on the extracellular portion of the receptor) their ability to inhibit VEGFR2, regardless of ligand subtype (i.e. VEGF₁₆₅ or VEGF_{165b}) may be due to their allosteric action (Zhang *et al.*, 2009; Dosch and Ballmer-Hofer, 2010; Gotink and Verheul, 2010; Leppanen *et al.*, 2010; Davis *et al.*, 2011). This result also suggests that these RTKIs have lipophilic properties, allowing them to diffuse through the cell membrane and bind to the intracellular portion of the receptor in a whole cell system. Their ability to readily cross the cell membrane is further implied by the similarity between the IC₅₀ values gained here and Davis' K_D values calculated from isolated catalytic domains (Table 3.2) (Gotink and Verheul, 2010; Davis *et al.*, 2011).

Sorafenib and vandetanib both caused a significant inhibition (below basal) of VEGF₁₆₅ NFAT-luciferase activation (P<0.05, paired T test; Figure 3.3.a, d). This was also seen for cediranib, (P<0.05, paired T test; Figure 3.6.b) with VEGF_{165b}-mediated NFAT-luciferase activation. When cediranib was incubated with unstimulated cells it produced an inhibition of the basal RLU reading (Figure 3.4). Therefore, it is likely that RTKI inhibition below basal is due to the multi-targeted

nature of these RTKIs, allowing them to reduce basal NFAT activity via a different tyrosine kinase system.

All of the RTKIs tested demonstrated classical non-competitive antagonism of VEGFR2 (a significant decrease in E_{max} without a marked change in VEGF₁₆₅/VEGF_{165b} EC_{50} (Figure 3.5)), an outcome that is likely to be due to the difference in ligand and drug receptor binding sites. A decrease in E_{max} occurs when an antagonist, in this case an RTKI, is able to remove a proportion of the signalling receptor population from the system, reducing the ability for the agonist (in this case VEGF) to produce a full response, regardless of concentration, resulting in the EC_{50} remaining relatively constant.

3.4.4 Conclusion

In conclusion, cediranib, sorafenib, pazopanib and vandetanib have been shown to non-competitively (Figure 3.5) inhibit VEGF₁₆₅- and VEGF_{165b}-VEGFR2 mediated activation of the NFAT-luciferase reporter gene, demonstrating nano-molar IC_{50} values (Table 3.2, Table 3.4). Finally, both VEGF₁₆₅ and VEGF_{165b} were shown to stimulate VEGFR2-mediated NFAT-luciferase activation; however the efficacy of VEGF_{165b} at VEGFR2 was lower than VEGF₁₆₅ (Figure 3.6).

Based on the data discussed in this Chapter, vandetanib and pazopanib, two class I RTKIs with different IC_{50} values were selected to be characterised *in vivo*. By being able to relate the inhibition of VEGFR2 by pazopanib and vandetanib *in vitro* to the hypertensive side effect profile of vandetanib and pazopanib *in vivo*, the importance of VEGF signalling in VEGF RTKI induced hypertension can be further explored.

Chapter 4: The *In Vivo* Cardiovascular Actions of Vandetanib

4.1 Introduction

Approximately 23%, up to as many as 90%, of the patient populations taking VEGF therapies develop hypertension or experience a worsening in their existing hypertensive condition (Hamberg *et al.*, 2010; La Vine *et al.*, 2010; Aparicio-Gallego *et al.*, 2011; Bible *et al.*, 2014). The development and escalation of pre-existing hypertension in these patient populations has been linked to multiple severe complications including venous or arterial thrombo-embolisms, acute heart failure, proteinuria, haemorrhage and reversible posterior leukoencephalopathy syndrome (Govindarajan *et al.*, 2006; Chu *et al.*, 2007; Pouessel and Culine, 2008; Eschenhagen *et al.*, 2011). A deeper understanding of the acute and chronic hypertensive effects of RTKIs may help to elucidate the physiological sequelae responsible.

With this in mind, the hypertensive effect of vandetanib, a VEGFR2, VEGFR3, EGFR and RET kinase inhibitor (see Section 1.3.1.1) approved for the treatment of medullary thyroid cancer, was explored in the rat. Regular (1 min recording every 15 min) recordings of heart rate and mean arterial blood pressure were taken with the intention of exploring the long term effects of vandetanib (21 day treatment; 25 mgkg⁻¹day⁻¹ i.p) on blood pressure and heart rate. The post-treatment effects of vandetanib (measured for 10 days post-treatment) were also analysed with the aim of investigating whether vandetanib-induced cardiovascular physiological changes, such as vessel rarefaction.

Mesenteric mesothelium were taken from rats involved in the study described above and stained for ECs with the hope of better understanding the effects of vandetanib on vessel

structure over time. It is currently thought that a key mechanism by which VEGF RTKIs, such as vandetanib, cause hypertension is vascular rarefaction (Small *et al.*, 2014). Vascular rarefaction is the process of vessel regression, reducing the density of the microvascular network and therefore increasing blood pressure (Feihl *et al.*, 2006; see Section 1.2.5). Rarefaction has previously been described in *in vivo* models of hypertension, within multiple tissue types such as the mesentery, cremaster muscle, skin and brain showing these vascular changes (Triantafyllou *et al.*, 2015). Rarefaction has also been implicated as a possible cause of VEGF RTKI induced hypertension, with Steeghs *et al* demonstrating a reduction in capillary density in humans during a phase I trial for telatanib, a VEGFR2, VEGFR3 and PDGFR- β RTKI (Steeghs *et al.*, 2008; Mross *et al.*, 2011).

In the study presented herein, the regional haemodynamic effects of vandetanib on heart rate, mean arterial blood pressure and mesenteric, renal and hindquarter vascular conductances over a period of 4 days were also investigated. Although it is widely known that VEGF RTKIs cause hypertension in humans (Lankhorst *et al.*, 2015; Abi Aad *et al.*, 2015; Kruzliak *et al.*, 2014), there has been little or no investigation into the regional haemodynamic effects of these compounds in either animal models or human subjects. Understanding how vandetanib affects blood flow to specific vascular beds may help to elucidate some of the physiological processes responsible for the wide range of side effects caused by vandetanib.

4.2 Methodology

4.2.1 Time Course of the Effects of Vandetanib on Cardiovascular Variables, Measured By Radio-Telemetry

Rats were implanted with radio-telemetry devices as described in Chapter 2.4. Ten days post-surgical implantation of the radio-telemetry device, mean arterial blood pressure and heart rate were monitored and recorded for 1 min, every 15 min, for 9 days. Rats were randomly assigned to be administered 0.5 ml of either 25 mgkg⁻¹day⁻¹ vandetanib i.p (Sequoia research products, SRP0098v), diluted in vehicle (2% Tween, 5% propylene glycol in 0.9% saline solution) (n=7) or vehicle (n=5) for 21 days. A post-treatment monitoring period of 10 days was observed (Figure 4.1).



Figure 4.1 Schematic diagram of the vandetanib 25 mgkg⁻¹day⁻¹ i.p radio-telemetric experimental timeline.

4.2.1.1 Statistical Analysis

All data have been expressed as mean \pm SEM with significance being accepted at $P < 0.05$. A Kolmogorov-Smirnoff test was performed to test for normality. This test showed data was not normally distributed. A non-parametric, two-tailed within group comparison (Friedman's test) was performed to determine if any changes seen from the baseline value were significant. A non-parametric between group two tailed comparison (Mann Whitney-U test) was performed to analyse whether differences between test groups were significant. This was done using Graphpad prism 6.00.

4.2.2 The Action of Vandetanib on Mesenteric Vessel Structure Following *In Vivo* Dosing For 21 Days and a Post-Treatment Period of 10 Days

On the final day of the telemetric study, as described in Section 2.3, rats were killed with 50 mgkg⁻¹ pentobarbitone i.p and the mesentery was removed (as detailed in Section 2.4). The mesentery was washed with PBS and fixed in 4% paraformaldehyde (pH 7.4) before 4 mesenteric membranous panels were isolated, washed in PBX (0.5% Triton-X100 in PBS for 1 h) and incubated in 1% BSA-PBX for 1 h. Mesenteric panels were then incubated over night at 4°C with 10 µgml⁻¹ biotinylated Isolectin GS-IB4 (from *Griffonia simplicifolia*; Molecular Probes), washed with PBX for 1 h and incubated with 1 µgml⁻¹ TRITC-labelled streptavidin (S-870 Molecular Probes) for 2 h to stain ECs. Mesenteric panels were washed with PBX for 1 h and then incubated with Hoechst (2 µgml⁻¹ diluted in BSA-PBX 30 min), to stain for cell nuclei, before being mounted onto APES coated microscopy slides with fluorescence mounting media.

4.2.2.1 Data Analysis

Images (16 bit) were taken on a Zeiss Axio observer Z1 using a Hamamatsu Orca flash 4 C11440 HD camera and an EC-Plan neofluor 10x/-0.3 ph1 objective. Images were analysed using Angiotool 0.6b (Zudaire *et al.*, 2011). All analysis was blinded. Data were collated and plotted to show mean ± SEM using Microsoft Excel 2010 and GraphPad Prism 6.00. Statistical significance was determined using an unpaired one tailed Mann Whitney-U test (P<0.05).

4.2.3 Regional Haemodynamic Effects of Vandetanib Measured by Pulsed Doppler Flowmetry (i.v)

Rats were implanted with miniature pulsed Doppler flow probes and intra-vascular catheters as described in Section 2.6. Starting 24 h after catheter surgery, animals were randomly assigned to be administered with a 0.4 ml priming bolus dose of vandetanib (Sequoia research products, SRP0098v) at $12.5 \text{ mgkg}^{-1}\text{h}^{-1}$ (n=6), $25 \text{ mgkg}^{-1}\text{h}^{-1}$ (n=6) or vehicle (2% Tween 80, 5% propylene glycol in 0.9% saline) (n=6) i.v infused over 6 min once every 24 h. 0.4 ml of vandetanib or vehicle was then immediately infused over 45 min at a concentration of $12.5 \text{ mgkg}^{-1}\text{h}^{-1}$. Cardiovascular variables were recorded continuously for 4.5 h per day over a 4-day period (Figure 4.2).

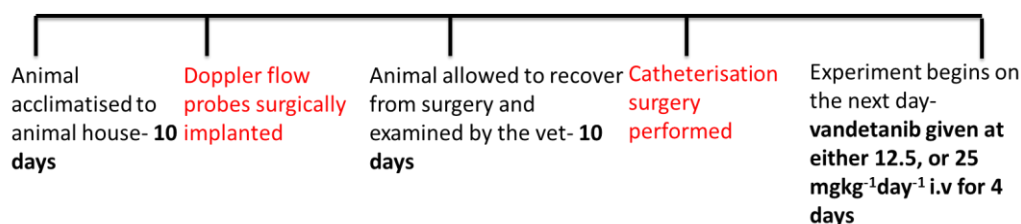


Figure 4.2 Schematic diagram of the vandetanib i.v Pulsed Doppler Flowmetry experimental timeline.

4.2.4 Regional Haemodynamic Effects of Vandetanib Measured by Pulsed Doppler Flowmetry (i.p)

Rats were implanted with miniature pulsed Doppler flow probes and intra-vascular catheters as described in Section 2.6. Starting 24 h after catheter surgery, animals were randomly assigned to be administered with a 0.5 ml bolus dose of vandetanib (Sequoia research products, SRP0098v) at $12.5 \text{ mgkg}^{-1}\text{day}^{-1}$ (n=8), $25 \text{ mgkg}^{-1}\text{day}^{-1}$ (n=8), $50 \text{ mgkg}^{-1}\text{day}^{-1}$ (n=8) or vehicle (n=8) (2% Tween 80, 5% propylene glycol in 0.9% saline), i.p once every 24 h.

Cardiovascular variables were recorded continuously for 4.5 h per day over a 4-day period (Figure 4.3).

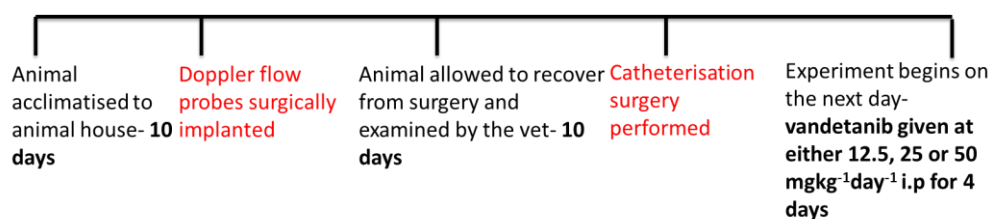


Figure 4.3 Schematic diagram of the vandetanib i.p Pulsed Doppler Flowmetry experimental timeline.

4.2.4.1 Statistical Analysis

All data have been expressed as mean \pm SEM with significance being accepted at $P < 0.05$. A Kolmogorov-Smirnoff test was performed to test for normality. This test showed data was not normally distributed. A non-parametric, two-tailed within group analysis (Friedman's test) was performed to determine if changes seen from baseline values were significant.

Non-parametric between group two tailed comparisons (Mann Whitney (for 2 groups) and Kruskal Wallis (more than 2 groups) were performed to test for significant differences between groups. All statistical analyses were performed using Biomedical version 3.4 (Nottingham, UK).

4.3 Results

4.3.1 Time Course of Effects of Vandetanib on Cardiovascular Variables Measured By Radio-Telemetry

Effects of vandetanib on cardiovascular variables measured by radio-telemetry are shown on Figure 4.1, Figure 4.2, Figure 4.3, Figure 4.4, Table 4.1 and Table 4.2.

4.3.1.1 Mean Arterial Blood Pressure

Mean arterial blood pressure remained steady throughout the 9 day pre-treatment period in both the vandetanib and vehicle groups, mean arterial blood pressure did not change significantly throughout the study for the vehicle group (Figure 4.4). In rats administered vandetanib ($25 \text{ mg kg}^{-1} \text{ day}^{-1}$) i.p, mean arterial blood pressure increased significantly by $4.5 \pm 0.3 \text{ mmHg}$ ($P < 0.05$, Friedman) during the first 24 h of the treatment period (Figure 4.4, Table 4.1). This pressor effect was maintained throughout the remainder of the dosing period. However, when the peak plasma concentration time range (4-8 h post-dosing) (Ton *et al.*, 2013) was analysed (see Section 1.3.1.1 for more detail), a significant increase of $+13.8 \pm 2.6 \text{ mmHg}$ from baseline was seen on day 2 of treatment (Figure 4.4, Table 4.1). This finding was mirrored when the data were analysed in 3 h time slots ($P < 0.05$, Friedman comparison against mean daytime (06:00-18:00) baseline data) (Figure 4.4). The rise in mean arterial blood pressure (mmHg) was significantly different from the vehicle group ($P < 0.05$, Mann Whitney; Figure 4.1) and was maintained throughout the 21 day dosing period ($P < 0.05$, Friedman; Figure 4.4, Table 4.1).

During the post-dosing observation period, mean arterial blood pressure decreased from $+10.9 \pm 0.4$ mmHg to $+8.4 \pm 0.6$ mmHg ($25 \text{ mgkg}^{-1}\text{day}^{-1}$ i.p) on the 7th day after treatment (Figure 4.4, Table 4.1). The decrease was maintained for the remainder of the post dosing period (Figure 4.4, Table 4.1). The steady decline in mean arterial blood pressure over the 10 day post-dosing observation period can be seen in more detail in Figure 4.4d., which shows the final day of treatment followed by the 10 day post-treatment observation period analysed in 3 h time slots. At the end of the study (Day 10 post-treatment period), there was no significant difference between the vandetanib and vehicle groups. The vandetanib treatment group had a mean arterial blood pressure of $+4.4 \pm 0.4$ mmHg, whereas the vehicle group had a mean arterial blood pressure of $+2.4 \pm 0.4$ mmHg above baseline (Table 4.1). Of interest a daytime/ night-time increase and decrease in mean arterial blood pressure can be clearly seen in Figure 4.4c, d. This was further explored in Figure 4.5.

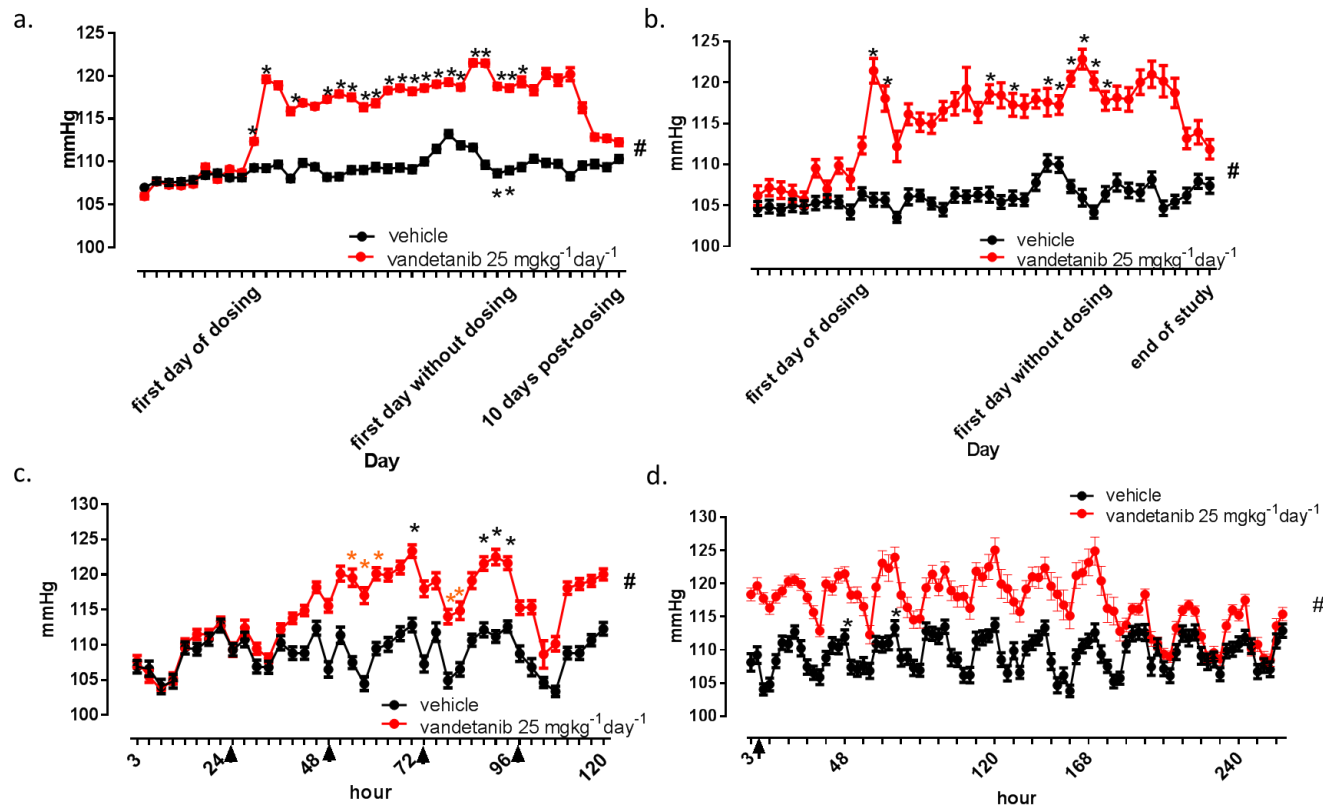


Figure 4.4. Mean arterial blood pressure of male Sprague Dawley rats dosed with vandetanib 25 mgkg⁻¹day⁻¹ i.p (n=7) vs vehicle (n=5). Data displayed as mean ± SEM. Data were analysed and displayed in 24 hour bins (a), 4-8 h after dosing (b) or in 3 h bins, separated into the last day prior to dosing and the first 4 days of dosing (c) or the last day of dosing followed by the 10 day post-treatment period (d). Red line- vandetanib 25 mgkg⁻¹day⁻¹ i.p, black line- vehicle i.p #-P<0.05 Mann Whitney between group comparison *-P<0.05 Friedman test with data points compared against the mean of the 9 day pre-treatment period (a, b) or against the mean daytime (06:00-18:00) (orange*) and mean nighttime (18:00-06:00) (black*) values (c, d). Arrows show dosing times (c, d)

	24 h Vehicle		24 h Vandetanib 25 mgkg ⁻¹ day ⁻¹		4-8 h Post-treatment vehicle		4-8 h Post-treatment vandetanib 25 mgkg ⁻¹ day ⁻¹	
	Mean	SEM	Mean	SEM	Mean	SEM	Mean	SEM
Baseline	0.0	0.2	0.0	0.1	0.0	0.3	0.0	0.7
Day 1	1.4	0.4	4.5	0.3	1.5	0.7	4.7	1.1
Day 2	1.3	0.4	11.7	0.4	0.7	0.8	13.8	1.6
Day 3	1.8	0.4	11.0	0.4	0.7	0.8	10.4	1.6
Day 4	0.1	0.4	8.0	0.4	-1.4	0.6	4.6	1.9
Day 5	1.9	0.4	9.0	0.3	1.1	1.0	8.5	1.4
Day 6	1.5	0.4	8.6	0.3	1.2	0.7	7.6	1.2
Day 7	0.3	0.4	9.4	0.3	0.3	0.7	7.4	1.3
Day 8	0.3	0.4	10.0	0.3	-0.5	0.8	9.0	1.2
Day 9	1.1	0.4	9.7	0.4	1.3	0.9	9.8	1.5
Day 10	1.1	0.4	8.5	0.4	1.1	0.7	11.6	2.7
Day 11	1.4	0.5	9.0	0.4	1.3	0.8	8.7	1.3
Day 12	1.3	0.5	10.4	0.3	1.3	0.9	11.0	1.2
Day 13	1.4	0.4	10.7	0.3	0.5	0.8	10.8	1.6
Day 14	1.2	0.4	10.3	0.4	0.9	0.9	9.7	1.5
Day 15	2.1	0.4	10.7	0.4	0.7	0.7	9.5	1.5
Day 16	3.6	0.4	11.2	0.3	2.8	1.0	10.4	1.2
Day 17	5.3	0.4	11.4	0.4	5.2	1.0	10.0	1.8
Day 18	4.0	0.4	10.8	0.4	5.0	0.9	9.6	1.3
Day 19	3.7	0.4	13.7	0.4	2.3	0.8	12.8	1.0
Day 20	1.7	0.4	13.6	0.3	1.0	1.0	15.2	1.3
Day 21	0.7	0.4	10.9	0.4	-0.8	0.8	12.6	1.2
Day 1	1.1	0.4	10.7	0.4	1.4	0.9	10.2	1.3
Day 2	1.5	0.4	11.5	0.6	2.8	1.1	10.6	1.5
Day 3	2.4	0.4	10.5	0.5	1.9	0.9	10.3	1.5
Day 4	1.9	0.4	12.4	0.6	1.6	1.0	12.4	1.6
Day 5	1.8	0.4	11.6	0.6	3.2	0.9	13.4	1.7
Day 6	0.4	0.4	12.4	0.8	-0.3	0.9	12.6	2.0
Day 7	1.6	0.4	8.4	0.6	0.5	0.8	11.1	1.9
Day 8	1.8	0.4	5.0	0.4	1.3	0.9	5.6	1.4
Day 9	1.4	0.4	4.9	0.4	3.0	0.9	6.3	1.5
Day 10	2.4	0.4	4.4	0.4	2.4	0.9	4.3	1.3

Table 4.1 Mean \pm SEM change from baseline (defined as the mean value of the 9 day pre-treatment period) mean arterial blood pressure of male Sprague Dawley rats dosed with vandetanib 25 mgkg⁻¹day⁻¹ i.p (n=7) vs vehicle (n=5). Data were analysed and displayed in 24 h bins (left) or 4-8 h Sections after dosing (right). Black baseline: average of 9 days pre-treatment period; blue text: treatment period; red text: post-treatment period.

Due to the daytime/ night-time pattern seen in the mean arterial blood pressure recordings (Figure 4.4d) the data were analysed in two 12 h slots (06:00-18:00 h or 18:00-06:00 h) (Figure 4.5). Changes in mean arterial blood pressure in response to vandetanib ($25 \text{ mgkg}^{-1}\text{day}^{-1}$ i.p) or vehicle, i.p followed the same trend (pre-, during- and post- treatment) as the data presented in Figure 4.4a, b (analysed over 24 h or 4-8 h post-dosing). The average mean arterial blood pressure was higher during the night-time throughout the study (Figure 4.5).

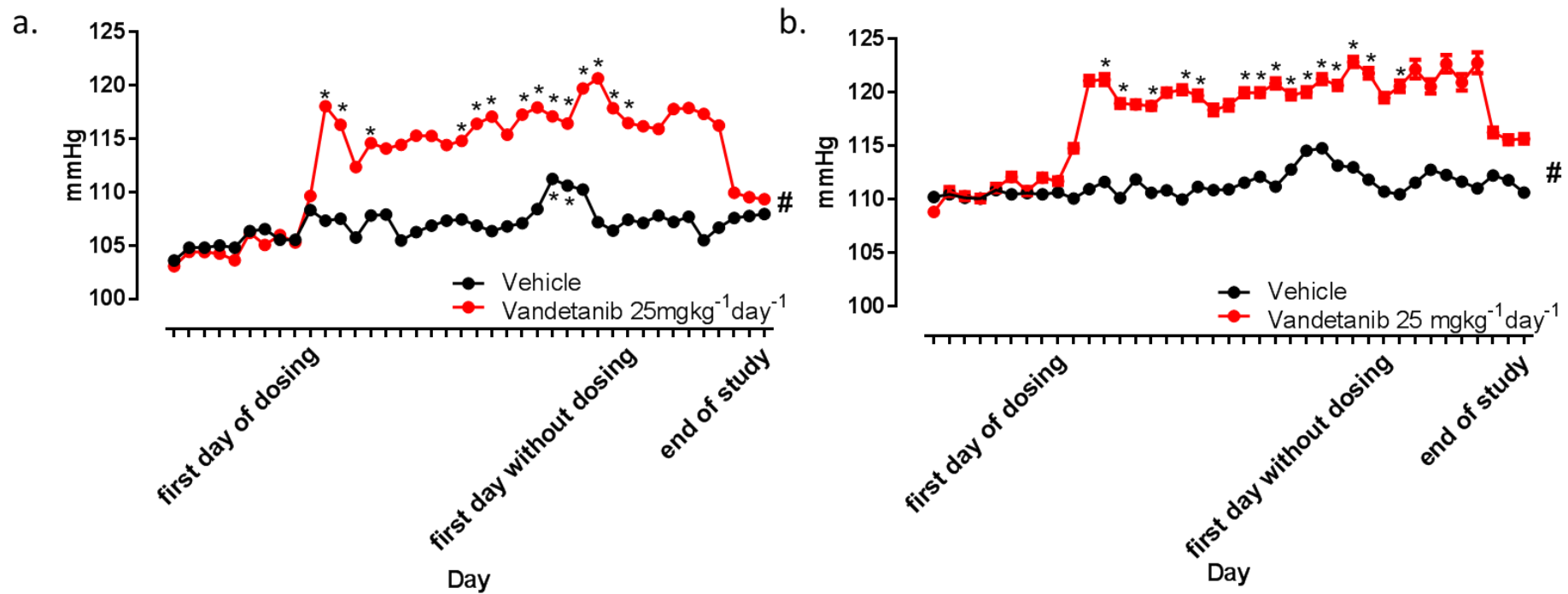


Figure 4.5 Mean arterial blood pressure of male Sprague Dawley rats dosed with vandetanib 25 mgkg⁻¹day⁻¹ i.p (n=7) vs vehicle (n=5). Data displayed are mean ± SEM. Data were analysed and displayed in 12 h bins, separated into (a) daytime (06:00-18:00) or (b) night-time (18:00-06:00). Red line- vandetanib 25 mgkg⁻¹day⁻¹ i.p, black line- vehicle i.p #-P<0.05 Mann Whitney between group comparison *-P<0.05 Friedman test with data points compared against the mean 9 day pre-treatment period.

4.3.1.2 Heart Rate

In the vehicle group, heart rate was significantly higher compared to the vandetanib group prior to vandetanib administration (Figure 4.6). Over the 21 day treatment period, and during the 10 day post-treatment period, heart rate in the vehicle group gradually reduced such that by the end of the study it was -40 ± 3 BPM lower than at the start (Table 4.2).

The pattern of heart rate change was similar in the vandetanib group to that seen in the vehicle-treated group (Figure 4.6, Table 4.2).

The average heart rate (throughout the study) was lower in the vehicle group in the 4-8 h post-dosing data analysis (330 ± 2 BPM) compared to the 24 h analysis (366 ± 2 BPM (Table 4.2)). There was a similar reduction in heart rate in the vandetanib group ($25 \text{ mgkg}^{-1}\text{day}^{-1}$, i.p). The average heart rate, over the entire study, was approximately 320 ± 1 BPM (4-8 h post-dosing) compared to 358 ± 1 BPM (24 h analysis (Figure 4.6, Table 4.2)) in the vandetanib group.

There was a significant difference between the vehicle and vandetanib groups ($P < 0.05$, Mann Whitney; Figure 4.6) during the last day of baseline recording and the first 4 days of treatment, however, there was no significant difference between groups in the last day of treatment and 10 days post-treatment observation period (Mann Whitney). There were no significant changes in heart rate in the vehicle or vandetanib groups during the last 10 days of dosing (Friedman compared to the last 24 h of dosing) (Figure 4.6).

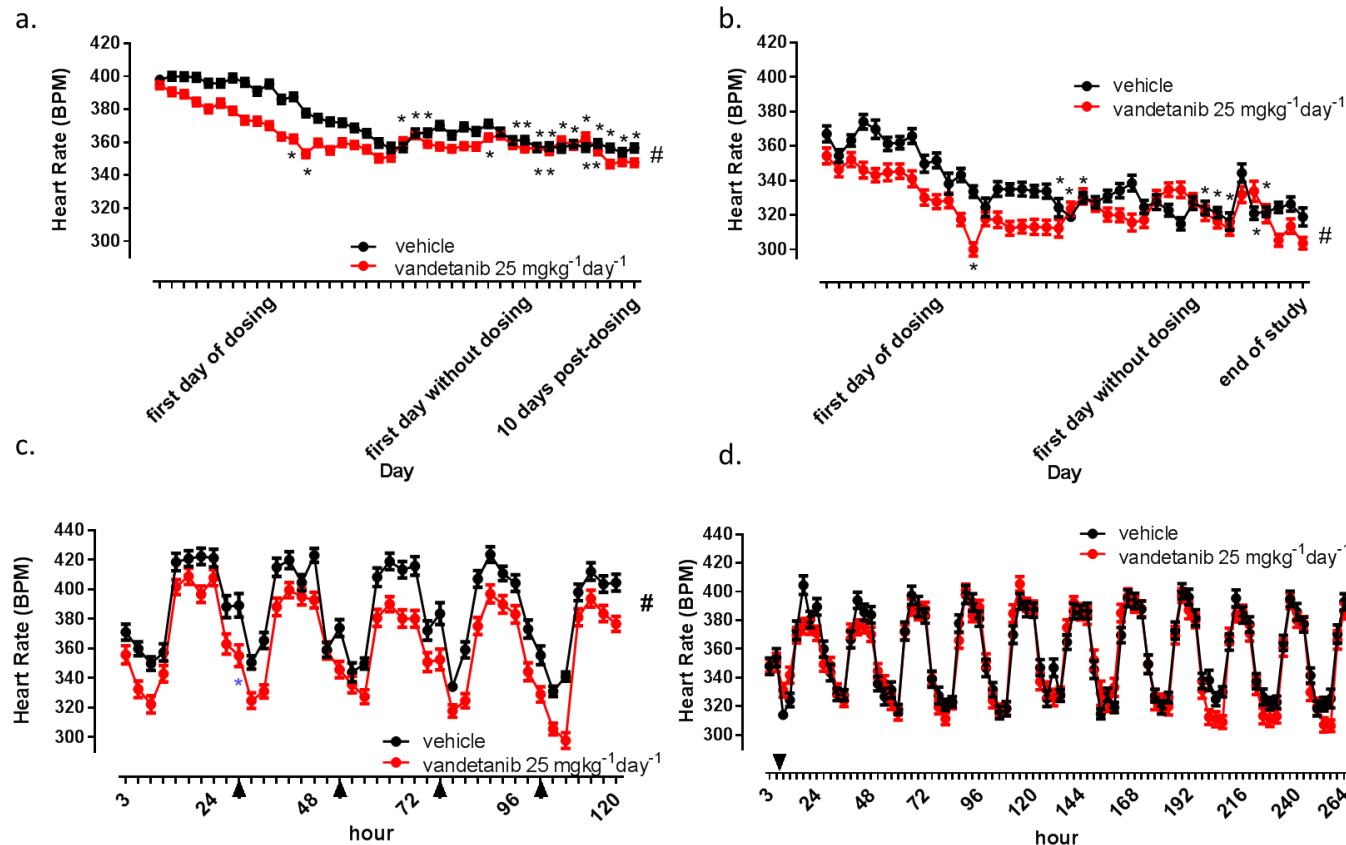


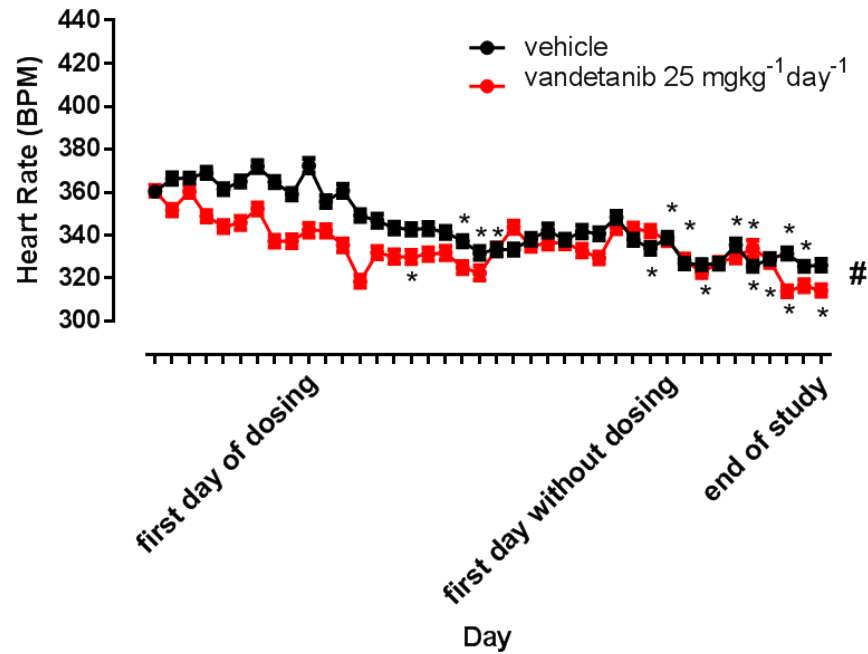
Figure 4.6 Mean heart rate of male Sprague Dawley rats dosed with vandetanib 25 mgkg⁻¹day⁻¹ i.p (n=7) vs vehicle (n=5). Data are displayed as mean \pm SEM. Data were analysed and displayed in 24 h bins (a), 4-8 h after dosing (b) or in 3 h bins, separated into the last day prior to dosing and the first 4 days of dosing followed by a 10 day post-treatment period (d). Red line shows data obtained with vandetanib 25 mgkg⁻¹day⁻¹ i.p. Black line shows the vehicle control i.p. #P<0.05 Mann Whitney between group comparison *-P<0.05 Friedman test with data points compared against the mean of the 9 day pre-treatment period (a, b) or against the mean daytime (06:00-18:00 h) (blue*) and mean night-time (18:00-06:00 h) (black*) values (c, d).-Arrows show dosing times (c, d)

	24 h Vehicle		24 h Vandetanib 25 mgkg ⁻¹ day ⁻¹		4-8 h Post-treatment vehicle		4-8 h Post-treatment vandetanib 25 mgkg ⁻¹ day ⁻¹	
	Mean	SEM	Mean	SEM	Mean	SEM	Mean	SEM
Baseline	0.0	1.1	0.0	0.1	0.0	4.1	0.0	3.2
Day 1	-2.0	2.5	4.5	0.3	-12.0	5.2	-15.9	4.6
Day 2	-11.3	2.5	11.7	0.4	-25.6	6.8	-15.2	4.8
Day 3	-9.7	2.5	11.0	0.4	-20.5	4.8	-26.3	4.2
Day 4	-19.5	2.5	8.0	0.4	-30.1	4.5	-43.6	4.5
Day 5	-22.7	2.5	9.0	0.3	-39.3	6.1	-25.9	4.5
Day 6	-24.9	2.4	8.6	0.3	-28.6	5.2	-26.5	5.0
Day 7	-25.4	2.4	9.4	0.3	-28.8	4.3	-31.4	4.5
Day 8	-28.6	2.4	10.0	0.3	-28.6	4.9	-30.4	4.3
Day 9	-31.8	2.4	9.7	0.4	-29.8	4.4	-30.5	4.9
Day 10	-37.7	2.6	8.5	0.4	-29.9	5.0	-30.7	4.7
Day 11	-40.7	2.9	9.0	0.4	-39.4	6.1	-31.4	5.6
Day 12	-40.4	2.6	10.4	0.3	-44.8	4.0	-20.1	4.6
Day 13	-31.6	2.6	10.7	0.3	-33.7	4.2	-12.9	4.9
Day 14	-31.5	2.5	10.3	0.4	-36.3	4.5	-18.2	4.0
Day 15	-27.2	2.6	10.7	0.4	-32.6	4.4	-23.4	4.4
Day 16	-32.9	2.4	11.2	0.3	-29.5	5.0	-23.8	4.3
Day 17	-28.0	2.5	11.4	0.4	-25.2	5.4	-27.9	5.4
Day 18	-30.7	2.5	10.8	0.4	-39.1	4.8	-26.6	4.8
Day 19	-26.1	2.4	13.7	0.4	-36.2	5.2	-13.5	4.7
Day 20	-31.1	2.5	13.6	0.3	-40.9	4.5	-9.0	4.5
Day 21	-36.2	2.5	10.9	0.4	-48.8	4.6	-8.9	5.0
Day 1	-36.0	2.3	10.7	0.4	-36.8	4.8	-14.7	4.2
Day 2	-40.4	2.6	11.5	0.6	-39.6	4.9	-22.5	4.8
Day 3	-39.8	2.5	10.5	0.5	-42.3	4.2	-27.4	4.4
Day 4	-40.9	2.5	12.4	0.6	-47.5	5.8	-31.8	4.2
Day 5	-38.3	2.3	11.6	0.6	-19.4	6.0	-11.8	5.1
Day 6	-40.5	2.4	12.4	0.8	-42.7	4.6	-9.9	6.2
Day 7	-38.0	2.5	8.4	0.6	-41.8	4.0	-22.8	5.7
Day 8	-40.7	2.4	5.0	0.4	-39.3	4.1	-38.2	4.1
Day 9	-43.3	2.4	4.9	0.4	-37.4	5.0	-30.1	4.8
Day 10	-40.7	2.6	4.4	0.4	-44.8	5.9	-40.0	4.0

Table 4.2 Mean \pm SEM change from baseline (defined as the mean value of the 9 day pre-treatment period) heart rate of male Sprague Dawley rats dosed with vandetanib 25 mgkg⁻¹day⁻¹ i.p (n=7) vs vehicle (n=5). Data displayed are mean \pm SEM. Data were analysed and displayed in 24 h bins (left) or 4-8 h Bins after dosing (right). Black baseline: average of 9 days pre-treatment period; blue text: treatment period; red text: post-treatment period.

A daytime/ night-time elevation and reduction in heart rate can be clearly seen in Figure 4.6c, d. Therefore data were analysed in as two 12 h slots (06:00-18:00 h or 18:00-16:00 h) (Figure 4.7). Changes in heart rate in response to vandetanib ($25 \text{ mgkg}^{-1}\text{day}^{-1}$, i.p) or vehicle i.p followed the same trend (pre-, during- and post-treatment) as the data presented in Figure 4.6a, b. (analysed over 24 h or 4-8 h post-treatment). However there was an average difference of 52 BPM between the daytime (Figure 4.7.a.) and night-time (Figure 4.7b) data, with the night-time heart rate being higher throughout the study (Figure 4.7).

a.



b.

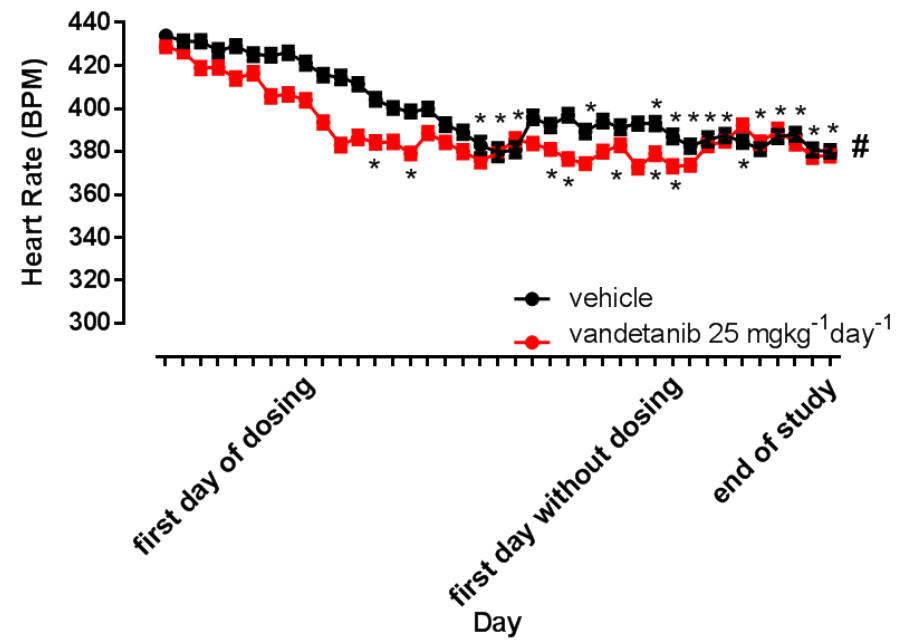


Figure 4.7 Mean heart rate of male Sprague Dawley rats dosed with vandetanib $25 \text{ mgkg}^{-1}\text{day}^{-1}$ i.p. ($n=7$) vs vehicle i.p. ($n=5$). Data displayed as Mean \pm SEM. Data were analysed and displayed in 12 h bins from 06:00-18:00 h (a) or from 18:00-06:00 h (b). Red line- vandetanib $25 \text{ mgkg}^{-1}\text{day}^{-1}$, i.p, black line- vehicle i.p #- $P<0.05$ Mann Whitney between group comparison *- $P<0.05$ Friedman test with data points compared against the mean of the 9 day pre-treatment period (a, b)

4.3.2 The Effects of Vandetanib on Mesenteric Vessel Structure Following *In Vivo* Dosing For 21 Days and a Post-treatment Treatment Period of 10 Days

In order to explore the possibility of structural vascular changes following treatment with vandetanib, mesenteric capillary beds were collected at the end of the experiment, stained for the presence of isolectin-B4, an EC marker, and evaluated for vessel length and the number of vessel junctions.

Mesenteric capillary beds taken from rats treated with vandetanib (25 mgkg⁻¹day⁻¹, i.p) showed a trend towards reduction in total vessel length and total vessel junction number compared to those taken from the vehicle-treated group (Figure 4.8, Figure 4.9, Figure 4.10), however this trend was not significant (P>0.05 Student T test). A reduction in total vessel length and total vessel junction number is suggestive of vessel rarefaction (Small *et al.*, 2014).

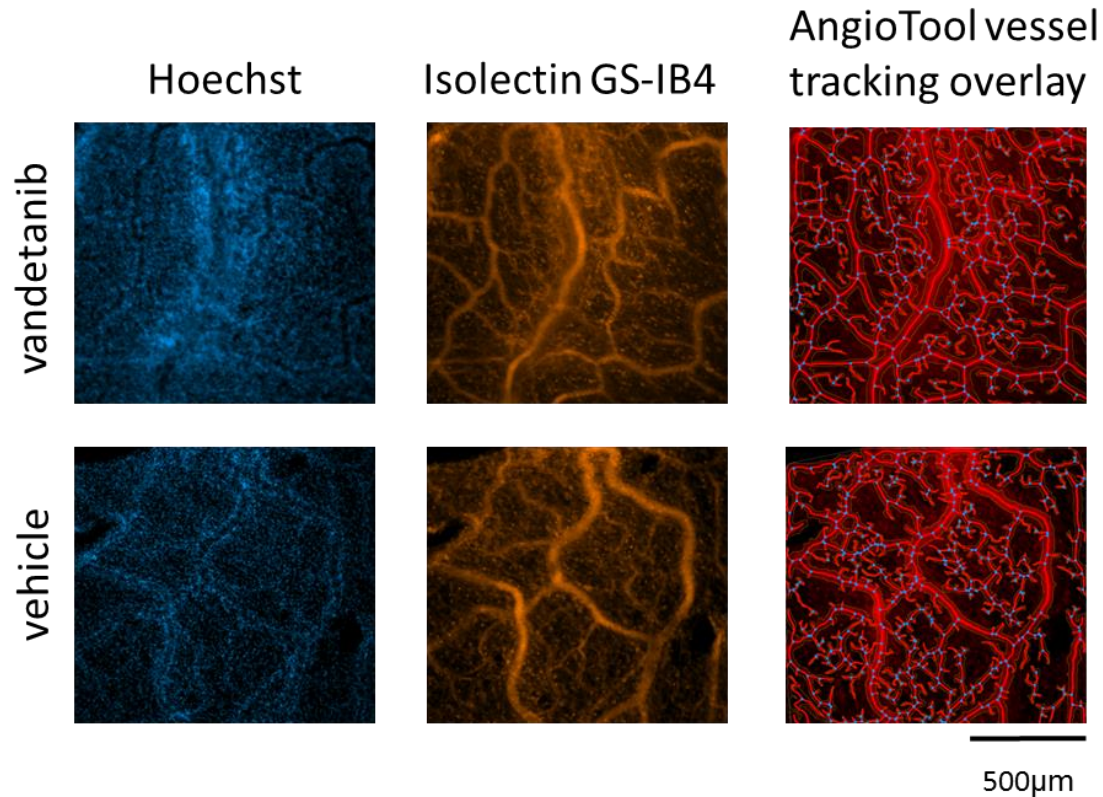


Figure 4.8 Representative images of the mesenteric vasculature of male Sprague Dawley rats treated with vandetanib $25 \text{ mgkg}^{-1}\text{day}^{-1}$, i.p or vehicle i.p for 21 days before a 10 day post-treatment observation period. The mesentery was harvested and stained for cell nuclei (images in blue), and Isolectin-B4 (a marker of ECs) (images in red). Images were analysed using AngioTool 6.0b. AngioTool 6.0b vessel tracking overlay is shown on the right, with red lines indicating vessel structure and blue dots indicating vessel junctions.

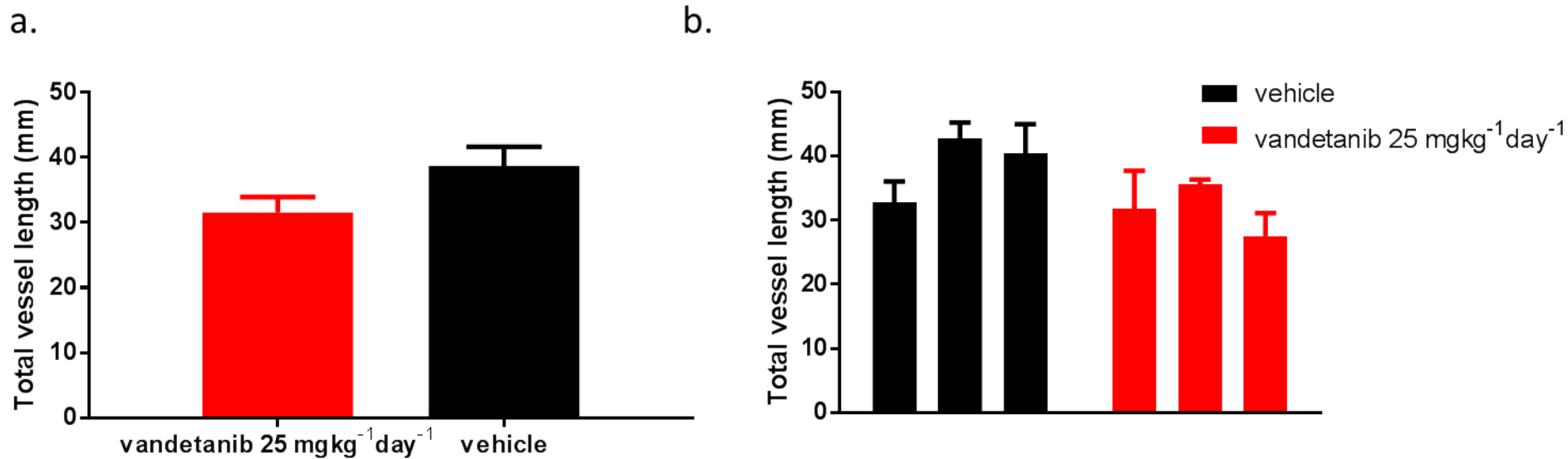
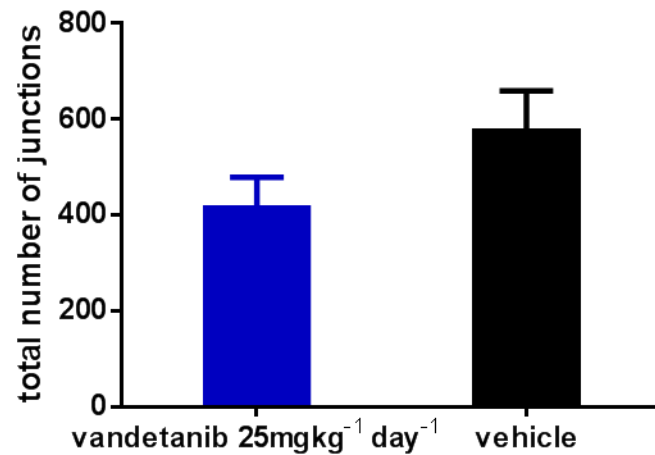


Figure 4.9 Total mesenteric vessel length (mm) in Sprague Dawley rats treated with vandetanib 25 mgkg⁻¹day⁻¹ i.p or vehicle i.p for 21 days before a 10 day post-treatment period. The mesentery was harvested and stained for cell nuclei and Isolectin-B4 (EC marker). 4 mesenteric panels were taken from each rat (n=3 rats for both groups). These data were pooled to give mean total vessel length of treated (red bar) and vehicle (black bar) groups (a). Individual rat data (mean of 4 mesenteric panels per animal) for treated (red bars) and vehicle (black bars) groups is shown in (b). Data displayed as mean ± SEM. Between group unpair Student T test showed no significant difference, P>0.05 (a).

a.



b.

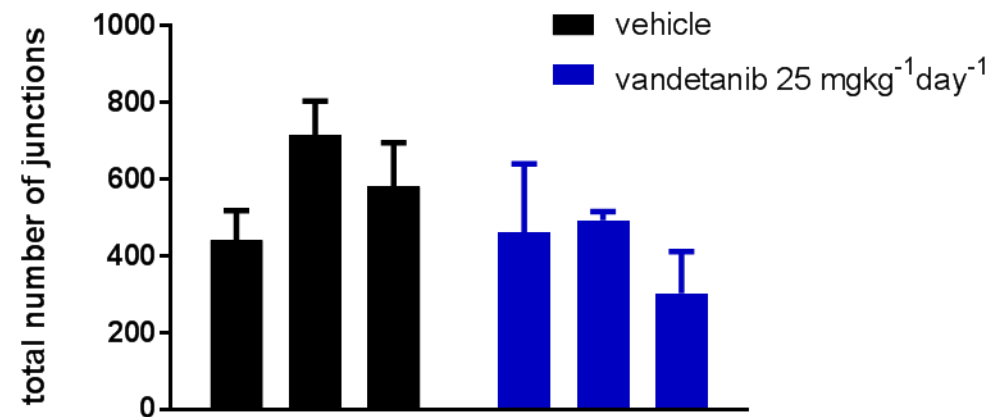


Figure 4.10 Total vessel junction number in Sprague Dawleys treated with vandetanib 25 mgkg⁻¹day⁻¹, i.p or vehicle i.p for 21 days before a 10 day post-treatment period. The mesentery was harvested and stained for cell nuclei and Isolectin-B4 (EC marker). 4 mesenteric panels were taken from each rat (n=3 rats for both groups). These data were pooled to give total vessel junction number mean total vessel junction number of treated (blue bar) and vehicle (black bar) groups (a). Individual rat data (mean of 4 mesenteric panels per animal) for treated (blue bars) and vehicle (black bars) groups are shown in (b). Data shown as mean ± SEM. Between group unpair Student T test showed no significant difference, P>0.05 (a).

4.3.3 Regional Haemodynamic Effects of Vandetanib Measured by Pulsed Doppler Flowmetry (i.v)

The cardiovascular effects of vandetanib ($12.5 \text{ mgkg}^{-1}\text{day}^{-1}$ or $25 \text{ mgkg}^{-1}\text{day}^{-1}$) or vehicle administered i.v are shown in Figure 4.11 and Table 4.3.

Prior to administration of vandetanib on day 1 of the experiment, there were no significant differences between any of the experimental groups (Table 4.3).

In rats given vehicle, there were no significant changes in heart rate and small rise in blood pressure compared to baseline ($P < 0.05$, Friedman) at 24-28 h, followed by a decrease from 48 h onwards with the exception of the 51 h and 72 h time points, compared to baseline (Figure 4.11). Renal vascular conductance showed small decreases towards the end of the study compared to baseline ($P < 0.05$, Friedman) at 51, 52, 75 and 76 h. There was no significant change in mesenteric vascular conductance compared to baseline. Hindquarters vascular conductance showed a reduction at 24-28 h ($P < 0.05$, Friedman) and then increased at 48-52 h ($P < 0.05$, Friedman) compared to baseline (Figure 4.11).

In rats administered $12.5 \text{ mgkg}^{-1}\text{day}^{-1}$ vandetanib i.v, there were no significant changes in heart rate, mean arterial blood pressure or hindquarters vascular conductance compared to baseline (Figure 4.11). However, there was a gradual reduction in renal vascular conductance, compared to baseline, which was significant from 48 h onwards (Figure 4.11). Mesenteric vascular conductance showed an early, transient fall at 1-4 h ($P < 0.05$, Friedman) and then a later, more persistent, significant decrease from 48 h onwards, with the exception of

the 72 h time point in comparison to baseline ($P < 0.05$, Friedman).

The heart rate, mean arterial blood pressure, and the 3 vascular conductance measurements for $12.5 \text{ mgkg}^{-1}\text{day}^{-1}$ vandetanib i.v group were not significantly different ($P > 0.05$, Mann Whitney) from the corresponding vehicle i.v measurements (Figure 4.11).

In rats given $25 \text{ mgkg}^{-1}\text{day}^{-1}$ vandetanib i.v, there was a gradual, modest decrease in heart rate at 50 h, 52 h and 76 h ($P < 0.05$, Friedman; Figure 4.11b.) compared to baseline. Mean arterial blood pressure significantly increased at 25-28 h and 49 h, 50 h, 51 h, 73 h and 74 h compared to baseline ($P < 0.05$, Friedman; Figure 4.11). No significant changes in renal vascular conductance were seen throughout the study (Figure 4.11), but there were significant decreases in mesenteric vascular conductance and hindquarters vascular conductance compared to baseline ($P < 0.05$, Friedman; Figure 4.11). The heart rate, mean arterial blood pressure, and the 3 vascular conductance measurements for $25 \text{ mgkg}^{-1}\text{day}^{-1}$ vandetanib i.v group were not significantly different ($P > 0.05$, Mann Whitney) from the corresponding vehicle i.v measurements (Figure 4.11).

The $25 \text{ mgkg}^{-1}\text{day}^{-1}$ vandetanib i.v and $12.5 \text{ mgkg}^{-1}\text{day}^{-1}$ vandetanib i.v were not significantly different in any of the cardiovascular variables measured ($P < 0.05$, Mann Whitney) (Figure 4.11).

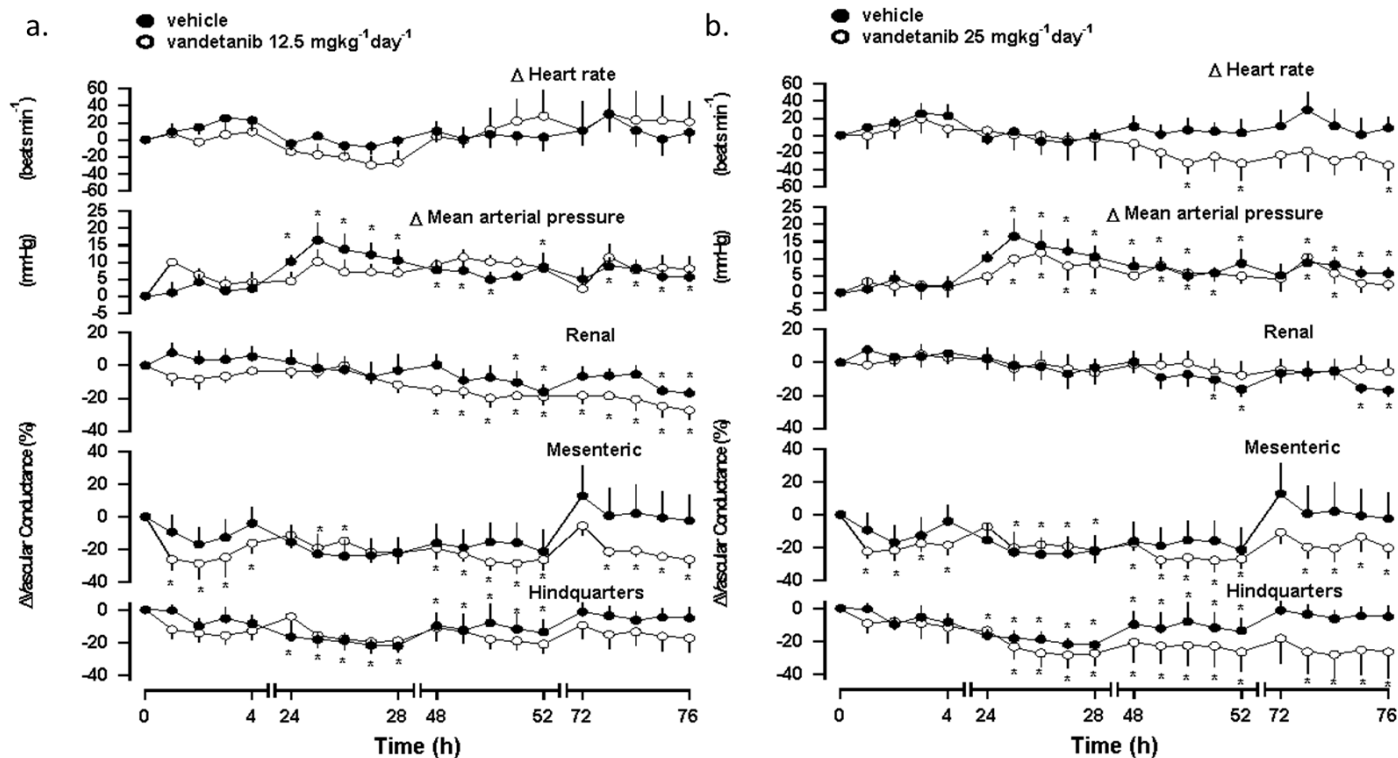


Figure 4.11 Regional haemodynamic effects of vandetanib in conscious male Sprague-Dawley rats following i.v administration of vandetanib at $12.5 \text{ mgkg}^{-1}\text{day}^{-1}$ (a, $n=6$), $25 \text{ mgkg}^{-1}\text{day}^{-1}$ (b, $n=6$) or vehicle (a, b, $n=6$). Data shown (mean \pm SEM) illustrate mean arterial blood pressure, heart rate and regional changes in vascular conductance over the entire study period (4 days). Open circle- vandetanib $12.5 \text{ mgkg}^{-1}\text{day}^{-1}$ i.v (a.) or vandetanib $25 \text{ mgkg}^{-1}\text{day}^{-1}$ i.v (b.), closed circle- vehicle i.v (a., b.). #- $p < 0.05$ Mann Whitney between group comparison*- $p < 0.05$ Friedman test with data points compared against baseline (defined as 0 h on day 1 (before treatment took place). Δ -change from baseline.

	Vehicle (i.v.)	12.5 mgkg ⁻¹ day ⁻¹ Vandetanib (i.v.)	25 mgkg ⁻¹ day ⁻¹ Vandetanib (i.v.)
HR (beats min ⁻¹)	345±11	361±19	365±16
MAP (mmHg)	99±2	106±3	104±3
Renal DS (KHz)	8.3±0.6	9.2±1.2	8.4±1.0
Mesenteric DS (KHz)	8.5±1.6	8.5±0.7	9.2±1.6
Hindquarters DS (KHz)	5.7±0.5	5.3±0.9	5.5±0.5
Renal VC ([KHz mmHg]10 ³)	83.8±7.8	87.7±13.0	79.6±7.9
Mesenteric VC ([KHz mmHg]10 ³)	85.1±15.4	79.0±5.8	90.1±17.6
Hindquarters VC ([KHz mmHg]10 ³)	57.8±4.9	50.3±9.4	51.9±4.2

Table 4.3 Resting (day 1 at least 30 min prior to drug administration) cardiovascular variables prior to the administration of vandetanib or vehicle i.v (n=6). Representative measurements were taken in the 30 min prior to i.v administration. Data displayed as mean ± SEM. HR: heart rate, MAP: mean arterial blood pressure, DS: Doppler shift, VC: vascular conductance. Mann Whitney between group comparison showed no significant differences between resting variables, P>0.05.

4.3.4 Regional Haemodynamic Effects of Vandetanib Measured by Pulsed Doppler Flowmetry (i.p)

Cardiovascular effects of vehicle or vandetanib administered i.p are shown in Figure 4.12, Figure 4.13, Figure 4.14, Table 4.4 and Table 4.5.

Prior to administration of vandetanib on day 1 of the experiment, there were no significant differences between any of the experimental groups (Table 4.4).

In rats given vehicle i.p, there was a significant decreases in heart rate ($P < 0.05$, Friedman; Figure 4.9) and a significant increases in mean arterial blood pressure at sporadic time points throughout the study, compared to baseline ($P < 0.05$, Friedman; Figure 4.12). There were no significant changes in renal and mesenteric vascular conductance compared to baseline (Figure 4.12). Hindquarters vascular conductance was significantly reduced during day 2, 3 and 4 of the study compared to baseline ($P < 0.05$, Friedman; Figure 4.12).

In rats given vandetanib ($12.5 \text{ mgkg}^{-1} \text{ day}^{-1}$) i.p there was a sporadic but significant change from baseline in heart rate ($P < 0.05$, Friedman). There was also a significant pressor effect relative to baseline ($P < 0.05$, Friedman) throughout day 2, 3 and 4 of the study (Figure 4.12). Renal vascular conductance significantly decreased ($P < 0.05$, Friedman) from 26 h onwards compared to baseline (Figure 4.12). Mesenteric vascular conductance significantly decreased ($P < 0.05$, Friedman) during the 24-76 h time points (excluding the 48 and 72 h time points) of the study compared to baseline (Figure 4.12). Hindquarters vascular conductance significantly decreased ($P < 0.05$, Friedman) in comparison to baseline 2 h after the

first dose of vandetanib was administered. This decrease was maintained from 4 h until the end of the study (Figure 4.12).

Mean arterial blood pressure and hindquarters vascular conductance for the vandetanib ($12.5 \text{ mgkg}^{-1} \text{ day}^{-1}$) i.p group were significantly different from the vehicle i.p group ($P < 0.05$, Mann Whitney; Figure 4.12, Table 4.5).

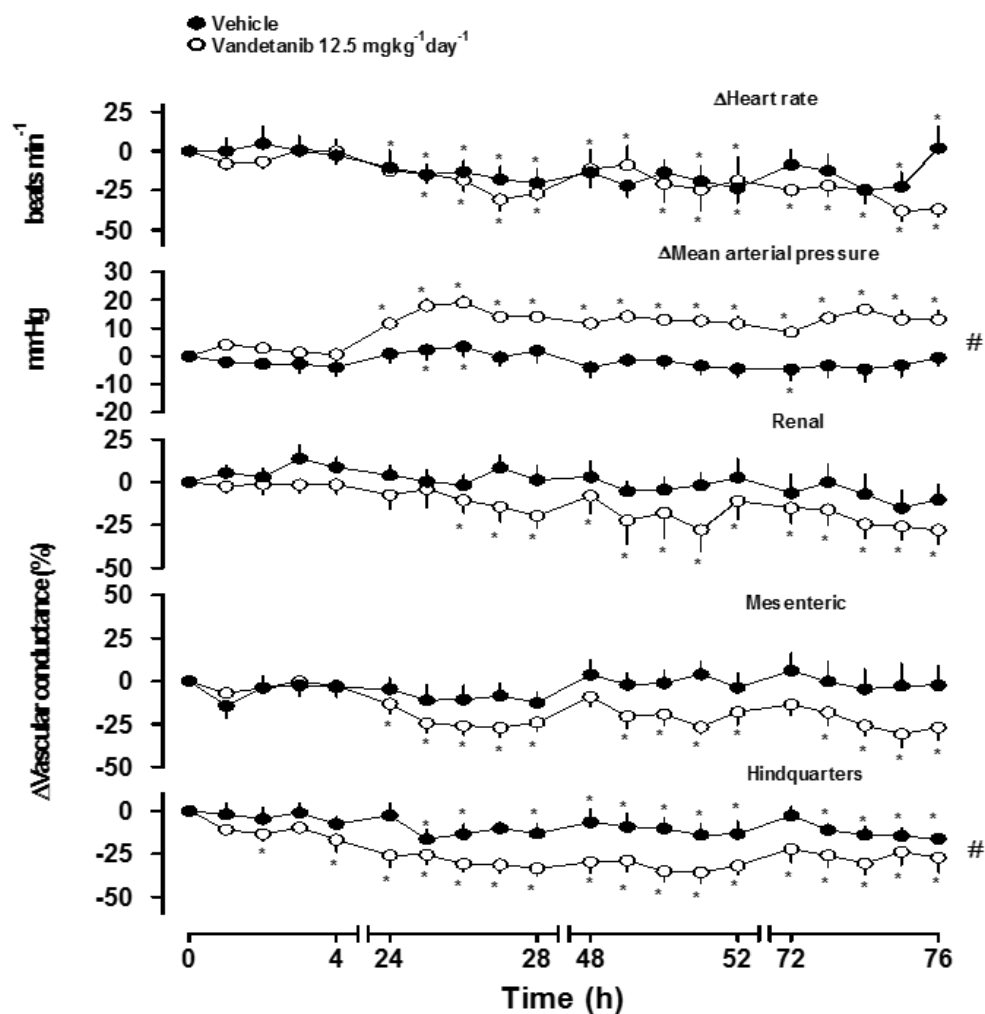


Figure 4.12 Regional haemodynamic effects of vandetanib in conscious male Sprague Dawley rats following i.p administration of vandetanib $12.5 \text{ mgkg}^{-1}\text{day}^{-1}$ ($n=8$) or vehicle i.p ($n=8$). Data shown (mean \pm SEM) illustrate mean arterial blood pressure, heart rate and regional changes in vascular conductance over the entire study period (4 days). Open circles show data obtained with vandetanib $12.5 \text{ mgkg}^{-1}\text{day}^{-1}$ i.p and closed circles show the corresponding vehicle control i.p # $p<0.05$ Mann Whitney between group comparison * $p<0.05$ Friedman test with data points compared against baseline (defined as 0 h on day 1 (before treatment was initiated)). Δ -change from baseline measurements.

In rats given vandetanib ($25 \text{ mgkg}^{-1}\text{day}^{-1}$) i.p there was a significant decrease in heart rate during day 2 and during the last 2 h of days 3 and 4 compared to baseline ($P < 0.05$, Friedman). Mean arterial blood pressure increased ($P < 0.05$, Friedman) throughout day 2, 3 and 4 of the study compared to baseline (Figure 4.13). Renal vascular conductance was significantly decreased ($P < 0.05$, Friedman) 25 h after dosing. This reduction was relatively consistent throughout the study (Figure 4.13). Mesenteric vascular conductance significantly decreased in comparison to baseline ($P < 0.05$, Friedman) 24 h after the first dose, and similarly to the renal effects, this reduction was maintained until the end of the study period (Figure 4.13). Hindquarters vascular conductance significantly decreased ($P < 0.05$, Friedman) in comparison to baseline at 24 h after the first dose of vandetanib ($25 \text{ mgkg}^{-1}\text{day}^{-1}$) i.p was administered. This decrease was maintained until the end of the study (Figure 4.13).

Mean arterial blood pressure, mesenteric and hindquarters vascular conductance for the Vandetanib ($25 \text{ mgkg}^{-1} \text{ day}^{-1}$) i.p group were significantly different from the vehicle i.p group ($P < 0.05$ Mann Whitney; Figure 4.13, Table 4.5).

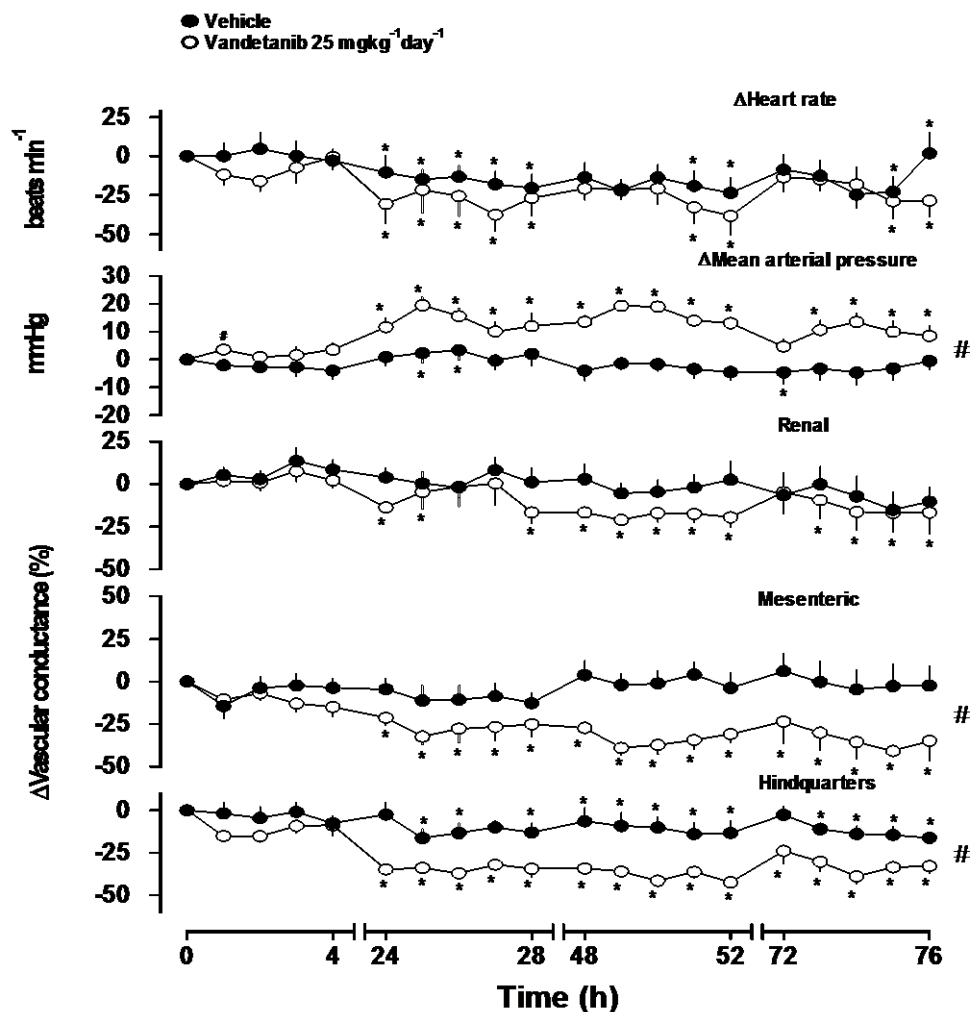


Figure 4.13 Regional haemodynamic effects of vandetanib in conscious male Sprague Dawley rats following i.p administration of vandetanib 25 mgkg⁻¹day⁻¹ (n=8) or vehicle i.p (n=8). Data shown (mean ± SEM) illustrate mean arterial blood pressure, heart rate and regional changes in vascular conductance over the entire study period (4 days). Open circle- vandetanib 25 mgkg⁻¹day⁻¹ i.p, closed circle- vehicle i.p #-p<0.05 Mann Whitney between group comparison *-p<0.05 Friedman test with data points compared against baseline (defined as 0 h on day 1 i.e. before treatment took place). Δ-change from baseline measurement

In rats given vandetanib ($50 \text{ mgkg}^{-1}\text{day}^{-1}$) i.p a significant decrease in heart rate ($P < 0.05$, Friedman) from 1 h-76 h (excluding the 4 h time point) was seen in comparison to baseline (Figure 4.14). The highest dose of vandetanib caused a significant pressor effect compared to baseline ($P < 0.05$, Friedman), which was apparent 1 h after drug administration. Mean arterial blood pressure was consistently higher than the baseline on days 2, 3 and 4 (Figure 4.14). Although there was little effect in the renal vascular bed at earlier time points, renal vascular conductance was significantly decreased ($P < 0.05$, Friedman) during day 4 in comparison to baseline (Figure 4.14). In contrast, mesenteric vascular conductance was significantly decreased 1 h after vandetanib administration and this vasoconstriction was sustained for the remainder of the study ($P < 0.05$, Friedman; Figure 4.14). Likewise, hindquarters vascular conductance significantly decreased ($P < 0.05$, Friedman) 1 h after the first dose of vandetanib in comparison to baseline (Figure 4.14). This decrease was also maintained until the end of the study, although there were some fluctuations throughout the study period (Figure 4.14).

The mean arterial blood pressure for the vandetanib ($50 \text{ mgkg}^{-1}\text{day}^{-1}$) i.p group was significantly different from the vehicle i.p group ($P < 0.05$, Mann Whitney; Figure 4.14, Table 4.5). No other measured variables were significantly different between groups.

There were no significant differences between all measured variables in the $12.5 \text{ mgkg}^{-1}\text{day}^{-1}$, $25 \text{ mgkg}^{-1}\text{day}^{-1}$ and $50 \text{ mgkg}^{-1}\text{day}^{-1}$ groups ($P < 0.05$, Kruskal Wallis).

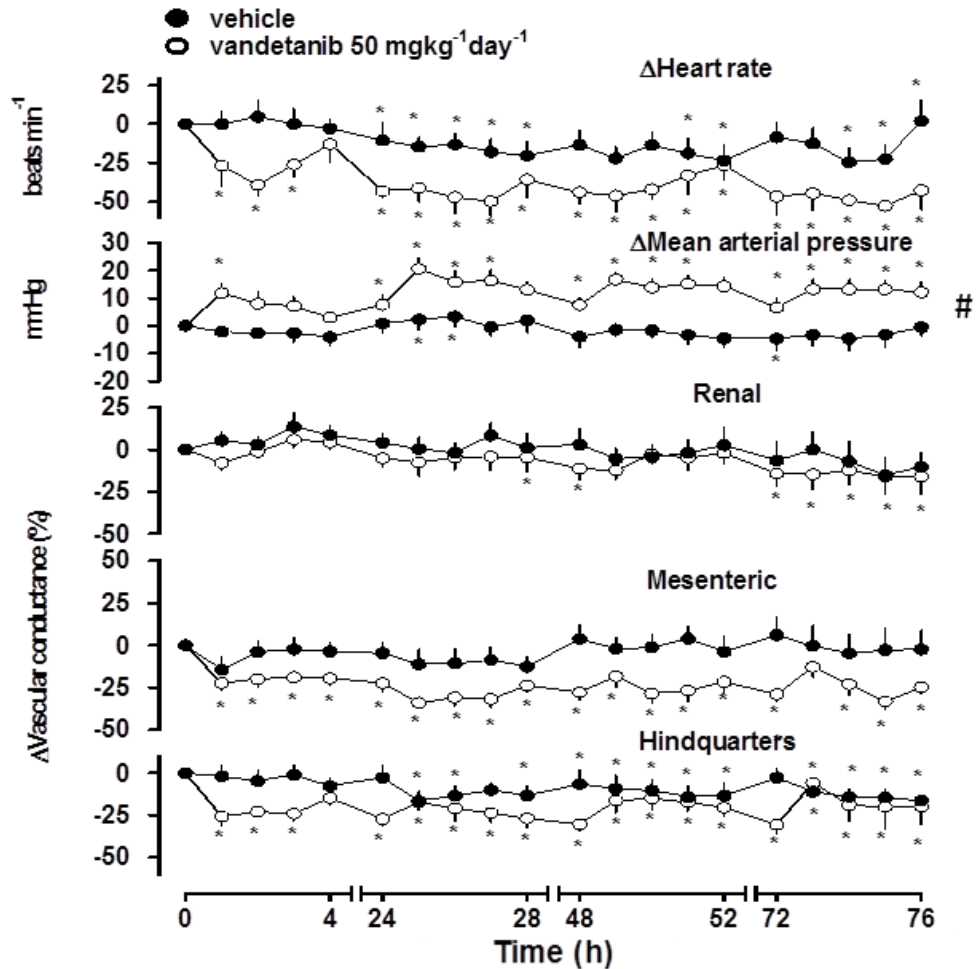


Figure 4.14 Regional haemodynamic effects of vandetanib in conscious male Sprague-Dawley rats following i.p administration of vandetanib 50 mgkg⁻¹day⁻¹ (n=8) or vehicle (n=8). Data shown (mean ± SEM) illustrate mean arterial blood pressure, heart rate and regional changes in vascular conductance over the entire study period (4 days). Open circle- vandetanib 50 mgkg⁻¹day⁻¹ i.p, closed circle- vehicle i.p #-p<0.05 Mann Whitney between group comparison*-p<0.05 Friedman test with data points compared against baseline (defined as 0 h on day 1 (before treatment took place). Δ-change from baseline measurement.

	Vehicle	12.5 mgkg ⁻¹ day ⁻¹ vandetanib	25 mgkg ⁻¹ day ⁻¹ vandetanib	50 mgkg ⁻¹ day ⁻¹ vandetanib
HR (beats min ⁻¹)	354±5	367±4	362±11	372±12
MAP (mmHg)	104±3	98±2	103±3	107±4
Renal DS (KHz)	8.9±1.4	8.8±0.9	8.9±1.0	9.4±1.0
Mesenteric DS (KHz)	11.4±1.4	10±1.3	12.5±1.1	8.7±0.9
Hindquarters DS (KHz)	5.8±0.4	6.2±0.5	6.2±0.7	5.9±0.4
Renal VC ([KHz mmHg]10 ³)	86±14.4	89.6±8.6	84.8±7.3	89.4±10.9
Mesenteric VC ([KHz mmHg]10 ³)	110.3±14.6	102.3±12.3	121.3±10.6	81.3±7.7
Hindquarters VC ([KHz mmHg]10 ³)	56.5±5.0	64.3±6.6	60.9±6.8	55.4±4.7

Table 4.4 Resting (day 1 at least 30 min prior to drug administration) cardiovascular variables prior to the administration of stated compound i.p (n=8). Representative measurements were taken 30 min prior to i.p administration. Data represented as mean ± SEM. HR: heart rate, MAP: mean arterial blood pressure, DS: Doppler shift, VC: vascular conductance. Mann Whitney between group comparison showed no significant differences between resting variables, P>0.05.

Vandetanib (i.p)	12.5 mgkg ⁻¹ day ⁻¹	25 mgkg ⁻¹ day ⁻¹	50 mgkg ⁻¹ day ⁻¹
Δ HR (beats min ⁻¹)	—	—	—
Δ MAP (mmHg)	↑	↑	↑
Renal DS (KHz)	—	—	—
Mesenteric DS (KHz)	—	↓	—
Hindquarters DS (KHz)	↓	↓	—
%Δ Renal VC	—	—	—
%Δ Mesenteric VC	—	↓	—
%Δ Hindquarters VC	↓	↓	—

Table 4.5 Summary of the regional haemodynamic effects of 12.5 mgkg⁻¹day⁻¹ vandetanib i.p (n=8), 25 mgkg⁻¹day⁻¹ vandetanib i.p (n=8) and 50 mgkg⁻¹day⁻¹ vandetanib i.p (n=8) over the entire study period (4 days). Arrows represent significant direction of change compared to vehicle group (n=8) (P<0.05, Mann Whitney). Dashes represent no significant change in comparison to vehicle (p>0.05 Mann Whitney). Δ-change in HR (heart rate), MAP (mean arterial blood pressure), renal, mesenteric and hindquarters DS (Doppler shift) and renal, mesenteric and hindquarters VC (vascular conductance).

4.4 Discussion

A greater understanding of how VEGF RTKIs cause hypertension is needed. Through examining the actions of vandetanib on cardiovascular variables such as heart rate and blood pressure, the cardiovascular side effect profile of vandetanib can be further elucidated. The data discussed in this Chapter demonstrate that vandetanib has a hypertensive and vasoconstrictive action in the rat.

4.4.1 Methodology

To examine the acute actions of vandetanib on heart rate, blood pressure and vascular conductance in the rat, vandetanib was first administered i.v. This decision was made based on previous experience with other RTKIs in this model (Woolard *et al.*; unpublished observations). The method of i.v administration allows vandetanib to enter the blood plasma instantly and avoid first pass metabolism. However, preliminary data (Figure 4.11) showed only very small increases in blood pressure vs vehicle. The hypertensive action of vandetanib has previously been reported to be a substantially larger than this (Janse, 2005; Gu *et al.*, 2009; Blasi *et al.*, 2012). This observation, coupled with the lack of immediate effect on blood pressure one would expect to see with i.v administration and the difficulties experienced in maintaining vandetanib in solution; made it clear that either an alternative route of administration or an alternative vehicle should be considered. The vehicle used in this study was a combination of previously published vandetanib vehicles (Advani *et al.*, 2007; Tai *et al.*, 2010; Wibom *et al.*, 2010). It was observed that vandetanib, although unable to solubilise fully in 0.4 ml vehicle (volumes used for i.v administration), it

was able to solubilise in a larger volume of vehicle. This led to the conclusion that the vandetanib concentrations administered (12.5 mgkg^{-1} , 25 mgkg^{-1}) were higher than the limit of solubility for our chosen vehicle. A lack of full compound solubility could lead to a reduction in drug exposure and therefore a reduction in the vandetanib-mediated effects seen. As vandetanib is given orally in humans, it was decided that i.p delivery would more closely mimic the route of administration in humans (Turner *et al.*, 2011). Logistically, changing the route of delivery to i.p allowed for a larger catheter to be implanted (see Section 2.6.2.4) and for vandetanib to be delivered in a larger volume of vehicle. i.v administration limits the volume that can be administered, as an increase in blood volume leads to a direct increase in blood pressure; this is not an issue with i.p delivery.

4.4.2 Mean Arterial Blood Pressure

In the telemetry study, vandetanib caused a significant increase in blood pressure within the first 24 h after the initial dose. This increase was sustained throughout the dosing period and for 7 days post-dosing, before decreasing to between $+5.0 \text{ mmHg} \pm 0.5 \text{ mmHg}$ and $+4.4 \text{ mmHg} \pm 0.5 \text{ mmHg}$ on day 7-10 post-dosing (Figure 4.4, Figure 4.5, Table 4.1). The hypertensive effect of vandetanib was shown to be time dependent (Figure 4.4) with mean arterial blood pressure being significantly higher 4-8 h after dosing compared to the mean 12 h (daytime) blood pressure ($P < 0.05$, Mann Whitney). This result indicates that vandetanib may reach its peak plasma volume concentration within 4-8 h of i.p administration. This conclusion is supported by vandetanib's FDA report which states that absorption typically took between 2-8 h in rats and dogs (Thornton *et al.*, 2012).

In the haemodynamic studies, a significant pressor effect was observed in all vandetanib (i.p) treatment groups within 24 h of dosing, compared to baseline. All concentrations of vandetanib showed a significant increase in blood pressure compared to the vehicle group (Figure 4.12, Figure 4.13 and Figure 4.14). However, there was no significant difference in mean arterial blood pressure between dose groups. The lack of dose-dependent response implies the maximum hypertensive effect of vandetanib has been reached with these doses. The ability for VEGF RTKIs, including vandetanib, to cause hypertension has been well documented (Gu *et al.*, 2009; Kappers *et al.*, 2010; Leigh Verbois, 2011; Blasi *et al.*, 2012; Grabowski *et al.*, 2012).

The reason as to why VEGF RTKIs cause hypertension is not fully understood. Currently it is thought that their action on VEGFR2 signalling activity is key as the VEGFR2 signalling pathway is involved in vascular growth and maintenance. A study by Mayer *et al* confirmed that vandetanib led to hypertension in humans within a 6 week treatment period (Mayer *et al.*, 2011). Mayer hypothesised that this action may be due to antagonism of VEGF NO-dependant vasodilatation and subsequently demonstrated the capacity of vandetanib to reduce resting brachial arterial diameter, increase vascular resistance and decrease systemic nitrate concentrations (Mayer *et al.*, 2011). VEGF-antagonism related hypertension has also been shown to not be related to the renin-angiotensin and sympathetic systems, further supporting hypertension in patient populations taking VEGF RTKIs as being primarily caused by vessel dysregulation (Veronese *et al.*, 2006).

Vascular rarefaction, which has been shown to occur in mice within 7 days of administration of AG-013736, a small

molecule inhibitor of VEGF/PDGF (Kamba and McDonald, 2007), has also been implicated as a cause of VEGF-RTKI induced hypertension. It has been shown that when vessels close down, for example due to pro-constrictive signalling or vessel damage, autonomic rarefaction can occur (Greene *et al.*, 1981). A reduction in vessel number and/or functioning vessels may go some way to explaining the prolonged hypertensive effect of vandetanib post-treatment regimen (Figure 4.4). Vessel regrowth, a process which would increase vessel surface area and therefore decrease blood pressure can take between 5-10 days to occur (*in vitro*) (Davis *et al.*, 2000, di Blasio *et al.*, 2015), and requires VEGF (Cai *et al.*, 2003).

However, in the preliminary staining study of mesenteric panels taken from rats treated with 25 mgkg⁻¹day⁻¹ (Figure 4.8, Figure 4.9, Figure 4.10), vandetanib showed no significant signs of rarefaction in comparison to the vehicle group. However, the 25 mgkg⁻¹day⁻¹ vandetanib group mesenteric staining showed a trend toward reduced total vessel length and total vessel junction number in the vandetanib group, compared to vehicle, which could indicate a reduction in vessel density and an increased degree of spacing between vessels. As animals in this study had a 10 day 'recovery' period before tissue was harvested, it is possible that during vandetanib treatment rarefaction may occur, although it is not permanent once vandetanib is removed. This theory is supported by the gradual trend of reduction in blood pressure when vandetanib treatment was removed. It would be interesting to perform this study on animals at different lengths of treatment period, for example 4 days, 10 days and 21 days to test this hypothesis. Whether sustained hypertension is a production of reduced VEGF-dependant vasodilatation, vascular rarefaction

or a combination of both is unknown and needs further investigation.

The most commonly seen hypertensive reaction in humans taking vandetanib is grade 2 hypertension (160-169 systolic over 100-109 mmHg diastolic; Qi *et al.*, 2012). Given the variation in age and the possible pre-existing cardiovascular pathophysiology's within the human patient population taking vandetanib, it is difficult to know the average increase in blood pressure seen due to vandetanib, rather than other variables. It is therefore difficult to compare the average increase in mean arterial blood pressure seen in the rat to the human. These results suggest more extensive human studies are needed to look at the off- as well as on-treatment development and progression of hypertension while taking vandetanib.

4.4.3 Vascular Conductance

Vandetanib (i.v or i.p) had no significant effect on the renal vascular bed in comparison the vehicle (Table 4.5). However, mesenteric (25 mgkg⁻¹day⁻¹ i.p) and hindquarter (12.5 mgkg⁻¹day⁻¹ and 25 mgkg⁻¹day⁻¹ i.p) vascular conductances were significantly reduced, in comparison to vehicle (Figure 4.12, Figure 4.13, Figure 4.14). There were no significant differences between the renal, mesenteric and hindquarter vascular conductances in the 12.5 mgkg⁻¹day⁻¹ and 25 mgkg⁻¹day⁻¹ groups i.v. These results suggest that vandetanib (i.p) has a vascular bed-specific vasoconstrictive effect in the hindquarters and mesenteric vascular beds at various doses. The 50 mgkg⁻¹day⁻¹ i.p group showed no significant differences compared to vehicle in any of the vascular beds studied. The variation between doses implies

that the vasoconstrictive effect of vandetanib is dose dependent and therefore may be due to inhibition of multiple receptors.

A reduction in vascular conductance is indicative of a reduction in vessel diameter and an increased resistance to blood flow. Vandetanib induced-vasoconstriction has been previously reported in resting brachial arteries in humans (Mayer et al., 2011) and implies that vessel function and signalling may be altered by vandetanib. Whether sustained hypertension is a product of reduced VEGF-dependant vasodilation or due to off-target, i.e inhibition of other vasoactive receptor tyrosine kinases, effects needs further investigation.

4.4.4 Heart Rate

Vandetanib produced a significant decrease in heart rate throughout the telemetry study, when dosed at 25 mgkg⁻¹day⁻¹ for 21 days (Figure 4.6, Figure 4.7). However, when the data was normalised to baseline (Table 4.2), the vandetanib group did not have as great a decrease in heart rate as the vehicle group. Vandetanib did not cause a significant decrease in heart rate compared to the vehicle group in both regional haemodynamic studies (i.p and i.v; Figure 4.11, Figure 4.12, Figure 4.13, Figure 4.14, Table 4.5), however the vandetanib 50 mgkg⁻¹day⁻¹ group had a significantly decreased heart rate in comparison to baseline, which looked to be time dependent, with heart rate decreasing throughout the day, after each dose, and then increasing at the beginning of the next day (prior to dosing). Overall, these results suggest vandetanib does not have a predominant bradycardic effect in the rat.

Vandetanib has been previously reported to induce bradycardia in orally dosed rats (Verbois, 2011). Although this is the only previously published record of vandetanib causing a decrease in heart rate, other VEGF-targeting RTKIs have also been shown to result in bradycardia, including pazopanib and sunitinib (Blasi *et al.*, 2012; Heath *et al.*, 2013). The bradycardic effect seen in the 50 mgkg⁻¹day⁻¹ haemodynamic study group may be a compensatory reaction to vandetanib-induced vessel constriction. A drug-induced consistent increase in blood pressure would be detected by baroreceptors found on the aortic arch and carotid bodies. When baroreceptors are activated through vessel stretching, negative feedback on heart rate occurs through vagal parasympathetic action (Janse, 2005). This would lead to a compensatory decrease in heart rate, and in turn blood pressure. However, this hypothesis needs to be explored further.

4.4.5 Conclusion

Vandetanib demonstrated a hypertensive effect when given chronically. It also caused vasoconstriction of the mesenteric and hindquarter vascular beds at 12.5 and 25 mgkg⁻¹day⁻¹. This and previously discussed data suggest that these effects may be due to antagonism of VEGFR2, which initially leads to inhibition of NO-dependent vasodilatation and subsequently endothelial dysfunction. This action would chronically manifest *in vivo* as a reduction in vessel conductance, seen in the regional haemodynamic studies in this Chapter, and an increase in blood pressure, which in turn may lead to a compensatory bradycardic effect (as seen with 50 mgkg⁻¹day⁻¹ vandetanib). The preliminary mesenteric vascular staining results also suggest that vandetanib, when given over a 3

week period, may cause a reduction in vessel number. This rarefractive response to vandetanib would further promote hypertension in the rat (Triantafyllou *et al.*, 2015). The constrictive effect of vandetanib in regionally specific vascular beds is a novel finding. However, whether the cardiovascular profile found here is unique to vandetanib is unknown. In order to gain a better understanding of VEGF RTKI cardiovascular profiles, it is important to be able to compare compounds. In order to look for similarities and differences between VEGF RTKIs, and therefore gain a better understanding of RTKI cardiovascular profiles, the next Chapter (Chapter 5) will study pazopanib, a class I VEGF RTKI with a greater potency at VEGFR2 than vandetanib (Chapter 3, (Davis *et al.*, 2011; Carter *et al.*, 2015)).

Chapter 5: The *In Vivo* Cardiovascular Actions of Pazopanib

5.1 Introduction

To determine whether mean arterial blood pressure, heart rate and vascular conductance in the renal, mesenteric and hindquarters vascular beds differ between RTKIs of the same class (Gotink and Verheul, 2010), but with differing potencies at VEGFR2 (Davis *et al.*, 2011; Carter *et al.*, 2015), pazopanib was studied in the rat as a comparison to vandetanib (Chapter 4). Pazopanib, like vandetanib, is a Class I RTKI. However, pazopanib demonstrates greater potency at VEGFR2 (Chapter 3) and a higher incidence and severity of hypertension in the human pazopanib-patient population has been reported (see Section 1.3.1.2, Table 1.2) (Hamberg *et al.*, 2010; Wells *et al.*, 2012; Bible *et al.*, 2014).

In order to compare the action of vandetanib with pazopanib; chronic, regular recordings of heart rate and blood pressure were analysed in order to explore the long-term effects of pazopanib on blood pressure and heart rate. The post-treatment effects of pazopanib were also analysed to assess pazopanib-induced cardiovascular changes, such as vessel rarefaction, which may lead to a sustained hypertensive response after pazopanib treatment was stopped.

Moreover, the regional haemodynamic effects of pazopanib on blood pressure, heart rate and the vascular conductance of the mesenteric, renal and hindquarter vascular beds over a period of 4 days were also investigated.

5.2 Methodology

5.2.1 Time Course of Effects of Pazopanib on Cardiovascular Variables Measured By Radio-Telemetry

Rats were implanted with radio-telemetry devices as described in Section 2.3. Ten days post-surgical implantation of the device, mean arterial blood pressure and heart rate were monitored and recorded for 1 min, every 15 min, for 3 days. Rats were randomly assigned to be given 0.5 ml of either pazopanib 30 mgkg⁻¹day⁻¹, i.p (Sequoia research products, SRP010772p), diluted in vehicle (2% Tween, 5% propylene glycol in 0.9% saline solution) (n=7) or vehicle (n=4) for 21 days. A post-treatment monitoring period of 10 days was observed (Figure 5.1).



Figure 5.1 Schematic diagram of the pazopanib 30 mgkg⁻¹day⁻¹ i.p radio-telemetric experimental timeline.

5.2.1.1 Statistical Analysis

All data have been expressed as mean \pm SEM with significance being accepted at $P < 0.05$. A Kolmogorov-Smirnoff test was performed to test for normality. This test showed data were not normally distributed. A non-parametric, two-tailed within group comparison (Friedman's test) was performed to determine if any changes seen from the baseline value were significant. A non-parametric between group two-tailed comparison (Mann Whitney-U test) was performed to analyse

whether differences between test groups were significant. This was done using Graphpad Prism 6.00.

5.2.2 Regional Haemodynamic Effects of Pazopanib Measured by Pulsed Doppler Flowmetry (i.p)

Rats were implanted with miniature pulsed Doppler flow probes and intra-vascular catheters as described in Section 2.6. 24 h after catheter surgery, animals were randomly assigned to be administered with a 0.5 ml bolus dose of pazopanib i.p (Sequoia research products, SRP010772p) at 10 mgkg⁻¹day⁻¹ (n=8), 30 mgkg⁻¹day⁻¹ (n=8), 100 mgkg⁻¹day⁻¹ (n=8) or vehicle (n=8) (2% Tween 80, 5% propylene glycol in 0.9% saline) i.p once every 24 h. Cardiovascular variables were recorded continuously for 4.5 h per day over a 4 day experimental period (Figure 5.2).

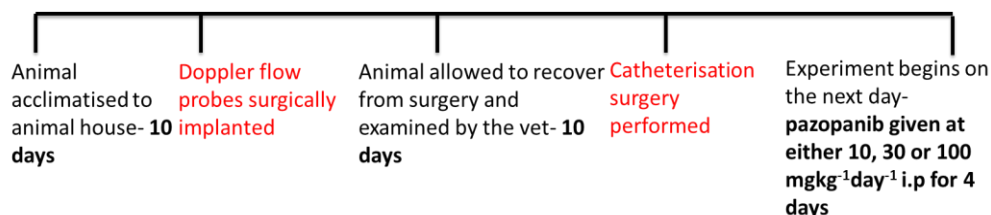


Figure 5.2 Schematic diagram of the pazopanib Pulsed Doppler Flowmetry experimental timeline.

5.2.2.1 Statistical Analysis

All data have been expressed as mean \pm SEM with significance being accepted at $P < 0.05$. A Kolmogorov-Smirnoff test was performed to test for normality. This test showed data were not normally distributed. A non-parametric, two-tailed within group (Friedman's test) was performed to determine if changes seen from baseline values were significant.

Non-parametric between group two tailed comparisons (Mann Whitney (for 2 groups) and Kruskal Wallis (more than 2

groups) were performed to test for significant differences between groups. All statistical analyses were performed using Biomedical version 3.4 (Nottingham, UK).

5.3 Results

5.3.1 Time Course of Effects of Pazopanib on Cardiovascular Variables Measured By Radio-Telemetry

The effects of pazopanib on cardiovascular variables measured by radio-telemetry are shown in Figure 5.3, Figure 5.4, Figure 5.5, Figure 5.6, Table 5.1 and Table 5.2.

5.3.1.1 Mean Arterial Blood Pressure

Mean arterial blood pressure, measured by radio-telemetry, remained consistent throughout the 3 day pre-treatment period in both the pazopanib and vehicle groups, and was steady thereafter in the vehicle group (Figure 5.3). In rats given pazopanib ($30 \text{ mgkg}^{-1}\text{day}^{-1}$ i.p), mean arterial blood pressure increased significantly by $+7.1 \pm 0.5 \text{ mmHg}$ ($P < 0.05$, Friedman) during day 8 of the treatment period (Figure 5.3, Table 5.1). This was maintained throughout the dosing and post-dosing periods. The increase in mean arterial blood pressure (mmHg) in the pazopanib $30 \text{ mgkg}^{-1}\text{day}^{-1}$ i.p group was significantly different from the vehicle group ($P < 0.05$, Mann Whitney; Figure 5.3). The vehicle group did not demonstrate a significant increase in mean arterial blood pressure throughout the study (Figure 5.3).

As the vehicle group had a higher starting mean arterial blood pressure (Table 5.1) data have been normalised (value - average of 3 day pre-treatment period) (Figure 5.3b, Table 5.1). In order to more easily see the differences within and between the pazopanib $30 \text{ mgkg}^{-1}\text{day}^{-1}$ i.p and vehicle i.p groups, this style of analysis has been adopted throughout.

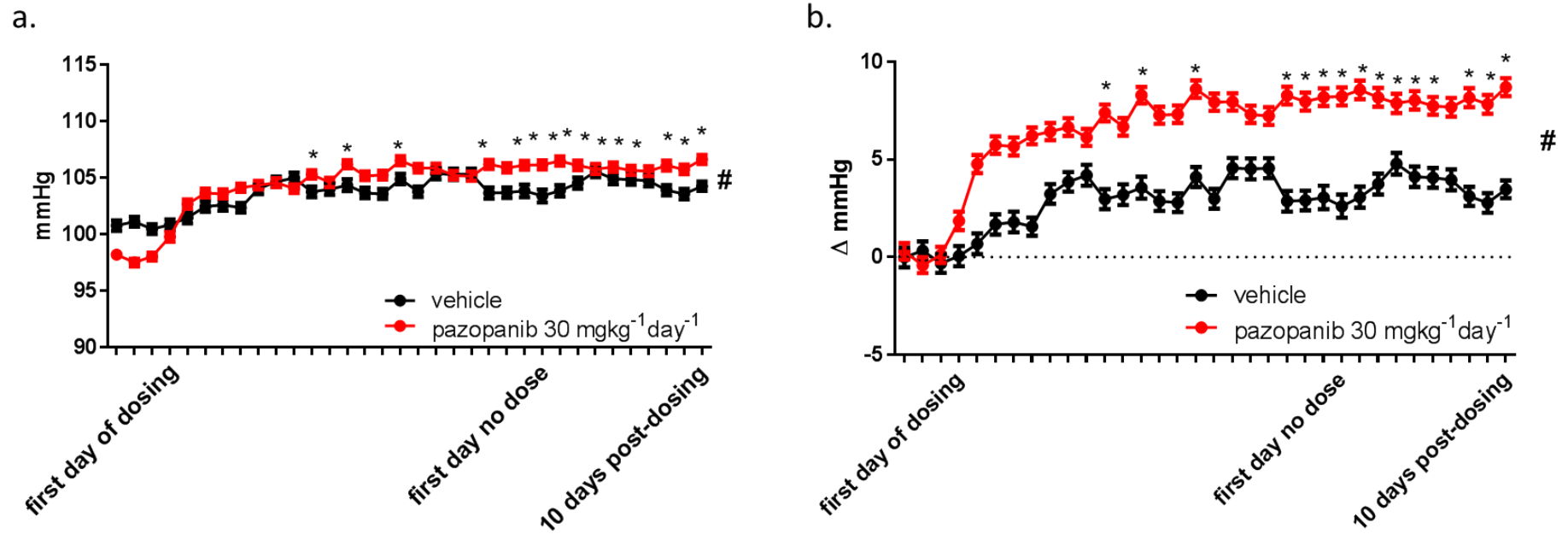


Figure 5.3 Mean arterial blood pressure (measured by radio-telemetry) of male Sprague Dawley rats dosed with pazopanib 30 mgkg⁻¹day⁻¹ i.p (n=7) or vehicle (n=4). Data are displayed as mean ± SEM. Data were analysed and displayed in 24 h bins (a), or as mean change from baseline (average of 3 day pre-treatment period) in 24 h bins (b). Red line-pazopanib 30 mgkg⁻¹day⁻¹ i.p and black-vehicle controls i.p #p<0.05 Mann Whitney (pazopanib vs vehicle) or *p<0.05 Friedman test with data points compared against the mean of the 3 day pre-treatment period.

	24 h Vehicle		24 h Pazopanib 30 mgkg ⁻¹ day ⁻¹		2-4 h Post-treatment vehicle		2-4 h Post-treatment pazopanib 30 mgkg ⁻¹ day ⁻¹	
	Mean	SEM	Mean	SEM	Mean	SEM	Mean	SEM
Baseline	0.0	0.3	0.0	0.3	0.0	1.4	0.0	0.6
Day 1	2.9	0.5	-1.0	0.5	-0.3	1.7	3.1	1.5
Day 2	3.6	0.5	1.9	0.5	0.2	2.0	6.4	1.6
Day 3	4.6	0.5	2.9	0.4	1.5	1.7	7.9	1.3
Day 4	4.7	0.5	2.8	0.4	0.9	1.9	7.2	1.3
Day 5	4.4	0.5	3.3	0.4	2.0	1.6	7.8	1.1
Day 6	6.1	0.5	3.6	0.4	3.4	1.8	8.0	1.3
Day 7	6.7	0.5	3.8	0.4	5.6	1.5	8.3	1.2
Day 8	7.1	0.5	3.3	0.4	3.8	1.5	5.0	1.2
Day 9	5.8	0.5	4.5	0.4	5.0	1.7	10.3	1.3
Day 10	6.1	0.5	3.8	0.5	4.2	1.9	9.2	1.3
Day 11	6.4	0.6	5.4	0.4	6.0	2.5	9.2	1.2
Day 12	5.7	0.5	4.4	0.4	4.0	1.6	9.6	1.3
Day 13	5.7	0.5	4.4	0.4	3.1	1.5	9.5	1.4
Day 14	7.0	0.5	5.7	0.4	3.6	1.7	10.9	1.3
Day 15	5.9	0.5	5.1	0.4	2.6	1.6	9.9	1.3
Day 16	7.4	0.5	5.1	0.4	5.3	2.1	10.7	1.3
Day 17	7.4	0.6	4.4	0.4	4.3	1.7	7.4	1.3
Day 18	7.4	0.5	4.4	0.4	2.8	1.3	7.8	1.1
Day 19	5.7	0.5	5.4	0.4	2.6	1.7	14.6	1.6
Day 20	5.8	0.5	5.1	0.5	1.4	1.6	9.6	1.5
Day 21	5.9	0.6	5.3	0.4	3.2	1.9	8.2	1.1
Day 1	5.5	0.6	5.4	0.4	4.0	2.3	9.2	1.4
Day 2	5.9	0.5	5.7	0.5	5.9	2.2	10.5	1.5
Day 3	6.6	0.5	5.3	0.5	3.6	1.8	8.5	1.3
Day 4	7.7	0.6	5.0	0.5	4.1	2.0	8.7	1.5
Day 5	7.0	0.5	5.2	0.5	2.4	1.9	8.1	1.2
Day 6	6.9	0.5	4.9	0.4	4.9	1.6	8.8	1.2
Day 7	6.8	0.5	4.8	0.5	2.5	1.7	8.4	1.5
Day 8	6.0	0.5	5.3	0.5	3.8	1.6	7.0	1.3
Day 9	5.6	0.5	5.0	0.5	4.6	1.8	12.4	1.7
Day 10	6.3	0.5	5.8	0.5	2.9	1.5	10.1	1.2

Table 5.1 Mean arterial blood pressure (mmHg) and change in mean arterial blood pressure (Δ mmHg) from baseline (defined as the mean value of the 3 day pre-treatment period) of male Sprague Dawley rats dosed with pazopanib 30 mgkg⁻¹day⁻¹ i.p (n=7) or vehicle (n=4). Data are presented as mean \pm SEM and were analysed and displayed in 24 h bins (left) or 2-4 h bins after dosing (right). Black baseline: average of 3 days pre-treatment period; blue text: treatment period; red text: post-treatment period.

Due to the daytime/ night-time pattern seen in the mean arterial blood pressure recordings, the data were analysed in two 12 h slots-segments: (a) daytime (06:00-18:00 h) and (b) night-time (18:00-06:00 h) (Figure 5.4). Changes in mean arterial blood pressure in response to pazopanib (30 mgkg⁻¹day⁻¹ i.p) or vehicle followed the same trend (pre-, during- and post-treatment) as the data presented in Figure 5.3 (analysed over 24 h). However there was a significant mean difference of 5.3 mmHg between the daytime (P<0.05, Mann Whitney) and night-time data (Figure 5.4), with the night-time mean arterial blood pressure higher in comparison throughout the study (Figure 5.4).

The peak plasma concentration time range (2-4 h post-treatment) (Justice and Robertson, 2008) for pazopanib was also analysed. Figure 5.4c shows a significant (P<0.05, Friedman) difference from baseline (+7.8 ± 1.1 mmHg) on day 5 of treatment (Figure 5.4, Table 5.1).

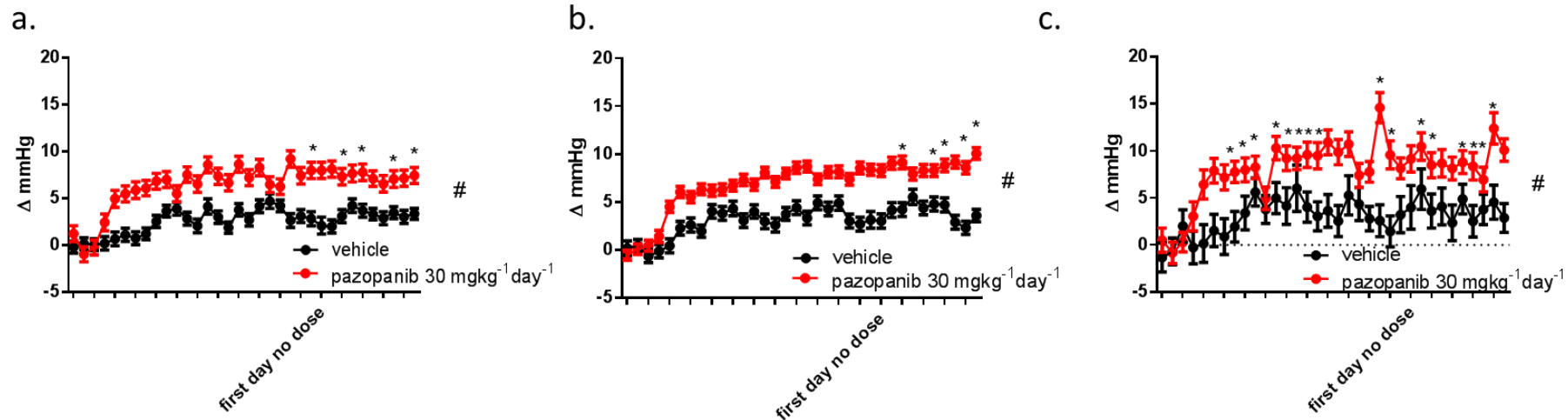


Figure 5.4 Change in mean arterial blood pressure from baseline of male Sprague Dawley rats dosed with pazopanib 30 $\text{mgkg}^{-1}\text{day}^{-1}$ i.p (n=7) or vehicle i.p (n=4). Data are displayed as mean \pm SEM. Data were analysed and displayed in 12 h bins, separated into daytime (06:00-18:00 h) (a), or night-time (18:00-06:00 h) (b) periods. Data collected 2-4 h after dosing are displayed in graph (c). Red line and symbols show data obtained following treatment with pazopanib 30 $\text{mgkg}^{-1}\text{day}^{-1}$ i.p The black line and symbols show the equivalent vehicle control i.p # $p < 0.05$ Mann Whitney between group comparison * $p < 0.05$ Friedman test with data points compared against the mean daytime (a), night-time (b) or 2-4 h after 9 am (scheduled dosing time) (c) of the 3 day pre-treatment period.

5.3.1.1 Heart Rate

Data have been normalised (value - average of 3 day pre-treatment period) (Figure 5.5, Table 5.2) to more clearly show the change in heart rate in comparison to baseline.

Over the 21 day treatment period and the 10 day post-treatment period, heart rate in the vehicle group showed a greater decline than the pazopanib group, such that at the end of the study it was -18.5 ± 4.0 BPM lower than at the start (Table 5.2). A significant difference between the pazopanib and the vehicle groups was seen ($P < 0.05$, Mann Whitney; Figure 5.5, Table 5.2) with the vehicle group showing a greater decrease in heart rate than pazopanib throughout the study.

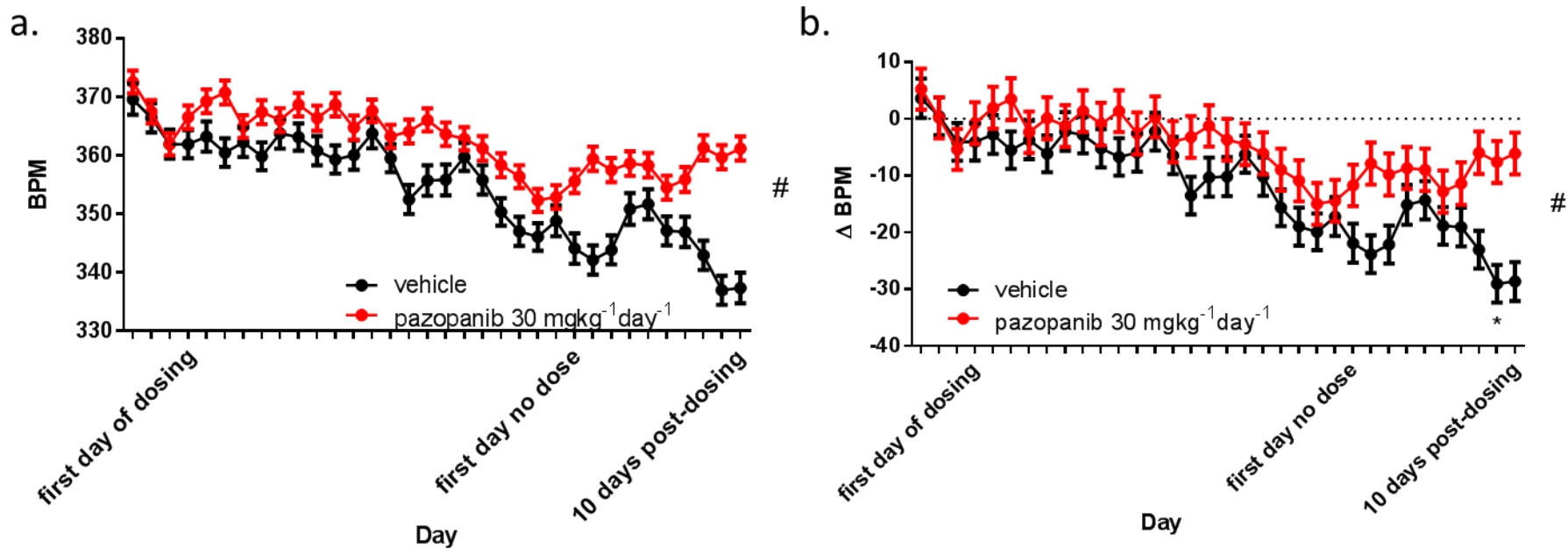


Figure 5.5 Mean heart rate of male Sprague Dawley rats dosed with pazopanib 30 mgkg⁻¹day⁻¹ i.p (n=7) or vehicle i.p (n=4). Data are displayed as mean ± SEM. Data were analysed and displayed in 24 h bins (a), or as mean change from baseline (average of 3 day pre-treatment period) in 24 h bins (b). Red line show data obtained with pazopanib 30 mgkg⁻¹day⁻¹ i.p Black line shows the vehicle controls i.p #p<0.05 Mann Whitney test performed for pazopanib vs vehicle *p<0.05 Friedman test with data points compared against the mean of the 3 day pre-treatment period.

	24 h Vehicle		24 h Pazopanib 30 mgkg ⁻¹ day ⁻¹		2-4 h Post-treatment vehicle		2-4 h Post-treatment pazopanib 30 mgkg ⁻¹ day ⁻¹	
	Mean	SEM	Mean	SEM	Mean	SEM	Mean	SEM
Baseline	0.0	4.3	0.0	3.1	0.0	2.2	0.0	3.9
Day 1	-5.4	3.9	0.5	3.0	-9.2	4.1	-9.6	4.9
Day 2	-4.1	4.0	3.3	3.0	-0.5	6.5	6.8	6.6
Day 3	-6.8	3.9	4.8	3.0	-1.9	4.9	13.4	6.6
Day 4	-5.1	4.0	-1.1	3.0	-1.4	5.7	5.4	5.5
Day 5	-7.5	3.9	1.4	3.0	-3.1	5.5	2.9	6.0
Day 6	-3.5	4.0	0.1	3.0	-0.3	6.1	-5.9	4.2
Day 7	-4.2	3.9	2.7	3.0	6.1	5.3	2.7	5.5
Day 8	-6.5	4.0	0.4	3.1	-11.9	3.3	-6.1	5.4
Day 9	-8.0	3.9	2.7	3.0	2.6	6.0	12.3	5.7
Day 10	-7.2	4.0	-1.3	3.1	-2.1	6.5	4.8	5.4
Day 11	-3.6	4.0	1.6	2.9	4.7	7.0	4.5	6.0
Day 12	-7.8	3.9	-2.7	3.0	-4.3	5.2	11.0	5.8
Day 13	-14.8	4.0	-1.9	3.0	-8.8	5.8	13.2	6.3
Day 14	-11.6	4.0	0.1	3.0	-13.3	4.2	4.8	4.7
Day 15	-11.5	4.0	-2.4	3.0	-13.2	4.6	9.1	6.2
Day 16	-7.6	3.9	-3.2	3.0	2.7	7.0	14.1	6.6
Day 17	-11.5	4.0	-4.8	3.1	-11.7	5.0	-4.4	5.6
Day 18	-17.0	3.9	-7.7	3.0	-14.3	3.7	-10.8	5.0
Day 19	-20.3	4.0	-9.6	3.0	-15.8	5.1	19.0	8.6
Day 20	-21.2	3.9	-13.7	3.0	-19.8	4.4	0.2	7.1
Day 21	-18.5	4.0	-13.1	3.0	-9.8	6.1	-21.1	4.1
Day 1	-23.2	4.0	-10.4	3.0	-15.2	7.5	-12.3	4.4
Day 2	-25.2	4.0	-6.6	3.0	-11.6	7.3	9.0	7.3
Day 3	-23.5	3.9	-8.5	3.0	-22.8	6.1	-12.8	5.0
Day 4	-16.5	4.1	-7.4	3.1	-16.6	4.1	-9.0	5.8
Day 5	-15.7	4.0	-7.7	3.1	-12.0	6.8	-13.4	4.8
Day 6	-20.2	3.9	-11.5	3.0	-12.1	5.8	-7.3	5.3
Day 7	-20.4	4.0	-10.1	3.1	-17.8	5.6	-9.3	4.7
Day 8	-24.4	4.0	-4.7	3.1	-16.9	5.4	-11.8	5.1
Day 9	-30.4	3.9	-6.3	3.0	-19.2	5.8	18.5	6.4
Day 10	-30.0	4.0	-4.8	3.0	-27.2	4.7	1.9	5.1

Table 5.2 Mean \pm SEM change from baseline (defined as the mean value of the 3 day pre-treatment period) heart rate of male Sprague Dawley rats dosed with pazopanib 30 mgkg⁻¹day⁻¹ i.p (n=7) vs vehicle (n=4). Data were analysed and displayed in 24 h bins (left) or 2-4 h bins after dosing (right). Black baseline: average of 3 days pre-treatment period; blue text: treatment period; red text: post-treatment period.

A daytime/ night-time fluctuations in heart rate was clearly seen. Therefore data were analysed in two 12 h time periods: (a) daytime (06:00-18:00 h) and (b) night-time (18:00-06:00 h) (Figure 5.6a, b). Changes in heart rate in response to pazopanib or vehicle i.p followed the same trend (pre-, during- and post-treatment) as the data presented in Figure 5.5a, b (analysed over 24 h). However, there was a significant mean difference of 50 BPM between the daytime ($P < 0.05$, Mann Whitney; Figure 5.6a.) and night-time (Figure 5.6b.) data, with the heart rate higher during the night-time period (Figure 5.6).

The peak plasma concentration time range (2-4 h post-treatment) for pazopanib was analysed (Justice and Robertson, 2008). There were no significant differences within the pazopanib and vehicle treatment groups in comparison to baseline ($P < 0.05$, Friedman). However, there was a significant difference between the pazopanib and vehicle group ($P < 0.05$, Mann Whitney; Figure 5.6).

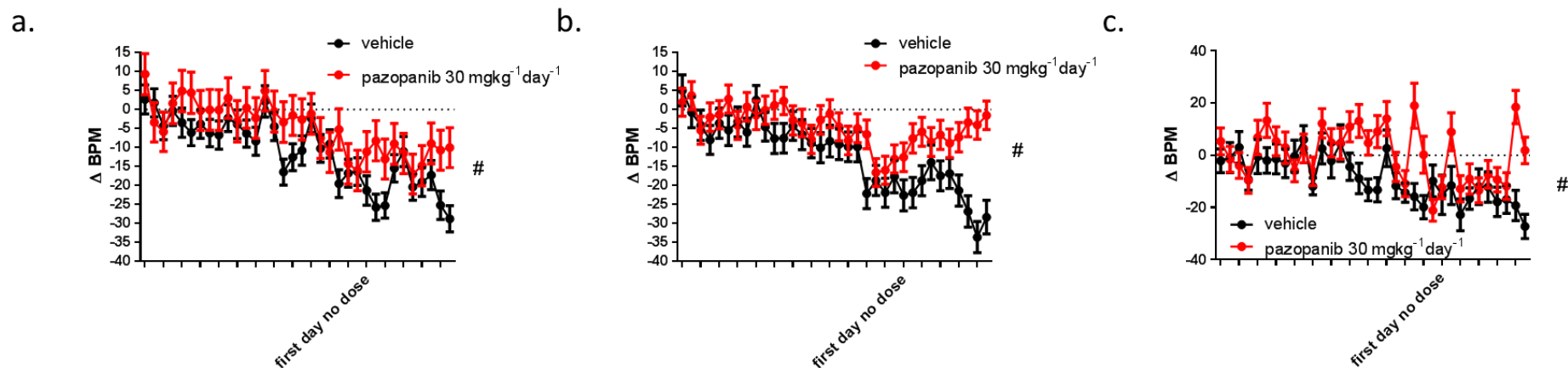


Figure 5.6 Change in heart rate from baseline of male Sprague Dawley rats dosed with pazopanib 30 mgkg⁻¹day⁻¹ i.p (n=7) or vehicle i.p (n=4). Data are displayed as mean ± SEM. Data were analysed and displayed in 12 h daytime bins (06:00-18:00 h) (a), 12 h night-time Sections (18:00-06:00 h) (b) or to show the 2-4 h period after treatment (c.). Red line- pazopanib 30 mgkg⁻¹day⁻¹ i.p, black line- vehicle i.p #p<0.05 Mann Whitney test performed for pazopanib vs vehicle groups *p<0.05 Friedman test with data points compared against the mean daytime (a.), night-time (b.) or 2-4 h after 9 am (scheduled dosing time) (c.) of the 3 day pre-treatment period.

5.3.2 Regional Haemodynamic Effects of Pazopanib Measured by Pulsed Doppler Flowmetry (i.p)

Cardiovascular effects of pazopanib or vehicle administered i.p are shown in Figure 5.7, Figure 5.8, Figure 5.9, Table 5.3 and Table 5.4.

Prior to administration of pazopanib on day 1 of the experiment, there were no significant differences between any of the experimental groups (Table 5.3).

In rats given vehicle i.p, heart rate significantly decreased compared to baseline, although not consistently, throughout the study ($P < 0.05$, Friedman). Mean arterial blood pressure significantly decreased, at 50 and 72-76 h, in comparison to baseline ($P < 0.05$, Friedman; Figure 5.7). Renal vascular conductance showed a continued significant decrease from baseline at 50-76 h ($P < 0.05$, Friedman; Figure 5.7).

Mesenteric vascular conductance increased significantly from baseline at 4 and 24 h ($P < 0.05$, Friedman; Figure 5.7).

Hindquarters vascular conductance was significantly reduced at 1 h and throughout days 2, 3 and 4 of the study ($P < 0.05$, Friedman; Figure 5.7).

In rats given pazopanib ($10 \text{ mg kg}^{-1} \text{ day}^{-1}$ i.p), there was a significant decrease in heart rate, in comparison to baseline, at 1 h and throughout days 2, 3 and 4 of the study (excluding 25 and 72 h) ($P < 0.05$, Friedman; Figure 5.7). Mean arterial blood pressure significantly increased, compared to baseline, 3 h after the initial dose, this increase was maintained and was significant throughout days 2 and 3 ($P < 0.05$ Friedman; Figure 5.7). There was no significant change in renal vascular conductance throughout the study ($P < 0.05$, Friedman; Figure

5.7). Mesenteric vascular conductance significantly decreased, compared to baseline ($P < 0.05$, Friedman) at 1 h and then from 25 h until the end of the study (Figure 5.7). Hindquarters vascular conductance significantly decreased ($P < 0.05$, Friedman), in comparison to baseline, at 1, 2 and 4 h. This significant decrease was maintained throughout the study (excluding time points 75 and 76 h) (Figure 5.7).

All measured variables of the pazopanib ($10 \text{ mg kg}^{-1} \text{ day}^{-1}$) i.p group were not significantly different from the vehicle i.p group ($P < 0.05$, Mann Whitney; Figure 5.7, Table 5.4).

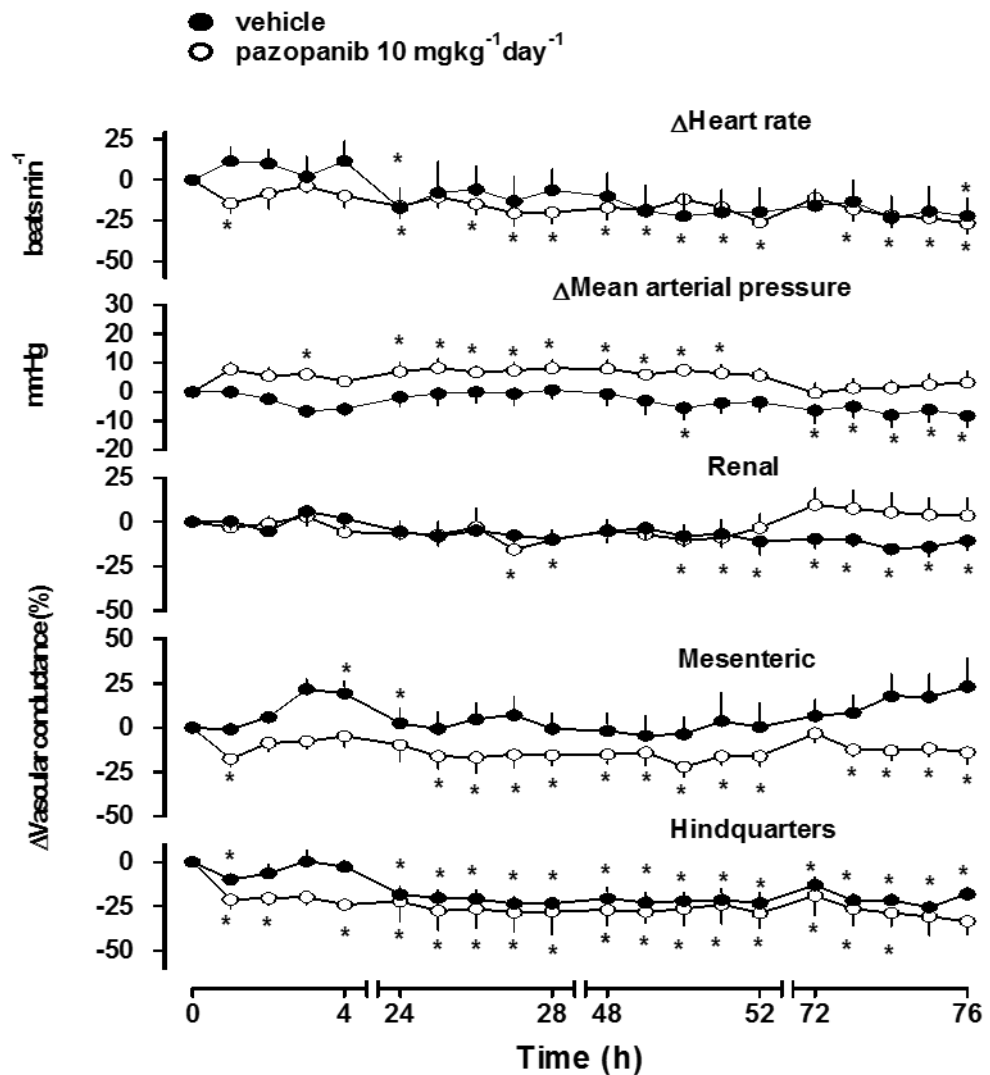


Figure 5.7 Regional haemodynamic effects of pazopanib in conscious male Sprague-Dawley rats following i.p administration of pazopanib 10 mgkg⁻¹day⁻¹ (n=8) or vehicle (n=8). Data shown (mean ± SEM) illustrate mean arterial blood pressure, heart rate and regional changes in vascular conductance over the entire study period (4 days). Open circle- pazopanib 10 mgkg⁻¹day⁻¹ i.p, closed circle- vehicle i.p #-p<0.05 Mann Whitney pazopanib vs vehicle groups *-p<0.05 Friedman test with data points compared against baseline (defined as 0 h on day 1 (before treatment took place). Δ-change from baseline measurement (0 h)

In rats given pazopanib ($30 \text{ mg kg}^{-1} \text{ day}^{-1}$ i.p) there was a significant decrease in heart rate during days 2, 3 and 4 ($P < 0.05$, Friedman Figure 5.8). Mean arterial blood pressure significantly increased from baseline throughout days 2, 3 and 4 ($P < 0.05$, Friedman Figure 5.8). There was a significant decrease in renal, mesenteric and hindquarters vascular conductance, from baseline, from 24 h onwards ($P < 0.05$, Friedman; Figure 5.8).

Mean arterial blood pressure, renal and mesenteric vascular conductance for the pazopanib ($30 \text{ mg kg}^{-1} \text{ day}^{-1}$ i.p) group were significantly different from the vehicle i.p group ($P < 0.05$, Mann Whitney; Figure 5.8, Table 5.4).

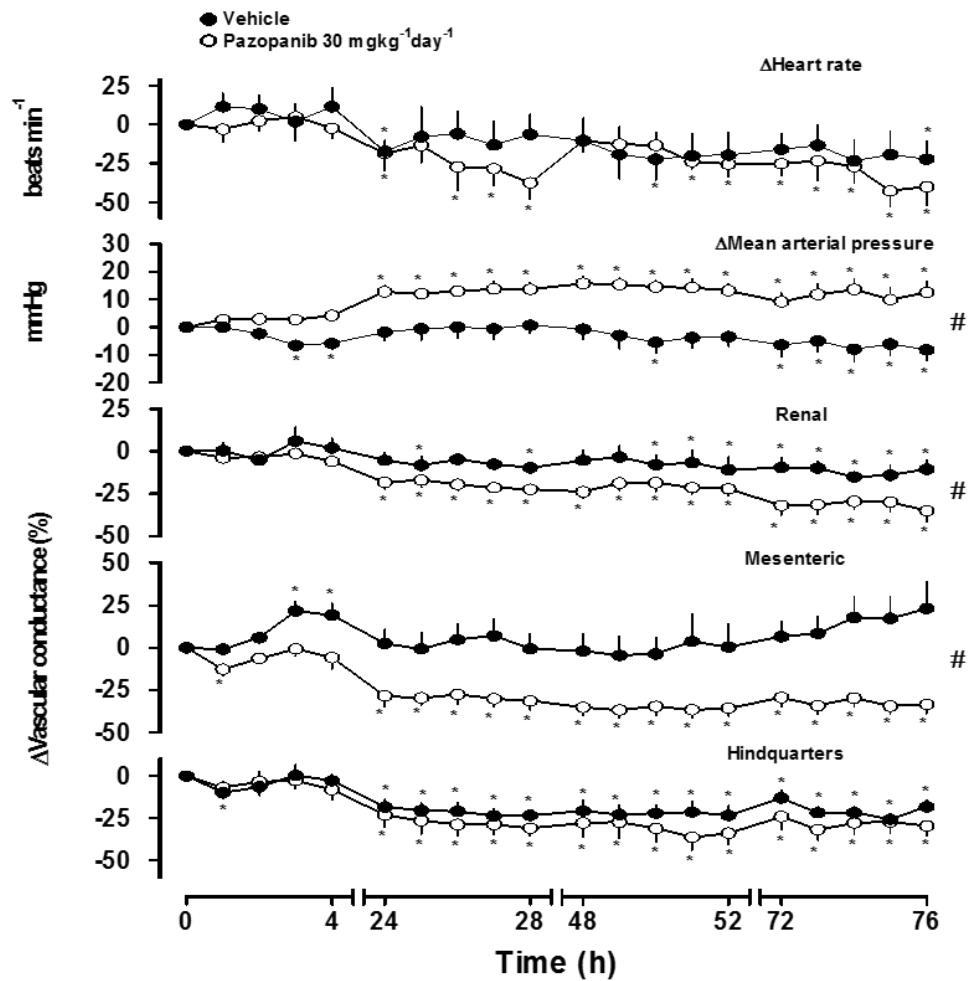


Figure 5.8 Regional haemodynamic effects of pazopanib in conscious male Sprague-Dawley rats following i.p administration of pazopanib 30 mg kg⁻¹ day⁻¹ (n=8) or vehicle (n=8). Data shown (mean ± SEM) illustrate mean arterial blood pressure, heart rate and regional changes in vascular conductance over the entire study period (4 days). Open circle show data obtained with pazopanib 30 mg kg⁻¹ day⁻¹ i.p. Closed circle show the corresponding vehicle controls i.p. #p < 0.05 Mann-Whitney test between pazopanib vs vehicle groups. *p < 0.05 Friedman test with data points compared against baseline (defined as 0 h on day 1 (before treatment took place)). Δ-change from baseline.

In rats given pazopanib ($100 \text{ mgkg}^{-1}\text{day}^{-1}$ i.p) there were significant decreases in heart rate compared to baseline, sporadically throughout the study ($P < 0.05$, Friedman; Figure 5.9). Mean arterial blood pressure significantly increased, in comparison to baseline, throughout days 2, 3 and 4 ($P < 0.05$, Friedman; Figure 5.9). There was a significant decrease in renal vascular conductance, compared to baseline, primarily during day 4 of the study ($P < 0.05$, Friedman; Figure 5.9). Mesenteric vascular conductance significantly decreased from 24 h onwards, in comparison to baseline ($P < 0.05$, Friedman; Figure 5.9). Hindquarters vascular conductance significantly decreased ($P < 0.05$, Friedman), in comparison to baseline, at 4 h; this was maintained for the remainder of the study (Figure 5.9).

Mean arterial blood pressure, mesenteric and hindquarters vascular conductance for the pazopanib ($100 \text{ mgkg}^{-1} \text{ day}^{-1}$ i.p) group were significantly different from the vehicle i.p group ($P < 0.05$, Mann Whitney; Figure 5.9, Table 5.4).

There were a no significant differences between heart rate, mean arterial blood pressure, mesenteric and hindquarters vascular conductance between the $10 \text{ mgkg}^{-1} \text{ day}^{-1}$, $30 \text{ mgkg}^{-1} \text{ day}^{-1}$ and $100 \text{ mgkg}^{-1} \text{ day}^{-1}$ groups. However, there was a significant difference between the renal vascular conductance in the $30 \text{ mgkg}^{-1} \text{ day}^{-1}$ and $100 \text{ mgkg}^{-1} \text{ day}^{-1}$ groups ($P < 0.05$, Kruskal Wallis).

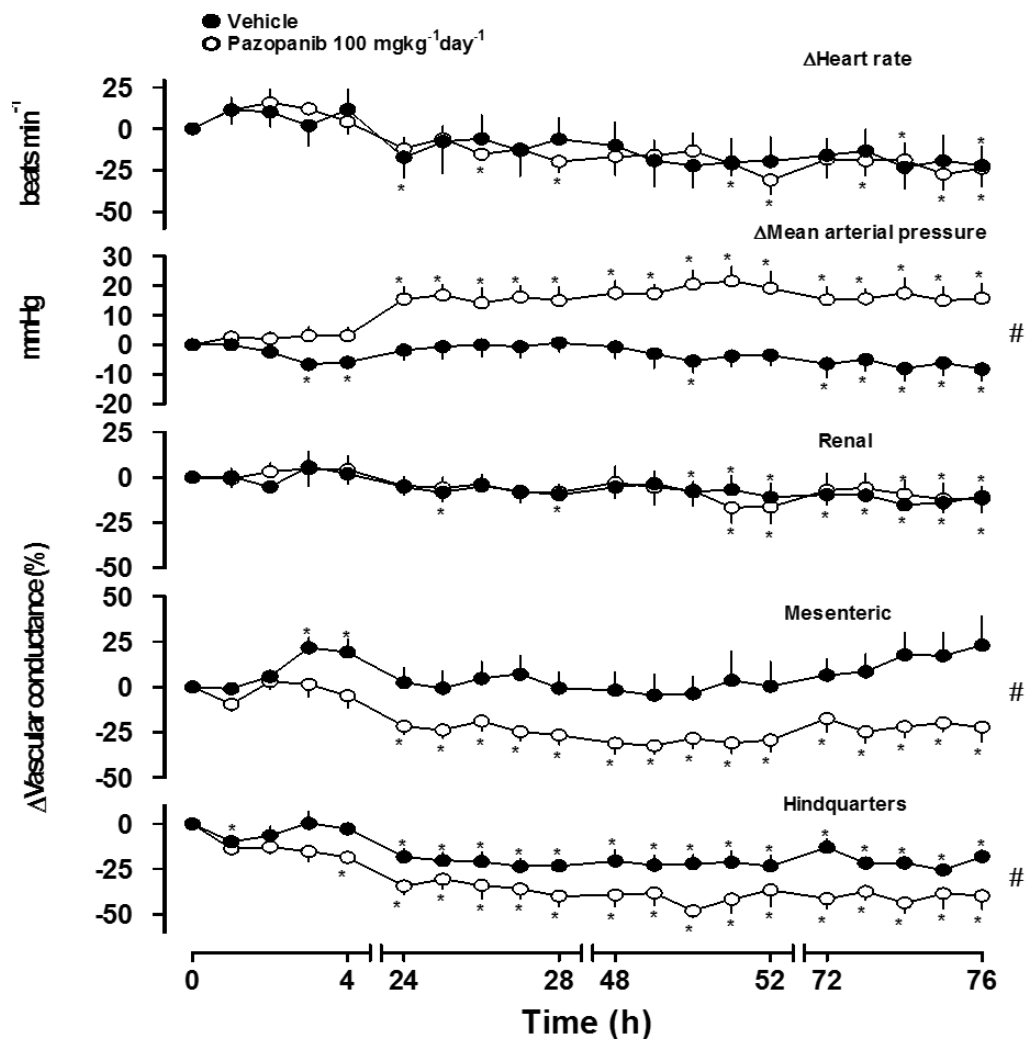


Figure 5.9 Regional haemodynamic effects of pazopanib in conscious male Sprague Dawley rats following i.p administration of pazopanib $100 \text{ mgkg}^{-1}\text{day}^{-1}$ ($n=8$) or vehicle ($n=8$). Data shown (mean \pm SEM) illustrates mean arterial blood pressure, heart rate and regional changes in vascular conductance over the entire study period (4 days). Open circle- pazopanib $100 \text{ mgkg}^{-1}\text{day}^{-1}$ i.p, closed circle- vehicle i.p. #- $p < 0.05$ Mann Whitney test for comparison between the pazopanib and vehicle groups *- $p < 0.05$ Friedman test with data points compared against baseline (defined as 0 h on day 1 (before treatment took place). Δ -change from baseline.

	Vehicle	10 mgkg ⁻¹ day ⁻¹ pazopanib	30 mgkg ⁻¹ day ⁻¹ pazopanib	100 mgkg ⁻¹ day ⁻¹ pazopanib
HR (beats min ⁻¹)	355±15.2	345±6.9	359±6.4	351±5.0
MAP (mmHg)	105±2.6	101±2.8	96±1.3	103±3.1
Renal DS (KHz)	10.1±1.6	8.4±0.6	9.2±0.5	8.1±0.6
Mesenteric DS (KHz)	9.9±1.1	12.4±0.8	11.4±1.2	11.2±0.4
Hindquarters DS (KHz)	6.0±0.3	5.6±0.2	5.5±0.4	5.3±0.4
Renal VC ([KHz mmHg]10 ³)	95.7±13.5	83.1±6.5	94.7±4.5	78.0±4.0
Mesenteric VC ([KHz mmHg]10 ³)	95.4±11.7	123.0±8.6	117.7±12.9	109.3±5.7
Hindquarters VC ([KHz mmHg]10 ³)	57.6±2.7	55.7±1.9	56.5±4.4	52.5±4.5

Table 5.3 Resting (day 1 at least 30 min prior to drug administration) cardiovascular variables prior to the administration of stated compound i.p (n=8). Representative measurements were taken 30 min prior to i.p administration. Data represented as mean ± SEM. HR: heart rate, MAP: mean arterial blood pressure, DS: Doppler shift, VC: vascular conductance. Mann Whitney between group comparison showed no significant differences between resting variables, P>0.05.

Pazopanib	10 mgkg ⁻¹ day ⁻¹	30 mgkg ⁻¹ day ⁻¹	100 mgkg ⁻¹ day ⁻¹
Δ HR (beats min ⁻¹)	—	—	—
Δ MAP (mmHg)	—	↑	↑
Renal DS (KHz)	—	↓	—
Mesenteric DS (KHz)	—	↓	↓
Hindquarters DS (KHz)	—	—	↓
%Δ Renal VC	—	↓	—
%Δ Mesenteric VC	—	↓	↓
%Δ Hindquarters VC	—	—	↓

Table 5.4 Summary of the regional haemodynamic effects of 10 mgkg⁻¹day⁻¹ pazopanib i.p (n=8), 30 mgkg⁻¹day⁻¹ pazopanib i.p (n=8) and 100 mgkg⁻¹day⁻¹ pazopanib i.p (n=8) over the entire study period (4 days). Arrows represent significant direction of change compared to vehicle group (n=8) (P<0.05, Mann Whitney between group comparison). Δ-change in HR (heart rate), MAP (mean arterial blood pressure), renal, mesenteric and hindquarters DS (Doppler shift) and renal, mesenteric and hindquarters VC (vascular conductance).

5.4 Discussion

Through examining the actions of pazopanib on cardiovascular variables such as heart rate and blood pressure, the cardiovascular side effect profile of pazopanib can be further elucidated. The data discussed in this Chapter demonstrate pazopanib has a dose dependent, time dependent hypertensive, vasoconstrictive action in the rat with the dosing schedules used here. This discussion will also compare these findings with those in Chapter 4: The *In vivo* Cardiovascular Actions of Vandetanib, with the purpose of highlighting differences and similarities between these two compounds.

5.4.1 Methodology

During the pazopanib (30 mgkg⁻¹day⁻¹) i.p telemetry experiment, variation between the baseline recordings of the pazopanib and vehicle groups made changes between and within the group, in non-normalised data, difficult to see (Figure 5.3). However, the difference between the baseline values of the vehicle group and pazopanib group were not significant (P>0.05; student T test, Figure 5.10). Variation between animals prior to treatment may be a consequence of genetic heterogeneity due to the strain of rat used (Ghirardi *et al.*, 1995; Rex *et al.*, 2007). This hypothesis is supported by Rex *et al.*, who demonstrated that populations of rats from the same stock, but bred separately, show different behavioural and genetic differences (Rex *et al.*, 2007). This study was performed over a 1 year period, allowing genetic variation between the cohorts of rats used to develop. This variation may lead to distortion of the power calculation, performed prior to performing the experiment, in order to justify the number of animals needed to gain statistical power. The power

calculation for this experiment stated that 3.29 rats were needed, per group, to gain statistical power to test changes in mean arterial blood pressure against $P=0.05$.

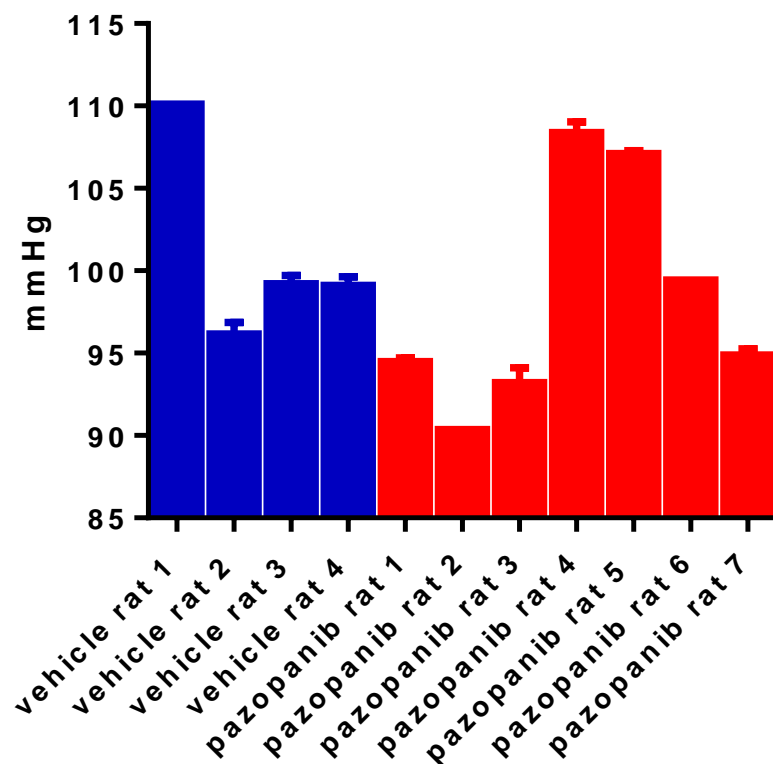


Figure 5.10 Mean 72 h baseline radio-telemetric recordings of mean arterial blood pressure of male Sprague Dawley rats prior to treatment with pazopanib 30 mgkg⁻¹day⁻¹ i.p (n=7, in red) or vehicle (n=4, in blue). Data are displayed as mean ± SEM. Between group Student T test demonstrated no significance.

5.4.2 Mean Arterial Blood Pressure

In the telemetry study, when the data were analysed as 12 h and 24 h data bins, pazopanib caused a significant pressor effect 8 days after the initial dose. However, when the data from 2-4 h after dosing were analysed, blood pressure was significantly higher 5 days after the initial dose. This result indicates that pazopanib has a greater pressor effect 2-4 h after administration. Pazopanib has been shown to reach its peak plasma volume concentration between 2-8 h in humans (Justice and Robertson, 2008). As the process of an i.p injection can cause animal stress and therefore elevate heart rate and blood pressure transiently, it is important to take into account the effect of post-injection stress when taking measurements close to the injection time. However, this is unlikely to have affected the analysis here, as seen in Figure 5.4, the 2-4 h post-administration data point is on average lower than the 3 h data point which includes the dose administration; implying dosing stress has not caused the increase in blood pressure.

The increase in blood pressure seen throughout the pazopanib telemetry dosing period was maintained throughout the 10 day no-treatment period, unlike vandetanib (Section 4.3.1). This difference between the two compounds is of particular interest as pazopanib is reported to have a shorter plasma half-life (vandetanib: 19 days vs pazopanib: 30.9 h see Sections 1.3.1.1 and 1.3.1.2). Therefore the results gained here suggest that pazopanib may lead to less severe but also less-reversible hypertension, in comparison to vandetanib. One explanation for this disparity could be a difference in the kinetic profile of pazopanib in comparison to vandetanib. Slow dissociation of drug from its target can lead to a disconnect

between the drugs pharmacokinetic profile and pharmacodynamic effects, with measured efficacy significantly outlasting detectable plasma concentrations of drug (Vauquelin and Charlton, 2010).

In the haemodynamic studies a significant rise in blood pressure was observed in all pazopanib (i.p) treatment groups within 24 h of dosing, compared to baseline. The 30 and 100 mgkg⁻¹ day⁻¹ pazopanib groups showed a significant elevation in mean arterial blood pressure compared to the vehicle group (Figure 5.8 and Figure 5.9). The pressor effect of pazopanib appears to be dose dependent, with the increase in blood pressure correlating to the increase in dose (Figure 5.7, Figure 5.8 and Figure 5.9). This was not seen with the vandetanib (Chapter 4).

Previous studies have shown that the ED₅₀ for pazopanib is 29.4 mgkg⁻¹day⁻¹ when given twice daily, orally (Justice and Robertson, 2008) in comparison to 25 mgkg⁻¹day⁻¹ for vandetanib (Ciardiello *et al.*, 2003) in mice i.p. Therefore assuming that the ED₅₀ in rat is the same as mouse and that the difference between a dose of 29.4 mgkg⁻¹day⁻¹ and 30 mgkg⁻¹day⁻¹ is negligible, it is possible to directly compare the effect of pazopanib and vandetanib at these doses. In the telemetry studies, vandetanib caused a significantly greater increase in daily (24 h) mean arterial blood pressure than pazopanib (P<0.05, Mann Whitney U). However, the difference between vandetanib-induced and pazopanib-induced hypertension in the haemodynamic study (over 4 days) was not significantly different.

The reasons why VEGF RTKIs may cause an increase in blood pressure have been previously discussed in Sections 1.5 and 4.4.2.

5.4.3 Vascular Conductance

Renal and mesenteric vascular conductances were significantly lower, in comparison to vehicle, in the 30 mgkg⁻¹day⁻¹ pazopanib treatment group, and mesenteric and hindquarter vascular conductances were significantly reduced, in comparison to vehicle, in the 100 mgkg⁻¹day⁻¹ i.p group (Figure 5.8, Figure 5.9). There was a significant difference in renal vascular conductance between the 30 mgkg⁻¹day⁻¹ and 100 mgkg⁻¹day⁻¹ i.p groups, however there was no significant difference in regional vascular conductances between the vandetanib 25 mgkg⁻¹day⁻¹ i.p and the pazopanib 30 mgkg⁻¹day⁻¹ i.p groups.

The implications of reduced vascular conductance have previously been discussed in Section 4.4.3.

5.4.4 Heart Rate

Throughout the telemetry study, no significant differences in heart rate from baseline were seen, and the heart rate in the pazopanib group was significantly higher than that of the vehicle group (Figure 5.5, Figure 5.6, Table 5.2). Pazopanib did not produce a significant decrease in heart rate, compared to vehicle, in the i.p regional haemodynamic study. However it did cause sustained significant decreases in heart rate compared to baseline in the 10 and 30 mgkg⁻¹day⁻¹ groups (Figure 5.7, Figure 5.8). These results suggest pazopanib does not have a prominent bradycardic effect.

However, in a published randomised, double blind placebo controlled study in humans, it was shown that pazopanib was able to induce concentration dependent bradycardia which occurred by day 9 of the study (Heath *et al.*, 2013).

Heart rate for vandetanib 25 mgkg⁻¹ day⁻¹ i.p and pazopanib 30 mgkg⁻¹ day⁻¹ i.p were not significantly different in either the haemodynamic or telemetry studies. Whether or not VEGF RTKIs cause bradycardia has not been well documented. Along with the above mentioned human study using pazopanib and the previously discussed published evidence of vandetanib-induced bradycardia (Section 4.4.4), sunitinib, a VEGF RTKI, has also been reported to cause a decrease in heart rate in telemetered rats, while not affecting cardiac structure or function (Blasi *et al.*, 2012). The reasons why RTKIs may lead to bradycardia have been previously discussed in Section 4.4.4.

5.4.5 Conclusion

The data shown here demonstrates that pazopanib causes hypertension and dose dependent constriction of the renal, mesenteric and hindquarter vascular beds (Figure 5.7, Figure 5.8, Figure 5.9). Of particular interest is the prolonged hypertension seen post-treatment with pazopanib. This finding is novel and suggests pazopanib is either able to cause more-permanent physiological changes within the rat's cardiovascular system or that it has a different kinetics profile in comparison to vandetanib (Chapter 4). Although vandetanib and pazopanib commonly inhibit VEGFR2, their IC₅₀ at VEGFR2 vary from 6.72 ± 0.03 to 8.25 ± 0.03, respectively (Chapter 3; Carter *et al.*, 2015). Potency at VEGFR2 seems to be directly comparable to the percentage of patients who develop

hypertension, with the more potent compounds such as pazopanib, having a wider spread hypertensive effect in the populous taking them (Hamberg *et al.*, 2010; Wells *et al.*, 2012; Bible *et al.*, 2014). However, in the rat, vandetanib was shown to cause a numerically greater and more transient increase in mean arterial blood pressure, in comparison to pazopanib, highlighting the need for further research into RTKI pharmacodynamic and pharmacokinetic profiles.

As the *in vivo* data collected here and in Chapter 4, along with the literature discussed (Section 1.2.5) suggest that the hypertensive side effect profile of VEGF RTKIs may be, in part, linked to endothelial dysfunction and changes in vessel tone, Chapter 6 will primarily focus on the effect of vandetanib on vessel tone.

Chapter 6: The Actions of Vandetanib, Pazopanib, hVEGF₁₆₅ and Acetylcholine on Vessel Diameter

6.1 Introduction

Current literature (Fan *et al.*, 2014; Kruzliak *et al.*, 2014; Lankhorst *et al.*, 2014; Abi Aad *et al.*, 2015; Lankhorst *et al.*, 2015) and the data discussed so far suggest that the hypertensive side effect profile of VEGF RTKIs may be linked to endothelial dysfunction and vessel tone. Therefore this Chapter focuses on the actions of vandetanib and pazopanib on vessel tone. It will also explore the effect of vandetanib on VEGF₁₆₅ and ACh-mediated vasodilatation.

It has previously been shown that haemodynamic force is a key stimulus for the production of vasoactive and vasodilatory, substances, such as NO, by ECs (Rubanyi *et al.*, 1986). Haemodynamic force, created by the flow of blood, can be characterised into two major types; shear stress and cyclic circumferential stretch (Yamamoto and Ando, 2015; Gutterman *et al.*, 2016). Increases in force cause activation of calvoolae-situated mechanosensory complexes consisting of stretch activated (SA) channels, integrin proteins and platelet EC adhesion molecule-1 (PECAM) and VEGFR2 (Chatterjee and Fisher, 2014b), leading to the production of vasoactive signalling molecules, such as NO and PGI₂, as well as anti-thrombogenic mediators e.g. thrombomodulin and HSG (Ando and Yamamoto, 2009; Conway and Schwartz, 2012). Therefore, understanding the action of vandetanib and pazopanib on vessel tone, in pressurised vessels, may help to elucidate whether vandetanib and pazopanib-mediated hypertension is due to the inhibition of constitutive vasoactive substances.

Secondly, the inhibition of VEGF-mediated dilatation by vandetanib was explored. VEGF is a potent mediator of

vasodilatation (Section 1.2), and its inhibition by RTKIs is believed to be the most likely cause of hypertension in the patient populations taking VEGF targeted anti-angiogenic treatments (Kruzliak *et al.*, 2014; Lankhorst *et al.*, 2014; Small *et al.*, 2014; Lankhorst *et al.*, 2015). Although the above hypothesis is widely accepted, the actions of RTKIs on vessel tone in the presence of VEGF have not previously been explored.

Finally, due to the results obtained in Chapter 3, which demonstrate vandetanib is able to inhibit basal measurements of NFAT-mediated luciferase production (Section 3.4.3) and because of the reported multi-targeted nature of VEGF RTKIs (Section 1.3.1), the effects of vandetanib on ACh-mediated vasodilatation was explored. ACh is a neurotransmitter able to cause vasodilatation through activating the muscarinic (M_3) ACh receptor (mAChR) on vascular ECs (Kruse *et al.*, 2012). This leads to vasodilatation through the production of NO and PGI_2 (Durand and Gutterman, 2013), because ACh-mediated dilatation has been shown to use the same vasodilatory signalling molecules as VEGF (NO and PGI_2) but does not do this through activation of a receptor tyrosine kinase, knowing if vandetanib is able to inhibit ACh-mediated dilatation is indicative of whether vandetanib is able to potently inhibit the intracellular signalling kinases responsible for the production of NO and PGI_2 .

By understanding the action of vandetanib and pazopanib, 2 VEGF RTKIs and the action of vandetanib on VEGF and ACh-mediated dilatation, on vessel tone in the presence of cyclic circumferential stretch, the role of these vasoactive substances in VEGF RTKI-induced hypertension can be further elucidated.

6.2 Methodology

6.2.1 Living Systems Pressure Myography

Rats were killed using stunning and cervical dislocation in accordance with Schedule 1 of the UK, Animals Scientific Procedures Act (1986). Second order mesenteric vessels were harvested, cleaned of connective tissue and mounted on the pressure myograph (Living Systems pressure myograph, Section 2.7). The myography bath contained 10 ml PSS (118 mM NaCl, 4.8 mM KCl, 1.1 mM MgSO₄·7H₂O, 25 mM NaHCO₃, 1.2 mM KH₂PO₄, 12 mM Glucose, 1.25 mM CaCl₂·2H₂O) and was perfused with 95% air/ 5% CO₂ to maintain a pH of approximately 7.4. Temperature was maintained at 36-37°C. Intraluminal pressure was set to 90 mmHg and the vessel was allowed to equilibrate to these conditions for 30 min (Figure 6.1).

After 30 min, PEG vehicle (2% Tween, 5% poly ethylene glycol in 0.9% saline solution) (final concentrations of 0.001%-10%), vandetanib (stock: 10⁻² M diluted in DMSO, then further diluted in PSS to give final concentrations of 10⁻¹⁰ M-10⁻⁵ M), pazopanib (stock: 10⁻² M diluted in DMSO, then further diluted in PSS to give final concentrations of 10⁻¹⁰ M-10⁻⁵ M) or DMSO (equivalent volumes of DMSO to those found in the vandetanib and pazopanib final solutions, diluted in PSS) were added cumulatively to the bath to generate a concentration response curve. Each concentration was added for 10 min. Vessels were dilated using 10⁻⁵ M ACh (final concentration) at the end of the experiment to check for endothelial function. If there was no response the experiment was discounted from the analysis. Vessels were imaged using an inverted microscope attached to a camera, and the internal diameter was measured using a

dimension analyser (Living Systems Instrumentation), linked to a MacLab data acquisition system.

6.2.2 DMT 120CP myography

Rats were killed using stunning and cervical dislocation in accordance with Schedule 1 of the UK, Animals Scientific Procedures Act (1986). Second order mesenteric vessels were harvested, cleaned of connective tissue and mounted on the pressure myography (DMT 120CP, Section 2.7). The myography bath contained 10 ml PSS and was perfused with 95% air/ 5% CO₂ to maintain a pH of approximately 7.4. Temperature was maintained at 36-37°C. PSS contained 0.01% BSA if hVEGF₁₆₅ was used in the study, this was done to ensure the hVEGF₁₆₅ did not adhere to surfaces within the bath. Intraluminal pressure was set to 90 mmHg and the vessel was allowed to equilibrate to these conditions for 30 min (Figure 6.1). After 30 min vessels were constricted by 40-60% of the initial diameter using 10⁻⁷ M U46619 (9,11-dideoxy-9 α ,11 α -methanoepoxy prostaglandin *F*_{2 α}), this response was allowed to stabilise for 30 min before compounds: vandetanib (stock: 10⁻² M diluted in DMSO, then further diluted in PSS to give final concentrations of 10⁻¹⁰ M-10⁻⁵ M), DMSO (equivalent volumes of DMSO to those found in the vandetanib final solutions, diluted in PSS), ACh (diluted in PSS, final concentration range from 10⁻¹⁰ M-10⁻⁵ M) or hVEGF₁₆₅ (stock concentration: 10⁻⁶ M, stock diluted in PBS + 0.1% BSA final concentration range, diluted in PSS + 0.1% BSA, between 10⁻¹⁴ M-10⁻⁹ M) were added cumulatively to the bath to generate a concentration response curve (Figure 6.1). Each concentration was added and incubated with the vessel for 5 min (time taken to see full response). Vessels were dilated using 10⁻⁵ M ACh (final concentration) at the end of the

experiment to check for endothelial function. If there was no response the experiment was discounted from the analysis. Vessels were imaged using an inverted microscope attached to a camera, and the internal diameter was measured using a dimension analyser (DMT) linked to a computer with DMT MyoView II software (Figure 6.1).

6.2.3 Statistical Analysis

Data obtained from the DMT 120CP system were fitted using non-linear regression (3-parameter) in GraphPad Prism 6 (San Diego, CA) to obtain EC_{50} values (Section 2.8.3). All data have been expressed as mean \pm SEM with significance being accepted at $P < 0.05$. A non-parametric, two-tailed group comparison (Friedman) was performed to determine if any changes seen from the baseline value were significant. Non-parametric between group two-tailed comparisons (Mann Whitney U test for 2 groups and Kruskal Wallis for more than 2 groups) were performed to look for significant differences between groups. An unpaired Student's T test was used to compare E_{max} and pEC_{50} values which had been gained by averaging the individual n values from each experimental non-linear regression curve fit. This was done using Graphpad prism 6.00.

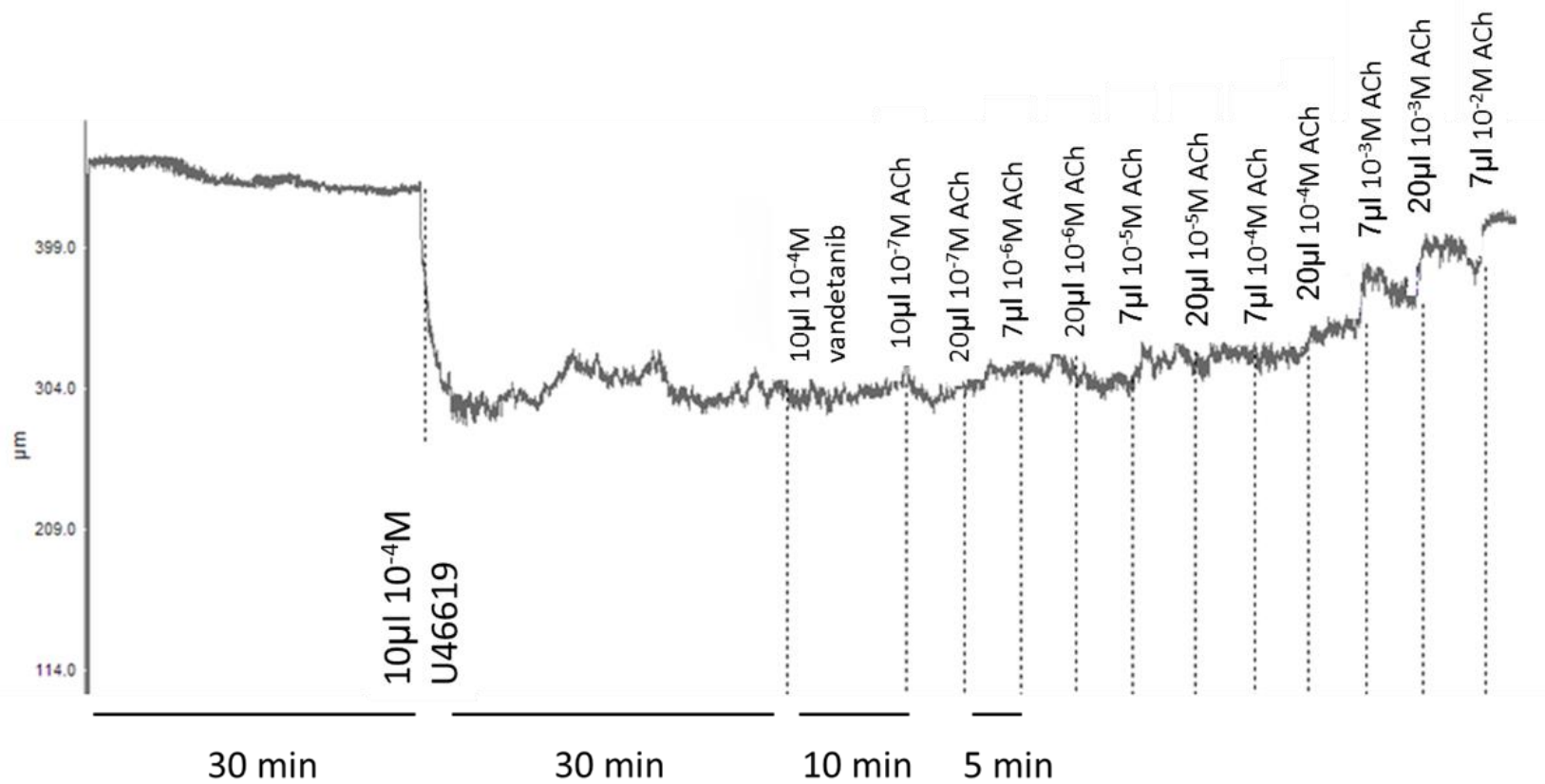


Figure 6.1 Representative trace showing the experimental protocol for pre-constriction of mesenteric arterioles with U46619. 30 min after precontraction, vandetanib ($10 \mu\text{l } 10^{-4} \text{ M}$, giving a final concentration of 10^{-7} M) was incubated with the vessel for 10 min and a concentration response curve for ACh was generated (10^{-10} M - 10^{-5} M -final concentrations).

6.3 Results

6.3.1 The Effects of Vandetanib and Pazopanib on Pressurised Vessel Diameter

Increasing concentrations of vandetanib, pazopanib and the corresponding vehicle control of DMSO caused no significant change in vessel diameter, compared to baseline measurements ($P < 0.05$, Friedman; Figure 6.2). However, there was a significant difference between the vandetanib concentration response vs the corresponding vehicle control of DMSO for vandetanib and pazopanib ($P < 0.05$, Mann Whitney; Figure 6.2).

The PEG vehicle used in the *in vivo* studies in Chapters 4 and 5, was also tested on pressurised mesenteric vessels, in order to explore whether the PEG vehicle has a constrictive effect on rat vessels. The PEG vehicle (2% tween80 + 5% PEG in 0.9% saline solution) showed no significant effect on vessel diameter at concentrations up to 10% vehicle (final concentration) in comparison to baseline (Friedman; Figure 6.2).

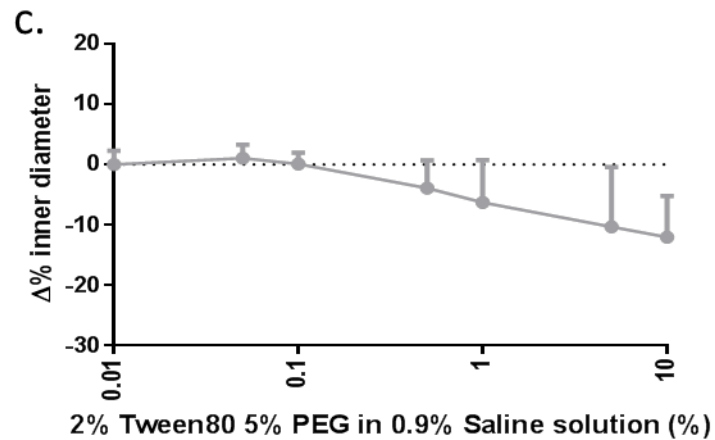
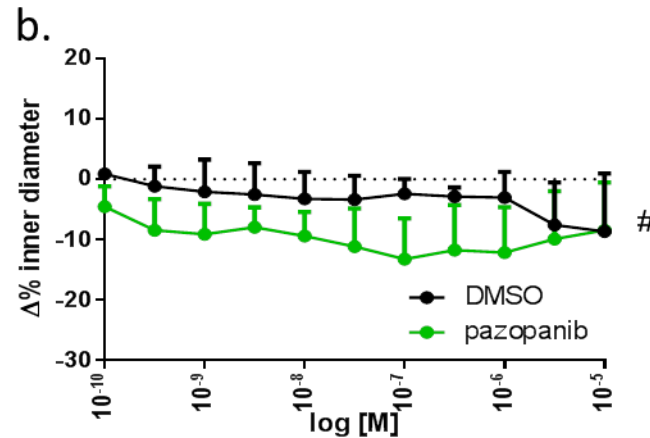
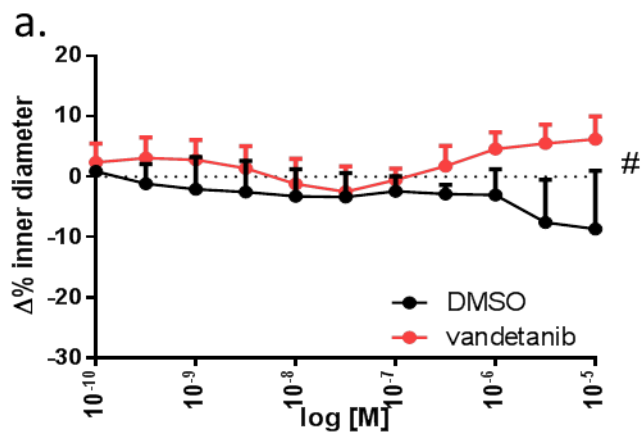


Figure 6.2 The effect of selected RTKIs on vessel diameter. Vessels were treated with increasing concentrations of vandetanib n=5 (a), pazopanib n=6 (b), equivalent DMSO vehicle concentrations n=4 (a, b) or the *in vivo* PEG vehicle used in Chapters 4 and 5 (2% tween80 + 5% PEG in 0.9% saline solution) n=7 (c). Data presented has been pooled and normalised to initial vessel diameter. Each point represents the mean \pm SEM. #-p<0.05 Mann Whitney between group comparison *-p<0.05 Friedman test with data points compared initial vessel diameter

6.3.2 The Effects of Vandetanib on the Vessel Diameter of Pre-Constricted Pressurised Vessels

Vandetanib significantly increased vessel diameter at concentrations between 3×10^{-7} M and 10^{-5} M in pre-constricted vessels in comparison to the vessel diameter produced by U46619 constriction ($P < 0.05$, Friedman; Figure 6.3). This increase in diameter was significantly different to the DMSO vehicle control ($P < 0.05$, Mann Whitney; Figure 6.3). The DMSO vehicle control, at the equivalent concentration of vandetanib 10^{-5} M, caused a significant increase in vessel diameter ($P < 0.05$, Friedman).

hVEGF₁₆₅ caused an increase in vessel diameter in pre-constricted vessels. This was significantly different, from baseline, at 3×10^{-9} M and 1×10^{-9} M ($P < 0.05$, Friedman; Figure 6.3). hVEGF₁₆₅ had a pEC₅₀ of 13.0 ± 0.5 . The increase in diameter was significantly different from the DMSO vehicle control group ($P < 0.05$, Mann Whitney; Figure 6.3). The DMSO concentration response data showed that DMSO caused a significant increase in vessel diameter at 3×10^{-10} M- 10^{-9} M ($P < 0.05$, Friedman).

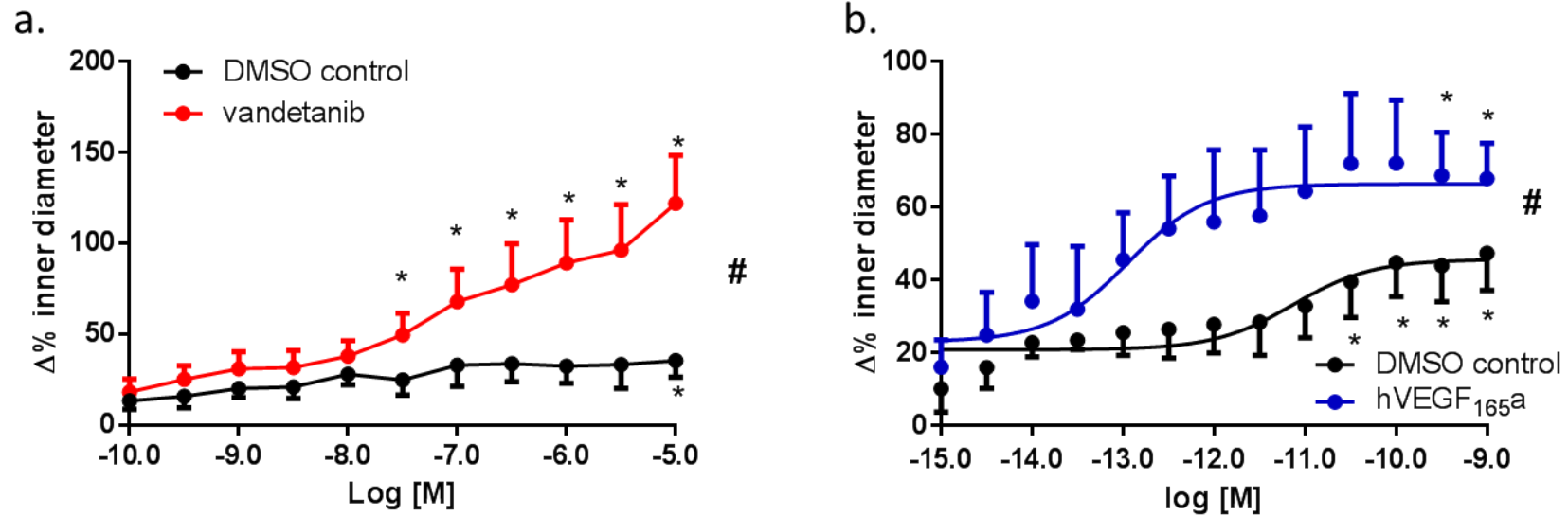


Figure 6.3 The effects of vandetanib and hVEGF₁₆₅ on vessel diameter after precontraction with U46619. Vessels were precontracted with U46619 (10⁻⁷ M), allowed to normalise of 30 min and then treated with increasing concentrations of vandetanib n=6 (a), VEGF n=5 (b) or the vehicle DMSO (n=6 (a) n=5 (b)). Data presented have been pooled and normalised to the vessel diameter produced by U46619 constriction. Each point represents the mean ± SEM. #-p<0.05 Mann Whitney between group comparison *-p<0.05 Friedman test with data points compared against the vessel diameter produced by U46619 constriction.

6.3.3 The Effects of Vandetanib on hVEGF₁₆₅ Mediated Vessel Dilatation

Vandetanib significantly inhibited hVEGF₁₆₅-mediated vessel dilatation in comparison to the DMSO control ($P < 0.05$, Mann Whitney; Figure 6.4). The hVEGF₁₆₅ + 10^{-7} M vandetanib concentration response curve experiment showed no significant change in vessel diameter throughout the concentration range tested ($P < 0.05$, Friedman; Figure 6.4). However, hVEGF₁₆₅ + DMSO control caused a significant increase in vessel diameter from 3×10^{-10} M onwards ($P < 0.05$, Friedman), with an E_{\max} of $110\% \pm 27\%$ compared to the mean hVEGF₁₆₅ + 10^{-7} M vandetanib E_{\max} of $37\% \pm 15\%$. The mean pEC_{50} for the hVEGF₁₆₅ + 10^{-7} M vandetanib group was 11.7 ± 0.6 , compared to the mean pEC_{50} of 12.2 ± 0.2 for the hVEGF_{165a} + DMSO, demonstrating that although vandetanib did not cause a significant shift in hVEGF₁₆₅ pEC_{50} it did cause a reduction in the efficacy of hVEGF₁₆₅.

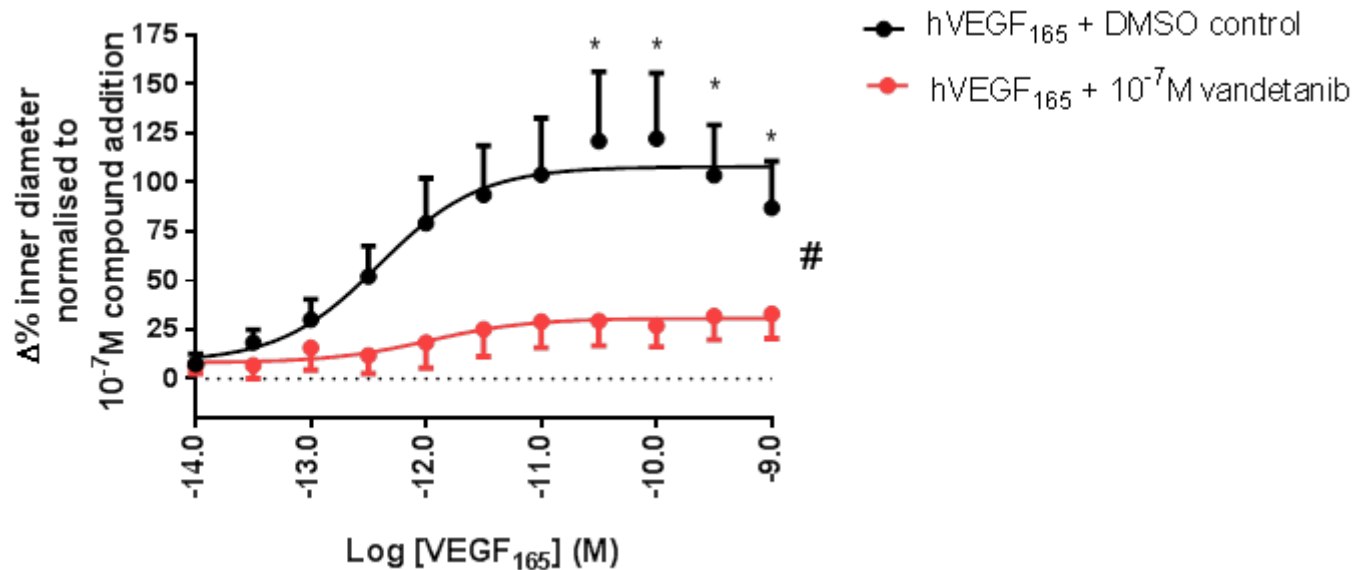


Figure 6.4 The effect of vandetanib on VEGF induced vessel dilatation after precontraction with U46619 (10^{-7} M) Vessels were precontracted with U46619, allowed to normalise of 30 min and then treated with 10^{-4} M vandetanib (10^{-7} M final concentration) (n=7), or the equivalent DMSO control (n=5) for 10 min before being exposed to increasing concentration of VEGF. Data presented have been pooled and normalised to the vessel diameter produced by the addition of vandetanib or DMSO, after U46619 constriction. Each point represents the mean \pm SEM from n separate experiments. #-p<0.05 Mann Whitney between group comparison*-p<0.05 Friedman test with data points compared against vandetanib/DMSO incubation step

6.3.4 The Effects of Vandetanib on ACh Mediated Vessel Dilatation

ACh + 10 μ l PSS elicited significant vessel dilatation between 10^{-7} M- 10^{-5} M ACh ($P < 0.05$, Friedman; Figure 6.5). The ACh + DMSO control group showed a significant increase in vessel diameter between 10^{-6} M- 10^{-5} M ACh ($P < 0.05$, Friedman; Figure 6.5). The ACh + 10^{-7} M vandetanib group demonstrated a significant increase in vessel diameter at 10^{-5} M ACh ($P < 0.05$, Friedman; Figure 6.5) The ACh + 10^{-7} M vandetanib group showed a significantly smaller increase in vessel diameter in comparison to ACh + 10 μ l PSS ($P < 0.05$, Kruskal Wallis). This difference was not seen between the ACh + 10^{-7} M vandetanib and ACh + DMSO control or between the ACh + DMSO control and ACh + 10 μ l PSS group ($P > 0.05$, Kruskal Wallis), demonstrating vandetanib significantly inhibits ACh-mediated dilatation. The pEC_{50} for ACh + PSS was 6.6 ± 0.2 . pEC_{50} values for the other experimental groups could not be calculated due to the non-linear regression curve not reaching the asymptote.

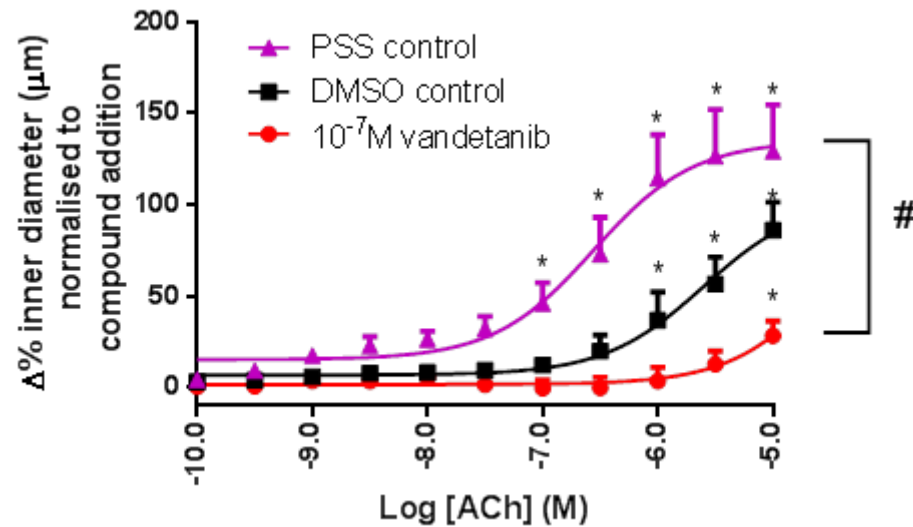


Figure 6.5 The effect of vandetanib, DMSO and PSS on ACh induced vessel dilatation after precontraction with U46619 (10^{-7} M). Vessels were precontracted with U46619, allowed to normalise of 30 min and then treated with $10 \mu\text{l}$ 10^{-4} M vandetanib (10^{-7} M final concentration) ($n=7$), or $10 \mu\text{l}$ of the equivalent DMSO concentration ($n=5$), or $10 \mu\text{l}$ PSS ($n=6$) for 10 min before being exposed to increasing concentration of ACh. Data presented has been pooled and normalised to the vessel diameter produced by the addition of vandetanib, DMSO or PSS after U46619 constriction. Each point represents the mean \pm SEM. #- $p < 0.05$ Kruskal Wallis between group comparison *- $p < 0.05$ Friedman test with data points compared against the PSS/ DMSO/ vandetanib incubation value after U46619 constriction.

6.4 Discussion

This Chapter set out to characterise the effects of vandetanib and pazopanib alone, and vandetanib in combination with hVEGF₁₆₅ or ACh on vessel tone. The effects of vandetanib in the presence of hVEGF₁₆₅ or ACh were explored due to the preliminary experimental results shown in Section 4.3.2. In vessels not pre-constricted with U46619, vandetanib and pazopanib had no significant effect (Figure 6.2). However, in pre-constricted vessels vandetanib caused a significant dilatation (Figure 6.3). Vandetanib was also shown to significantly reduce hVEGF₁₆₅ and ACh-mediated vessel dilatation (Figure 6.4, Figure 6.5). Here the possible reasons for these findings and how they relate to the current literature will be discussed.

6.4.1 The Effect of Vandetanib and Pazopanib on Pressurised Vessel Diameter

Vandetanib and pazopanib did not have a significant effect on vessel diameter in vessels which had not been pre-constricted with U46619 (Figure 6.2). The PEG vehicle used in Figure 6.2 and for the *in vivo* experiments in Chapters 4 and 5 had no significant effect on vessel tone.

The lack of effect of vandetanib and pazopanib on vessel diameter was somewhat unexpected as Mayer *et al* (2011) had previously reported vandetanib was able to reduce resting brachial arterial diameter and increase vascular resistance (Mayer *et al.*, 2011).

One explanation for the above result is that the vessels used in the experimental preparation were not under sufficient haemodynamic pressure to produce vascular cell signalling,

and therefore vandetanib/pazopanib targeted receptor tyrosine kinases were not activated. This would mean vandetanib and pazopanib were unable to bind to their target kinases (see Section 1.3.1 for explanation of class I RTKI mechanism) and could not elicit an effect. Haemodynamic pressure consists of 2 factors; shear stress and cyclic circumferential stretch (Chatterjee and Fisher, 2014a; Yamamoto and Ando, 2015,) In the isobaric myography protocol used here, vessels experienced cyclic circumferential stretch but not shear stress, as no flow through the vessel was allowed. The role of shear stress in the absence of cyclic circumferential stretch and *vice versa*, along with how ECs differentiate these mechano-signals is not fully understood (Yamamoto and Ando, 2015). However, there is an emerging theme in the literature that suggests cyclic stress in the absence of shear stress is primarily linked to endothelial remodelling. Sipkema *et al* demonstrated that in intact vessels, cyclic stretch lead to reorganisation of the endothelial cytoskeleton, with actin filaments realigned toward the direction of the cyclic stress (Sipkema *et al.*, 2003). Cyclic circumferential stretch has also been linked to the regulation of cell and vessel remodelling by Wang *et al* who showed human ECs exposed to cyclic stress had increased expression of metalloproteinases (Michel, 2003; Wang *et al.*, 2003). The myography experiments discussed herein would need to be repeated with the addition of shear stress to test this hypothesis further.

Vandetanib- and pazopanib-mediated vasodilatation would go relatively unseen in vessel preparations that had not been pre-constricted, as the vessel diameter does not have as much capacity to dilate. In order to test this vandetanib was added in a cumulative manner to vessel pre-constricted with U46619.

6.4.2 The Effect of Vandetanib on the Vessel Diameter of Pre-Constricted Pressurised Vessels

Vandetanib led to a significant dilatation in vessels pre-constricted with U46619 (Figure 6.3). This result was unexpected and contradicts the current literature (Bhargava, 2009; Kruzliak *et al.*, 2014; Lankhorst *et al.*, 2014; Abi Aad *et al.*, 2015; Lankhorst *et al.*, 2015).

U46619, used to constrict the vessels, is a thromboxane A₂ (TxA₂) agonist (Scornik and Toro, 1992). TxA₂ production in the EC is initiated by shear stress, which triggers the Ca²⁺ dependent production of arachidonic acid; this is converted into prostaglandin H₂ and subsequently to TxA₂ by TxA₂ synthase (otherwise known as CYP5). TxA₂ binds to thromboxane receptors (TP) on smooth muscle cells. TP is coupled to both Gq/11 and G12/13 G proteins, and therefore signals via the PLC and Rho kinase pathways to elicit contraction (Tsai and Jiang, 2006; Ellinsworth *et al.*, 2014). TxA₂ has been shown to reduce NO and PGI₂-mediated vessel relaxation (Feletou *et al.*, 2011). Vandetanib has been shown to bind to intracellular kinases involved in the vascular smooth muscle contraction mediated by TxA₂, for example Davis *et al* showed that vandetanib was able to bind to MEK with a K_d of 49 nM (Davis *et al.*, 2011). Vandetanib has been shown to be able to bind to the active conformation of tyrosine kinase domains (Gotink and Verheul, 2010), this paired with its ability to cross the cell membrane (Carter *et al.*, 2015) and reverse U46619-mediated constriction suggests that vandetanib may inhibit tyrosine kinase activity in vasoconstrictive as well as vasodilatory signalling pathways.

6.4.3 The Effects of Vandetanib on hVEGF_{165a}-Mediated Vessel Dilatation

Vandetanib was shown to non-competitively inhibit hVEGF_{165a}-mediated dilatation (Figure 6.4) significantly reducing the maximal effect of hVEGF_{165a} while not causing a significant shift in hVEGF_{165a} pEC₅₀ (Figure 6.4), in keeping with the *in vitro* findings in Chapter 3. The inhibition of VEGF-mediated dilatation in isolated vessel preparations supports the hypothesis that VEGF RTKIs cause vasoconstriction.

hVEGF₁₆₅ had a pEC₅₀ of 13.0 ± 0.5 (Figure 6.3) in pre-constricted rat mesenteric arterioles. This is significantly different from the potency of hVEGF_{165a} in HEK293 cells transfected with VEGFR2 and NFAT-RE-luc2P (Chapter 3, hVEGF_{165a} pEC₅₀= 9.66 ± 0.05 p<0.05, student T test). This in part may be due to the use of human VEGF₁₆₅, rather than the equivalent rat VEGF₁₆₄ (Ishii *et al.*, 2001). The protein sequence for rat VEGF₁₆₄ has 88% homology with the human VEGF_{165a} (Figure 6.6). Although this does not rule out a difference between the potency of the two VEGF isoforms at VEGFR2, it does show that these 2 isoforms are similar. Comparing the effect of rat VEGF₁₆₄ in this experimental set up to human VEGF₁₆₅ data shown here (Figure 6.3) would allow for any difference between the actions of these two isoforms on rat mesenteric arterioles to be further explored.

	Score	Expect	Method	Identities	Positives	Gaps
	299 bits(766)	7e-111	Compositional matrix adjust.	146/165(88%)	150/165(90%)	1/165(0%)
Human VEGF165	1		APMAEGGGQNHHEVVKFMDVYQRSYCHPIETLVDIFQEYPDEIEYIFKPSCVPLMRCGGC			60
Rat VEGF164	1		APTEGE-QKAHEVVKFMDVYQRSYCRPIETLVDIFQEYPDEIEYIFKPSCVPLMRCAGC			59
Human VEGF165	61		CNDEGLECVPTESNITMQIMRIKPHQGHIGEMSFLOHNKCECRPKKDRARQENPCGPC			120
Rat VEGF164	60		CNDE LECVPT ESN+TMQIMRIKPHQ QHIGEMSFLOH++CECRPKKDR + EN C PC			119
Human VEGF165	121		SERRKHLFVQDPQTCKCCKNTDSRCKARQLELNERTCRCDKPRR	165		
Rat VEGF164	120		SERRKHLFVQDPQTCKCCKNTDSRCKARQLELNERTCRCDKPRR	164		

Figure 6.6 Protein sequence homology between human VEGF₁₆₅ (obtained from uniprot.org, UNIPROT-KB-P15692, 03.05.2016) and rat VEGF₁₆₄ (obtained from uniprot.org, UNIPROT-KB-P16612, 03.05.2016). Protein sequence alignment was performed using blast.ncbi.nlm.nih.gov/Blast 03.05.2016.

The difference in the potency of VEGF in the recombinant VEGF-NFAT cell line vs the isolated rat mesenteric arteriole could also be due to the physiological and structural differences between tissues and cell lines. Unlike the recombinant cell line, the arteriole is comprised of multiple cell phenotypes which natively express VEGFR2 and the corresponding signalling proteins needed to produce a vasoactive response. As the vessel is intact, its ability to increase a vasodilatory/ vasoconstrictive response through electrical transduction is maintained (Segal *et al.*, 1999). This process primarily occurs through gap junction signalling. Gap junctions are comprised of two connexons, one provided by each cell to form small 'pores' between cells in very close proximity. Gap junctions allow small molecules (<1000 Da) and electrical current to pass between cells (Salameh *et al.*, 2005). Propagation of electrical signals between endothelial and vascular smooth muscle cells leads to a fast response to stimuli and smooth coordinated constriction/dilatation of the vessel (Lehoux *et al.*, 2006). As each cell does not have to be

stimulated individually, less agonist is needed reducing the EC₅₀ of stimulatory molecules.

6.4.4 The Effects of Vandetanib on ACh-Mediated Vessel Dilatation

ACh causes endothelium dependent relaxation of vascular smooth muscle, and therefore vessel dilatation (Furchgott and Zawadzki, 1980). ACh binds to M₃ mAChR on ECs. This in turn leads to the production of NO and PGI₂ via the activation of the PLC and PI3K pathways (Socha *et al.*, 2012; Kang, 2014). ACh uses the same signalling pathways as VEGFR2 to produce NO and PGI₂. Therefore inhibition of ACh-mediated dilatation by VEGF RTKIs, which have not been shown to interact with GPCRs, such as the M₃ mAChR, would demonstrate vandetanib is able to functionally inhibit intracellular signalling kinases alongside receptor tyrosine kinases. Figure 6.5 shows vandetanib is able to significantly inhibit ACh-mediated vessel dilatation. This result, and the findings from Davis *et al.* and others (Kumar *et al.*, 2007; Davis *et al.*, 2011), which demonstrate RTKIs are able to bind to catalytic domains of intracellular kinases, as well as the data in Chapter 3, which shows vandetanib is able to penetrate the cell membrane, suggests that vandetanib does not specifically inhibit receptor tyrosine kinases. This result shows the need for a better understanding of RTKI targets. It is possible that the multi-targeted actions of RTKIs, like vandetanib, lead to an inhibition of vessel dilatation, regardless of the initiating signalling molecule.

6.4.5 Conclusion

Vandetanib and pazopanib produced no significant effect on vessel diameter in non-preconstricted vessels. Vandetanib has been shown to inhibit VEGF and ACh-mediated vessel dilatation. Vandetanib was also shown to elicit vasodilatation in the presence of a vasoconstrictor, a novel finding. Overall this Chapter clearly demonstrates the importance of the multi-targeted nature of pazopanib and vandetanib. A clearer understanding of the effects of RTKIs on endothelial signalling in vessels or in the whole animal is needed to gain a greater understanding of the underlying mechanisms that lead to hypertension.

Chapter 7: General Discussion

7.1 Introduction

One of the main side effects of anti-angiogenic VEGF therapies is the development of cardio-toxicity, specifically hypertension. The main objectives of this work were to determine the haemodynamic profile of VEGF therapies and to elucidate the possible signalling sequelae involved in the development of RTKI-induced hypertension. Through characterising the haemodynamic, cardiovascular and signalling profile of a panel of RTKIs *in vitro* and *in vivo* the detrimental hypertensive effect of these compounds and the possible mechanisms of action by which hypertension occurs were explored. With this in mind the specific aims of this project were:

- a) To determine the pharmacological characteristics of a panel of receptor tyrosine kinase inhibitors (RTKIs) (cediranib, sorafenib, pazopanib and vandetanib) in a whole cell system using VEGF-stimulated Nuclear Factor of Activated T-cell (NFAT) signalling in HEK293 cells expressing the human VEGFR2 and an NFAT reporter gene linked to firefly luciferase. The actions of the above RTKIs were also explored in the presence of two VEGF-A isoforms, VEGF_{165a} and VEGF_{165b}.
- b) To investigate the chronic effects of vandetanib and pazopanib on heart rate and blood pressure in male Sprague Dawley rats.
- c) To assess the effect of various concentrations of vandetanib and pazopanib on heart rate, mean arterial blood pressure, hindquarter, renal and mesenteric vascular conductances in male Sprague Dawley rats.
- d) To assess the action of vandetanib and pazopanib on isolated pressurised mesenteric arterioles, and to

elucidate the effect of vandetanib on VEGF and ACh-mediated vessel dilatation.

7.2 The Pharmacological Characteristics of a Panel of Receptor Tyrosine Kinase Inhibitors (RTKIs) (Cediranib, Sorafenib, Pazopanib and Vandetanib) in a Whole Cell System

This aim was addressed in Chapter 3, where cediranib, sorafenib, pazopanib and vandetanib were shown to non-competitively inhibit VEGF₁₆₅ and VEGF_{165b}-VEGFR2 mediated activation of the NFAT-luciferase reporter gene. Both VEGF₁₆₅ and VEGF_{165b} were shown to stimulate VEGFR2 - mediated NFAT-luciferase activation; however the efficacy of VEGF_{165b} at VEGFR2 was lower than VEGF₁₆₅.

The findings from the study described in Chapter 3 raised several questions:

1. Do RTKIs have the same order of potency at VEGFRs in human tissue?
2. Do RTKIs show a bias toward blocking certain signalling pathways over others, for example by blocking certain tyrosine kinase residues at a higher potency than others?
3. Does the order of potency found *in vitro* translate to the extent and commonality of hypertension in the rat/human?

Question 1 is important as it allows for the results gained here to be related to physiologically relevant tissue, and therefore give more insight onto RTKI potency. In order to answer this question, human primary cells from various tissues, e.g. resistance arterioles and the heart could be exposed to

cumulative concentrations of VEGF₁₆₅ in the presence of varying concentrations of RTKI and *vice versa*, similar to the experiments performed in Chapter 3. This would allow for a comparison in the order of potency of cediranib, sorafenib, pazopanib and vandetanib in more relevant tissue types.

An answer to question 2 would give a greater understanding of RTKI pathway bias. This is important as different VEGFR2 signalling pathways have different outcomes for the cell (Figure 1.1), and therefore RTKI bias may be, in part, responsible for the differences seen between various RTKI side effect profiles. In order to address this question, reporter gene assays, such as the one used in Chapter 3 could be used. Rather than looking at the activation of NFAT, the activation of serum response element (SRE), a response element of the MAPK pathway (Hill *et al.*, 2001) could be used. The MAPK pathway in ECs is linked to cell proliferation and vasodilatation (Figure 1.1): processes important for tumour growth and blood pressure control, respectively.

Question 3 addresses whether the order of potency found in the cell line translates to the extent and commonality of hypertension in the rat/human. In order to investigate this, cediranib, sorafenib, pazopanib and vandetanib would need to be given to rats/humans at equivalent ED₅₀ values. This would allow for a direct comparison between the severity and commonality of hypertension between compound populations. In Chapters 4 and 5, vandetanib and pazopanib were given to rats at equivalent ED₅₀ values, these studies elucidated that although pazopanib has a greater potency at VEGFR2 *in vitro* it did not cause a greater increase in mean arterial blood pressure over a 21 day dosing period, but rather produced a more sustained increase in mean arterial blood pressure after

treatment. This result suggests that vandetanib and pazopanib may have different pharmacokinetic profiles (Section 5.4.2).

Understanding the link between *in vitro* VEGFR2 receptor potency and the *in vivo* hypertensive side effect profile is important for new VEGF RTKI compound design.

7.3 The Chronic Effects of Vandetanib and Pazopanib on Heart Rate and Blood Pressure in Male Sprague Dawley Rats

In long-term telemetry studies (Chapter 4 and 5), vandetanib appeared to demonstrate significant hypertensive effects within 24 h of the first dose. This was maintained throughout the dosing period and for 7 days after dosing for the vandetanib 25 mgkg⁻¹day⁻¹ treatment group. In a preliminary staining study of the mesenteric vasculature performed on tissue taken from the vandetanib treatment group in the telemetry study, no significant signs of rarefaction were seen, however there was a trend toward rarefaction, suggesting that rarefaction may have occurred during the treatment period and been reversed post-treatment. In comparison pazopanib produced a significant increase in mean arterial blood pressure from day 10 day of dosing. This effect persisted throughout the measured post-treatment period. Patient populations taking pazopanib have been shown to be more likely to develop hypertension than those prescribed vandetanib (Hamberg *et al.*, 2010; Wells *et al.*, 2012; Bible *et al.*, 2014). This knowledge, combined with the results from Chapters 4 and 5 indicate that VEGF RTKI induced hypertension may be, in part, due to physiological cardiovascular changes such as rarefaction. It is also possible that pazopanib has a different kinetics profile to vandetanib (previously discussed in Section

5.4.2). These findings are novel and have raised multiple research questions:

1. Do vandetanib and pazopanib cause rarefaction after 3 weeks of treatment, and does this process reverse after treatment stops?
2. Do VEGF RTKIs cause endothelial dysfunction?
3. Are the kinetics profile between vandetanib and pazopanib different?

In order to address the first question further mesenteric studies would need to be undertaken. By looking at the mesenteric vasculature at different stages of treatment length as well as post-treatment it would be possible to ascertain if rarefaction is a contributing factor to VEGF RTKI induced hypertension.

Question 2 addresses the hypothesis that VEGF RTKIs cause endothelial dysfunction which consequently leads to hypertension. In order to explore this further, blood plasma concentrations of endothelial dysfunction markers and inflammatory molecules, such as c-reactive protein and interleukin 6, respectively (Lopez-Garcia *et al.*, 2004), from humans/ rats which had been subject to VEGF RTKI treatment vs no/vehicle treatment should be measured and compared.

Finally, the higher potency of pazopanib at VEGFR2 ($IC_{50}=8.25 \pm 0.03$) in comparison to vandetanib ($IC_{50}=6.72 \pm 0.03$; Carter *et al.*, 2015) leads to the prediction that pazopanib would cause a greater increase in blood pressure than vandetanib. This hypothesis is supported by the greater number of patients who experience hypertension with pazopanib compared to vandetanib in the clinic (Hamberg *et*

al., 2010; Bible *et al.*, 2014; Wells *et al.*, 2012). The considerably shorter plasma half-life of pazopanib in comparison to vandetanib (Section 1.3.1.1 and 1.3.1.2) would also lead to the prediction that the hypertensive effects of pazopanib would wane prior to those of vandetanib. However this was not the case (Chapter 4 and 5). One explanation for this observation is a difference in the kinetic profile of pazopanib in comparison to vandetanib. Slow dissociation of a drug from its target can lead to a disengagement between its pharmacokinetic profile and the compounds pharmacodynamic effects, with measured efficacy significantly outlasting detectable plasma concentrations of drug (Vauquelin and Charlton, 2010). If radiolabelled versions of the compounds were available, their dissociation rates could be directly measured using scintillation proximity assays with an immobilised version of the catalytic domain of the VEGFR (Park *et al.*, 1999), allowing further exploration of this hypothesis.

7.4 The Effect of Various Concentrations of Vandetanib and Pazopanib on Heart Rate, Mean Arterial Blood Pressure, Hindquarter, Renal and Mesenteric Vascular Conductances in Male Sprague Dawley Rats.

The dose dependent effects of pazopanib i.p and vandetanib i.p on heart rate, mean arterial blood pressure, and vascular conductance of the renal, mesenteric and hindquarter vascular beds were investigated over 4 days. Both vandetanib and pazopanib lead to hypertension and vasoconstriction of the mesenteric and hindquarter vascular beds, pazopanib also caused significant vasoconstriction of the renal vascular bed. None of the variables measured in the haemodynamic studies

significantly differed between the 30 mgkg⁻¹day⁻¹ pazopanib and 25 mgkg⁻¹day⁻¹ vandetanib groups. The effect of vandetanib and pazopanib on vascular conductance is a novel finding and suggests these compounds may lead to hypertension via a vasoactive mechanism. The results gained in these studies raised multiple questions:

1. Are the cardiovascular effects of vandetanib and pazopanib persistent when rats are dosed chronically and are they consistent once treatment has stopped?
2. Do vandetanib and pazopanib affect vessel tone?
3. Are the effects of vandetanib and pazopanib on blood pressure and vascular conductance negated in the presence of a NO-donor or PGI₂?

Question 1 is aimed toward characterising the long term effects of RTKIs and will give more information about the incidence of permanent physiological adaptations in the presence of VEGF RTKIs. This question was addressed in Chapters 4 and 5 and was discussed in Section 7.3.

With the evidence that vandetanib and pazopanib lead to reduced vascular conductance, there is a likely possibility that RTKI-induced hypertension, is in part, caused by their effect on vessel tone. In order to investigate this hypothesis further, and address question 2, myography studies were performed in Chapter 6. The results from these studies will be further discussed in Section 7.5.

Finally, an understanding of the signalling processes involved in the hypertensive and vasoconstrictive effects of pazopanib and vandetanib is needed. Chapter 3 and previously discussed published data suggest that these effects may be due to

antagonism of VEGFR2, which initially leads to inhibition of NO-dependent vasodilatation and in turn endothelial dysfunction. By looking at the effects of vandetanib and pazopanib on heart rate, blood pressure and vascular conductance in the presence of an NO donor and/or epoprostenol (PGI₂), the underlying signalling mechanisms behind VEGF RTKI induced hypertension can be further explored.

7.5 The Action of Vandetanib and Pazopanib on Isolated Pressurised Mesenteric Arterioles, and the Effect of Vandetanib on VEGF and Acetylcholine Mediated Vessel Dilatation.

This aim was addressed in Chapter 6 where pazopanib and vandetanib were shown to have no significant effect on vessel diameter in non-precontracted vessels. Vandetanib was shown to inhibit VEGF- and ACh-mediated vessel dilatation, a novel finding. Vandetanib was also able to induce vasodilatation in the presence of a vasoconstrictor (U46619), a previously unseen finding. The results in Chapter 6 clearly demonstrate the importance of the multi-targeted nature of pazopanib and vandetanib. Finally, hVEGF_{165a} was shown to be significantly more potent in rat mesenteric arterioles than in the VEGF NFAT recombinant HEK293 cell line, this result was expected due to the ability for ECs, which contain the full plethora of VEGFR signalling machinery, to propagate vasoactive signals through cell-cell interactions (discussed fully in Chapter 6). These results, combined with those previously discussed raise multiple questions:

1. Does vandetanib and pazopanib affect vessel structure?

2. Do vandetanib and pazopanib exert the same effect in the presence of other vasoactive substances?
3. Do class II and class III RTKIs demonstrate the same effect as vandetanib and pazopanib in non-precontracted vessels?

Vessel stiffness has been noted as a physiological marker of hypertension (Chirinos, 2012). Vessel stiffness is characterised by a thickening of the vessel wall and leads to the vessel being less responsive to vasoactive substances and haemodynamic stress, reducing the ability for the vessel to dilate. Whether this is a marker of hypertension or a cause, is currently disputed in the literature (Hall *et al.*, 2012). In order to look for structural changes in the vessel, vessel biopsies from rats/humans treated with vandetanib/ pazopanib could be harvested and histological staining of the vascular smooth muscle performed.

Previous research has shown that vandetanib and pazopanib are able to bind to multiple receptor tyrosine kinases as well as intracellular signalling kinases (Davis *et al.*, 2011); however the effect of this on their hypertensive side effect profile is unknown. In order to address question 2, the experiments in Chapter 6 Sections 6.3.3 and 6.3.4 should be repeated in the presence of vasoactive stimuli shown to be inhibited by vandetanib and pazopanib. One example of this would be PDGF. The inhibition of PDGF signalling has been shown to reduce pericyte recruitment during angiogenesis, therefore reducing vessel stability (Heldin, 2013). Understanding the effects of VEGF RTKIs multi-targeted action on their vasoactive profile will help to further improve future drug design.

Finally, vandetanib and pazopanib were shown to have no effect on unstimulated vessel preparations. Both vandetanib and pazopanib are class I RTKIs. They exert their inhibitory effects by binding to the active conformation of the receptor, competitively antagonising ATP binding at various intracellular kinase groups (Gotink and Verheul, 2010). However, class II and class III RTKIs are able to bind to their targets while they are in the non-active conformational state (Zhang *et al.*, 2009; Gotink and Verheul, 2010; Davis *et al.*, 2011). By repeating the experiments in Figure 6.2, with sorafenib and neratinib a greater understanding of how an RTKI's mechanism of action affects VEGF RTKI vasoactivity would be gained.

7.6 Overall Conclusion

Targeted therapeutics, as opposed to traditional cytotoxic therapies, were first brought to the clinic in the hope that they would reduce many of the side effects seen with non-specific cytotoxic chemotherapy. VEGF RTKIs, which are multi-targeted, have become a popular therapeutic tool as they have been shown to be relatively well tolerated in comparison to cytotoxic chemotherapies and drug resistance is a less common problem.

The inhibition of VEGF, a potent stimulant for angiogenesis (Gacche and Meshram, 2014), by VEGF RTKIs has been shown to reduce vessel density, cancer metastasis and tumour size (Liang *et al.*, 2014). Significant increases in progression free survival for a multitude of cancer types has led to VEGF RTKIs being FDA approval for the treatment of various solid tumours. For example, sorafenib and pazopanib have been shown to significantly improve progression free survival in renal cell

cancer, with patients taking these compounds on average living 3 to 9 months longer (Meadows and Hurwitz, 2012).

However, anti-VEGF RTKIs have been shown to have class specific side effects such as hypertension. Hypertension can lead to life threatening conditions such as stroke, arterial thrombo-embolisms and acute heart failure (Eschenhagen *et al.*, 2011). Therefore, clinicians must weigh up the cost-benefit ratio of prescribing these compounds, as although they extend a patient's progression free survival they are also able to produce serious side effects for those taking them. Whether a chosen VEGF RTKI will be prescribed depends on the age of the patient, any pre-existing conditions the patient may have, the tumour type and its genetic profile as well as any other concomitant treatments prescribed eg, surgical removal of the tumour mass. A better understanding of how VEGF RTKIs cause hypertension may help to further inform clinicians about the best treatments to prescribe VEGF-RTKI mediated hypertension as well as assist the research and development of anti-VEGF compounds that prolong patient progression free survival while not being cardio-toxic.

The body of work undertaken here has given novel insight into the ability for anti-VEGF RTKIs work non-competitively to inhibit VEGF mediated effects in the cell. It has also produced a validated method of reproducing hypertension in a rat model, both in the short and long term. These models have shown that different anti-VEGF RTKIs have different regional haemodynamic and post-treatment hypertensive side effect profiles. Finally, an isolated vessel myography technique was developed that demonstrated VEGF RTKIs are able to cause vessel dilatation, while also inhibiting VEGF and ACh mediated

vessel dilatation, implying these compounds may have further off target effects.

The ability to use validated in vivo models to reproduce anti-VEGF RTKI mediated hypertension allows for future investigation into the mechanisms behind how hypertension occurs as well as how best to reverse it. The models tested here also allow for further study into the post-treatment hypertensive profile of these compounds – an important issue for patients who stop taking drugs like pazopanib, shown here to have a more sustained hypertensive effect in the rat after treatment in comparison to vandetanib. Finally, the experimental model of myography developed here enables further research into the direct effect of VEGF RTKIs on vessel diameter. This may provide an opportunity to re-define the proteins compounds like vandetanib interact with. Not only is this important for understanding the mechanisms behind the therapeutic and non-therapeutic effects of vandetanib but may also aid development of the next generation of safer anti-angiogenic therapies.

References

- Abi Aad, S., Pierce, M., Barmaimon, G., Farhat, F. S., Benjo, A. and Mouhayar, E. (2015) Hypertension induced by chemotherapeutic and immunosuppressive agents: a new challenge. *Crit Rev Oncol Hematol* 93(1): pp.28-35.
- Abrams, J. (1996) Beneficial actions of nitrates in cardiovascular disease. *Am J Cardiol* 77(13): pp.31c-37c.
- Advani, A., Kelly, D. J., Advani, S. L., Cox, A. J., Thai, K., Zhang, Y., White, K. E., Gow, R. M., Marshall, S. M., Steer, B. M., Marsden, P. A., Rakoczy, P. E. and Gilbert, R. E. (2007) Role of VEGF in maintaining renal structure and function under normotensive and hypertensive conditions. *Proc Natl Acad Sci USA* 104(36): pp.14448-14453.
- Ahn, G. O., Seita, J., Hong, B. J., Kim, Y. E., Bok, S., Lee, C. J., Kim, K. S., Lee, J. C., Leeper, N. J., Cooke, J. P., Kim, H. J., Kim, I. H., Weissman, I. L. and Brown, J. M. (2014) Transcriptional activation of hypoxia-inducible factor-1 (HIF-1) in myeloid cells promotes angiogenesis through VEGF and S100A8. *Proc Natl Acad Sci USA* 111(7): pp.2698-2703.
- Ando, J. and Yamamoto, K. (2009) Vascular mechanobiology: EC responses to fluid shear stress. *Circ J* 73(11): pp.1983-1992.
- Aparicio-Gallego, G., Afonso-Afonso, F. J., Leon-Mateos, L., Firvida-Perez, J. L., Vazquez-Estevez, S., Lazaro-Quintela, M., Ramos-Vazquez, M., Fernandez-Calvo, O., Campos-Balea, B. and Anton-Aparicio, L. M. (2011) Molecular basis of hypertension side effects induced by sunitinib. *Anticancer Drugs* 22(1): pp.1-8.

Arakawa, H. (2005) Interaction between isolation rearing and social development on exploratory behavior in male rats. *Behav Processes* 70(3): pp.223-234.

Arganda-Carreras, I., Fernandez-Gonzalez, R., Munoz-Barrutia, A. and Ortiz-De-Solorzano, C. (2010) 3D reconstruction of histological Sections: Application to mammary gland tissue. *Microsc Res Tech* 73(11): pp.1019-1029.

Arjaans, M., Schroder, C. P., Oosting, S. F., Dafni, U., Kleibeuker, J. E. and de Vries, E. G. (2016) VEGF pathway targeting agents, vessel normalization and tumor drug uptake: from bench to bedside. *Oncotarget* 7(16): pp.21247-21258.

Armesilla, A. L., Lorenzo, E., Gomez del Arco, P., Martinez-Martinez, S., Alfranca, A. and Redondo, J. M. (1999) Vascular endothelial growth factor activates nuclear factor of activated T cells in human ECs: a role for tissue factor gene expression. *Mol Cell Biol* 19(3): pp.2032-2043.

Azizi, M., Chedid, A. and Oudard, S. (2008) Home blood-pressure monitoring in patients receiving sunitinib. *N Engl J Med* 1: pp.95-97.

Bachelder, R. E., Crago, A., Chung, J., Wendt, M. A., Shaw, L. M., Robinson, G. and Mercurio, A. M. (2001) Vascular endothelial growth factor is an autocrine survival factor for neuropilin-expressing breast carcinoma cells. *Cancer Res* 61(15): pp.5736-5740.

Bagri, A., Kouros-Mehr, H., Leong, K. G. and Plowman, G. D. (2010) Use of anti-VEGF adjuvant therapy in cancer: challenges and rationale. *Trends Mol Med* 3: pp.122-132.

Bates, D. O., Mavrou, A., Qiu, Y., Carter, J. G., Hamdollah-Zadeh, M., Barratt, S., Gammons, M. V., Millar, A. B., Salmon, A. H., Oltean, S., Harper, S. J. (2013) Detection of VEGF-A(xxx)b isoforms in human tissues. *PLoS One* 7(8): pp.e68399

Bates, D. O., MacMillan, P. P., Manjaly, J. G., Qiu, Y., Hudson, S. J., Bevan, H. S., Hunter, A. J., Soothill, P. W., Read, M., Donaldson, L. F. and Harper, S. J. (2006) The endogenous anti-angiogenic family of splice variants of VEGF, VEGFxxx_b, are down-regulated in pre-eclamptic placentae at term. *Clin Sci* 110(5): pp.575-585.

Bates, R. C., Goldsmith, J. D., Bachelder, R. E., Brown, C., Shibuya, M., Oettgen, P. and Mercurio, A. M. (2003) Flt-1-dependent survival characterizes the epithelial-mesenchymal transition of colonic organoids. *Curr Biol* 13(19): pp.1721-1727.

Bauer, V. and Sotnikova, R. (2010) Nitric oxide-the endothelium-derived relaxing factor and its role in endothelial functions. *Gen Physiol Biophys* 29(4): pp.319-340.

Belcik, J. T., Qi, Y., Kaufmann, B. A., Xie, A., Bullens, S., Morgan, T. K., Bagby, S. P., Kolumam, G., Kowalski, J., Oyer, J. A., Bunting, S. and Lindner, J. R. (2012) Cardiovascular and systemic microvascular effects of anti-vascular endothelial growth factor therapy for cancer. *J Am Coll Cardiol* 7: pp.618-625.

Benest, A. V. and Bates, D. O. (2009) Measurement of angiogenic phenotype by use of two-dimensional mesenteric angiogenesis assay. *Methods Mol Biol* 467: pp.251-270.

Benjamin, B., Sahu, M., Bhatnagar, U., Abhyankar, D. and Srinivas, N. R. (2012) The observed correlation between in

vivo clinical pharmacokinetic parameters and in vitro potency of VEGFR-2 inhibitors. Can this be used as a prospective guide for the development of novel compounds?

Arzneimittelforschung 62(4): pp.194-201.

Bentley, K., Mariggi, G., Gerhardt, H. and Bates, P. A. (2009) Tipping the balance: robustness of tip cell selection, migration and fusion in angiogenesis. *PLoS Comput Biol.* 5(10): pp.e1000549.

Bhargava, P. (2009) VEGF kinase inhibitors: how do they cause hypertension? *Am J Physiol Regul Integr Comp Physiol* 1: pp.R1-5.

Bible, K. C. and Ryder, M. (2016) Evolving molecularly targeted therapies for advanced-stage thyroid cancers. *Nat Rev Clin Oncol* 7: pp.403-416.

Bible, K. C., Suman, V. J., Menefee, M. E., Smallridge, R. C., Molina, J. R., Maples, W. J., Karlin, N. J., Traynor, A. M., Kumar, P., Goh, B. C., Lim, W. T., Bossou, A. R., Isham, C. R., Webster, K. P., Kukla, A. K., Bieber, C., Burton, J. K., Harris, P. and Erlichman, C. (2012) A multiinstitutional phase 2 trial of pazopanib monotherapy in advanced anaplastic thyroid cancer. *J Clin Endocrinol Metab* 9: pp.3179-3184.

Bible, K. C., Suman, V. J., Molina, J. R., Smallridge, R. C., Maples, W. J., Menefee, M. E., Rubin, J., Karlin, N., Sideras, K., Morris Iii, J. C., McIver, B., Hay, I., Fatourech, V., Burton, J. K., Webster, K. P., Bieber, C., Traynor, A. M., Flynn, P. J., Cher Goh, B., Isham, C. R., Harris, P. and Erlichman, C. (2014) A Multicenter Phase 2 Trial of Pazopanib in Metastatic and Progressive Medullary Thyroid Carcinoma. *J Clin Endocrinol Metab*: MCH057H. 99(5): pp1687-1693.

Blanc, J., Geney, R. and Menet, C. (2013) Type II kinase inhibitors: an opportunity in cancer for rational design. *Anticancer Agents Med Chem* 5: pp.731-747.

Blancher, C., Moore, J. W., Robertson, N. and Harris, A. L. (2001) Effects of ras and von Hippel-Lindau (VHL) gene mutations on hypoxia-inducible factor (HIF)-1 α , HIF-2 α , and vascular endothelial growth factor expression and their regulation by the phosphatidylinositol 3-kinase/Akt signaling pathway. *Cancer Res* 61(19): pp.7349-7355.

Blasi, E., Heyen, J., Patyna, S., Hemkens, M., Ramirez, D., John-Baptiste, A., Steidl-Nichols, J. and McHarg, A. (2012) Sunitinib, a receptor tyrosine kinase inhibitor, increases blood pressure in rats without associated changes in cardiac structure and function. *Cardiovasc Ther* 30(5): pp.287-294.

Blowey, D. L. (2016) Diuretics in the treatment of hypertension. *Pediatr Nephrol*. [Epub ahead of print]

Bretz, C. A., Savage, S., Capozzi, M. and Penn, J. S. (2013) The role of the NFAT signaling pathway in retinal neovascularization. *Invest Ophthalmol Vis Sci* 54(10): pp.7020-7027.

Brockway, B. P., Mills, P. A. and Azar, S. H. (1991) A new method for continuous chronic measurement and recording of blood pressure, heart rate and activity in the rat via radio-telemetry. *Clin Exp Hypertens A* 13(5): pp.885-895.

Brozzo, M. S., Bjelic, S., Kisko, K., Schleier, T., Leppanen, V. M., Alitalo, K., Winkler, F. K. and Ballmer-Hofer, K. (2012) Thermodynamic and structural description of allosterically regulated VEGFR-2 dimerization. *Blood* 119(7): pp.1781-1788.

Cahill, P. A. and Redmond, E. M. (2016) Vascular endothelium - Gatekeeper of vessel health. *Atherosclerosis* 248: pp.97-109.

Cai, J., Ahmad, S., Jiang, W. G., Huang, J., Kontos, C. D., Boulton, M. and Ahmed, A. (2003) Activation of vascular endothelial growth factor receptor-1 sustains angiogenesis. *Diabetes* 52(12): pp.2959-2968.

Cao, Y., E, G., Wang, E., Pal, K., Dutta, S. K., Bar-Sagi, D. and Mukhopadhyay, D. (2012) VEGF exerts an angiogenesis-independent function in cancer cells to promote their malignant progression. *Cancer Res* 72(16): pp.3912-3918.

Carlomagno, F., Guida, T., Anaganti, S., Vecchio, G., Fusco, A., Ryan, A. J., Billaud, M. and Santoro, M. (2004) Disease associated mutations at valine 804 in the RET receptor tyrosine kinase confer resistance to selective kinase inhibitors. *Oncogene* 23(36): pp.6056-6063.

Carmeliet, P., Ferreira, V., Breier, G., Pollefeyt, S., Kieckens, L., Gertsenstein, M., Fahrig, M., Vandenhoock, A., Harpal, K., Eberhardt, C., Declercq, C., Pawling, J., Moons, L., Collen, D., Risau, W. and Nagy, A. (1996) Abnormal blood vessel development and lethality in embryos lacking a single VEGF. *Nature* 380(6573): pp.435-439.

Carmeliet, P. and Jain, R. K. (2011) Molecular mechanisms and clinical applications of angiogenesis. *Nature* 7347: pp.298-307.

Carmeliet, P., Moons, L., Luttun, A., Vincenti, V., Compernelle, V., De Mol, M., Wu, Y., Bono, F., Devy, L., Beck, H., Scholz, D., Acker, T., DiPalma, T., Dewerchin, M., Noel, A., Stalmans, I., Barra, A., Blacher, S., VandenDriessche, T., Ponten, A., Eriksson, U., Plate, K. H., Foidart, J. M., Schaper, W.,

Charnock-Jones, D. S., Hicklin, D. J., Herbert, J. M., Collen, D. and Persico, M. G. (2001) Synergism between vascular endothelial growth factor and placental growth factor. *Nat Med* 7(5): pp.575-583.

Carter, J. J., Wheal, A. J., Hill, S. J. and Woolard, J. (2015) Characterisation of VEGF_{165a}- and VEGF_{165b}-stimulated NFAT-mediated gene transcription in HEK-293 cells expressing the human vascular endothelial growth factor receptor 2 (VEGFR2): Influence of receptor tyrosine kinase inhibitors. *Br J Pharmacol.* 8(2): pp.540-8

Catena, R., Larzabal, L., Larrayoz, M., Molina, E., Hermida, J., Agorreta, J., Montes, R., Pio, R., Montuenga, L. M. and Calvo, A. (2010) VEGF_{121b} and VEGF_{165b} are weakly angiogenic isoforms of VEGF-A. *Mol Cancer* 9: pp.320.

Cebe Suarez, S., Pieren, M., Cariolato, L., Arn, S., Hoffmann, U., Bogucki, A., Manlius, C., Wood, J. and Ballmer-Hofer, K. (2006) A VEGF-A splice variant defective for heparan sulfate and neuropilin-1 binding shows attenuated signaling through VEGFR-2. *Cell Mol Life Sci* 63(17): pp.2067-2077.

Cella, D. and Beaumont, J. L. (2016) Pazopanib in the treatment of advanced renal cell carcinoma. *Ther Adv Urol* 8(1): pp.61-69.

Chambers, A. F., Groom, A. C. and MacDonald, I. C. (2002) Dissemination and growth of cancer cells in metastatic sites. *Nat Rev Cancer*, 2(8) pp.563-572.

Chapleau, M. W., Hajduczuk, G. and Abboud, F. M. (1991) Paracrine role of prostanoids in activation of arterial baroreceptors: an overview. *Clin Exp Hypertens A* 13(5): pp.817-824.

Chatterjee, S. and Fisher, A. B. (2014a) Mechanotransduction in the endothelium: role of membrane proteins and reactive oxygen species in sensing, transduction, and transmission of the signal with altered blood flow. *Antioxid Redox Signal* 20(6): pp.899-913.

Chatterjee, S. and Fisher, A. B. (2014b) Mechanotransduction: forces, sensors, and redox signalling. *Antioxid Redox Signal* 20(6): pp.868-871.

Chau, N. G. and Haddad, R. I. (2013) Vandetanib for the treatment of medullary thyroid cancer. *Clin Cancer Res* 19(3): pp.524-529.

Chaudhary, B., Khaled, Y. S., Ammori, B. J. and Elkord, E. (2014) Neuropilin 1: function and therapeutic potential in cancer. *Cancer Immunol Immunother* 63(2): pp.81-99.

Chen, H. X. and Cleck, J. N. (2009) Adverse effects of anticancer agents that target the VEGF pathway. *Nat Rev Clin Oncol* 6(8): pp.465-477.

Chen, S., So, E. C., Strome, S. E. and Zhang, X. (2015) Impact of Detachment Methods on M2 Macrophage Phenotype and Function. *J Immunol Methods* 426: pp.56-61.

Cheung, N., Wong, M. P., Yuen, S. T., Leung, S. Y. and Chung, L. P. (1998) Tissue-specific expression pattern of vascular endothelial growth factor isoforms in the malignant transformation of lung and colon. *Hum Pathol* 29(9): pp.910-914.

Chirinos, J. A. (2012) Arterial stiffness: basic concepts and measurement techniques. *J Cardiovasc Transl Res* 5(3): pp.243-255.

Cho, S., Grazioso, R., Zhang, N., Aykac, M. and Schmand, M. (2011) Digital timing: sampling frequency, anti-aliasing filter and signal interpolation filter dependence on timing resolution. *Phys Med Biol* 56(23): pp.7569-7583.

Christensen, K. L. and Mulvany, M. J. (2001) Location of resistance arteries. *J Vasc Res* 38(1): pp.1-12.

Chu, T. F., Rupnick, M. A., Kerkela, R., Dallabrida, S. M., Zurakowski, D., Nguyen, L., Woulfe, K., Pravda, E., Cassiola, F., Desai, J., George, S., Morgan, J. A., Harris, D. M., Ismail, N. S., Chen, J. H., Schoen, F. J., Van den Abbeele, A. D., Demetri, G. D., Force, T. and Chen, M. H. (2007) Cardiotoxicity associated with tyrosine kinase inhibitor sunitinib. *Lancet* 370(9604): pp.2011-2019.

Ciardiello, F., Caputo, R., Damiano, V., Troiani, T., Vitagliano, D., Carlomagno, F., Veneziani, B. M., Fontanini, G., Bianco, A. R. and Tortora, G. (2003) Antitumor effects of ZD6474, a small molecule vascular endothelial growth factor receptor tyrosine kinase inhibitor, with additional activity against epidermal growth factor receptor tyrosine kinase. *Clin Cancer Res* 9(4): pp.1546-1556.

Conway, D. and Schwartz, M. A. (2012) Lessons from the endothelial junctional mechanosensory complex. *F1000 Biol Rep* 4: pp.1.

Cutler, J. A. (1996) High blood pressure and end-organ damage. *J Hypertens Suppl* 14(6): pp.S3-6.

Davis, G. E., Black, S. M. and Bayless, K. J. (2000) Capillary morphogenesis during human EC invasion of three-dimensional collagen matrices, *In Vitro Cell Dev Biol Anim.* 36(8): pp.513-519.

Davis, M. I., Hunt, J. P., Herrgard, S., Ciceri, P., Wodicka, L. M., Pallares, G., Hocker, M., Treiber, D. K. and Zarrinkar, P. P. (2011) Comprehensive analysis of kinase inhibitor selectivity. *Nat Biotechnol* 29(11): pp.1046-1051.

De Bock, K., De Smet, F., Leite De Oliveira, R., Anthonis, K. and Carmeliet, P. (2009) Endothelial oxygen sensors regulate tumor vessel abnormalization by instructing pericyte ECs. *J Mol Med* 87(6): pp.561-956.

Deveney, A. M., Kjellstrom, A., Forsberg, T. and Jackson, D. M. (1998) A pharmacological validation of radiotelemetry in conscious, freely moving rats. *J Pharmacol Toxicol Methods* 40(2): pp.71-79.

di Blasio, L., Bussolino, F. and Primo, L. (2015) Three-dimensional in vitro assay of EC invasion and capillary tube morphogenesis. *Methods Mol Biol* 1214: pp.41-47.

Djonov, V., Baum, O. and Burri, P. H. (2003) Vascular remodeling by intussusceptive angiogenesis. *Cell Tissue Res* 314(1): pp.107-117.

Djordjevic, S. and Driscoll, P. C. (2013) Targeting VEGF signalling via the neuropilin co-receptor. *Drug Discov Today* 18(9-10): pp.447-455.

Domigan, C. K., Ziyad, S. and Iruela-Arispe, M. L. (2014) Canonical and Noncanonical Vascular Endothelial Growth Factor Pathways: New Developments in Biology and Signal Transduction. *Arterioscler Thromb Vasc Biol* 35(1): pp.30-39

Dosch, D. D. and Ballmer-Hofer, K. (2010) Transmembrane domain-mediated orientation of receptor monomers in active VEGFR-2 dimers. *Faseb j* 24(1): pp.32-38.

Dougher-Vermazen, M., Hulmes, J. D., Bohlen, P. and Terman, B. I. (1994) Biological activity and phosphorylation sites of the bacterially expressed. *Biochem Biophys Res Commun* 205(1): pp.728-738.

Du, X., Ou, X., Song, T., Zhang, W., Cong, F., Zhang, S. and Xiong, Y. (2015) Adenosine A2B receptor stimulates angiogenesis by inducing VEGF and eNOS in human microvascular ECs. *Exp Biol Med* 240(11): pp.1472-1479.

Dumont, D. J., Jussila, L., Taipale, J., Lymboussaki, A., Mustonen, T., Pajusola, K., Breitman, M. and Alitalo, K. (1998) Cardiovascular failure in mouse embryos deficient in VEGF receptor-3. *Science* 282(5390): pp.946-949.

Durand, M. J. and Gutterman, D. D. (2013) Diversity in mechanisms of endothelium-dependent vasodilatation in health and disease. *Microcirculation* 20(3): pp.239-247.

Ehling, M. and Mazzone, M. (2016) Vessel Normalization in the Spot-LIGHT of Cancer Treatment. *Trends Mol Med* 22(2): pp.85-87.

Eilken, H. M. and Adams, R. H. (2010) Dynamics of EC behavior in sprouting angiogenesis. *Curr Opin Cell Biol.* 5: pp.617-625.

Ellinsworth, D. C., Shukla, N., Fleming, I. and Jeremy, J. Y. (2014) Interactions between thromboxane A(2) thromboxane/prostaglandin (TP) receptors, and endothelium-derived hyperpolarization. *Cardiovasc Res* 102(1): pp.9-16.

Eschenhagen, T., Force, T., Ewer, M. S., de Keulenaer, G. W., Suter, T. M., Anker, S. D., Avkiran, M., de Azambuja, E., Balligand, J. L., Brutsaert, D. L., Condorelli, G., Hansen, A.,

Heymans, S., Hill, J. A., Hirsch, E., Hilfiker-Kleiner, D., Janssens, S., de Jong, S., Neubauer, G., Pieske, B., Ponikowski, P., Pirmohamed, M., Rauchhaus, M., Sawyer, D., Sugden, P. H., Wojta, J., Zannad, F. and Shah, A. M. (2011) Cardiovascular side effects of cancer therapies: a position statement from the Heart Failure Association of the European Society of Cardiology. *Eur J Heart Fail* 13(1): pp.1-10.

Eskens, F. A. and Verweij, J. (2006) The clinical toxicity profile of vascular endothelial growth factor (VEGF) and vascular endothelial growth factor receptor (VEGFR) targeting angiogenesis inhibitors; a review. *Eur J Cancer* 18: pp.3127-3139.

Estanol, B., Porrás-Betancourt, M., Padilla-Leyva, M. A. and Senties-Madrid, H. (2011) A brief history of the baroreceptor reflex: from Claude Bernard to Arthur C. Guyton. Illustrated with some classical experiments. *Arch Cardiol Mex* 81(4): pp.330-336.

Even, M. S., Sandusky, C. B. and Barnard, N. D. (2006) Serum-free hybridoma culture: ethical, scientific and safety considerations. *Trends Biotechnol* 24(3): pp.105-108.

Fan, M., Zhang, J., Wang, Z., Wang, B., Zhang, Q., Zheng, C., Li, T., Ni, C., Wu, Z., Shao, Z., Hu, X. (2014) Phosphorylated VEGFR2 and hypertension: potential biomarkers to indicate VEGF-dependency of advanced breast cancer in anti-angiogenic therapy. *Breast Cancer Res Trust* 143(1):PP. 141-151

Fallah, F. (2015) Recent strategies in treatment of pulmonary arterial hypertension, a review. *Glob J Health Sci* 7(4): pp.307-322.

Falloon, B. J., Bund, S. J., Tulip, J. R. and Heagerty, A. M. (1993) In vitro perfusion studies of resistance artery function in genetic hypertension. *Hypertension* 22(4) pp.486-495.

Feihl, F., Liaudet, L., Waeber, B. and Levy, B. I. (2006) Hypertension: a disease of the microcirculation? *Hypertension* 6: pp.1012-1017.

Feletou, M., Huang, Y. and Vanhoutte, P. M. (2011) Endothelium-mediated control of vascular tone: COX-1 and COX-2 products. *Br J Pharmacol* 164(3): pp.894-912.

Feng, D., Nagy, J. A., Hipp, J., Dvorak, H. F. and Dvorak, A. M. (1996) Vesiculo-vacuolar organelles and the regulation of venule permeability to macromolecules by vascular permeability factor, histamine, and serotonin. *J Exp Med* 183(5): pp.1981-1986.

Fenger-Gron, J., Mulvany, M. J. and Christensen, K. L. (1995) Mesenteric blood pressure profile of conscious, freely moving rats. *J Physiol* 488 (3): pp.753-760.

Ferrara, N. (2001) Role of vascular endothelial growth factor in regulation of physiological angiogenesis. *Am J Physiol Cell Physiol* 280(6): pp.C1358-1366.

Ferrara, N., Carver-Moore, K., Chen, H., Dowd, M., Lu, L., OShea, K. S., Powell-Braxton, L., Hillan, K. J. and Moore, M. W. (1996) Heterozygous embryonic lethality induced by targeted inactivation of the VEGF. *Nature* 380(6573): pp.439-442.

Ferrara, N. and Henzel, W. J. (1989) Pituitary follicular cells secrete a novel heparin-binding growth factor specific for

vascular ECs. *Biochem Biophys Res Commun* 161(2): pp.851-858.

Flecknell, P. (2010) *Laboratory Animal Anaesthesia*. London, UK: Elsevier.

Foekens, J. A., Peters, H. A., Grebenchtchikov, N., Look, M. P., Meijer-van Gelder, M. E., Geurts-Moespot, A., van der Kwast, T. H., Sweep, C. G. and Klijn, J. G. (2001) High tumor levels of vascular endothelial growth factor predict poor response to systemic therapy in advanced breast cancer. *Cancer Res* 61(14): pp.5407-5414.

Folkman, J. (1971) Tumor angiogenesis: therapeutic implications. *N Engl J Med* 285(21): pp.1182-1186.

Folkman, J. (1972) Anti-angiogenesis: new concept for therapy of solid tumors. *Ann Surg* 175(3): pp.409-416.

Fong, G. H., Zhang, L., Bryce, D. M. and Peng, J. (1999) Increased hemangioblast commitment, not vascular disorganization, is the primary defect in flt-1 knock-out mice. *Development* 126(13): pp.3015-3025.

Fujino, S., Enokibori, T., Tezuka, N., Asada, Y., Inoue, S., Kato, H. and Mori, A. (1996) A comparison of epidermal growth factor receptor levels and other prognostic parameters in non-small cell lung cancer. *Eur J Cancer* 32a (12): pp.2070-2074.

Furchgott, R. F. and Zawadzki, J. V. (1980) The obligatory role of ECs in the relaxation of arterial smooth muscle by acetylcholine. *Nature* 288(5789): pp.373-376.

Gacche, R. N. and Meshram, R. J. (2014) Angiogenic factors as potential drug target: efficacy and limitations of anti-angiogenic therapy. *Biochim Biophys Acta* 1846(1): pp.161-179.

Galdiero, M. R., Bonavita, E., Barajon, I., Garlanda, C., Mantovani, A. and Jaillon, S. (2013) Tumor associated macrophages and neutrophils in cancer. *Immunobiology* 218(11): pp.1402-1410.

Gardiner, S. M., Compton, A. M., Bennett, T. and Hartley, C. J. (1990) Can pulsed Doppler technique measure changes in aortic blood flow in conscious rats? *Am J Physiol* 259(2): pp.H448-456.

Gartner, K., Buttner, D., Dohler, K., Friedel, R., Lindena, J. and Trautschold, I. (1980) Stress response of rats to handling and experimental procedures. *Lab Anim* 14(3): pp.267-274.

Gelinas, D. S., Bernatchez, P. N., Rollin, S., Bazan, N. G. and Sirois, M. G. (2002) Immediate and delayed VEGF-mediated NO synthesis in ECs: role of PI3K, PKC and PLC pathways. *Br J Pharmacol* 137(7): pp.1021-1030.

Gerhardt, H., Golding, M., Fruttiger, M., Ruhrberg, C., Lundkvist, A., Abramsson, A., Jeltsch, M., Mitchell, C., Alitalo, K., Shima, D. and Betsholtz, C. (2003) VEGF guides angiogenic sprouting utilizing endothelial tip cell filopodia. *J Cell Biol* 161(6): pp.1163-1177.

Ghirardi, O., Cozzolino, R., Guaraldi, D. and Giuliani, A. (1995) Within- and between-strain variability in longevity of inbred and outbred rats under the same environmental conditions. *Exp Gerontol* 30(5): pp.485-494.

Gille, H., Kowalski, J., Li, B., LeCouter, J., Moffat, B., Zioncheck, T. F., Pelletier, N. and Ferrara, N. (2001) Analysis of biological effects and signaling properties of Flt-1 (VEGFR-1) and KDR (VEGFR-2). A reassessment using novel receptor-specific vascular endothelial growth factor mutants. *J Biol Chem* 276(5): pp.3222-3230.

Goel, H. L. and Mercurio, A. M. (2013) VEGF targets the tumour cell. *Nat Rev Cancer* 13(12): pp.871-882.

Gomez-Manzano, C., Holash, J., Fueyo, J., Xu, J., Conrad, C. A., Aldape, K. D., de Groot, J. F., Bekele, B. N. and Yung, W. K. (2008) VEGF Trap induces antiglioma effect at different stages of disease. *Neuro Oncol* 10(6): pp.940-945.

Gotink, K. J. and Verheul, H. M. (2010) Anti-angiogenic tyrosine kinase inhibitors: what is their mechanism of action? *Angiogenesis* 13(1): pp.1-14.

Govindarajan, R., Adusumilli, J., Baxter, D. L., El-Khoueiry, A. and Harik, S. I. (2006) Reversible posterior leukoencephalopathy syndrome induced by RAF kinase inhibitor BAY 43-9006. *J Clin Oncol* 28: pp.e48.

Grabowski, P., Briest, F., Baum, R. P., Zaknun, J. J., Kulkarni, H. R., Zeitz, M. and Horsch, D. (2012) Vandetanib therapy in medullary thyroid cancer. *Drugs Today* 11: pp.723-733.

Graham, F. L., Smiley, J., Russell, W. C. and Nairn, R. (1977) Characteristics of a human cell line transformed by DNA from human adenovirus type 5. *J Gen Virol* 36(1): pp.59-74.

Grandis, J. R. and Sok, J. C. (2004) Signaling through the epidermal growth factor receptor during the development of malignancy. *Pharmacol Ther* 102(1): pp.37-46.

Granito, A., Marinelli, S., Negrini, G., Menetti, S., Benevento, F. and Bolondi, L. (2016) Prognostic significance of adverse events in patients with hepatocellular carcinoma treated with sorafenib. *Therap Adv Gastroenterol* 9(2): pp.240-249.

Greene, A. N., Clapp, S. L. and Alper, R. H. (2007) Timecourse of recovery after surgical intraperitoneal implantation of radiotelemetry transmitters in rats. *J Pharmacol Toxicol Methods* 56(2): pp.218-222.

Greene, E. R., Blair, W. F. and Hartley, C. (1981) Noninvasive pulsed Doppler blood velocity measurements and calculated flow in human digital arteries. *ISA Trans* 20(2): pp.15-24.

Gu, J. W., Manning, R. D., Jr., Young, E., Shparago, M., Sartin, B. and Bailey, A. P. (2009) Vascular endothelial growth factor receptor inhibitor enhances dietary salt-induced hypertension in Sprague-Dawley rats. *Am J Physiol Regul Integr Comp Physiol* 297(1): pp.R142-148

Guiol, C., Ledoussal, C. and Surge, J. M. (1992) A radiotelemetry system for chronic measurement of blood pressure and heart rate in the unrestrained rat validation of the method. *J Pharmacol Toxicol Methods* 28(2): pp.99-105.

Gutterman, D. D., Chabowski, D. S., Kadlec, A. O., Durand, M. J., Freed, J. K., Ait-Aissa, K. and Beyer, A. M. (2016) The Human Microcirculation: Regulation of Flow and Beyond. *Circ Res* 118(1): pp.157-172.

Hall, J. E., Granger, J. P., do Carmo, J. M., da Silva, A. A., Dubinion, J., George, E., Hamza, S., Speed, J. and Hall, M. E. (2012) Hypertension: physiology and pathophysiology. *Compr Physiol* 2(4): pp.2393-2442.

Hall, P. S., Harshman, L. C., Srinivas, S. and Witteles, R. M. (2013) The frequency and severity of cardiovascular toxicity from targeted therapy in advanced renal cell carcinoma patients. *JACC Heart Fail* 1(1): pp.72-78.

Halpern, W. and Mulvany, M. J. (1977) Tension responses to small length changes of vascular smooth muscle cells. *J Physiol* 265(1): pp.21p-23p.

Hamberg, P., Verweij, J. and Sleijfer, S. (2010) (Pre-) clinical pharmacology and activity of pazopanib, a novel multikinase angiogenesis inhibitor. *Oncologist* 6: pp.539-547.

Hamerlik, P., Lathia, J. D., Rasmussen, R., Wu, Q., Bartkova, J., Lee, M., Moudry, P., Bartek, J., Jr., Fischer, W., Lukas, J., Rich, J. N. and Bartek, J. (2012) Autocrine VEGF-VEGFR2-Neuropilin-1 signaling promotes glioma stem-like cell viability and tumor growth. *J Exp Med* 209(3): pp.507-520.

Hanahan, D. and Weinberg, R. A. (2000) The hallmarks of cancer. *Cell* 1: pp.57-70.

Hanahan, D. and Weinberg, R. A. (2011) Hallmarks of cancer: the next generation. *Cell* 5: pp.646-674.

Hansen, W., Hutzler, M., Abel, S., Alter, C., Stockmann, C., Kliche, S., Albert, J., Sparwasser, T., Sakaguchi, S., Westendorf, A. M., Schadendorf, D., Buer, J. and Helfrich, I. (2012) Neuropilin 1 deficiency on CD4+Foxp3+ regulatory T cells impairs mouse melanoma growth. *J Exp Med* 209(11): pp.2001-2016.

Hapani, S., Sher, A., Chu, D. and Wu, S. (2010) Increased risk of serious hemorrhage with bevacizumab in cancer patients: a meta-analysis. *Oncology* 79(1-2): pp.27-38.

Hartley, C. J. and Cole, J. S. (1974) An ultrasonic pulsed Doppler system for measuring blood flow in small vessels. *J Appl Physiol* 37(4): pp.626-629.

Hasskarl, J. (2014) Sorafenib: targeting multiple tyrosine kinases in cancer, Recent Results. *Cancer Res* 201: pp.145-164.

Hauzer, W., Bujok, J., Czerski, A., Rusiecka, A., Pecka, E., Gnus, J., Zawadzki, W. and Witkiewicz, W. (2014) beta-adrenergic antagonists influence abdominal aorta contractility by mechanisms not involving beta-adrenergic receptors. *Folia Biol* 62(3): pp.243-250.

Hayman, S. R., Leung, N., Grande, J. P. and Garovic, V. D. (2012) VEGF inhibition, hypertension, and renal toxicity. *Curr Oncol Rep* 14(4): pp.285-294.

Haywood, J. R., Shaffer, R. A., Fastenow, C., Fink, G. D. and Brody, M. J. (1981) Regional blood flow measurement with pulsed Doppler flowmeter in conscious rat. *Am J Physiol* 241(2): pp.H273-H278.

Heath, E. I., Infante, J., Lewis, L. D., Luu, T., Stephenson, J., Tan, A. R., Kasubhai, S., LoRusso, P., Ma, B., Suttle, A. B., Kleha, J. F., Ball, H. A. and Dar, M. M. (2013) A randomized, double-blind, placebo-controlled study to evaluate the effect of repeated oral doses of pazopanib on cardiac conduction in patients with solid tumors. *Cancer Chemother Pharmacol* 71(3): pp.565-573.

Heldin, C. H. (2013) Targeting the PDGF signaling pathway in tumor treatment. *Cell Commun Signal* 11: pp.97.

Hellstrom, M., Phng, L. K., Hofmann, J. J., Wallgard, E., Coultas, L., Lindblom, P., Alva, J., Nilsson, A. K., Karlsson, L., Gaiano, N., Yoon, K., Rossant, J., Iruela-Arispe, M. L., Kalen, M., Gerhardt, H. and Betsholtz, C. (2007) Dll4 signalling through Notch1 regulates formation of tip cells during angiogenesis. *Nature* 7129: pp.776-780.

Hennequin, L. F., Stokes, E. S., Thomas, A. P., Johnstone, C., Ple, P. A., Ogilvie, D. J., Dukes, M., Wedge, S. R., Kendrew, J. and Curwen, J. O. (2002) Novel 4-anilinoquinazolines with C-7 basic side chains: design and structure activity relationship of a series of potent, orally active, VEGF receptor tyrosine kinase inhibitors. *J Med Chem* 45(6): pp.1300-1312.

Herbst, R. S., Sun, Y., Eberhardt, W. E., Germonpre, P., Saijo, N., Zhou, C., Wang, J., Li, L., Kabbinavar, F., Ichinose, Y., Qin, S., Zhang, L., Biesma, B., Heymach, J. V., Langmuir, P., Kennedy, S. J., Tada, H. and Johnson, B. E. (2010) Vandetanib plus docetaxel versus docetaxel as second-line treatment for patients with advanced non-small-cell lung cancer (ZODIAC): a double-blind, randomised, phase 3 trial. *Lancet Oncol* 11(7): pp.619-626.

Hill, S. J., Baker, J. G. and Rees, S. (2001) Reporter-gene systems for the study of G-protein-coupled receptors. *Curr Opin Pharmacol* 1(5): pp.526-532.

Hiratsuka, S., Minowa, O., Kuno, J., Noda, T. and Shibuya, M. (1998) Flt-1 lacking the tyrosine kinase domain is sufficient for normal development and angiogenesis in mice. *Proc Natl Acad Sci USA* 95(16): pp.9349-9354.

Hogan, P. G., Chen, L., Nardone, J. and Rao, A. (2003) Transcriptional regulation by calcium, calcineurin, and NFAT. *Genes Dev* 17(18): pp.2205-2232.

Holden, S. N., Eckhardt, S. G., Basser, R., de Boer, R., Rischin, D., Green, M., Increasednthal, M. A., Wheeler, C., Barge, A. and Hurwitz, H. I. (2005) Clinical evaluation of ZD6474, an orally active inhibitor of VEGF and EGF receptor signaling, in patients with solid, malignant tumors. *Ann Oncol* 8: pp.1391-1317.

Hong, D. S., Garrido-Laguna, I., Ekmekcioglu, S., Falchook, G. S., Naing, A., Wheler, J. J., Fu, S., Moulder, S. L., Piha-Paul, S., Tsimberidou, A. M., Wen, Y., Culotta, K. S., Anderes, K., Davis, D. W., Liu, W., George, G. C., Camacho, L. H., Percy Ivy, S. and Kurzrock, R. (2014) Dual inhibition of the vascular endothelial growth factor pathway: a phase 1 trial evaluating bevacizumab and AZD2171 (cediranib) in patients with advanced solid tumors. *Cancer* 120(14): pp.2164-2173.

Hong, S., Tan, M., Wang, S., Luo, S., Chen, Y. and Zhang, L. (2015) Efficacy and safety of angiogenesis inhibitors in advanced non-small cell lung cancer: a systematic review and meta-analysis. *J Cancer Res Clin Oncol*. 141(5): pp.909-921.

Hood, J. D., Meininger, C. J., Ziche, M. and Granger, H. J. (1998) VEGF upregulates ecNOS message, protein, and NO production in human ECs. *Am J Physiol* 274(3): pp.H1054-H1058.

Horii, D., Kanayama, T., Mori, M., Shibasaki, M. and Ikegami, S. (1978) Vasodilatation produced by prostacyclin (PGI₂) and 9(O)-thiaprostacyclin (PGI₂-S) in the canine femoral circulation. *Eur J Pharmacol* 51(3): pp.313-316.

Horowitz, J. R., Rivard, A., van der Zee, R., Hariawala, M., Sheriff, D. D., Esakof, D. D., Chaudhry, G. M., Symes, J. F. and Isner, J. M. (1997) Vascular endothelial growth factor/vascular permeability factor produces nitric oxide-dependent hypotension. Evidence for a maintenance role in quiescent adult endothelium. *Arterioscler Thromb Vasc Biol* 17(11): pp.2793-2800.

Huang, S. and Kauffman, S. (2013) How to escape the cancer attractor: rationale and limitations of multi-target drugs. *Semin Cancer Biol* 23(4): pp.270-278.

Huetteman, D. A. and Bogie, H. (2009) Direct blood pressure monitoring in laboratory rodents via implantable radio telemetry. *Methods Mol Biol* 573: pp.57-73.

Data Sciences International (DSI). (2013) Telemetry User manual Data Sciences International St Paul MN, USA: Data Sciences International p. appendix A.

Ishii, H., Oota, I., Takuma, T. and Inomata, K. (2001) Developmental expression of vascular endothelial growth factor in the masseter muscle of rats. *Arch Oral Biol* 46(1): pp.77-82.

Ito, N., Wernstedt, C., Engstrom, U. and Claesson-Welsh, L. (1998) Identification of vascular endothelial growth factor receptor-1 tyrosine. *J Biol Chem* 273(36): pp.23410-23418.

J.J. Van Dongen, R. R., J.W.Rensema, G.H.J. Van Wunnik (1990) Manual of Microsurgery on the Laboratory Rat. Techniques in the Behavioral and Neural Sciences volume 4 1 edn. Amsterdam, Netherlands: Elsevier, p. 81-160.

Janse, M. J. (2005) Sympathetic innervation of the heart. *Heart Rhythm* 6: pp.610.

Jia, H., Cheng, L., Tickner, M., Bagherzadeh, A., Selwood, D. and Zachary, I. (2010) Neuropilin-1 antagonism in human carcinoma cells inhibits migration and enhances chemosensitivity. *Br J Cancer* 102(3): pp.541-552.

Joyner, M. J. and Casey, D. P. (2014) Muscle blood flow, hypoxia, and hypoperfusion. *J Appl Physiol* 116(7): pp.852-857.

Justice, R. and Robertson, K. (2008) FDA Report: Pazopanib.

Kamba, T. and McDonald, D. M. (2007) Mechanisms of adverse effects of anti-VEGF therapy for cancer. *Br J Cancer* 12: pp.1788-1795.

Kandel, S. and Lampe, J. N. (2014) Role of Protein-Protein Interactions in Cytochrome P450-Mediated Drug Metabolism and Toxicity. *Chem Res Toxicol* 27(9): pp.1474-1486.

Kang, K. T. (2014) Endothelium-derived Relaxing Factors of Small Resistance Arteries in Hypertension. *Toxicol Res* 30(3): pp.141-148.

Kappers, M. H., van Esch, J. H., Sluiter, W., Sleijfer, S., Danser, A. H. and van den Meiracker, A. H. (2010) Hypertension induced by the tyrosine kinase inhibitor sunitinib is associated with increased circulating endothelin-1 levels. *Hypertension* 56(4): pp.675-681.

Katz, A. M. (2002) Ernest Henry Starling, his predecessors, and the "Law of the Heart". *Circulation* 106(23): pp.2986-2992.

Kaur, B., Khwaja, F. W., Severson, E. A., Matheny, S. L., Brat, D. J. and Van Meir, E. G. (2005) Hypoxia and the hypoxia-inducible-factor pathway in glioma growth and angiogenesis. *Neuro Oncol* 7(2): pp.134-153.

Kawamura, H., Li, X., Harper, S. J., Bates, D. O. and Claesson-Welsh, L. (2008) Vascular endothelial growth factor (VEGF)-A165b is a weak in vitro agonist for VEGF receptor-2 due to lack of coreceptor binding and deficient regulation of kinase activity. *Cancer Res* 68(12): pp.4683-4692.

Kawasaki, T., Kitsukawa, T., Bekku, Y., Matsuda, Y., Sanbo, M., Yagi, T. and Fujisawa, H. (1999) A requirement for neuropilin-1 in embryonic vessel formation. *Development* 126(21): pp.4895-4902.

Kieran, M. W., Kalluri, R. and Cho, Y. J. (2012) The VEGF pathway in cancer and disease: responses, resistance, and the path forward. *Cold Spring Harb Perspect Med* 2(12): pp.a006593.

Kitsukawa, T., Shimono, A., Kawakami, A., Kondoh, H. and Fujisawa, H. (1995) Overexpression of a membrane protein, neuropilin, in chimeric mice causes anomalies in the cardiovascular system, nervous system and limbs. *Development* 121(12): pp.4309-4318.

Klijn, J. G., Berns, P. M., Schmitz, P. I. and Foekens, J. A. (1992) The clinical significance of epidermal growth factor receptor (EGF-R) in human breast cancer: a review on 5232 patients. *Endocr Rev* 13(1): pp.3-17.

Knosel, T., Kampmann, E., Kirchner, T. and Altendorf-Hofmann, A. (2014) Tyrosine kinases in soft tissue tumors. *Pathologie* 35 (2): pp.198-201.

Knowles, P. P., Murray-Rust, J., Kjaer, S., Scott, R. P., Hanrahan, S., Santoro, M., Ibanez, C. F. and McDonald, N. Q. (2006) Structure and chemical inhibition of the RET tyrosine kinase domain. *J Biol Chem* 281(44): pp.33577-33587.

Koch, S., Tugues, S., Li, X., Gualandi, L. and Claesson-Welsh, L. (2011) Signal transduction by vascular endothelial growth factor receptors. *Biochem J* 2: pp.169-183.

Kramer, K. and Kinter, L. B. (2003) Evaluation and applications of radiotelemetry in small laboratory animals. *Physiol Genomics* 13(3): pp.197-205.

Kramer, K., van Acker, S. A., Voss, H. P., Grimbergen, J. A., van der Vijgh, W. J. and Bast, A. (1993) Use of telemetry to record electrocardiogram and heart rate in freely moving mice. *J Pharmacol Toxicol Methods* 30(4): pp.209-215.

Kruse, A. C., Hu, J., Pan, A. C., Arlow, D. H., Increasednbaum, D. M., Increasedmond, E., Green, H. F., Liu, T., Chae, P. S., Dror, R. O., Shaw, D. E., Weis, W. I., Wess, J. and Kobilka, B. K. (2012) Structure and dynamics of the M3 muscarinic acetylcholine receptor. *Nature* 482(7386): pp.552-556.

Kruzliak, P., Kovacova, G. and Pechanova, O. (2013) Therapeutic potential of nitric oxide donors in the prevention and treatment of angiogenesis-inhibitor-induced hypertension. *Angiogenesis* 16(2): pp.289-295.

Kruzliak, P., Novak, J. and Novak, M. (2014) Vascular endothelial growth factor inhibitor-induced hypertension: from pathophysiology to prevention and treatment based on long-acting nitric oxide donors. *Am J Hypertens* 27(1): pp.3-13.

Kumar, R., Knick, V. B., Rudolph, S. K., Johnson, J. H., Crosby, R. M., Crouthamel, M. C., Hopper, T. M., Miller, C. G., Harrington, L. E., Onori, J. A., Mullin, R. J., Gilmer, T. M., Truesdale, A. T., Epperly, A. H., Bloor, A., Stafford, J. A., Luttrell, D. K. and Cheung, M. (2007) Pharmacokinetic-pharmacodynamic correlation from mouse to human with pazopanib, a multikinase angiogenesis inhibitor with potent antitumor and antiangiogenic activity. *Mol Cancer Ther* 6(7): pp.2012-2021.

La Vine, D. B., Coleman, T. A., Davis, C. H., Carbonell, C. E. and Davis, W. B. (2010) Frequent dose interruptions are required for patients receiving oral kinase inhibitor therapy for advanced renal cell carcinoma. *Am J Clin Oncol* 33(3): pp.217-220.

Lamas, S. and Rodriguez-Puyol, D. (2012) Endothelial control of vasomotor tone: the kidney perspective. *Semin Nephrol* 2: pp.156-166.

Lamprecht, F., Williams, R. B. and Kopin, I. J. (1973) Serum dopamine-beta-hydroxylase during development of immobilization-induced hypertension. *Endocrinology* 92(3): pp.953-956.

Lankhorst, S., Kappers, M. H., van Esch, J. H., Danser, A. H. and van den Meiracker, A. H. (2014) Hypertension during vascular endothelial growth factor inhibition: focus on nitric oxide, endothelin-1, and oxidative stress. *Antioxid Redox Signal* 20(1): pp.135-145.

Lankhorst, S., Saleh, L., Danser, A. J. and van den Meiracker, A. H. (2015) Etiology of angiogenesis inhibition-related hypertension. *Curr Opin Pharmacol* 21: pp.7-13.

Le, D. L., Cao, H. and Yang, L. X. (2014) Cardiotoxicity of molecular-targeted drug therapy. *Anticancer Res* 34(7): pp.3243-2349.

Lee, J., Ku, T., Yu, H., Chong, K., Ryu, S. W., Choi, K. and Choi, C. (2012) Blockade of VEGF-A suppresses tumor growth via inhibition of autocrine signaling through FAK and AKT. *Cancer Lett* 318(2): pp.221-225.

Lee, S., Jilani, S. M., Nikolova, G. V., Carpizo, D. and Iruela-Arispe, M. L. (2005) Processing of VEGF-A by matrix metalloproteinases regulates bioavailability and vascular patterning in tumors. *J Cell Biol* 169(4): pp.681-691.

Lehoux, S., Castier, Y. and Tedgui, A. (2006) Molecular mechanisms of the vascular responses to haemodynamic forces. *J Intern Med* 259(4): pp.381-392.

Leigh Verbois, S. 2011. Pharmacology/toxicology nda/bla review and evaluation-Vandetanib *AstraZeneca*.

Leppanen, V. M., Prota, A. E., Jeltsch, M., Anisimov, A., Kalkkinen, N., Strandin, T., Lankinen, H., Goldman, A., Ballmer-Hofer, K. and Alitalo, K. (2010) Structural determinants of growth factor binding and specificity by VEGF receptor 2. *Proc Natl Acad Sci USA* 107(6): pp.2425-2430.

Leung, D. W., Cachianes, G., Kuang, W. J., Goeddel, D. V. and Ferrara, N. (1989) Vascular endothelial growth factor is a secreted angiogenic mitogen. *Science* 246(4935): pp.1306-1309.

Levy, P. (1989) Effects of prazosin on blood pressure and diabetic control in patients with type II diabetes mellitus and mild essential hypertension. *Am J Med* 86(1b): pp.59-62.

Liang, X., Xu, F., Li, X., Ma, C., Zhang, Y. and Xu, W. (2014) VEGF signal system: the application of antiangiogenesis. *Curr Med Chem* 21(7): pp.894-910.

Liang, X., Xu, F., Ma, C., Zhang, Y. and Xu, W. (2013) VEGF Signal System: The Application of Antiangiogenesis. *Curr Med Chem* 21(7): pp.894-910

Lopez-Garcia, E., Schulze, M. B., Fung, T. T., Meigs, J. B., Rifai, N., Manson, J. E. and Hu, F. B. (2004) Major dietary patterns are related to plasma concentrations of markers of inflammation and endothelial dysfunction. *Am J Clin Nutr* 80(4): pp.1029-1035.

Lowe, J., Araujo, J., Yang, J., Reich, M., Oldendorp, A., Shiu, V., Quarmby, V., Lowman, H., Lien, S., Gaudreault, J. and Maia, M. (2007) Ranibizumab inhibits multiple forms of biologically active vascular endothelial growth factor in vitro and in vivo. *Exp Eye Res* 85(4): pp.425-430.

Maddox, P. H. and Jenkins, D. (1987) 3-Aminopropyltriethoxysilane (APES): a new advance in Section adhesion. *J Clin Pathol* 40(10): pp.1256-1257.

Mahalingam, D., Malik, L., Beeram, M., Rodon, J., Sankhala, K., Mita, A., Benjamin, D., Ketchum, N., Michalek, J., Tolcher, A., Wright, J. and Sarantopoulos, J. (2014) Phase II study evaluating the efficacy, safety, and pharmacodynamic correlative study of dual antiangiogenic inhibition using bevacizumab in combination with sorafenib in patients with advanced malignant melanoma. *Cancer Chemother Pharmacol* 74(1): pp.77-84.

Mak, P., Leav, I., Pursell, B., Bae, D., Yang, X., Taglienti, C. A., Gouvin, L. M., Sharma, V. M. and Mercurio, A. M. (2010)

ERbeta impedes prostate cancer EMT by destabilizing HIF-1alpha and inhibiting VEGF-mediated snail nuclear localization: implications for Gleason grading. *Cancer Cell* 17(4): pp.319-332.

Malkesman, O., Maayan, R., Weizman, A. and Weller, A. (2006) Aggressive behaviour and HPA axis hormones after social isolation in adult rats of two different genetic animal models for depression. *Behav Brain Res* 175(2): pp.408-414.

Mason, R. P., Marche, P. and Hintze, T. H. (2003) Novel vascular biology of third-generation L-type calcium channel antagonists: ancillary actions of amlodipine. *Arterioscler Thromb Vasc Biol* 23(12): pp.2155-2163.

Mavromoustakos, T., Apostolopoulos, V. and Matsoukas, J. (2001) Antihypertensive drugs that act on Renin-Angiotensin System with emphasis in AT(1) antagonists. *Mini Rev Med Chem* 1(2): pp.207-217.

Maxwell, P. H., Pugh, C. W. and Ratcliffe, P. J. (2001) Activation of the HIF pathway in cancer. *Curr Opin Genet Dev* 3: pp.293-299.

Mayer, E. L., Dallabrida, S. M., Rupnick, M. A., Redline, W. M., Hannagan, K., Ismail, N. S., Burstein, H. J. and Beckman, J. A. (2011) Contrary effects of the receptor tyrosine kinase inhibitor vandetanib on constitutive and flow-stimulated nitric oxide elaboration in humans. *Hypertension* 58(1): pp.85-92.

McCormack, T., Krause, T. and OFlynn, N. (2012) Management of hypertension in adults in primary care: NICE guideline. *Br J Gen Pract* 62(596): pp.163-164.

Meadows, K. L. and Hurwitz, H. L. (2012) Anti-VEGF Therapies in the Clinic. *Cold Spring Harb Perspect Med* 2(10): pp. 6577

Meunier, V., Bourrie, M., Berger, Y. and Fabre, G. (1995) The human intestinal epithelial cell line Caco-2; pharmacological and pharmacokinetic applications. *Cell Biol Toxicol* 11(4): pp.187-194.

Michel, J. B. (2003) Anoikis in the cardiovascular system: known and unknown extracellular mediators. *Arterioscler Thromb Vasc Biol* 23(12): pp.2146-2154.

Mimeault, M. and Batra, S. K. (2013) Hypoxia-inducing factors as master regulators of stemness properties and altered metabolism of cancer- and metastasis-initiating cells. *J Cell Mol Med* 17(1): pp.30-54.

Minguet, J., Smith, K. H., Bramlage, C. P. and Bramlage, P. (2015) Targeted therapies for treatment of renal cell carcinoma: recent advances and future perspectives. *Cancer Chemother Pharmacol* 76(2): pp.219-233.

Mir, O., Ropert, S., Alexandre, J. and Goldwasser, F. (2009) Hypertension as a surrogate marker for the activity of anti-VEGF agents. *Ann Oncol* 5: pp.967-970.

Mitchell, J. A., Ali, F., Bailey, L., Moreno, L. and Harrington, L. S. (2008) Role of nitric oxide and prostacyclin as vasoactive hormones released by the endothelium. *Exp Physiol* 93(1): pp.141-147.

Moncada, S. and Higgs, E. A. (2006) Nitric oxide and the vascular endothelium. *Handb Exp Pharmacol* (176)(1): pp.213-254.

Mourad, J. J., des Guetz, G., Debbabi, H. and Levy, B. I. (2008) Blood pressure rise following angiogenesis inhibition by bevacizumab. A crucial role for microcirculation. *Ann Oncol* 5: pp.927-34.

Mourad, J. J. and Levy, B. I. (2011) Mechanisms of antiangiogenic-induced arterial hypertension. *Curr Hypertens Rep* 13(4): pp.289-293.

Mross, K., Frost, A., Scheulen, M. E., Krauss, J., Strumberg, D., Schultheiss, B., Fasol, U., Buchert, M., Kratzschmer, J., Delesen, H., Rajagopalan, P. and Christensen, O. (2011) Phase I study of telatinib (BAY 57-9352): analysis of safety, pharmacokinetics, tumor efficacy, and biomarkers in patients with colorectal cancer. *Vasc Cell* 3: pp.16.

Mulders, P., Hawkins, R., Nathan, P., de Jong, I., Osanto, S., Porfiri, E., Protheroe, A., van Herpen, C. M., Mookerjee, B., Pike, L., Jurgensmeier, J. M. and Gore, M. E. (2012) Cediranib monotherapy in patients with advanced renal cell carcinoma: results of a randomised phase II study. *Eur J Cancer* 48(4): pp.527-537.

Mulvany, M. J. and Halpern, W. (1976) Mechanical properties of vascular smooth muscle cells in situ. *Nature* 260(5552): pp.617-619.

Mulvany, M. J. and Halpern, W. (1977) Contractile properties of small arterial resistance vessels in spontaneously hypertensive and normotensive rats. *Circ Res* 41(1): pp.19-26.

Murakami, M., Iwai, S., Hiratsuka, S., Yamauchi, M., Nakamura, K., Iwakura, Y. and Shibuya, M. (2006) Signaling

of vascular endothelial growth factor receptor-1 tyrosine kinase. *Blood* 108(6): pp.1849-1856.

Murohara, T., Horowitz, J. R., Silver, M., Tsurumi, Y., Chen, D., Sullivan, A. and Isner, J. M. (1998) Vascular endothelial growth factor/vascular permeability factor enhances vascular. *Circulation* 97(1): pp.99-107.

Nakayama, T. (2006) Prostacyclin analogues: prevention of cardiovascular diseases. *Cardiovasc Hematol Agents Med Chem* 4(4): pp.351-359.

Nicoli, S., Standley, C., Walker, P., Hurlstone, A., Fogarty, K. E. and Lawson, N. D. (2010) MicroRNA-mediated integration of haemodynamics and Vegf signalling during angiogenesis. *Nature* 7292: pp.1196-1200.

Nieminen, T., Toivanen, P. I., Rintanen, N., Heikura, T., Jauhiainen, S., Airene, K. J., Alitalo, K., Marjomaki, V. and Yla-Herttuala, S. (2014) The impact of the receptor binding profiles of the vascular endothelial growth factors on their angiogenic features. *Biochim Biophys Acta* 1840(1): pp.454-463.

Norrby, K. (2006) In vivo models of angiogenesis. *J Cell Mol Med* 10(3): pp.588-612.

Norrby, K. (2008) Drug testing with angiogenesis models. *Expert Opin Drug Discov* 3(5): pp.533-549.

Norrby, K., Jakobsson, A. and Sorbo, J. (1986) Mast-cell-mediated angiogenesis: a novel experimental model using the rat mesentery. *Cell Pathol Incl Mol Pathol* 52(3): pp.195-206.

Norrby, K. C. (2011) Rat mesentery angiogenesis assay. *J Vis Exp* 18(52) [abstract].

Ohuchi, E., Imai, K., Fujii, Y., Sato, H., Seiki, M. and Okada, Y. (1997) Membrane type 1 matrix metalloproteinase digests interstitial collagens and other extracellular matrix macromolecules. *J Biol Chem* 272(4): pp.2446-2451.

Olsson, A. K., Dimberg, A., Kreuger, J. and Claesson-Welsh, L. (2006) VEGF receptor signalling - in control of vascular function. *Nat Rev Mol Cell Biol* 5: pp.359-371.

World Health Organisation. (2016) Cancer Available at: <http://www.who.int/cancer/en/> (Accessed: 23.03.2016 2016).

Pan, Q., Chathery, Y., Wu, Y., Rathore, N., Tong, R. K., Peale, F., Bagri, A., Tessier-Lavigne, M., Koch, A. W. and Watts, R. J. (2007) Neuropilin-1 binds to VEGF₁₂₁ and regulates EC migration and sprouting. *J Biol Chem* 282(33): pp.24049-24056.

Park, Y. W., Cummings, R. T., Wu, L., Zheng, S., Cameron, P. M., Woods, A., Zaller, D. M., Marcy, A. I. and Hermes, J. D. (1999) Homogeneous proximity tyrosine kinase assays: scintillation proximity assay versus homogeneous time-resolved fluorescence. *Anal Biochem* 269(1): pp.94-104.

Parker, M. W., Xu, P., Li, X. and Vander Kooi, C. W. (2012) Structural basis for selective vascular endothelial growth factor-A (VEGF-A) binding to neuropilin-1. *J Biol Chem* 287(14): pp.11082-11089.

Patel, N. S., Li, J. L., Generali, D., Poulosom, R., Cranston, D. W. and Harris, A. L. (2005) Up-regulation of delta-like 4 ligand

in human tumor vasculature and the role of basal expression in EC function. *Cancer Res* 19: pp.8690-8697.

Pawlik, T. M., Reyes, D. K., Cosgrove, D., Kamel, I. R., Bhagat, N. and Geschwind, J. F. (2011) Phase II trial of sorafenib combined with concurrent transarterial chemoembolization with drug-eluting beads for hepatocellular carcinoma. *J Clin Oncol* 29(30): pp.3960-3967.

Persson, P. B., Skalweit, A. and Thiele, B. J. (2004) Controlling the release and production of renin. *Acta Physiol Scand* 4: pp.375-381.

Ponchon, P. and Elghozi, J. L. (1996) Contribution of the renin-angiotensin and kallikrein-kinin systems to short-term variability of blood pressure in two-kidney, one-clip hypertensive rats. *Eur J Pharmacol* 297(2): pp.61-70.

Potente, M., Gerhardt, H. and Carmeliet, P. (2011) Basic and therapeutic aspects of angiogenesis. *Cell* 6: pp.873-387.

Pouessel, D. and Culine, S. (2008) High frequency of intracerebral hemorrhage in metastatic renal carcinoma patients with brain metastases treated with tyrosine kinase inhibitors targeting the vascular endothelial growth factor receptor. *Eur Urol* 53(2): pp.376-381.

Pritchard-Jones, R. O., Dunn, D. B., Qiu, Y., Varey, A. H., Orlando, A., Rigby, H., Harper, S. J. and Bates, D. O. (2007) Expression of VEGF(xxx)b, the inhibitory isoforms of VEGF, in malignant melanoma. *Br J Cancer* 2: pp.223-230.

Qi, W. X., Shen, Z., Lin, F., Sun, Y. J., Min, D. L., Tang, L. N., He, A. N. and Yao, Y. (2012) Incidence and Risk of Hypertension with Vandetanib in Cancer Patients: A

Systematic review and Meta-analysis of clinical trials. *Br J Clin Pharmacol.* 75(4): pp.919-930

Ramos-Vara, J. A. (2005) Technical aspects of immunohistochemistry, *Vet Pathol*, 42(4) pp.405-426.

Ranieri, G., Mammi, M., Donato Di Paola, E., Russo, E., Gallelli, L., Citraro, R., Gadaleta, C. D., Marech, I., Ammendola, M. and De Sarro, G. (2014) Pazopanib a tyrosine kinase inhibitor with strong anti-angiogenetic activity: A new treatment for metastatic soft tissue sarcoma. *Crit Rev Oncol Hematol* 89(2): pp.322-329.

Rennel, E., Waine, E., Guan, H., Schuler, Y., Leenders, W., Woolard, J., Sugiono, M., Gillatt, D., Kleinerman, E., Bates, D. and Harper, S. (2008) The endogenous anti-angiogenic VEGF isoform, VEGF165b inhibits human tumour growth in mice. *Br J Cancer* 98(7): pp.1250-1257.

Rex, A., Kolbasenko, A., Bert, B. and Fink, H. (2007) Choosing the right wild type: behavioral and neurochemical differences between 2 populations of Sprague-Dawley rats from the same source but maintained at different sites. *J Am Assoc Lab Anim Sci* 46(5): pp.13-20.

Rini, B. I., Cohen, D. P., Lu, D. R., Chen, I., Hariharan, S., Gore, M. E., Figlin, R. A., Baum, M. S. and Motzer, R. J. (2011) Hypertension as a biomarker of efficacy in patients with metastatic renal cell carcinoma treated with sunitinib. *J Natl Cancer Inst* 103(9): pp.763-73.

Robinson, E. S., Matulonis, U. A., Ivy, P., Berlin, S. T., Tyburski, K., Penson, R. T. and Humphreys, B. D. (2010) Rapid development of hypertension and proteinuria with

cediranib, an oral vascular endothelial growth factor receptor inhibitor. *Clin J Am Soc Nephrol* 5(3): pp.477-483.

Rubanyi, G. M., Romero, J. C. and Vanhoutte, P. M. (1986) Flow-induced release of endothelium-derived relaxing factor. *Am J Physiol* 250(2): pp.H1145-H1149.

Ruscito, I., Gasparri, M. L., Marchetti, C., De Medici, C., Bracchi, C., Palaia, I., Imboden, S., Mueller, M. D., Papadia, A., Muzii, L. and Panici, P. B. (2016) Cediranib in ovarian cancer: state of the art and future perspectives. *Tumour Biol.* 37(3): pp.2833-2839

Salameh, A., Galvagni, F., Bardelli, M., Bussolino, F. and Oliviero, S. (2005) Direct recruitment of CRK and GRB2 to VEGFR-3 induces proliferation, migration and survival of endothelial cells through the activation of ERK, AKT, and JNK pathways.. *Blood* 106(10): pp.3423-31.

Sato, Y., Nakajima, S., Shiraga, N., Atsumi, H., Yoshida, S., Koller, T., Gerig, G. and Kikinis, R. (1998) Three-dimensional multi-scale line filter for segmentation and visualization of curvilinear structures in medical images. *Med Image Anal* 2(2): pp.143-168.

Sawano, A., Takahashi, T., Yamaguchi, S. and Shibuya, M. (1997) The phosphorylated 1169-tyrosine containing region of flt-1 kinase (VEGFR-1) is a major binding site for PLCgamma. *Biochem Biophys Res Commun* 238(2): pp.487-491.

Scappaticci, F. A., Fehrenbacher, L., Cartwright, T., Hainsworth, J. D., Heim, W., Berlin, J., Kabbinavar, F., Novotny, W., Sarkar, S. and Hurwitz, H. (2005) Surgical wound healing complications in metastatic colorectal cancer

patients treated with bevacizumab. *J Surg Oncol* 91(3): pp.173-180.

Scartozzi, M., Galizia, E., Chiorrini, S., Giampieri, R., Berardi, R., Pierantoni, C. and Cascinu, S. (2009) Arterial hypertension correlates with clinical outcome in colorectal cancer patients treated with first-line bevacizumab. *Ann Oncol* 20(2): pp.227-230.

Scornik, F. S. and Toro, L. (1992) U46619, a thromboxane A₂ agonist, inhibits K_{Ca} channel activity from pig coronary artery. *Am J Physiol* 262(1): pp.C708-C713.

Schmidt C (2015) Cediranib aims for a comeback. *J Natl Cancer Inst.* 107: pp.6-8.

Segal, S. S., Welsh, D. G. and Kurjiaka, D. T. (1999) Spread of vasodilatation and vasoconstriction along feed arteries and arterioles of hamster skeletal muscle. *J Physiol* 516 (1): pp.283-291.

Semenza, G. L., Agani, F., Booth, G., Forsythe, J., Iyer, N., Jiang, B. H., Leung, S., Roe, R., Wiener, C. and Yu, A. (1997) Structural and functional analysis of hypoxia-inducible factor 1. *Kidney Int* 51(2): pp.553-555.

Senger, D. R., Galli, S. J., Dvorak, A. M., Perruzzi, C. A., Harvey, V. S. and Dvorak, H. F. (1983) Tumor cells secrete a vascular permeability factor that promotes accumulation of ascites fluid. *Science* 219(4587): pp.983-5.

Senger, D. R., Perruzzi, C. A., Feder, J. and Dvorak, H. F. (1986) A highly conserved vascular permeability factor secreted by a variety of human and rodent tumor cell lines. *Cancer Res* 46(11): pp.5629-5632.

Senger, D. R. and Van De Water, L. (2000) VEGF expression by epithelial and stromal cell compartments: resolving a controversy. *Am J Pathol* 157(1): pp.1-3.

Sgoifo, A., Stilli, D., Medici, D., Gallo, P., Aimi, B. and Musso, E. (1996) Electrode positioning for reliable telemetry ECG recordings during social stress in unrestrained rats. *Physiol Behav* 60(6): pp.1397-1401.

Shalaby, F., Rossant, J., Yamaguchi, T. P., Gertsenstein, M., Wu, X. F., Breitman, M. L. and Schuh, A. C. (1995) Failure of blood-island formation and vasculogenesis in Flk-1-deficient mice. *Nature* 376(6535): pp.62-66.

Sharma, T., Dhingra, R., Singh, S., Sharma, S., Tomar, P., Malhotra, M. and Bhardwaj, T. R. (2013) Aflibercept: a novel VEGF targeted agent to explore the future perspectives of anti-angiogenic therapy for the treatment of multiple tumors. *Mini Rev Med Chem* 13(4): pp.530-540.

Shibuya, M. (2014) VEGF-VEGFR Signals in Health and Disease. *Biomol Ther* 22(1): pp.1-9.

Sipkema, P., van der Linden, P. J., Westerhof, N. and Yin, F. C. (2003) Effect of cyclic axial stretch of rat arteries on endothelial cytoskeletal morphology and vascular reactivity. *J Biomech* 36(5): pp.653-659.

Sleijfer, S., Ray-Coquard, I., Papai, Z., Le Cesne, A., Scurr, M., Schoffski, P., Collin, F., Pandite, L., Marreaud, S., De Brauwier, A., van Glabbeke, M., Verweij, J. and Blay, J. Y. (2009) Pazopanib, a multikinase angiogenesis inhibitor, in patients with relapsed or refractory advanced soft tissue sarcoma: a phase II study from the European organisation for research and treatment of cancer-soft tissue and bone

sarcoma group (EORTC study 62043). *J Clin Oncol* 19: pp.3126-3132.

Small, H. Y., Montezano, A. C., Rios, F. J., Savoia, C. and Touyz, R. M. (2014) Hypertension due to antiangiogenic cancer therapy with vascular endothelial growth factor inhibitors: understanding and managing a new syndrome. *Can J Cardiol* 30(5): pp.534-543.

Smith, J. (2005) Erlotinib: small-molecule targeted therapy in the treatment of non-small-cell lung cancer. *Clin Ther* 27(10): pp.1513-1534.

Socha, M. J., Behringer, E. J. and Segal, S. S. (2012) Calcium and electrical signalling along endothelium of the resistance vasculature. *Basic Clin Pharmacol Toxicol* 110(1): pp.80-86.

Soker, S., Takashima, S., Miao, H. Q., Neufeld, G. and Klagsbrun, M. (1998) Neuropilin-1 is expressed by endothelial and tumor cells as an isoform-specific receptor for vascular endothelial growth factor. *Cell* 92(6): pp.735-745.

Souza, V. B., Silva, E. N., Ribeiro, M. L. and Martins Wde, A. (2015) Hypertension in patients with cancer. *Arq Bras Cardiol* 104(3): pp.246-52.

Stankov, K., Popovic, S. and Mikov, M. (2013) C-KIT Signaling in Cancer Treatment. *Curr Pharm Des.*

Steeghs, N., Gelderblom, H., Roodt, J. O., Christensen, O., Rajagopalan, P., Hovens, M., Putter, H., Rabelink, T. J. and de Koning, E. (2008) Hypertension and rarefaction during treatment with telatinib, a small molecule angiogenesis inhibitor. *Clin Cancer Res* 14(11): pp.3470-3476.

Stewart, B., Wild, C.P. (2014) World Cancer Report 2014. world health organisation p.630.

Stewart, W. J., Galvin, K. A., Gillam, L. D., Guyer, D. E. and Weyman, A. E. (1985) Comparison of high pulse repetition frequency and continuous wave Doppler echocardiography in the assessment of high flow velocity in patients with valvular stenosis and regurgitation. *J Am Coll Cardiol* 6(3): pp.565-571.

Stitham, J., Arehart, E. J., Gleim, S. R., Douville, K. L. and Hwa, J. (2007) Human prostacyclin receptor structure and function from naturally-occurring and synthetic mutations, *Prostaglandins Other Lipid Mediat*, 82(1-4): pp.95-108.

Strilic, B., Kucera, T., Eglinger, J., Hughes, M. R., McNagny, K. M., Tsukita, S., Dejana, E., Ferrara, N. and Lammert, E. (2009) The molecular basis of vascular lumen formation in the developing mouse aorta. *Dev Cell* 4: pp.505-515.

Stuttfield, E. and Ballmer-Hofer, K. (2009) Structure and function of VEGF receptors. *IUBMB Life* 61(9): pp.915-922.

Tai, J. H., Tessier, J., Ryan, A. J., Hoffman, L., Chen, X. and Lee, T. Y. (2010) Assessment of acute antivasular effects of vandetanib with high-resolution dynamic contrast-enhanced computed tomographic imaging in a human colon tumor xenograft model in the nude rat. *Neoplasia* 12(9): pp.697-707.

Thomas, P. and Smart, T. G. (2005) HEK293 cell line: a vehicle for the expression of recombinant proteins. *J Pharmacol Toxicol Methods* 51(3): pp.187-200.

Thornton, K., Kim, G., Maher, V. E., Chattopadhyay, S., Tang, S., Moon, Y. J., Song, P., Marathe, A., Balakrishnan, S., Zhu,

H., Garnett, C., Liu, Q., Booth, B., Gehrke, B., Dorsam, R., Verbois, L., Ghosh, D., Wilson, W., Duan, J., Sarker, H., Miksinski, S. P., Skarupa, L., Ibrahim, A., Justice, R., Murgu, A. and Pazdur, R. (2012) Vandetanib for the treatment of symptomatic or progressive medullary thyroid cancer in patients with unresectable locally advanced or metastatic disease: U.S. Food and Drug Administration drug approval summary. *Clin Cancer Res* 14: pp.3722-3730.

Toi, M., Matsumoto, T. and Bando, H. (2001) Vascular endothelial growth factor: its prognostic, predictive, and therapeutic implications. *Lancet Oncol* 2(11): pp.667-673.

Ton, G. N., Banaszynski, M. E. and Kolesar, J. M. (2013) Vandetanib: A novel targeted therapy for the treatment of metastatic or locally advanced medullary thyroid cancer. *Am J Health Syst Pharm* 70(10): pp.849-855.

Triantafyllou, A., Anyfanti, P., Pырpasopoulou, A., Triantafyllou, G., Aslanidis, S. and Douma, S. (2015) Capillary rarefaction as an index for the microvascular assessment of hypertensive patients. *Curr Hypertens Rep* 17(5): pp.33.

Tsai, M. H. and Jiang, M. J. (2006) Rho-kinase-mediated regulation of receptor-agonist-stimulated smooth muscle contraction. *Pflugers Arch* 453(2): pp.223-232.

Turner, V. P. Brabb, T., Pekow, C., Vasbinder, M (2011) Administration of Substances to Laboratory Animals: Routes of Administration and Factors to Consider. *JAALAS* 50 (5): pp. 600-613

Valnes, K. and Brandtzaeg, P. (1985) Retardation of immunofluorescence fading during microscopy. *J Histochem Cytochem* 33(8): pp.755-761.

Varey, A. H., Rennel, E. S., Qiu, Y., Bevan, H. S., Perrin, R. M., Raffy, S., Dixon, A. R., Paraskeva, C., Zaccheo, O., Hassan, A. B., Harper, S. J. and Bates, D. O. (2008) VEGF 165 b, an antiangiogenic VEGF-A isoform, binds and inhibits bevacizumab treatment in experimental colorectal carcinoma: balance of pro- and antiangiogenic VEGF-A isoforms has implications for therapy. *Br J Cancer* 98(8): pp.1366-1379.

Vauquelin, G. and Charlton, S. J. (2010) Long-lasting target binding and rebinding as mechanisms to prolong in vivo drug action. *Br J Pharmacol* 161(3): pp.488-508.

Verbois, L., Justice, R. and Robertson, K. (2008) FDA Report: Pazopanib.

Veronese, M. L., Mosenkis, A., Flaherty, K. T., Gallagher, M., Stevenson, J. P., Townsend, R. R. and ODwyer, P. J. (2006) Mechanisms of hypertension associated with BAY 43-9006. *J Clin Oncol* 24(9): pp.1363-1369.

Vidal, M., Wells, S., Ryan, A. and Cagan, R. (2005) ZD6474 suppresses oncogenic RET isoforms in a Drosophila model for type 2 multiple endocrine neoplasia syndromes and papillary thyroid carcinoma. *Cancer Res* 65(9): pp.3538-3541.

Visakorpi, T., Kallioniemi, O. P., Koivula, T., Harvey, J. and Isola, J. (1992) Expression of epidermal growth factor receptor and ERBB2 (HER-2/Neu) oncoprotein in prostatic carcinomas. *Mod Pathol* 5(6): pp.643-648.

Voon, D. C., Subrata, L. S., Baltic, S., Leu, M. P., Whiteway, J. M., Wong, A., Knight, S. A., Christiansen, F. T. and Daly, J. M. (2005) Use of mRNA- and protein-destabilizing elements to develop a highly responsive reporter system. *Nucleic Acids Res* 33(3): pp.e27.

Wang, B. W., Chang, H., Lin, S., Kuan, P. and Shyu, K. G. (2003) Induction of matrix metalloproteinases-14 and -2 by cyclical mechanical stretch is mediated by tumor necrosis factor-alpha in cultured human umbilical vein ECs. *Cardiovasc Res* 59(2): pp.460-469.

Wang, R., Chadalavada, K., Wilshire, J., Kowalik, U., Hovinga, K. E., Geber, A., Fligelman, B., Leversha, M., Brennan, C. and Tabar, V. (2010) Glioblastoma stem-like cells give rise to tumour endothelium. *Nature*. 7325:pp.829-33.

Wedge, S. R., Kendrew, J., Hennequin, L. F., Valentine, P. J., Barry, S. T., Brave, S. R., Smith, N. R., James, N. H., Dukes, M., Curwen, J. O., Chester, R., Jackson, J. A., Boffey, S. J., Kilburn, L. L., Barnett, S., Richmond, G. H., Wadsworth, P. F., Walker, M., Bigley, A. L., Taylor, S. T., Cooper, L., Beck, S., Jurgensmeier, J. M. and Ogilvie, D. J. (2005) AZD2171: a highly potent, orally bioavailable, vascular endothelial growth factor receptor-2 tyrosine kinase inhibitor for the treatment of cancer. *Cancer Res* 65(10): pp.4389-4400.

Wedge, S. R., Ogilvie, D. J., Dukes, M., Kendrew, J., Chester, R., Jackson, J. A., Boffey, S. J., Valentine, P. J., Curwen, J. O., Musgrove, H. L., Graham, G. A., Hughes, G. D., Thomas, A. P., Stokes, E. S., Curry, B., Richmond, G. H., Wadsworth, P. F., Bigley, A. L. and Hennequin, L. F. (2002) ZD6474 inhibits vascular endothelial growth factor signaling, angiogenesis, and tumor growth following oral administration. *Cancer Res* 62(16): pp.4645-4655.

Weiss, J. M., Villaruz, L. C., Socinski, M. A., Ivanova, A., Grilley-Olson, J., Dhruva, N. and Stinchcombe, T. E. (2014) A single-arm phase II trial of pazopanib in patients with advanced non-small cell lung cancer with non-squamous

histology with disease progression on bevacizumab containing therapy. *Lung Cancer* 86(2): pp.288-290.

Wells, S. A., Jr., Robinson, B. G., Gagel, R. F., Dralle, H., Fagin, J. A., Santoro, M., Baudin, E., Elisei, R., Jarzab, B., Vasselli, J. R., Read, J., Langmuir, P., Ryan, A. J. and Schlumberger, M. J. (2012) Vandetanib in patients with locally advanced or metastatic medullary thyroid cancer: a randomized, double-blind phase III trial. *J Clin Oncol* 30(2): pp.134-141.

White, B. J., Smith, P. A. and Dunn, W. R. (2013) Hydrogen sulphide-mediated vasodilatation involves the release of neurotransmitters from sensory nerves in pressurized mesenteric small arteries isolated from rats. *Br J Pharmacol* 168(4): pp.785-793.

Wibom, C., Sandstrom, M., Henriksson, R., Antti, H., Johansson, M. and Bergenheim, A. T. (2010) Vandetanib alters the protein pattern in malignant glioma and normal brain in the BT4C rat glioma model. *Int J Oncol* 37(4): pp.879-890.

Widakowich, C., de Castro, G., Jr., de Azambuja, E., Dinh, P. and Awada, A. (2007) Review: side effects of approved molecular targeted therapies in solid cancers. *Oncologist* 12: pp.1443-1455.

Wong, P. P., Demircioglu, F., Ghazaly, E., Alrawashdeh, W., Stratford, M. R., Scudamore, C. L., Cereser, B., Crnogorac-Jurcevic, T., McDonald, S., Elia, G., Hagemann, T., Kocher, H. M. and Hodivala-Dilke, K. M. (2015) Dual-action combination therapy enhances angiogenesis while reducing tumor growth and spread. *Cancer Cell* 27(1): pp.123-137.

Woolard, J., Bevan, H. S., Harper, S. J. and Bates, D. O. (2009) Molecular diversity of VEGF-A as a regulator of its biological activity. *Microcirculation*: 7: pp.572-592.

Woolard, J., Wang, W. Y., Bevan, H. S., Qiu, Y., Morbidelli, L., Pritchard-Jones, R. O., Cui, T. G., Sugiono, M., Waine, E., Perrin, R., Foster, R., Digby-Bell, J., Shields, J. D., Whittles, C. E., Mushens, R. E., Gillatt, D. A., Ziche, M., Harper, S. J. and Bates, D. O. (2004) VEGF165b, an inhibitory vascular endothelial growth factor splice variant: mechanism of action, in vivo effect on angiogenesis and endogenous protein expression. *Cancer Res* 64(21): pp.7822-7835.

Wyckoff, J. B., Jones, J. G., Condeelis, J. S. and Segall, J. E. (2000) A critical step in metastasis: in vivo analysis of intravasation at the primary tumor. *Cancer Res* 60(9) pp.2504-2511.

Yamamoto, K. and Ando, J. (2015) Vascular EC membranes differentiate between stretch and shear stress through transitions in their lipid phases. *Am J Physiol Heart Circ Physiol* 309(7): pp.H1178-1185.

Yasky, J., Verho, M., Erasmus, T. P., Luus, H. G., Angela, M., Grandin, L., Akbary, M. A. and Rangoonwala, B. (1996) Efficacy of ramipril versus enalapril in patients with mild to moderate essential hypertension. *Br J Clin Pract* 50(6): pp.302-310.

Yoon, S. and Seger, R. (2006) The extracellular signal-regulated kinase: multiple substrates regulate diverse cellular functions. *Growth Factors* 1: pp.21-44.

Zachary, I. (2014) Neuropilins: role in signalling, angiogenesis and disease. *Chem Immunol Allergy* 99: pp.37-70.

- Zachary, I. and Glik, G. (2001) Signaling transduction mechanisms mediating biological actions of the vascular endothelium growth. *Cardiovasc Res* 49(3): pp.568-581.
- Zhang, C., Wu, X., Zhang, M., Zhu, L., Zhao, R., Xu, D., Lin, Z., Liang, C., Chen, T., Chen, L., Ren, Y., Zhang, J., Qin, N. and Zhang, X. (2013) Small molecule R1498 as a well-tolerated and orally active kinase inhibitor for hepatocellular carcinoma and gastric cancer treatment via targeting angiogenesis and mitosis pathways. *PLoS One* 8(6): pp.e65264.
- Zhang, J., Yang, P. L. and Gray, N. S. (2009) Targeting cancer with small molecule kinase inhibitors. *Nat Rev Cancer* 1: pp.28-39.
- Zhang, Y., Lin, Y., Bowles, C. and Wang, F. (2004) Direct cell cycle regulation by the fibroblast growth factor receptor (FGFR) kinase through phosphorylation-dependent release of Cks1 from FGFR substrate 2, *J Biol Chem* 279(53): pp.55348-55354.
- Zou, A. P. and Cowley, A. W., Jr. (1999) Role of nitric oxide in the control of renal function and salt sensitivity. *Curr Hypertens Rep* 1(2): pp.178-186.
- Zudaire, E., Gambardella, L., Kurcz, C. and Vermeren, S. (2011) A computational tool for quantitative analysis of vascular networks. *PLoS One* 6(11): pp.e27385.